

# Università degli studi di Milano



Corso di Dottorato di Ricerca  
In Scienze e Tecnologie Chimiche  
XXVIII Ciclo

Dipartimento di Chimica

“NEW INSIGHTS IN ELECTRON DENSITY AND ELECTRON SPIN DENSITY THROUGH  
TOPOLOGICAL DESCRIPTORS BASED ON BADER’S THEORY OF ATOMS IN  
MOLECULES”

Chim/02

Tesi di Dottorato di ricerca di:  
Ahmed Muhamed Orlando  
R10067

Tutor: Leonardo Lo Presti  
Co-Tutor: Carlo Gatti

Coordinatore del corso di dottorato: Prof.ssa Emanuela Licandro

Anno accademico: 2015/2016

Introduction	4
Chapter 1	10
Single N–C bond becomes shorter than formally double N=C bond in a thiazete-1,1-dioxide crystal: an experimental and theoretical study of strong crystal field effects	
1.1 Introduction	11
1.2 Materials and Methods	14
1.2.1 X-ray diffraction	14
1.2.2 In vacuo quantum mechanical calculations	15
1.2.3 Solid–state quantum mechanical calculations	15
1.3 Multipole analysis	15
1.4 Results and discussion	16
1.4.1 Bond conjugation effects in the thiazete ring: gas–phase results	16
1.4.2 Bond lengths and charge density at the bcp	17
1.4.3 Charge density Laplacian and bond ellipticities	19
1.5 Crystal field effects	22
1.5.1 Crystal packing	22
1.5.2 Thiazete geometry	23
1.5.3 Charge redistribution along the conjugated system	24
1.5.4 Integrated source function	27
1.5.5 Dipole moment enhancement	29
1.6 Conclusions	32
Chapter 2	38
Source Function for the electron spin density: development and application of a new QTAIM based chemical descriptor	
2.1 Introduction	39
2.2 Source Function for electron density	40
2.3 Source Function for electron spin density	41
2.3.1 Theory	41
2.3.2 Comparison between the electron density and spin electron density behaviour	42
2.3.3 Total atomic spin population and atomic laplacian of the spin density	45
2.3.4 Numerical accuracy of $\square(r)$ and $s(r)$ reconstruction	49
2.3.5 On the interpretation of $s(r)$ information using SFs QTAIM based descriptor	51
2.3.6 Electron spin density in terms of its SFS percentage	59
2.3.7 Transferability of $\rho(r)$ and $s(r)$ in n-alkanes and n-alkyl radicals: similarities and differences as viewed through the Source Function descriptors	67
2.4 Interpretation of ferro-magnetic interactions in Azido Cu(II) di-nuclear complexes using the SFs based topological descriptors	80
2.4.1 Introduction	80
2.4.2 Results and discussion	82
2.5 Non-Innocent role of ligands in some Ni organometallic complexes as viewed through the Spin Density Source Function	94
General remarks and conclusions	102
Appendix A1	110
A1. Experimental procedures: full discussion	110
A1.1 Specimens.	110
A1.2 X–ray diffraction.	110

A1.3 Multipole Model.	114
A1.4. Accuracy of geometric and thermal parameters of DTC in the solid state at $T = 100$ K	116
A1.5. Statistical assessment of the weighting scheme.	116
A1.6 Correlations.	119
A2. Gas-phase optimized structures.	119
A2.1 Bond polarization and bond strength.	119
A2.2 Delocalization indices.	121
. A2.3 Source function values.	123
A3. Crystal field effects	125
Appendix A2	136

# **INTRODUCTION:**

1900 could be considered as year of birth of quantum mechanics, in fact in that year Max Plank has published his well known work on the distribution of the blackbody radiation<sup>[1]</sup>. Since that work, during the following 25 years, a huge amount of discussions and comparisons were done; this challenge has involved almost all the most important scientist of the last century, shaking the foundation of classical physics. In fact in 1925 W. K. Heisenberg published a landmark paper on quantum mechanics<sup>[2]</sup> and, in 1927, he proposed the uncertainty principle<sup>[3]</sup>. This led to a new microscopic science, also helped by the experimental techniques that were becoming available in that period. The birth of quantum mechanics originated because classical physics models were unable to explain the following phenomena:

- i) The problem of blackbody radiation: the classical electromagnetic theory does not interpret the spectrum emitted by hot black bodies
  
- ii) The problem of specific heat in solids: according to classical statistical mechanics, all the energetic levels in a molecular system should equally contribute to the specific heat of a crystal, but this leads to an incorrect behaviour of thermal capacity with temperature (T) at low T.
  
- iii) The problem of atomic spectra: experiment shows that the radiations emitted (or absorbed) by elements are restricted to well-defined frequencies, typical of each element. This is in contradiction with the classical model relying on continuous electron energies.

The introduction of a quantum approach in chemistry was performed by Heitler and London<sup>[4]</sup>, that showed how the use of Schroedinger equation could help to explain chemical bonding. In any case Schrodinger formalism is unable to translate the outcome of a calculation in the usual chemical language. For this reason chemical paradigms (as for example the Lewis theory of chemical bonding<sup>[5]</sup>) are customarily used and the problem remains of finding a link between them and the rigorous quantum physics. A huge amount of effort has been done in the last century to meet this goal. The most general and useful approach is the introduction of descriptors, i.e. theoretical tools and procedures which yield information close to the classical chemical language and at the same time ultimately relies on the wavefunction. An interesting subset of descriptors is represented by the ones based on the Electron Density (ED) distribution which represents the probability of finding an

electron at the position  $\mathbf{r}$  regardless the position and the spin of the other electrons within the molecular system. Electron density can be obtained from the wavefunction by

$$\rho(\mathbf{r}) = \int \Psi^*(r_1, r_2, \dots, r_N; R) \Psi(r_1, r_2, \dots, r_N; R) d s_1 d r_2, d s_2 d s_3 \dots d s_N, d r_N \quad eq. 1$$

where  $\Psi$  represents the wavefunction,  $r_i$  and  $s_i$  are the space and spin coordinates of the  $i$ -th electron and  $R$  collectively indicates the position of nuclei; it is important to stress that eq.1 is valid in the well known Born-Oppenheimer approximation so that the nuclei are considered static with respect electrons, which move in the field created by nuclei in their fixed positions. ED is a physical observable defined in real space and thus very suited for the study of chemical phenomena. Furthermore, as showed by Hohenberg and Kohn,<sup>[6]</sup> the external potential of a molecular system is uniquely determined by its  $\rho(\mathbf{r})$ , i.e. energy is a functional of ED ( $E[\rho(\mathbf{r})]$ ); as a consequence, all the properties of a system can be determined in principle by the knowledge of its  $\rho(\mathbf{r})$ .

Chemical descriptors based on Quantum Theory of Atoms in Molecules (QTAIM<sup>[7]</sup>) are the most used in our research group as they present a very important advantage: they can be applied on the same grounds to experimental and theoretical ED's. In fact  $\rho(\mathbf{r})$  is not only a quantum mechanical observable, but it is also a measurable quantity. In particular it is possible to obtain the electron density distribution of a physical system from X-ray diffraction experiments, which measure structure factors that are the Fourier transform of  $\rho(\mathbf{r})$

$$F_{hkl} = \int_V \langle \rho(r) \rangle e^{2\pi i H \cdot r} dr \quad eq.2$$

In eq.2  $h,k,l$  are the Miller indices which define vectors  $H$  in the reciprocal space<sup>[8]</sup>. There exist several approaches to obtain  $\rho(\mathbf{r})$  from X-ray diffraction data<sup>[9]</sup>, the most used is the multipolar model approach. A very relevant and important aspect of QTAIM is the possibility of partition molecules (and crystals) into atomic regions. Of course QTAIM is not the only method of partitioning the real space belonging to the physical system into atomic contributions, but it is the only one leading to quantum objects, whose energy may be defined unequivocally.

The atomic basins are defined in Bader's theory by

$$\nabla \rho(\mathbf{r}) \cdot \mathbf{n}(\mathbf{r}) = 0 \quad eq.3$$

where  $\nabla \rho(\mathbf{r})$  is the gradient of the electron density distribution and  $\mathbf{n}(\mathbf{r})$  is the vector normal to the basin surface. All the points that fulfill eq.3 define a zero-flux surface which encloses all the

---

<sup>1</sup> to obtain a charge density-quality set of structure factors from an X-ray diffraction experiment an accurate and high-resolution experiment is required, possibly performed at low T. The interested reader is addressed to [8].

electrons belonging to an atomic basin, the boundaries among atoms being defined by the zero-flux surfaces. The atomic regions so defined are non-overlapping and exhaustive and all the atomic basins built by eq.3 are defined as proper quantum open systems. A very important consequence is that in a system all molecular properties (volume, charge, electrostatic moments, energy, etc.) can be partitioned into atomic contributions. One fundamental aspect of QTAIM is the study of  $\rho(\mathbf{r})$  in terms of its scalar field topology. It is performed through the analysis of the critical points (CPs), i.e. those points where the gradient of the electron density vanishes. Critical points are labeled by two numbers  $m$  and  $n$ , the rank<sup>2</sup> of the CP and the algebraic sum of the signs of the curvatures. For topologically stable structures,  $m = 3$ ; as consequence, for them it is possible to distinguish four types of CPs, each of which indicates univocally a structural feature of the system:

- (3,-3) are maxima in the  $\rho(\mathbf{r})$  distribution, are (roughly) located at the position of nuclei (with a few exceptions<sup>3</sup>) and are thus associated to them. Since all the gradient lines terminate at these maxima, they are also called 3D attractors.
- (3,-1) are saddle points called bond critical points (BCPs); this kind of CPs are particularly important because they are related to chemical interactions.
- (3,+1) are saddle points which are found at the center of rings (ring critical points, RCP).
- (3,+3) are minima in ED, associated to cages and corresponding to the minimum ED values within them .

In QTAIM, the line formed by the juxtaposition of the two  $\nabla\rho(\mathbf{r})$  trajectories connecting two (3,-3) critical points is defined as bond path (BP). The bcp lies at the minimum ED along the bond path, along which  $\rho(\mathbf{r})$  is maximally concentrated with respect to any other direction. In general in a molecular system all the chemical bonds supposed by a chemist are topologically described by a bond path but the inverse relationship not always holds. In fact in many cases BPs are found among atomic basins whose interaction would be classified as repulsive by common chemical thinking (e.g. among anions in a crystal).<sup>[10]</sup>

This Ph.D. thesis is focused on the application of QTAIM based chemical descriptors to challenging chemical test-cases, as well as on the development of novel topological descriptors, like the Source Function for the spin density.

The thesis is organized as follows:

In chapter 1 the ED of a very unusual structural feature in a synthetic  $\beta$ -sultamic analogue (DTC)<sup>[11,12]</sup>, has been explored by both low-T single-crystal X-ray diffraction and quantum mechanical simulations to gain insights into the subtle interplay between structure, electron

---

<sup>2</sup> the rank is the number of non zero ED curvatures (eigenvalues of the Hessian matrix) at CP.

<sup>3</sup> in very few cases the  $\rho(\mathbf{r})$  maxima (and associated zero-flux basins) were found in points where no nuclei are present. In such cases the (3,-3) CP are called non-nuclear attractors.

delocalization and crystal field polarization effects. The core chemical moiety in DTC is an uncommon 4-membered thiazete-1,1-dioxide heterocycle, where the formally single N–C bond is, on average, 0.018 Å shorter than the formally double N=C bond. Both local and non-local topological descriptors provided by QTAIM have been employed in the analysis of DTC in comparison with chemically related derivatives and possible implications from the viewpoint of the accurate *in silico* modelling of crystal structures are discussed. Particular attention is dedicated on such kind of issues in chemical and pharmaceutical industries, because the control of the crystal structure is really problematic in some cases; in fact different polymorphs of the same substance have different intensive physical properties, such as solubility, refraction index and conductivity and problems may arise in industrial processes related to the synthesis of chemicals and drugs on large scale<sup>[13]</sup>. Results of this part of work have been published in Ref [12, 14].

In chapter 2, we focused on the source function (SF) QTAIM based topological descriptor. The ED at any point  $r$  within a system may be regarded as consisting of a sum of Source Function (SF) contributions  $S(r; \Omega)$ <sup>[15]</sup> representing a measure of how the various atomic basins or groups of atomic basins defined through QTAIM contribute to determine the  $\rho(r)$  at  $r$ . Recently it was shown that the SF is able to reveal electron delocalization effects in planar electron conjugated systems, in terms of an increased capability of determining the ED along a given bond by the distant, though through-bonds connected, atomic basins and, at the same time, into a decreased ability to do so by the two atoms directly involved in the bond. Such an adjustment of sources then translates into a pictorial pattern of enhanced and reduced atomic SF contributions from, respectively, distant and nearby atoms, compared to the case of a partially or fully saturated network of bonds.<sup>[16,17]</sup>

In the present PhD thesis, we have extended such an analysis to the non planar conjugated systems, where the usual  $\sigma/\pi$  electron separation does no longer apply. Being based on the total ED, the SF analysis may be safely applied also in these less conventional electron delocalized systems. The obtained results have been published in Ref. [18]. Then we have extended the SF reconstruction approach also to the electron density spin counterparts<sup>[19]</sup> *in vacuo*. Such reconstruction was investigated both on simple (but chemically meaningful) spin-polarized molecular systems<sup>[19]</sup> and on more complex single-molecule magnets<sup>[18,20]</sup>. This investigation has showed that the difference between the two spin counterparts of electron density distribution can be reconstructed with a sufficient accuracy, analogously to the case of the total ED<sup>[19]</sup>. Moreover, it was found that the SF for the electron spin density brings in precious chemical information, neatly distinguishing the quite different roles played by the unpaired electrons ED and the spin polarized ED due to the remaining electrons<sup>[19]</sup>. Furthermore, quantitative answers to questions related to the transferability of the spin density in alkyl radicals<sup>[18]</sup> or to the transmission of spin information in metal(s)-ligand systems

were provided<sup>[20]</sup>. Understanding, from a real space perspective, by which mechanisms spin information transmits, might be of relevance to interpret the fundamental magnetic interactions present in complex materials, such as for example coordination polymers or Heussler and half-Heussler alloys<sup>[21]</sup>. As these interactions have a key role in spintronics, characterization of the chemical bond and interpretation of the electron spin density distributions in these systems through the SF analysis, could hopefully disclose structure-property relationships extremely useful for the design of materials with particular physical properties.



## REFERENCES

- [1] M. Planck *Verh. Dtsch. Phys. Ges. Berlin* (1900), **2**, 202
- [2] W. Heisenberg *Zeit. f. Physik* (1925), **33**, 879
- [3] W. Heisenberg *Zeit. f. Physik* 1927, **43**, 172-198
- [4] W. Heitler, F. London, *Zeitschrift für Physik*, (1927), **44**, 455
- [5] G. N. Lewis *J. Am. Chem. Soc.* (1916), **33**, 762–785.
- [6] P. Hohenberg, W. Kohn, *Phys. Rev.* (1964), B864, 136
- [7] R. F. W. Bader *Atoms In Molecules: A Quantum Theory* Oxford: Clarendon Press, 1990
- [8] Giacovazzo, C., Monaco, H. L., Artioli, G., Viterbo, D., Ferraris, G., Gilli, G., Zanotti, G., Catti, M. (2002) *Foundamentals of Crystallography. Secon Edition*. Edited by C. Giacovazzo. New York: Oxford University Press
- [9] C. Gatti and P. Macchi (Eds.), *Modern Charge Density Analysis*, Springer, Dordrecht Heidelberg-London- New York, 2012
- [10] C. Gatti, *Z. Kristallogr.*, 2005, **220**, 399-457
- [11] Clerici, F. ; Gelmi, M. L. ; Soave, R. ; Lo Presti, L. *Tetrahedron* (2002), **58**, 5173-5178
- [12] Orlando, A. M. ; Lo Presti, L. ; Soave, R. *Acta Cryst.* (2010), **E66**, o2032-o2033
- [13] . Bauer, S. Spanton, R. Quick, J. Quick, W. Dziki, W. Porter, J. Morris. *Pharm. Res.* (2001), **18**, 859–866
- [14]L. Lo Presti, A. M. Orlando, L. Loconte, R. Destro, E. Ortoleva, R. Soave, C. Gatti, *Cryst. Growth Des.*, 2014, **14** (9), pp 4418–4429
- [15] Bader R.F.W., Gatti C. *Chem Phys Lett* (1998), **287**, 233-238
- [16] C. Gatti, The Source Function Descriptor as a Tool to Extract Chemical Information from Theoretical and Experimental Electron Densities, *Struct. Bond.*, 2012, **147**, 193-286
- [17] E. Monza, C. Gatti, L. Lo Presti, E. Ortoleva, “Revealing Electron Delocalization through the Source Function”, *J. Phys. Chem. A*, 2011, 115, 12864–12878
- [18] R. Chauvin et al (eds.), *Applications of Topological Methods in Molecular Chemistry, Challenges and Advances in Computational Chemistry and Physics 22*, DOI 10.1007/978-3-319-29022-5\_5 Springer International Publishing Switzerland 2016
- [19] C. Gatti, A. M. Orlando and L. Lo Presti *Chem. Sci.*, 2015,**6**, 3845-3852
- [20] C. Gatti, A. M. Orlando, L. Lo Presti, *Acta Cryst.*, 2014, **A70**, C281
- [21] C. Felser, G.H. Fecher, B. Balke *Angew. Chem. Int. Ed.* (2007), **46**, 668-699

# CHAPTER 1

**Single N–C bond becomes shorter than formally double N=C bond in a thiazete-1,1-dioxide crystal: an experimental and theoretical study of strong crystal field effects**

## 1.1 Introduction

In modern theoretical and applied chemistry, electron localization and delocalization effects play an important role, providing an easy-to-grasp conceptual framework to forecast and rationalize molecular structure and reactivity.<sup>[1,2]</sup> Furthermore, these effects are also rooted at the core of several relevant molecular properties, such as the well-known requirement of bond length alternation to prompt nonlinear optic responses.<sup>[3,4]</sup> Translating the description of bonding (de)localization from the realm of quantum mechanics to the language of the electron density,  $\rho(\mathbf{r})$ , has been a major object of study during the past decades.<sup>[5,8]</sup> In this sense one of the most popular density-based tool to explore the chemical bond in the real space is the Quantum Theory of Atoms in Molecules (QTAIM) developed by R. F. W. Bader<sup>[5]</sup> and co-workers in early 90s.<sup>[9]</sup> Since  $\rho(\mathbf{r})$  is a scalar field which *is* also a quantum-mechanical observable, it is accessible from both theoretical simulations and accurate single-crystal X-ray tests carried out at low temperature,<sup>[10]</sup> as already pointed out in the introductory chapter of this thesis. In a physical perspective, the root of localization and delocalization effects actually consists in the correlated motion of electrons, that can be fully described by the two-electron (pair) density and by the consequent ‘electron sharing indices’ (ESI).<sup>[11]</sup> Among the latter, localization,  $\lambda(A,A)$ , and delocalization,  $\delta(A,B)$  indices are undoubtedly the most widely used ESI.<sup>[12]</sup> When employed in the QTAIM framework, they provide a *direct* estimate of the number of electrons localized within the same QTAIM atomic basin A, and, respectively, of the number of electron pairs delocalized between a couple of atomic basins A and B, regardless their nuclei are connected by a bond path or not. Even though these pair density-based indices are not experimentally accessible, investigating non-local electronic effects is possible thanks to the Source Function (SF) descriptor.<sup>[13]</sup> (For an introduction to the SF, see Chapter 2). Although SF lacks of any direct connection with pair density, it can provide *indirect* hints on the magnitude of electron delocalization within the system, revealing how the individual atomic basins *influence* both their close and far surroundings.<sup>[14]</sup> Moreover, SF is easily computed from the charge density Laplacian,  $\nabla^2\rho(\mathbf{r})$ , and it allows to relate the electron density at every reference point  $\mathbf{r}$  to the influence that each atomic basin has on determining the electron density at that point.

Electron delocalization features may be also deeply influenced by crystal packing: for example, the energy gain caused by electrostatic interactions among molecules in the crystal may strengthen the role of those molecular resonance forms leading to higher charge separation in the molecule.<sup>[15]</sup> The result of this process is often a remarkable enhancement of the molecular dipole moment  $\boldsymbol{\mu}$  in the crystal<sup>[15,16]</sup>: as revealed by a ground-breaking work on urea crystal<sup>[15a]</sup>,  $|\boldsymbol{\mu}|$  increases in the crystal respectively by 37% and by 53% relative to the isolated molecules at crystal

or at in vacuo optimized geometry. The main cause of such large dipole moment enhancement in the bulk can be attributed to the significant magnitude increase of the charge transfer component  $\mu_{CT}$ , which is a measure of charge separation among the atoms in the molecule.

More in detail the total molecular dipole is given by<sup>[45]</sup>

$$\boldsymbol{\mu} = \boldsymbol{\mu}_A + \boldsymbol{\mu}_{CT}$$

where  $\boldsymbol{\mu}_A$  is the atomic polarization term due to the atomic first moments  $\boldsymbol{\mu}_\Omega$  and it is evaluated as

$$\boldsymbol{\mu}_A = \sum_{\Omega} \boldsymbol{\mu}_\Omega$$

$$\boldsymbol{\mu}_\Omega = - \int_{\Omega} \rho(\mathbf{r}) \mathbf{r}_\Omega$$

with  $\mathbf{r}_\Omega$  being the local atomic position vector  $\mathbf{r}_\Omega = \mathbf{r} - \mathbf{X}_\Omega$ , defined relative to its associated nucleus position  $\mathbf{X}_\Omega$ . The charge transfer (CT) component  $\boldsymbol{\mu}_{CT}$  is evaluated as

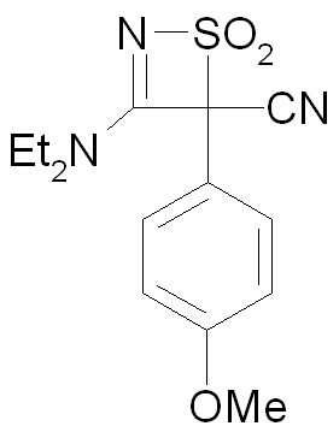
$$\boldsymbol{\mu}_{CT} = \sum_{\Omega} q_{\Omega} \mathbf{X}_{\Omega}$$

where  $q_{\Omega}$  is the net charge of atom  $\Omega$ , obtained by

$$q_{\Omega} = Z_{\Omega} - N_{\Omega};$$

$Z_{\Omega}$  and  $N_{\Omega}$  being the nuclear charge and the atomic electron population of  $\Omega$ .

In this chapter, we're going to focus on the experimental and theoretical charge density distribution of 3-diethylamino-4-(4-methoxyphenyl)-1,1-dioxo-4H-1 $\lambda$ ,2-thiazete-4-carbonitrile, a synthetic thiazete-1,1-dioxide derivative (hereinafter DTC). As shown in Scheme 1 and Figure 1, DTC's core structure shows a significant similarity with 4-membered  $\beta$ -sultam antibiotics.<sup>[17]</sup> The central moiety of the title compound is a heavy functionalized four-membered 1,2-thiazete-1,1-dioxide ring bearing a N-bonded sulfonyl group.



Scheme 1

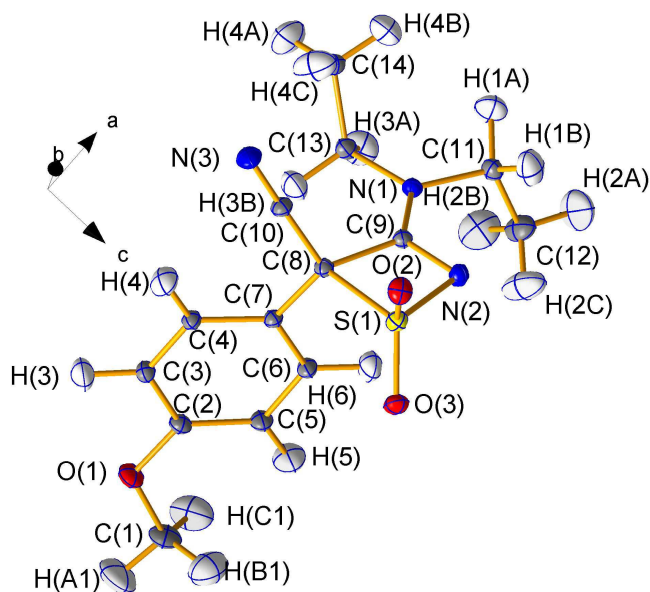


Fig. 1: Experimentally-derived asymmetric unit of DTC at  $T = 100(2)$  K, with the atom numbering scheme. Thermal ellipsoids are drawn at 50 % probability level.

This system shows remarkable unusual features: out of the 632626 entries within the current release of the Cambridge Structural Database (CSD),<sup>[18]</sup> just 16 (0.03 %) contain a 4-membered ring bearing a N–SO<sub>2</sub> system. Furthermore, most of them are 1,2-thiazetidine derivatives, i.e. their heterocyclic core is completely saturated. Just DTC<sup>[19]</sup> (codes: LOZII, LOZII2) and one closely related compound<sup>[20]</sup> (code: TAYCUR) display the unsaturated thiazete ring. At a structural level, a very unusual bonding feature was revealed by former room-temperature (RT) crystallographic investigation within the independent atom model (IAM) approximation<sup>[21]</sup> on different DTC polymorphs<sup>[19]</sup> and TAYCUR<sup>[20]</sup>: in the –N–C=N–SO<sub>2</sub>– moiety (Scheme 1), the formally single N–C bond is indeed found to be, on average, 0.018(3) Å shorter than the formally double N=C bond. In the current CSD release just other two structures,<sup>[22]</sup> markedly different from DTC, show a R<sub>2</sub>N–C=N–R (R = any substituent) bond pattern where  $d_{\text{C–N}} < d_{\text{C=N}}$ , being  $d$  the geometric bond length. Thus, a deep investigation of the DTC crystal seems to be particularly intriguing as it may shed light on the subtle interplay between electron delocalization and crystal field polarization effects. By comparing a series of *in vacuo* systems, including DTC molecule and DTC crystal, our analysis aims to clarify the peculiar properties of the uncommon conjugated –N–C=N–SO<sub>2</sub>– moiety and how crystal packing influences them. Considering the relevance of accurate estimates in describing the geometry of the conjugated bond patterns in DTC crystal and the electronic effects that cause them, we performed single-crystal X-ray diffraction experiments at low  $T$  in order to deconvolute the thermal motion from the static electron density and to provide better estimates either of geometrical and electronic parameters.

# 1.2 Materials and Methods

## 1.2.1 X-ray diffraction

We performed X-ray data collections with graphite-monochromated Mo K $\alpha$  radiation ( $\lambda = 0.71073 \text{ \AA}$ ) at a nominal source power of 50 kV x 30 mA on a three-circle Bruker SMART APEX II goniometer equipped with a CCD area detector and an Oxford Cryostream N<sub>2</sub> gas blower; details of synthetic route to obtain title compound have been reported elsewhere.<sup>[19a]</sup> We employed the SAINT program package<sup>[23]</sup> throughout to obtain data reductions and the final dataset results by merging diffraction data collected on two distinct crystals at  $T = 100(2) \text{ K}$ . A detailed description of the experimental procedure can be found in the appendix A1; Table 1 summarizes the overall statistics of the data employed for the charge density analysis.<sup>[24]</sup> Generally, the completeness was as large as 99.7 %, with an internal agreement factor  $R_{\text{int}}$  as low as 0.0443.

Crystal data	$F_{\text{exp}}$
$a$ (Å)	8.5421(26)
$b$ (Å)	13.2390(6)
$c$ (Å)	13.0443(40)
$\beta$ (deg)	95.079(26)
$V$ (Å <sup>3</sup> )	1469.37(35)
Density (g·cm <sup>-3</sup> )	1.389
Crystal size (mm)	//
Data collection ( $\sin\theta/\lambda_{\text{MAX}} = 0.65 \text{ \AA}^{-1} / 0.90 \text{ \AA}^{-1}$ )	
Measured reflections	86720 / 157389
Unique reflections	3375 / 8956
$I > 2\sigma(I)$ reflections	3117 / 7688
Completeness (%)	100.0 / 99.7
$R_{\text{int}}$	0.0397 / 0.0441
<b>Refinement</b>	
$R(F)$ , $wR(F^2)$ , Goodness-of-fit <sup>4</sup>	0.0297, 0.0798, 0.999
	0.0168, 0.0290, 1.099
$\Delta\rho_{\text{min}}$ , $\Delta\rho_{\text{max}}$ (eÅ <sup>-3</sup> ), data-to-parameters ratio	-0.341, +0.372, 13.80
	-0.144, +0.151, 13.37
Experimental ( $F_{\text{exp}}$ ) spherical ( $\zeta = \kappa\alpha$ ) and deformation ( $\zeta' = \kappa'\alpha'$ ) exponents <sup>5</sup>	S: $\zeta = 4.306$ , $\zeta' = 4.26(2)$ , 4.54(1)
	O: $\zeta = 4.345$ , $\zeta' = 4.98(2)$
	N: $\zeta = 3.797$ , $\zeta' = 3.28(1)$
	C: $\zeta = 3.151$ , $\zeta' = 2.667(3)$
	H: $\zeta = 2.436(3)$ , $\zeta' = 3.00(2)$

Table 1: Data collection statistics and relevant refinement details of the 'A' polymorph of DTC (C<sub>14</sub>H<sub>17</sub>N<sub>3</sub>O<sub>3</sub>S, molecular weight 307.37 g mol<sup>-1</sup>, space group P2<sub>1</sub>/n,  $\mu = 0.234 \text{ mm}^{-1}$ ,  $F_{000} = 648 e$ ).

<sup>4</sup> First row: IAM results from shelx,<sup>[21]</sup> with the thermal motion of H atoms treated as isotropic and  $(\sin\theta/\lambda)_{\text{MAX}} = 0.65 \text{ \AA}^{-1}$ . Second row: multipole model (XD2006<sup>[31]</sup>) on experimental ( $F_{\text{exp}}$ ) structure factor amplitudes up to  $\sin\theta/\lambda = 0.9 \text{ \AA}^{-1}$ .

<sup>5</sup> Values in bohr<sup>-1</sup>. Where not reported, least-squares estimated standard deviations are smaller than the last digit.

### 1.2.2 *In vacuo* quantum mechanical calculations

For the *in vacuo* simulations we employed the Gaussian09 program.<sup>[25]</sup> The non-local hybrid DFT B3LYP Hamiltonian,<sup>[26]</sup> in conjunction with a 6-311G(p,d) basis set<sup>[27]</sup> was selected. Full geometry optimizations were performed on (i) DTC, (ii) the two independent molecules in the asymmetric unit of TAYCUR<sup>[20]</sup> and (iii) a series of appropriate model systems for investigating the covalent bonding properties of the N-C-N-SO<sub>2</sub> atom sequence. To guarantee that a true energy minimum has been effectively reached, we performed full vibration mode analyses. We also performed a single-point calculation on the DTC molecule *in vacuo*, keeping frozen the atomic coordinates to those determined by the X-ray diffraction experiment at  $T = 100$  K. In all this chapter,  $\rho_{\text{VQM}}$  and  $\rho_{\text{VQM-FROZEN}}$  label, respectively, the charge density distributions corresponding to the *in vacuo* relaxed and frozen geometries. An analysis of charge density topologies was carried out by a modified version of the PROAIM program package.<sup>[28]</sup>

### 1.2.3 *Solid-state* quantum mechanical calculations

We employed the same B3LYP<sup>[26]</sup> Hamiltonian and 6-311G(p,d) basis set<sup>[27]</sup> used for *in vacuo* calculations, for the single-point periodic wavefunction calculation of DTC corresponding to the experimentally determined crystal structure at  $T = 100$  K using the CRYSTAL09 program.<sup>[29]</sup> The Fourier transform of the periodic wavefunction was employed to compute a set of  $\approx 9000$  theoretical structure factor amplitudes,  $F_{\text{theo}}$ , within the same  $0.9 \text{ \AA}^{-1}$  resolution in  $\sin\theta/\lambda$  as the experimental dataset. Then, these synthetic data have been employed to obtain a multipole-projected charge density distribution, hereinafter referred to as  $\rho_{\text{MM-PQM}}$  (MM = Multipole Model; PQM= Periodic Quantum Mechanical), while its related primary density, i.e. before the multipole model projection, is referred to as  $\rho_{\text{PQM}}$ .

## 1.3 Multipole analysis

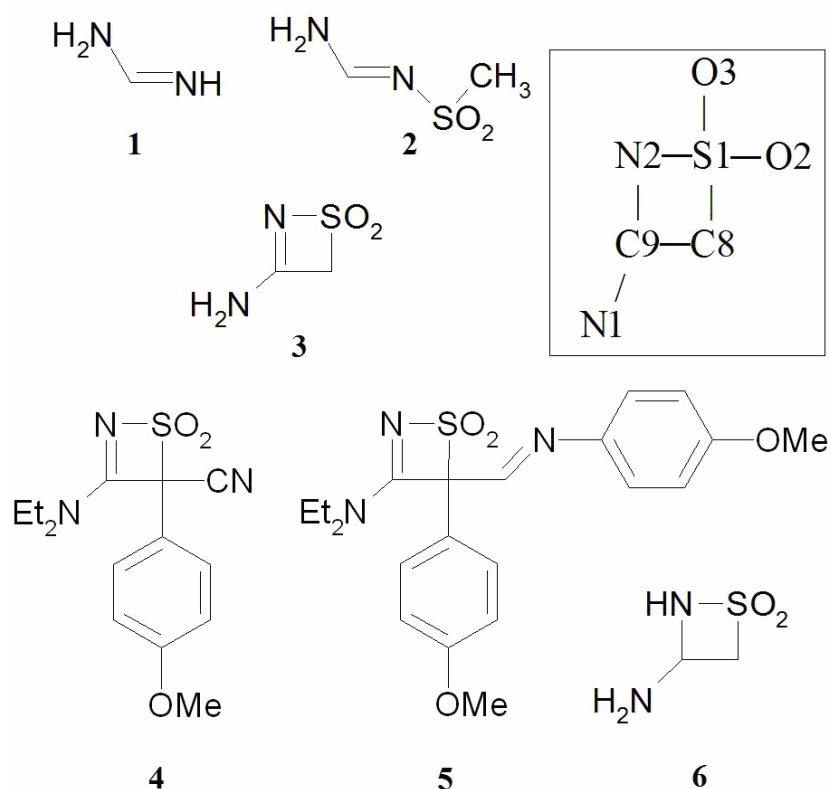
In order to extract the static charge density ( $\rho_{\text{EXP}}$ ) from the observed squared structure factor amplitudes ( $F_{\text{exp}}^2$ ) at  $T = 100$  K we employed the Hansen-Coppens multipole formalism<sup>[30]</sup> as implemented in the XD2006 software package<sup>[31]</sup>. The multipole-projected density  $\rho_{\text{MM-PQM}}$  was instead refined against  $F_{\text{theo}}$  (see Section 5.3). See Table 1 for global refinement parameters, while a full description on the multipole refinement can be found in the appendix A1 along with a full assessment of the final least-squares model from the statistical and physical viewpoints<sup>[32]</sup>. The final

model employed a multipole expansion up to  $l = 4$  for S,  $l = 3$  for C, O, N and  $l = 2$  for H. The description of thermal motion of hydrogen atoms as anisotropic was performed by means of the SHADE2 server.<sup>[33]</sup>

## 1.4 Results and discussion

### *1.4.1 Bond conjugation effects in the thiazete ring: gas-phase results*

For as we know, 1,2-thiazetidines or 1,2-thiazetes rings have never been investigated before in terms of a charge density analysis. Thus, quantum-mechanical calculations on a series of chemically related derivatives, i.e. methanimidamide, 1-(methylsulfonyl)-methanimidamide and 3-amino-1,1-dioxo-4*H*- $\lambda^6$ ,2-thiazete (Scheme 2, structures 1–3) were performed in order to understand the basic conjugation effects in the DTC heterocycle.



Scheme 2

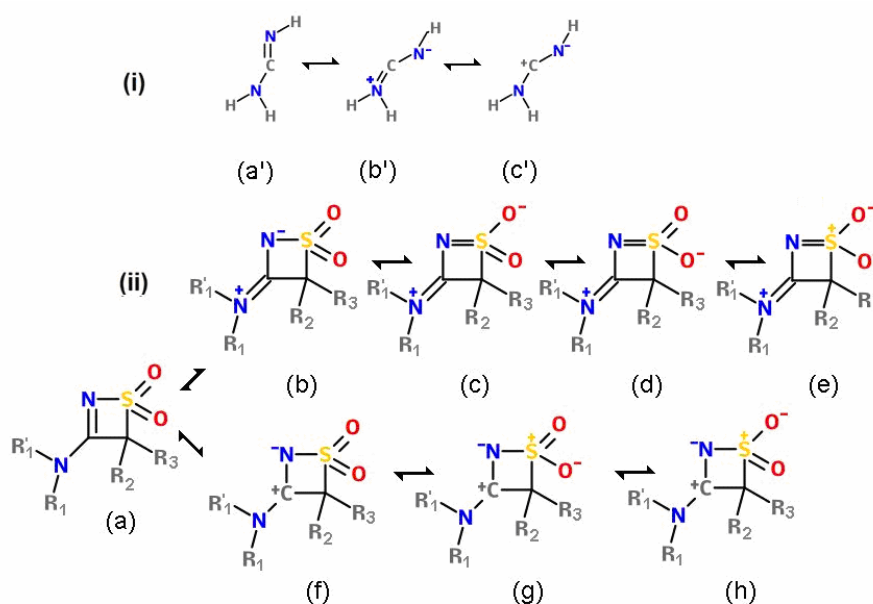
Moreover, we considered the minimum geometries of isolated DTC (Scheme 2, structure **4**) and of both the symmetry-independent molecules of TAYCUR (Scheme 2, structure **5**).<sup>[20]</sup> Since the latter show a marked similarity in terms of chemical bonding descriptors,<sup>[34]</sup> in the following discussion



we shall consider the related average values. The analogue fully saturated 3-amino-1,1-dioxo-thiazetidene cycle (Scheme 2, compound **6**) was also employed as a proper unconjugated reference. A further examination of those individual local and non-local topological descriptors for the thiazete cycle not openly discussed in the text have been reported in the appendix A1 as well as the delocalization indices and integrated Source Function.

#### 1.4.2 Bond lengths and charge density at the bcp

Considering conjugated systems, the measure of individual bond lengths through adjacent bonds allows to provide a first indication of remarkable electron localization or delocalization effects.<sup>[3]</sup> Differently with the solid-state X-ray results, all the evaluated gas-phase systems show the bond length alternation pattern predicted by the supposedly dominant resonance structure *a* (or *a'*) displayed in Scheme 3,<sup>[35]</sup> as  $d_{C=N}$  invariably results to be shorter than  $d_{C-N}$  in all the conjugated structures **1–5** (see tab. 2).



Scheme 3

Regarding the not-conjugated structure **6**, a bond alternation scheme more similar to the X-ray one, with the exocyclic C9–N1 bond shorter than the in-cycle C9–N2 bond was instead retrieved. The possible influence of the electron correlation on the refined geometrical parameters was also checked: we employed the same 6-311G(p,d) triple zeta basis set to perform geometry optimizations on the isolated DTC molecule at the PBE0,<sup>[36]</sup> M06<sup>[37]</sup> and MP2<sup>[38]</sup> levels of theory, resulting in the geometrical results reported in appendix A1. However, all the levels of theory adopted provided the same  $d_{C=N} < d_{C-N}$  result, suggesting that crystal field effects may be

essentially the cause of the bond length inversion in crystalline DTC. In the following discussion we will always refer – if not otherwise specified – to the B3LYP results and we will investigate the variation of the bond lengths and the related charge density properties within the core N–C=N moiety, as its degree of similarity with the title compound increases (see figure 2). Table 2 and Figure 2a (red triangles) show that, on shifting from system **1** to **5**, the C9=N2 bond distance undergoes a monotonic lengthening (up to  $\approx + 3.9\%$ ), while its conjugated C9–N1 bond (red circles) similarly shortens by almost the same amount ( $\approx -3.4\%$ ). Defining a 'bond length difference parameter', BDP, as  $d_{C9-N1} - d_{C9=N2}$ , i.e. as the distance between the red curves in Figure 2a, the latter amounts to 0.11 Å in the conjugated methanimidamide **1**, but reduces to  $\approx 0.02-0.01$  Å in DTC and TAYCUR. The nature of the substituents at C8 has a minor influence on the thiazete properties since generally, all the geometric and topological point descriptors for compounds **4** and **5** are quite similar. The formally single and formally double C–N bond distances show respectively the largest decrease ( $-0.037$  Å) and the largest increase ( $+0.018$  Å) going from **1** to **2**, upon insertion of the electron–attractor sulfonyl group. This may be clearly related to the attained availability of resonance forms *c-e* (and *g-h*, Scheme 3) after introducing such group, while the different S–N distances in systems **2-5** (see tab. 2) may match to different relative weight of the resonance structures *a, b, c-d, e, g-h* in such compounds.

	1 <sup>1</sup>	2 <sup>2</sup>	3 <sup>3</sup>	4 <sup>4</sup>	5 <sup>5</sup>	6 <sup>6</sup>
Bonds						
S1–N2	//	1.6916	1.7277	1.7013	1.6963	1.7149
N2=C9	1.2721	1.2896	1.3048	1.3159	1.3212	1.5109
C9–N1	1.3799	1.3434	1.3401	1.3330	1.3327	1.4312
C9–C8	//	//	1.5125	1.5407	1.5349	1.5486
S1–C8	//	1.7992	1.8577	1.9686	1.9465	1.8251
Angles						
S1–N2–C9	//	115.2	91.9	95.0	94.5	93.8
N2–C9–N1	129.3	121.8	125.8	125.0	124.1	116.4
N2–C9–C8	//	//	108.2	108.5	108.1	94.9
N2–S1–C8	//	100.2	79.1	78.1	78.6	79.1
Torsions						
S1–N2–C9–C8	//	//	0.0	–2.5	2.1	16.4
S1–N2–C9–N1	//	–177.6	180.0	177.8	–176.1	136.5

Table 2: Bond length and angles estimates (Å, deg) as retrieved from the gas–phase quantum–mechanical optimizations of compounds 1–6 at the B3LYP 6–311G(p,d) theory level. See Figure 1 and Scheme 2 for the atom numbering.

<sup>1</sup> Methanimidamide.

<sup>2</sup> 1-(methylsulfonyl)-methanimidamide.

<sup>3</sup> 3-amino-1,1-dioxo-4*H*-1λ<sup>6</sup>,2-thiazete.

<sup>4</sup> Title compound.

<sup>5</sup> For TAYCUR, the unweighted average between the two symmetry-independent molecules is here reported.

<sup>6</sup> Unconjugated thiazetidone cycle.

As expected,<sup>[5,8,9]</sup> at the bond critical point (bcp), a contravariant correspondence occurs between the changes in bond distances and the adjustments of the electron density  $\rho_{\text{bcp}}$ : the shorter the bond, the greater the electron density value at the related critical point (dashed lines in Figure 2a), so that the  $\rho_{\text{bcp}}$  values prove to be remarkably more similar in the substitutes thiazete eterocycles than in the linear compounds **1** and **2**.

### 1.4.3 Charge density Laplacian and bond ellipticities

Looking for further details, we shall consider the electron density Laplacian at the bond critical point,  $\nabla^2\rho_{\text{bcp}}$ , and the related bond ellipticity,  $\varepsilon$  (Figure 2b). It is defined as  $\varepsilon = (\lambda_1/\lambda_2 - 1)$ , with  $\lambda_1$  and  $\lambda_2$  being the two negative curvatures of the  $\rho(\mathbf{r})$  distribution at the bcp, and it measures the electron density accumulation in the plane orthogonal to the bond path.<sup>[5,6]</sup> Specifically, the eigenvector related to  $\lambda_2$  describes the major axis of the elliptical contour of the electron density about the bond path. Homopolar conjugated and aromatic systems show adjacent bonds with  $\varepsilon > 0$  and major axes tend to be parallel to each other.<sup>[6,39]</sup>

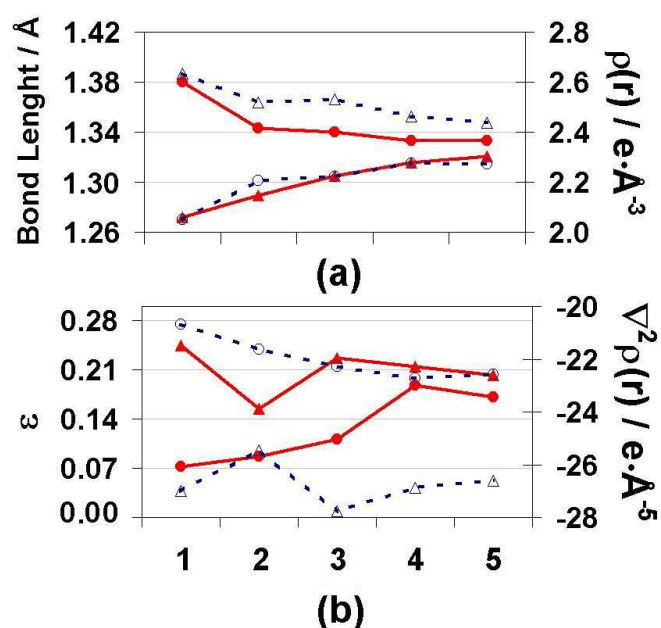


Figure 2: Point topological descriptors for the N–C=N bond pattern in gas-phase optimized molecules **1–5** (Scheme 2). Quantities referring to the C9=N2 bond are marked as triangles, those referring to C9–N1 as circles. (a) bond length (full red lines, left scale) and electron density at the bcp (dotted blue lines, right scale); (b) bond ellipticity (full red lines, left scale) and electron density Laplacian at the bcp (dotted blue lines, right scale).

On the contrary, bond ellipticity has a less straightforward interpretation in heteropolar bonds<sup>[40-42]</sup> as the bcp usually falls in the valence shell charge concentration (VSCC)<sup>[5]</sup> of the less

electronegative atom, expected therefore to rule the direction of the major bond axis.<sup>[41]</sup> The overlap of major axes of neighbouring bonds in the  $-\text{N}-\text{C}=\text{N}$  (**1**) or  $-\text{N}-\text{C}=\text{N}-\text{S}$  (**2-5**) moieties was very close to one ( $>0.9985$  at least) for all **1-5** compounds. Moreover, ellipticities retrieved in all of these bonds are significant in absolute value. On the other hand, the  $p-\pi$  system in the sulphonyl group shows no remarkable overlap ( $<0.3$ ) with the  $\pi$  system in the  $-\text{N}-\text{C}=\text{N}-\text{S}$  moiety. Hence, the two systems are substantially decoupled, as for the resonance effects. Considering figure 2b, the two C–N bonds clearly display quite a different behaviour through the series of compounds **1-5**. In the formally single C9–N1 bond a neat increase of the magnitude of the electron density Laplacian occurs at the bcp (Figure 2b, open blue circles), while for the double C9=N2 bond (open blue triangles)  $\nabla^2\rho_{\text{bcp}}$  tends to oscillate; eventually, the title compound (**4**) and TAYCUR (**5**) have quite similar  $\nabla^2\rho_{\text{bcp}}$  values with respect to the reference methanimidamide **1**. Such trends are reflected in bond ellipticities, since  $\epsilon_{\text{C9-N1}}$  (full red circles) almost monotonically grows to values very similar to those shown by the double bond C9=N2 in compounds **4** and **5**, while  $\epsilon_{\text{C9=N2}}$  (red full triangles) displays a clear ellipticity minimum connected to the lower Laplacian magnitude in **2** and then grows again stabilizing at a value slightly smaller than that in **1**, namely at  $\approx 0.20-0.22$ . For both  $\epsilon$  and  $\nabla^2\rho_{\text{bcp}}$ , the most abrupt and off-trend variations clearly concern the C9=N2 bond upon insertion of the electron-attractor sulphonyl group at the N2 atom (**1** to **2** transition). On the contrary, once the 4-membered cycle is formed (**2** to **3** transition), the N2–S1 bond weakens, as it lengthens by 0.0361 Å (Table 2), while the  $\nabla^2\rho_{\text{bcp}}$  value for the adjacent C9=N2 bond turns out to be even more negative than in methanimidamide **1**. However, the related  $\rho_{\text{bcp}}(\text{C9=N2})$  grows only by 0.01  $\text{e}\cdot\text{Å}^{-3}$  while  $d_{\text{C9=N2}}$  increases its length even further (Figure 2a). Looking for the possible origin of such apparently inconsistent behaviour we have to consider the mutual interplay of several factors: (i) the electronic factors originated by the insertion of the  $\text{SO}_2$  group; (ii) the ring strain, revealing itself in the general weakening of the bonds of the cycle relative to the analogue linear compounds, and (iii) the sensitivity of the electron density (ED) Laplacian to the position of the bcp along the internuclear vector in polar bonds, as  $\nabla^2\rho(\mathbf{r})$  is a fast varying function of the position of the point considered in those VSCC zones lying close to the core depletion region.

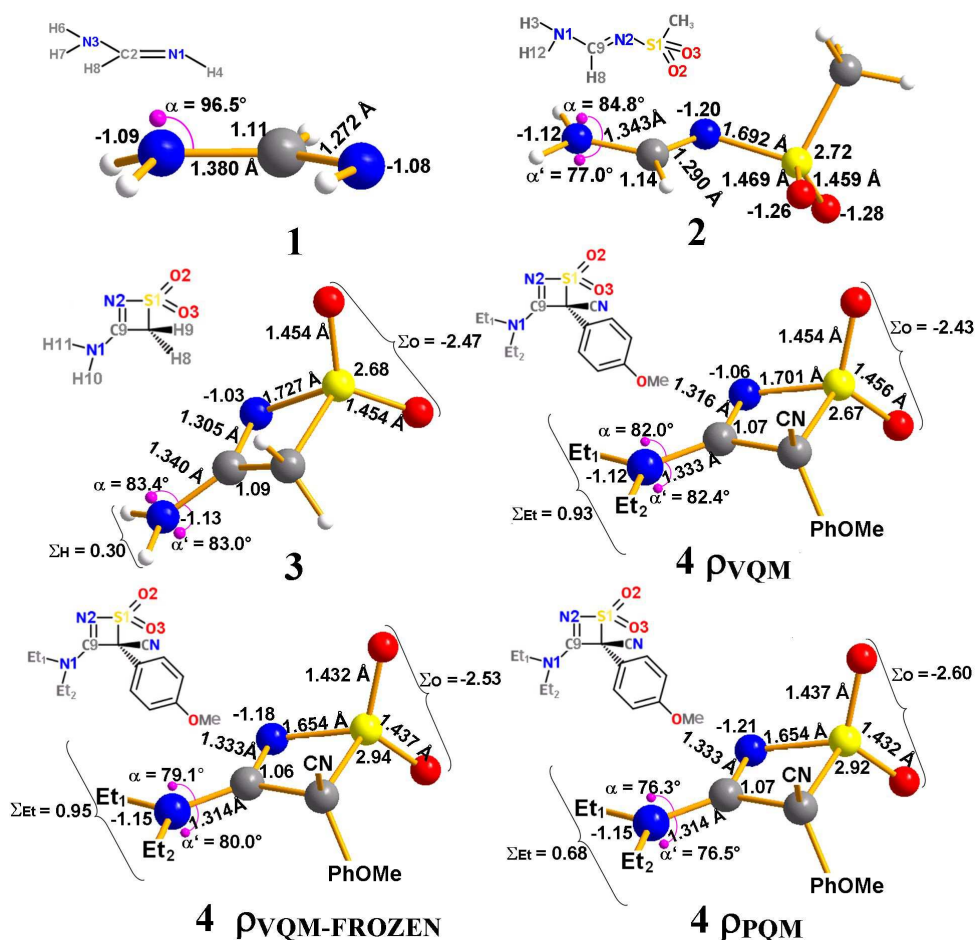


Figure 3: Location of  $-\nabla^2\rho(\mathbf{r})$  non-bonded maxima around N1 (purple dots, see text), together with relevant bond lengths (Å) and QTAIM integrated charges (electrons) for case systems **1-4** (see Scheme 2 and the text for the meaning of the various labels). ‘Et’ stands for ethyl group.

By inspecting resonance forms in Scheme 3 and analysing the VSCC non bonded maxima (nbms), it is possible to see how the abrupt reduction of the C=N ellipticity and Laplacian magnitude from **1** to **2** are triggered by the increased availability of resonance forms like *c-e*, as confirmed and pictorially visible by a corresponding abrupt variation, from  $sp^3$  to  $sp^2$  hybridization of the N involved in the formally single C-N bond. Figure 3 displays the remarkable pyramidalization this N atom acquires in **1**, with a N-H-C-H’ torsion of about 20°, having just one non bonded maximum (nbm) in its VSCC and forming a nbm-N-C angle, hereinafter referred to as  $\alpha$  angle, of about 97°. The corresponding N atom in **2** shows a significant pyramidalization decrease, in reason of the N-H-C-H’ torsion lowered to 3°. Two nbms now appear above and below the N atom, almost perpendicular to the H-N-C plane. Since the two nbms form, respectively, an  $\alpha$  and an  $\alpha'$  angle of 84.8° and 77.0°, they are not equivalent in placement. The enhanced double bond character of C-N and the consequent decrease of such character for C=N is directly suggested by the evident decrease of the  $\alpha$  angle from **1** to **2**. Then, once the 4-membered cycle is formed on passing from **2** to **3**, the

N pyramidalization gets completely lost. The  $\alpha$  and  $\alpha'$  angles turn to be almost equivalent and progressively lower along the series **2-4**, conforming with the C-N bond length monotonic decrease. In details, such angles further decrease to about  $79.5^\circ$  as the DTC molecule is constrained to the crystal geometry and to about  $76.3^\circ$  as in the crystal the DTC molecule is surrounded by other DTC molecules. Note once more how the  $\alpha$  and  $\alpha'$  angle decrease mirrors the C-N bond length diminishing, and its remarkable change upon crystallization and single/double CN bond length inversion.<sup>[43]</sup> As previously stated, the N-S bond weakens from **2** to **3** because of the insertion of the 4-membered ring constraint, but then it systematically strengthens and decreases in length along the cyclic series, from 1.723 Å in **3**, to 1.701 Å in **4** and further down to 1.654 Å in the DTC crystal. Again, a possible interpretation of this evidence may be given in terms of resonance structures *c-e* increasing their impact, which is validated (Figure 3), for the DTC system, by the progressive, large increase in the global negative charge of the oxygen atoms, namely from 2.427e in the geometry optimized molecule up to 2.596e in the crystal. Since charge separation does not necessarily imply bond lengthening for heteropolar bonds, also structures *g-h* may be significant players in this process. Inspection of trends in bond polarization and in delocalization indices and integrated Source Function non-local descriptors of the charge density, provide other interesting hints on the changes occurring in the N1-C9=N2-S1 conjugation pattern. They are all reported in appendix A1.

## 1.5 Crystal field effects

### *1.5.1 Crystal packing*

Concerning solid DTC, we can not recognize noteworthy directional atom-atom intermolecular extended patterns because of the lacking of strong hydrogen bond (HB) donors in this system. Actually, close contacts involving the backbone thiazete atoms are discouraged due to the presence of cumbersome substituents. The most significant HB contact at T = 100 K is C5-H5...N2 ( $d_{\text{H}\cdots\text{N}} = 2.54$  Å,  $\alpha_{\text{C5-H5-N2}} \approx 164$  deg), which involves a phenyl CH group and the N2 nitrogen in the thiazete cycle. In general, phenyl C-H donors always trigger the most favourable interactions in terms of geometrical descriptors in this system. Interestingly, an acceptor for weak CH... $\pi$  interaction is also the localized  $\pi$ -system of the cyano group, whereas the methoxy oxygen O1 accepts a couple of very weak HB's from the dangling ethyl groups of a translationally-related

molecule. In contrast, atom N1 is excluded from any intermolecular HB, while, as expected, the sulphonyl oxygen atoms O2 and O3 can also act as weaker CH...O HB acceptors.

### 1.5.2 Thiazete geometry.

In the N=C=N system, the uncommon bond length alternation pattern manifests clearly within the DTC and TAYCUR crystal structures (Table 5), where the previously defined bond length difference parameter (BDP) is always negative. Considering individual structures, however, the low-*T* DTC structure is the only one where the sign of BDP is statistically significant, with BDP =  $-0.0181(7)$  Å, whereas it is poorly relevant, in terms of the corresponding estimated standard deviations (esd's), at room temperature ( $-0.009(4)$  Å). Generally, the comparison among the geometrical parameters reported in Tables 2 and 3 implies that remarkable structural changes on the bond lengths and angles within the thiazete cycle are due to crystal field. On the contrary, upon crystallization no important variations in the torsion angles occur. The main conformational adjustments involve the exocyclic substituents, especially the methoxy group orientation. The thiazete cycle is not rigidly distorted, as the minor and the major diagonals, C9...S1 and C8...N2, undergo a significant but asymmetric reduction in length [C9...S1: from 2.2402 to 2.1942(6) Å; C8...N2: from 2.3219 Å to 2.3021(9) Å] when comparing solid state and the optimized *in vacuo* outcomes. As a result,  $d_{S1-N2}$  is decreased by 0.0474 Å (MP2: 0.0473 Å), while, as previously stated,  $d_{S1-C8}$  shortens even by 0.0727 Å upon crystallization. (Tables 2, 5). On the contrary, the C9-C8 and the C9=N2 bonds, slightly lengthen by  $\approx 0.01$  Å. In the crystal, the sign inversion of the BDP parameter is due to the simultaneous C9=N2 bond length increase ( $\approx 0.016$  Å) and the larger C9-N1 bond length decrease ( $\approx 0.019$  Å).

Bonds	DTC, 100(2) K <sup>1</sup>	DTC, RT <sup>2</sup>	DTC, RT <sup>3</sup>	TAYCUR, RT <sup>4</sup>	
S1–N2	1.6539(4)	1.6494(18)	1.6421(19)	1.6514(49)	1.6478(69)
N2=C9	1.3325(5)	1.3266(25)	1.3308(27)	1.3293(80)	1.3286(85)
C9–N1	1.3144(5)	1.3175(25)	1.3074(24)	1.3084(85)	1.3087(109)
C9–C8	1.5343(5)	1.5213(24)	1.5317(29)	1.5332(75)	1.5344(109)
S1–C8	1.8959(6)	1.8930(19)	1.8777(20)	1.8788(65)	1.8649(57)
Angles					
S1–N2–C9	93.92(3)	94.3(1)	93.8(1)	94.0(4)	93.9(5)
N2–C9–N1	126.52(3)	126.6(2)	127.0(2)	126.6(5)	126.3(6)
N2–C9–C8	106.68(3)	106.5(2)	106.1(2)	106.1(4)	105.7(5)
N2–S1–C8	80.58(2)	80.36(8)	80.93(9)	80.7(2)	80.9(3)
Torsions					
S1–N2–C9–C8	–2.55(4)	–2.5(2)	–5.6(2)	1.2(4)	1.8(5)
S1–N2–C9–N1	177.27(4)	177.0(2)	177.0(2)	–176.9(5)	–176.7(7)

Table 3: Experimental estimates for relevant bond length and angles ( $\text{\AA}$ , deg) describing the thiazete ring in DTC and related compounds. See Figure 1 and Scheme 2 for the atom numbering. Esd's in parentheses.

It is worth stressing that the changes examined before remarkably decrease when electron correlation effects are studied at the MP2 theory level. For instance, at the MP2 level, the *in vacuo* estimate for BDP in **4**, yet still positive, lowers from +0.017  $\text{\AA}$  to +0.006  $\text{\AA}$ , while the large reduction of the S1–C8 distance upon change of phase decreases from 0.073 to just 0.020  $\text{\AA}$ . However, it shall be noted that both DFT and MP results predicted the same geometrical trends, providing a further validation that the detected crystal field effects are not fake products of model shortcomings.

### 1.5.3 Charge redistribution along the conjugated system

The  $\nabla^2\rho(\mathbf{r})$  and  $\epsilon(\mathbf{r})$  profiles along the N2–S1, C9=N2 and C9–N1 bond paths for *in vacuo* and solid-state DTC are compared, respectively in Figures 4 and 5. Regarding the isolated molecule (compound **4**), we reported results coming from both  $\rho_{\text{VQM}}$  and  $\rho_{\text{VQM-FROZEN}}$  (ED for *in vacuo* QM optimization and for *in vacuo* QM simulation at frozen geometry, respectively), whereas the condensed-phase curves refer to the experimental ED distribution,  $\rho_{\text{EXP}}$ , for the molecule extracted from the crystal, the multipole-projected theoretical periodic ED distribution,  $\rho_{\text{MM-PQM}}$ , and the corresponding primary density  $\rho_{\text{PQM}}$  (ED from the solid state QM periodic wave function). The

<sup>1</sup> Polymorph A, this work. The reported parameters derive from the final multipole model against experimental structure factors.

<sup>2</sup> Polymorph A, see ref. 19a. IAM model (shelx).

<sup>3</sup> Polymorph B, see ref. 19b. IAM model (shelx).

<sup>4</sup> The asymmetric unit of TAYCUR contains 2 independent molecules (molecule A on the left, molecule B on the right). See ref. 20. IAM model (shelx).



$\nabla^2\rho(\mathbf{r})$  and  $\epsilon(\mathbf{r})$  profiles of the primary periodic density are compared with those from  $\rho_{\text{VQM}}$  and  $\rho_{\text{VQM-FROZEN}}$  densities in Figure 4. , Figure 5 compares the experimental profiles and those obtained from the periodic calculation before and after the multipolar projection on the theoretical structure factors. Therefore, Figure 4 is useful to disentangle matrix effects from pure geometric effects caused by crystallization, while Figure 5 allows to evaluate the overall agreement between experiment and theory, and in particular the effect of the multipolar model bias. <sup>[14b]</sup> As expected, the  $\rho(\mathbf{r})$  bcp invariably falls in the VSCC region of the less electronegative atom, i.e. S1 or C9 (plots on the right of Figures 4 and 5). Moreover, remarkable changes in terms of charge density distribution occur through the *in vacuo*–solid transition (Figure 4), which may be mostly due to the change of geometry.

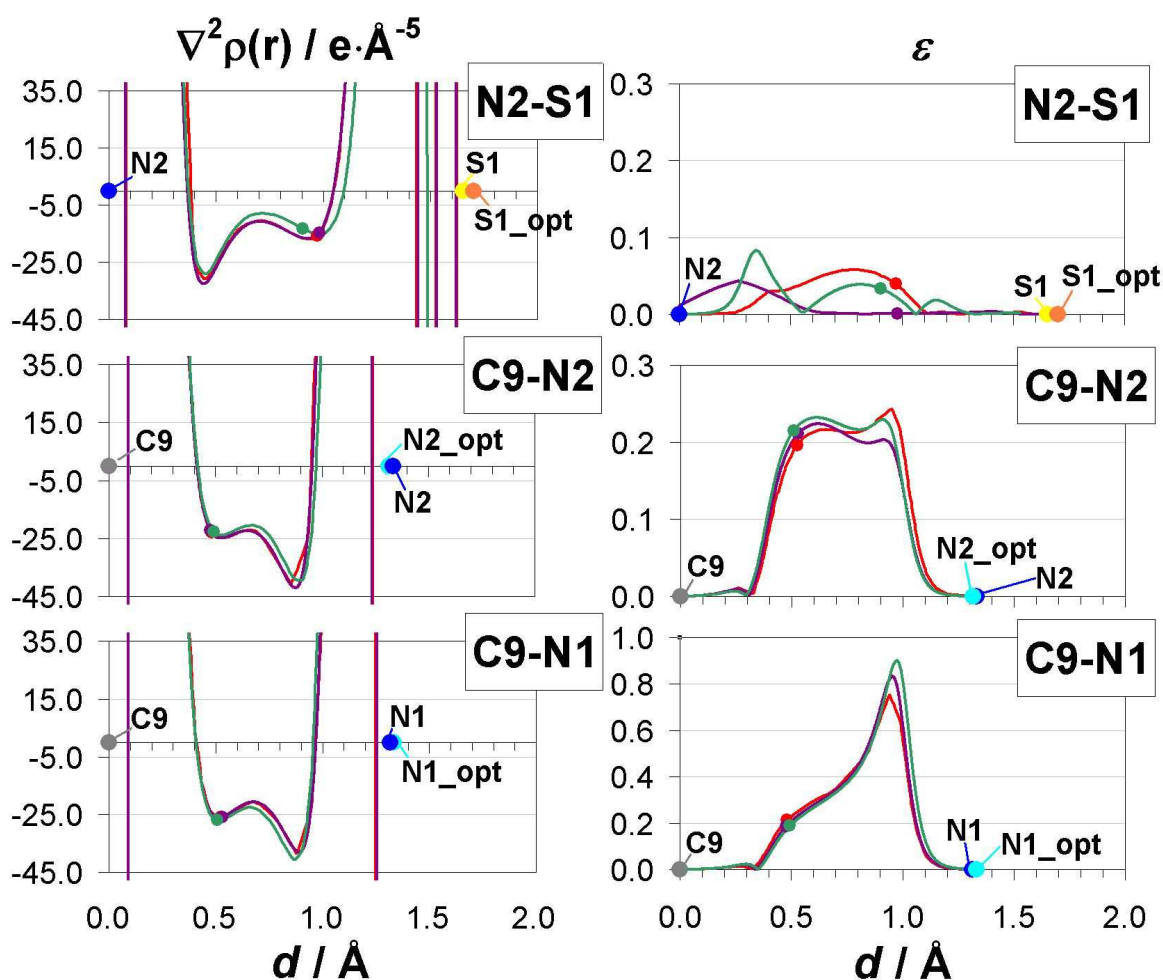


Figure 4: Electron density Laplacian (left) and ellipticity (right) profiles along the N2–S1, C9–N2 and C9–N1 bond vectors in DTC, comparing theoretical *in vacuo* and solid-state electron density models.  $d$  is the distance from the atom on the left and the indicated atomic locations. The position of the  $\rho(\mathbf{r})$  bcp is marked by a coloured dot. Different colours refer to the electron density model employed to compute the  $\nabla^2\rho(\mathbf{r})$  and  $\epsilon(\mathbf{r})$  profiles: (i) green:  $\rho_{\text{VQM}}$ ; (ii) purple:  $\rho_{\text{VQM-FROZEN}}$ ; (iii) red:  $\rho_{\text{PQM}}$ .

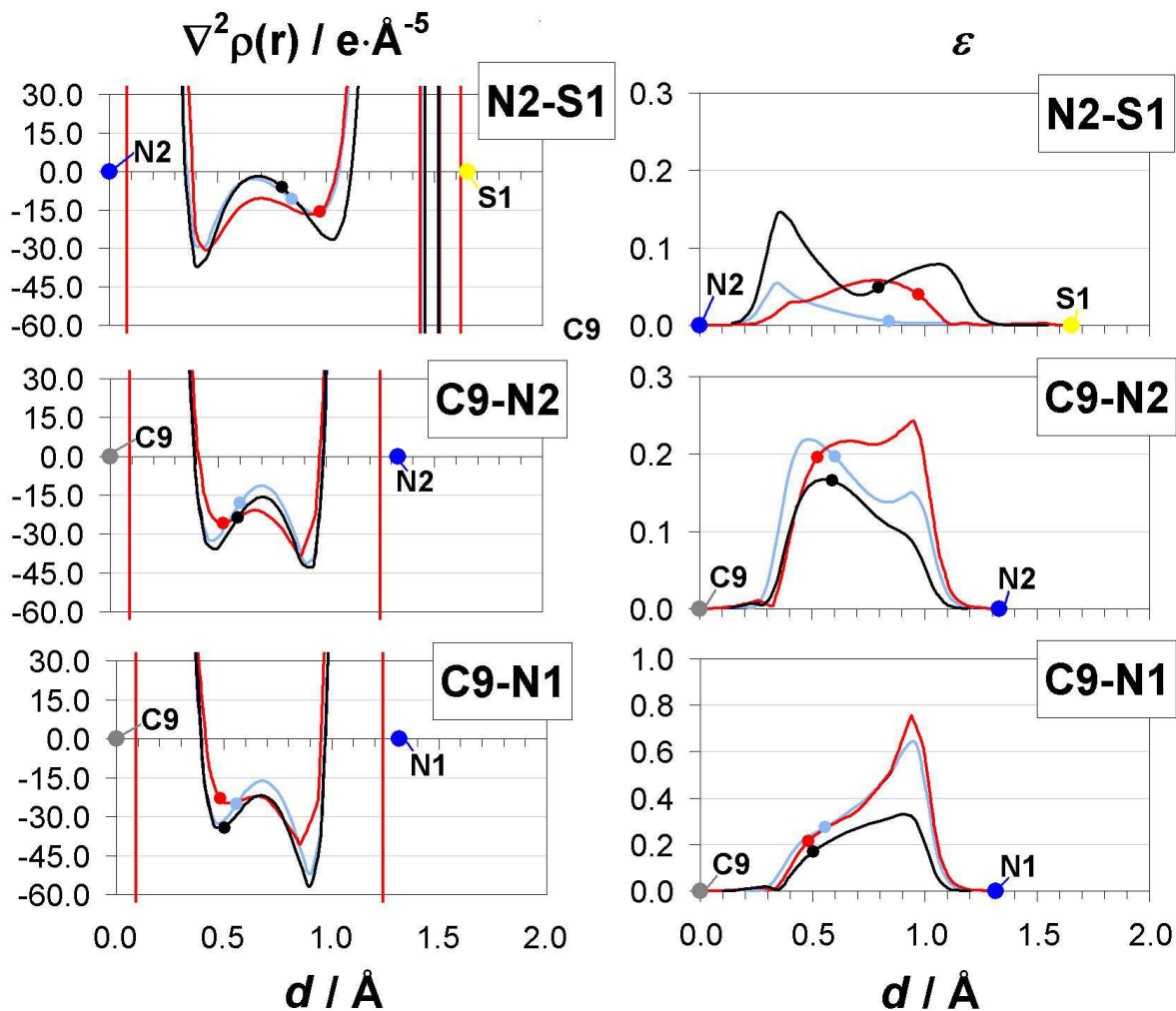


Figure 5: Same as Figure 4, but comparing charge density models of DTC in the solid state. The colour-code is here defined as follows: (i) black:  $\rho_{\text{EXP}}$ ; (ii) light blue:  $\rho_{\text{MM-PQM}}$ ; (iii) red:  $\rho_{\text{PQM}}$ .

In detail:

- (i) opposite variations with phase changes occur in the C9-N1 and C9=N2 bonds, the former slightly growing and the latter slightly reducing their shared character, as underlined by the respectively larger and smaller uniformity of their Laplacian distributions in the bonding regions;
- (ii) the ellipticity of the C9-N1 bond is in the crystal somewhat less peaked near N1, since the nitrogen  $p$ -lone pair is more involved in the bond, as already shown by the decrease of  $\alpha$  and  $\alpha'$  angles (Figure 3). For N2 just the opposite is true;
- (iii) the N2-S1 bond has a less straightforward behaviour, as it is not simply triggered by the geometry change: in the crystal the ellipticity is larger and more uniform along the bonding region, while the bcp is remarkably further displaced towards the S atom. The roots of the changes described above for C-N and S-N bonds are clearly detectable. The reverse behaviour of C9-N1 and C9=N2 bonds conforms with the shortening of the former and lengthening of the latter and with the

large growth of the N2 negative charge, from  $-1.06 e$  in the *in vacuo* optimized geometry to  $-1.21 e$  in the crystal (increased weight of resonance forms *b-d*). The S atom largely increases its electronic charge as well, namely from  $+2.67 e$  up to  $+2.92 e$  upon shortening of the S-N bond; the S-N bcp further shifts itself towards the electropositive S atom because of the bond largely enhanced polarity. The larger ellipticity for the S-N bond in the crystal suggests that the resonance forms *c-d* become more and more relevant, as they conform with an increase of the negative charge on the oxygen atoms, along with the (*e-h*) implying a larger positive charge on S. Actually, the oxygen atoms global negative charge notably increases in magnitude, in details from  $2.43 e$  (in the *in vacuo* optimized geometry) to  $2.60 e$  (in the crystal).

Two main conclusions may be drawn looking at the ED Laplacian profiles displayed in Figure 5. First, there is a remarkable agreement between theory and experiment concerning the description of the bonding features in the conjugated C–N=C–S system, provided that structure factors are both projected on the multipole model. Second, a significant bias is introduced by this model, since the shape of profiles from  $\rho_{MM-PQM}$  are definitely more alike to those from  $\rho_{EXP}$  than to those resulting from the primary density  $\rho_{PQM}$ . Specifically, the trend retrieved in the multipole model is a decrease of the shared character of the bonds, leading to deeper ED Laplacian minima and higher ED Laplacian maxima in the bonding region.

#### 1.5.4 Integrated source function

The experimental Source Function percentage contributions (SF%) of the various atomic basins  $\Omega$  in solid DTC for the N1–C9, C9=N2 and N2–S1 bcp's are graphically represented in Figure 6, while table 6 reports theoretical SF% data for *in vacuo* and in-crystal DTC. As we can observe in Figure 6, generally the thiazete substituents have a minor influence (individual SF% being  $< 5\%$ ) on the conjugated system features, except for the contributions of the two ethyl groups to the C9–N1 bcp, which are slightly higher than 5 % because of their proximity to this bond and their well-known inductive (+I) effect<sup>[16]</sup>. A further confirmation of the increasing equalization of N1–C9 and N2=C9 bonds upon crystallization for  $\rho_{VQM}$  and  $\rho_{PQM}$  model densities can be deduced from the integrated SF results on the  $\rho_{VQM}$  and  $\rho_{PQM}$  densities (Table 6), as the SF%<sub>C9+N2</sub> value becomes slightly closer to SF%<sub>C9+N1</sub>.<sup>[44]</sup>

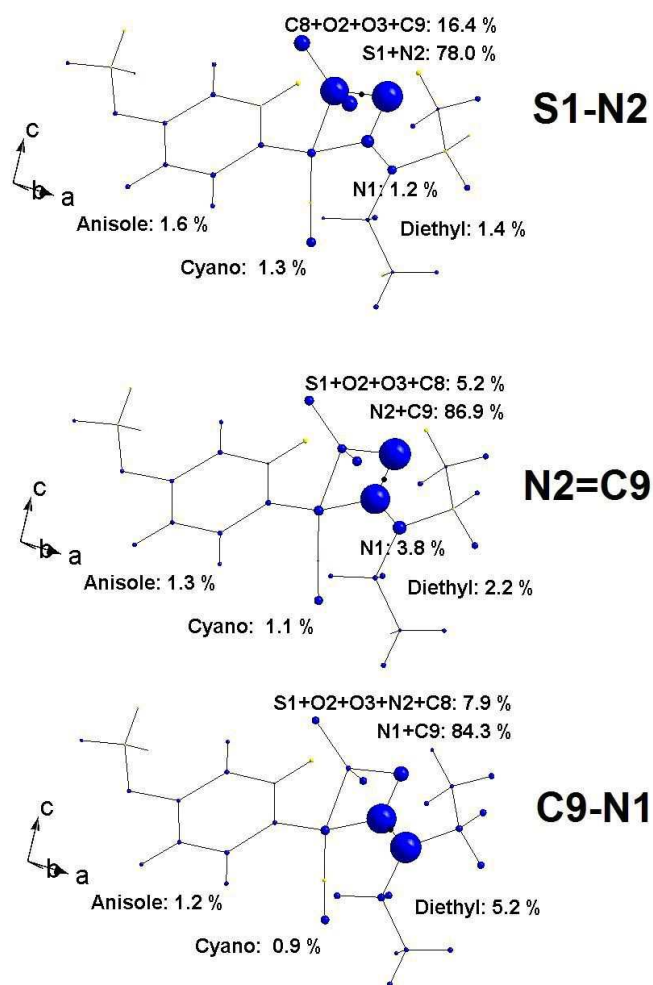


Figure 6: Source Function percentage contributions (SF%) to the charge density values at the S1–N2, C9=N2 and C9–N1 bcp's in DTC, as computed from the in–crystal experimentally derived multipole model  $\rho_{\text{EXP}}$ . The position of each bcp is denoted by a black dot. Each atom  $\Omega$  is displayed as a sphere whose volume is proportional to the SF% contribution from  $\Omega$  to the electron density at the indicated bcp. The colour of the sphere is blue if the SF% contribution is positive and yellow if negative.

	Percentage Source Function values, SF%( $\Omega$ ,bcp)								
	C9-N1			C9-N2			S1-N2		
	N1	C9	N2	N2	C9	N1	N2	S1	N1
$\rho_{\text{VQM}}$	44.2	38.8	6.3	46.7	39.7	4.2	35.9	40.8	1.2
$\rho_{\text{VQM-FRO}}$	44.7	38.9	5.8	46.4	39.3	4.4	35.6	39.9	1.2
$\rho_{\text{PQM}}$	44.5	39.1	5.6	46.1	39.3	4.5	35.8	39.2	1.2
$\rho_{\text{MM-PQM}}$	44.8	39.7	4.5	47.2	39.3	3.6	42.1	34.6	1.2
$\rho_{\text{EXP}}$	45.0	39.3	5.0	47.8	39.1	3.8	43.7	34.3	1.3

Table 4: Values of integrated Source Function for the DTC molecule from various models. See Figure 1 and Scheme 2 in the main text for the atom numbering.

The decrease of the N2 SF contribution at the C1-N9 bcp ED agrees with the negative charge enhancement at N2, while for N1 the opposite occurs: upon crystallization, its contribution slightly raises at C2=N9 bcp, complying with its improved ability to release its p- $\pi$  electrons (see  $\alpha$ ,  $\alpha'$  angles in Figure 3). Despite bond length values become more similar, the combination of the two effects mentioned above, which may be described through enhanced contributions from resonance structures *b-e*, does not increase electron delocalization in the N-C=N moiety. Upon crystallization, the SF% contributions from S1+N2 atoms to their bcp density reduce (-1.7) rather than augment, despite the S1-N2 becomes shorter. Basically, only the SF% from S1 diminishes (-1.6), implying a stronger impact from those resonance structures featuring a positive S atom and an increased positive charge on it and on O atoms (see Figure 3). Experimentally derived SF data are only qualitatively close to those resulting from the crystal periodic wavefunction and actually closer to those derived by projecting the theoretical structure factors onto the multipolar model.

### 1.5.5 Dipole moment enhancement.

In the previous pages we discussed atomic charges  $q(\Omega)$ , defined according to QTAIM and displayed in Figure 3. From them, we may provide a quantitative measure of the actual larger polarization, as a whole, of the DTC molecule in the crystal, by evaluating the molecular dipole moment  $\boldsymbol{\mu}$ . This quantity is strongly model-dependent<sup>[32 f,i,j,k,l]</sup> and it is notoriously quite difficult to be accurately determined. By using QTAIM, molecular boundaries are naturally defined also in the crystal, through the zero-flux surfaces of the composing atoms.<sup>[9,15b]</sup> Hence, it is possible to gain an accurate evaluation of  $\boldsymbol{\mu}$  in the condensed phase, using a method equally applicable to the *in vacuo* estimate.<sup>[9,15a,15b]</sup> Comparing this latter value with the (formally equivalent) value one obtains from the usual procedure implemented in the quantum chemical codes, like Gaussian-09, provides a check on the numerical accuracy of the QTAIM estimate.<sup>[15b]</sup> Discrepancies between the modules of the two values, due to numerical errors in the QTAIM basin integration, were found to be lower than 0.1% for all systems **1-4**. The total molecular dipole  $\boldsymbol{\mu}$  has then been partitioned into a first moment contribution,  $\boldsymbol{\mu}_A$ , representing the atomic polarization term due to the atomic first moments plus a charge transfer (CT) component  $\boldsymbol{\mu}_{CT}$  developing from the net atomic charges (see section 1 and Ref [45]). Since both composing terms are not origin-dependent for a neutral system, they thus maintain a physical meaning by themselves.<sup>[15]</sup> Total dipole moment module  $|\boldsymbol{\mu}|$  values are listed in Table 7, together with their components  $|\boldsymbol{\mu}_A|$  and  $|\boldsymbol{\mu}_{CT}|$ , for DTC *in vacuo* (optimized geometry and crystal frozen geometry), in-crystal, and from experiment. The two vectors are almost

collinear, but as expected, oppositely directed,<sup>a</sup> as denoted by the angle  $\gamma$  between  $\underline{\mu}_A$  and  $\underline{\mu}_{CT}$ , reported in Table 5 as well. Values for systems **1-3** are also reported, in order to provide exhaustive data.<sup>[46]</sup>

System, density	$ \underline{\mu} $	$ \underline{\mu}_A $	$ \underline{\mu}_{CT} $	$\gamma$
<b>1</b> , $\rho_{VQM}$	3.5	1.8	4.2	122.1
<b>2</b> , $\rho_{VQM}$	6.1	3.3	8.6	146.2
<b>3</b> , $\rho_{VQM}$	8.1	4.1	12.1	166.5
<b>4</b> , $\rho_{VQM}$	9.6	5.8	15.2	167.4
<b>4</b> , $\rho_{VQM-FROZEN}$	9.7	5.1	14.7	167.7
<b>4</b> , $\rho_{PQM}$	13.0	5.0	17.8	163.1
<b>4</b> , $\rho_{EXP}$	15.4 (1.5)	5.7	20.3	153.6

Table 5: Values (Debye) of the molecular total dipole moment module,  $|\underline{\mu}|$ , and of its charge transfer,  $|\underline{\mu}_{CT}|$ , and atomic polarization,  $|\underline{\mu}_A|$ , components for the molecules 1-4, from various theoretical models and experiment. The angle  $\gamma$  between  $\underline{\mu}_A$  and  $\underline{\mu}_{CT}$  is also reported.

A remarkable result is surely the agreement - within almost one experimental esd - between the theoretical evaluation for the DTC molecular dipole module in the bulk and the analogue multipole-derived evaluation from X-ray diffraction data. However, the neat enhancement of the DTC molecular dipole module, on passing from the *in vacuo* optimized geometry to the crystal (from 9.6 to 13.0 D, see Table 5), is to be considered the most important result. The observed 35% enhancement nicely parallels that found, theoretically, for the urea crystal<sup>[15b]</sup> (+37%). As the only geometrical change due to crystallization bears a negligible increase (from 9.6 to 9.7 Debye), such large enhancement is to be ascribed to the matrix effect of the crystal, resulting from the interplay between two cooperating effects. First, an augmentation of the CT component (from 15.2 to 17.8 Debye), due to the discussed general increase of the atomic charges magnitudes in the thiazete ring and in the sulphonyl groups. Then, the packing constraints caused by crystallization lead to a reduction in the magnitude of the atomic polarization (from 5.8 down to 5.0 Debye), as already retrieved in other systems.<sup>[15a,15c,48]</sup> Since the  $\underline{\mu}_A$  and  $\underline{\mu}_{CT}$  vectors in DTC (**4**) are almost antiparallel ( $\gamma > 160^\circ$ ), the two effects concur in enhancing the molecular dipole moment upon crystallization. The enhancement is, however, mostly (76%) provided by the CT component, and so by the increased charge separation of bonded atoms in the bulk, implying that crystallization of DTC is driven by electrostatics. The resonance forms of the DTC molecule leading to an increase of charge separation, hence to an increase of the electrostatic energy gain produced by molecules interacting among each other, turn out to be largely energy-stabilized upon crystallization. Moreover, the increase of their influence, induce large geometrical distortions to occur, so that the single N-C bond turns out to be shorter than the formally double N=C bond in the crystal.

<sup>a</sup> Atoms usually polarize in a direction counter to the electric field created by charge transfer (see Ref. 45 and Ref 15a).

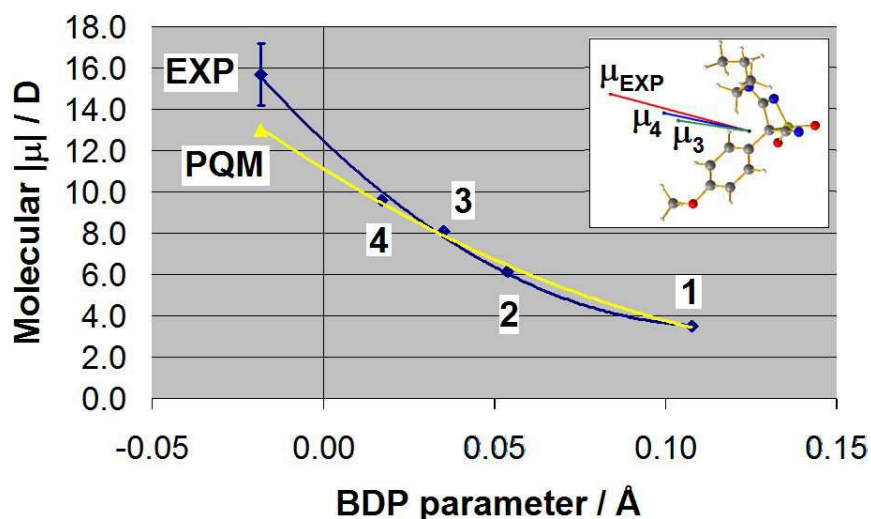


Figure 7: Molecular dipole vector modulus *vs.* the bond difference parameter,  $BDP = d_{C9-N1} - d_{C9=N2}$ , through the compound series **1–4** in Scheme 2, plus the values computed from the  $\rho_{exp}$  (blue rhombus) and  $\rho_{PQM}$  (yellow triangle) models. Units are Debye and Å and the reported entries come from the QTAIM partitioning of the corresponding charge density distributions. The esd for the  $\rho_{exp}$  dipole moment is also shown. The two linear least-squares fittings displayed in the Figure differ in the last point: the blue curve includes the  $\rho_{exp}$  model and has equation  $|\mu| = 6.8(9) \cdot (10 \cdot BDP)^2 - 1.57(9) \cdot 10^2 \cdot BDP + 12.5(2)$ , with correlation coefficient  $R^2 = 0.997$ , while the yellow curve includes the  $\rho_{PQM}$  model and has equation  $|\mu| = 2.8(7) \cdot (10 \cdot BDP)^2 - 1.02(9) \cdot 10^2 \cdot BDP + 11.1(2)$  with  $R^2 = 0.997$ . Inset: mutual orientation and moduli of molecular dipole moments of gas-phase optimized compounds **3** and **4**, plus the solid-state  $\rho_{exp}$ .

Despite the change of geometry (see above) seems to be the only factor influencing most of the bonding properties in the DTC crystal, the molecular dipole moment module enhancement clearly shows a different behaviour. In fact, shortening of N1-C9 and lengthening of N2=C9 bonds only occur when an enhancement of the molecular dipole moment module can stabilize the DTC molecule. In other words, bond length inversion turn out to be manifest in a *real* system only in the bulk, where such a change is exploited because it becomes, there, energetically convenient.

Table 5 and Figure 7 show that in the series of compounds **1–4** a systematic increase of the total molecular dipole moment module occurs, and a fairly well inverse quadratic correlation is evident between its module and the bond difference parameter  $BDP = d_{C9-N1} - d_{C9=N2}$  (Figure 7). Note also that the total dipole moment has always a very similar orientation with respect to the thiazete ring (Figure 7, inset). Therefore, the increment of the  $\mu$  vector modulus is likely the main cause of all the  $\rho(\mathbf{r})$  rearrangements previously commented, or *viceversa*, those  $\rho(\mathbf{r})$  rearrangements dictate the observed dipole moment enhancement.

## 1.6 Conclusions

This chapter is focused on 3-diethylamino-4-(4-methoxyphenyl)-1,1-dioxo-4*H*-1 $\lambda$ <sup>6</sup>,2-thiazete-4-carbonitrile (DTC), a synthetic compound whose core chemical moiety is an uncommon 4-membered thiazete-1,1-dioxide heterocycle showing significant similarity with  $\beta$ -sultamic drugs. Crystallographic investigations carried out at room temperature on DTC polymorphs revealed that in the conjugated  $\text{-N-C=N-SO}_2\text{-}$  system the formally single N-C bond is, on average, 0.018 Å shorter than the formally double N=C bond. To clarify the subtle interplay between structure, electron delocalization and crystal field polarization effects, we investigated the charge density distribution of DTC either by single-crystal X-ray diffraction at  $T = 100(2)$  K and quantum mechanical simulations. We employed to this purpose both local and non-local topological descriptors provided by the Quantum Theory of Atoms in Molecules, relating topological and structural changes of crystalline and *in vacuo* DTC to the smaller or larger importance of resonance forms in the  $\text{-N-C=N-SO}_2\text{-}$  moiety. As a result, we provided a rationale for the aforementioned C-N/C=N bond length inversion: the large DTC dipole moment enhancement occurring in the crystal stabilizes highly polar resonant forms so as to exploit more convenient electrostatic interactions with neighbouring molecules. As a consequence, a significant electronic rearrangement occurs within the molecule, resulting in an unusual and counterintuitive bond length alternation pattern. Such findings also lead to further possible implications we discussed in this chapter, aiming at an accurate *in silico* modelling of crystal structures. From the results obtained it is possible to draw the following conclusions:

(i) the C-N/C=N bond length inversion in the solid state of DTC with respect the DTC structure *in vacuo*, is due to a significant ( $\approx +35\%$ ) in-crystal DTC dipole moment enhancement that has its roots in a concomitant growth of the charge transfer, along with a decrease in the magnitude of the atomic polarization term. In particular such dipole enhancement derives at most (76%) from the charge transfer component, hence from the augmented charge separation of bonded atoms in the bulk. As a consequence, upon crystallization the highly polar resonant forms in Scheme 3 (*c-e* and *g-h*) are stabilized and the increase of their weight significantly influences the molecular geometry. The electrostatic contribution to the total cohesive energy of DTC represents the ultimate leading force of this process. As this system lacks strong directional hydrogen bond networks, higher first and second electrostatic moment magnitudes need to be explored to achieve more favourable electrostatic interactions with neighbouring molecules. .

(ii) The bias introduced by the multipolar model may lead to wrong conclusions when subtle changes are discussed, and ones where delocalization effects are mainly intertwined with the



polarization effects caused by the crystal matrix. In these cases, correct conclusions can be safely achieved only if the changes are assessed through comparable approaches, like the examination of theoretical and experimental structural EDs, both filtered through the same multipolar model expansion .<sup>[48]</sup>

(iii) As it is well known, the interplay between the molecular and the crystal structure determines essential bulk features in a material, among which second-harmonic generation, pyroelectricity and piezoelectricity. Despite none of these properties can be exploited by DTC itself because of its centrosymmetric space group, it emerges as an interesting test case to shed light on how crystallization may produce changes in the molecular structure, that in turn define the crystal field itself. Since these changes are essentially quantum-mechanical in nature, the suitability of methods intrinsically neglecting quantum effects in accurately displaying the crystalline matrix effects and/or predicting crystal structures are questioned. This is the case, for instance, of those based on force fields methods.

The joint theoretical and experimental approach employed in this study overcomes such limitations, as it detects and rationalizes also subtle and counterintuitive effects. However, we cannot ignore its lack of predictability. Aiming at a further improvement of the computational recipes for *in silico* modelling of crystalline materials in terms of accuracy and reliability, we sense that the knowledge of *accurate* single-crystal X-ray structures and experimentally-derived charge densities will be more and more relevant in the next future, providing precious hints as well as paradigmatic cases to be interpreted.

## **REFERENCES:**

- [1] Poater, J.; Duran, M.; Solà, M.; Silvi, B. *Chem. Rev.* **2005**, *105*, 3911–3947.
- [2] Merino, G.; Vela, A.; Heine, T. *Chem. Rev.* **2005**, *105*, 3812–3841.
- [3] Nalwa, H. S. ; Miyata, S. *Nonlinear Optics of Organic Molecules and Polymers*, CRC press Inc, Boca Raton (FL), **1997**.
- [4] Beverina, L.; Sanguineti, A.; Battagliarin, G.; Ruffo, R.; Roberto, D.; Righetto, S.; Soave, R.; Lo Presti, L.; Ugo, R.; Pagani, G. A. *Chem. Commun.* **2011**, *47*, 292-294.
- [5] (a) Bader, R. F. W. *Atoms in molecules. A quantum theory*; Oxford University Press, Oxford (UK), **1990**; (b) *Modern Charge Density Analysis*, Editors: Gatti, C. & Macchi, P. **2012**, Springer, Dordrecht (D)
- [6] Bader, R. F. W.; Slee, S.; Cremer, D.; Kraka, E. *J. Am. Chem. Soc.* **1983**, *105*, 5061–5068.
- [7] Cremer, D.; Kraka, E.; Slee, S.; Bader, R. F. W.; Lau, C. D. H.; Nguyen-Dang, T. T.; MacDougall, P. J. *J. Am. Chem. Soc.* **1983**, *105*, 5069–5075.
- [8] Matta, C. F. ; Boyd, R. J. *The Quantum Theory of Atoms in Molecules. From Solid State to DNA and Drug Design*; Wiley-VCH, Weinheim, (D) **2007**.
- [9] Gatti, C. *Z. Kristallogr.* **2005**, *220*, 399–457.
- [10] Destro, R.; Lo Presti, L. ; Soave, R.; Goeta, A. E. *Multi-Temperature Electron Density Studies*, in *Modern Charge Density Analysis*, Editors: Gatti, C. & Macchi, P. **2012**, Springer, Dordrecht (D)
- [11] (a) Fulton, R. L. ; Mixon, S. T. *J. Phys. Chem.* **1993**, *97*, 7530–7534; (b) Fulton, R. L. *J. Phys. Chem.* **1993**, *97*, 7516–7529; (c) Matito, E. ; Solà, M. ; Salvador, P. ; Duran, M. *Faraday Discuss.* **2007**, *135*, 325–345
- [12] (a) Bader, R. F. W. ; Stephens, M. E. *J. Am. Chem. Soc.* **1975**, *97*, 7391–7399; (b) Fradera, X. ; Austen, M. A. ; Bader, R. F. W. *J. Phys. Chem. A* **1999**, *103*, 304–314
- [13] (a) Bader, R. F. W.; Gatti, C. *Chem. Phys. Lett.* **1998**, *287*, 233–238; (b) Gatti, C. ; Cargnoni, F. ; Bertini, L. *J. Comput. Chem.* **2003**, *24*, 422–436; (c) Gatti, C. *Struct. Bond.* **2012**, *147*, 193–286.
- [14] (a) Monza, E. ; Gatti, C. ; Lo Presti, L. ; Ortoleva, E. *J. Phys. Chem. A* **2011**, *115*, 12864–12878; (b) Lo Presti, L.; Gatti, C. *Chem. Phys. Lett.* **2009**, *476*, 308–316. (c) Lo Presti, L., Ellern, A, Destro, R., Soave, R., Lunelli, B. *J. Phys. Chem. A* **2011**, *115*, 12695–12707; (d) Saleh, G.; Soave, R.; Lo Presti, L., Destro, R. *Chem. Eur. J.* **2013**, *19*, 3490–3503.
- [15] (a) Gatti, C; Saunders, V. R.; Roetti, C *J Chem Phys* **1994**, *101* 10686-10696; (b) May, E.; Destro, R.; Gatti, C. *J Am Chem Soc* **2001**, *123*, 12248-12254; (c) Gatti, C. *Phys. Scripta* **2013**, *87*, 048102 (38pp); (d) Jarzemska, K. N.; Kamiński, R. ; Wenger, E. ; Lecomte, C. ; Dominiak, P. M. *J. Phys. Chem. C*, **2013**, *117*, 7764–7775.

- [16] (a) Spackman, M. A. *Chem Rev* **1992**, 92 1769-1797; (b) Spackman, M. A.; Byrom, P.G.; Alfredsson, M.; Hermansson, K. *Acta Crystallogr.* 1999, A55, 30-47; (c) Gatti, C.; Silvi, B.; Colonna, F. *Chem Phys Lett* **1995**, 247, 135-142; (d) Volkov, A.; Gatti, C.; Abramov, Y.; Coppens, P. *Acta Crystallogr.* **2000**, A56, 252-258
- [17] Page, M. *Acc. Chem. Res.* **2004**, 37, 297-303.
- [18] Allen, H. *Acta Crystallogr.*, **2002**, B58, 380-388.
- [19] (a) Clerici, F. ; Gelmi, M. L. ; Soave, R. ; Lo Presti, L. *Tetrahedron* **2002**, 58, 5173-5178; (b) Orlando, A. M. ; Lo Presti, L. ; Soave, R. *Acta Cryst.* **2010**, E66, o2032-o2033
- [20] Clerici, F. ; Galletti, F. ; Pocar, D. ; Roversi, P. *Tetrahedron* **1996**, 52, 7183-7200.
- [21] Sheldrick, G. M. *Acta Cryst.* **2008** A64, 112-122.
- [22] (a) Kirschke, K.; Hubner, P.; Lutzem, G.; Grundemann, E; Ramm, M. *Liebigs Ann.* **1994**, 159-165; (b) Marihart, E.A.; Greving, J.-B.: Frohlich, R.; Wurthwein, E.-U. *Eur.J.Org.Chem.* **2007**, 5071-5081.
- [23] Bruker. SMART and SAINT. Bruker AXS Inc., **1999** Madison, Wisconsin, USA
- [24] CCDC 998124 contains the supplementary crystallographic data for this paper. These data can be obtained free of charge from The Cambridge Crystallographic Data Centre via [www.ccdc.cam.ac.uk/data\\_request/cif](http://www.ccdc.cam.ac.uk/data_request/cif).
- [25] Frisch, M. J. ; Trucks, G. W. ; Schlegel, H. B. ; Scuseria, G. E. ; Robb, M. A.; Cheeseman, J. R.; Scalmani, G. ; Barone, V. *et al. Gaussian 09 (Revision A.1)*, **2009**, Gaussian, Inc., Wallingford CT.
- [26] Becke, A. D. *J. Chem. Phys.* **1993**, 98, 5648 –5652.
- [27] Krishnan, R. ; Binkley, J. S. ; Seeger, R. ; Pople, J. A. *J. Chem. Phys.* **1980**, 72, 650 –654.
- [28] (a) Biegler-König, F. W. ; Bader, R. F. W. ; Tang, T.-H. *J. Comput. Chem.* **1982**, 3, 317-328; (b) AIMPAC download page: <http://www.chemistry.mcmaster.ca/aimpac/imagemap/imagemap.htm>
- [29] Dovesi, R.; Saunders, V. R.; Roetti, C.; Orlando, R.; Zicovich-Wilson, C. M.; Pascale, F.; Civalieri, B.; Doll, K.; Harrison, N. M.; Bush, I. J.; D'Arco, P.; Llunell, M.; CRYSTAL09 User's Manual. University of Torino: Torino, 2009.
- [30] Hansen, N. K.; Coppens, P. *Acta Crystallogr* **1978**, A34, 909–921.
- [31] Volkov, A. ; Macchi, P. ; Farrugia, L. J. ; Gatti, C. ; Mallinson, P. ; Richter, T.; Koritsanszky, T. *XD2006-A Computer Program Package for Multipole Refinement, Topological Analysis of Charge Densities and Evaluation of Intermolecular Energies from Experimental and Theoretical Structure Factors*, **2006**. See also <http://xd.chem.buffalo.edu/>.
- [32] On the statistical assessment of multipole models see (a) Zhurov, V. V.; Zhurova, E. A.; Pinkerton, A. A. *J. Appl. Cryst.* **2008**, 41, 340–349; (b) Jorgensen, M. R. V.; Svendsen, H.; Schmøkel, M. S.; Overgaard, J.; Iversen, B. B. *Acta Crystallogr. Section A*, **2012**, 68, 301–303. On the problem of correlations among refined parameters see (c) Dittrich B.; Hübschle, C. B.; Holstein,

J. J.; Fabbiani F. P. A. *J. Appl. Cryst.*, **2009**, *42*, 1110–1121; On the problem of modelling the charge density when sulfur atoms are present see (d) Dominiak, P.; Coppens, P., *Acta Crystallogr. Section A* **2006**, *62*, 224–227 (e) Leusser, D.; Henn, J.; Kocher, N.; Engels, B.; Stalke, D. *J. Am. Chem. Soc.*, **2004**, *126*, 1781–1793; (f) Sledz, P.; Kaminski, R.; Chruszcz, M.; Zimmerman, M. D.; Minor, W.; Wozniak, K. *Acta Crystallogr. Section B*, **2010**, *66*, 482–492; (g) Schmökel, M. S.; Cenedese, S.; Overgaard, J.; Jørgensen, M. R. V.; Chen, Y.-S.; Gatti, C.; Stalke, D.; Iversen, B. B. *Inorg. Chem.*, **2012**, *51*, 8607–8616; (h) Lo Presti L.; Destro, R. *J. Chem. Phys.*, **2008**, *128*, 044710; On the modelling of electrostatic moments, see (i) Munshi, P.; Jelsch, C.; Hathwar, V. R.; Guru Row, T. N. *Cryst. Growth Des.*, **2010**, *10*, 1516–1526; (j) Durka, K.; Kamiński, R.; Luliński, S.; Serwatowski, J.; Woźniak, K. *Phys. Chem. Chem. Phys.*, **2010**, *12*, 13126–13136; (k) Bak, J. M.; Dominiak, P. M.; Wilson, C.C.; Wozniak, K. *Acta Crystallogr. Section A*, **2009**, *65*, 490–500; (l) Poulain-Paul, A.; Nassour, A.; Jelsch, C.; Guillot, B.; Kubicki, M.; Lecomte, C. *Acta Crystallogr. Section A*, **2012**, *68*, 715–728.

[33] Østergaard Madsen, A. *J. Appl. Crystallogr.* **2006**, *39*, 757–758.

[34] For example, the average absolute differences in quantum mechanical estimates of bond lengths, angles and torsions in the thiazete system between the two symmetry-independent molecules in TAYCUR amount to  $6 \cdot 10^{-4}$  Å,  $5 \cdot 10^{-2}$  deg and  $2 \cdot 10^{-1}$  deg, respectively. Actually, the most important conformational differences in the asymmetric unit of TAYCUR concern the exocyclic groups (see ref. 20).

[35] Resonance forms a-h relate to systems **2-5**, while forms a'-b' and f' to system **1**. In the system **2**, there is no 4MR and the C bonded to S bears 3 hydrogen atoms.

[36] Adamo, C.; Barone, V. *Chem. Phys. Lett.* **1998**, *298* 113–119.

[37] a) Zhao, Yan; Donald G. Truhlar. *J. Phys. Chem.* **2006**, *110*, 13126-13130; b) Zhao, Yan; Donald G. Truhlar. *Theor. Chem. Account* **2008**, *120*, 215-241.

[38] a) Møller, C.; Plesset, M. S. *Phys. Rev.* **1934**, *46*, 618–622; b) Head-Gordon, M.; Pople, J. A.; Frisch, M. J. *Chemical Physics Letters* **1988**, *153*, 503–506.

[39] The alignment of adjacent major axes reflects that of  $\pi$  orbitals

[40] Cheesman, J. R., Carroll, M. T., Bader, R. F. W. *Chem. Phys. Lett.* **1988**, *143*, 450-458.

[41] Tafipolski, M.; Scherer, W.; Öfele, K.; Artus, G.; Pedersen, B.; Hermann, W. A.; McGrady, G. S. *J. Am. Chem. Soc.* **2002**, *124*, 5865-5880.

[42] Farrugia, L. J.; Khalaji, A. D. *J. Phys. Chem. A*, **2011**, *115*, 12512-12522.

[43] The off-trend low value for  $\alpha'$  (but not for  $\alpha$ ) in **2** is likely due to the quite different orientation of the sulphonyl group and consequent magnitude of the C=N-S-O (O') torsion angles in this not cyclic compound (these angles are equal in magnitude for all other compounds, while they differ by more than  $100^\circ$  in **2**). The lack of the 4-membered ring constraint largely differentiates the orientation of the two O atoms and make them largely not equivalent with respect to both the N-C=N(S) and the  $\pi$ -delocalization planes. Indeed **2** is the only compound in the **2-5** series, where the two S-O distances are appreciably different.

[44] More in detail, the  $SF\%_{C9+N2} - SF\%_{C9+N1}$  difference decreases from 3.4 in the *in vacuo* optimized geometry VQM down to 1.8 in the crystal (PQM).

[45] Bader, R.F.W.; Larouche, A.; Gatti, C.; Carroll, M.T.; MacDougall, P.J.; Wiberg, K.B. *J. Chem. Phys.* **1987**, *87*, 1142-1152.

[46] The same angle  $\gamma$  is considerably lower in compounds **1** and **2**, but it should be remembered that the latter necessarily exhibit very different conformations with respect to DTC, as they lack a closed 4-membered ring.

[47] Gatti, C.; Silvi, B.; Colonna, F. *Chem Phys Lett* **1995**, *247*, 135-142.

[48] Volkov, A.; Abramov, Y.; Coppens, P.; Gatti, C. *Acta Crystallogr.* **2000**, *A56*, 332-339.

# **CHAPTER 2**

## **SOURCE FUNCTION FOR THE ELECTRON SPIN DENSITY: DEVELOPEMENT AND APPLICATION OF A NEW QTAIM BASED CHEMICAL DESCRIPTOR**

## **2.1 Introduction:**

*On the electron spin density distribution:*

Electron spin density distribution is a physical observable that can be obtained experimentally through magnetic scattering of polarized X-rays and neutrons diffraction techniques<sup>[1,2]</sup>. In a couple of very recent works, M. Deutsch *et al.* have performed a joint refinement of X-ray and polarized neutron diffraction data using a split-spin version of the well-known Hansen & Coppens  $\varphi\rho$ <sup>[3]</sup>, leading to accessible much improved experimental  $s(\mathbf{r})$  and to first spin-resolved electron density distributions  $\rho(\mathbf{r})_s$ <sup>[4,5]</sup>. It is clear that with the increased availability of large scale facilities providing intense neutron and synchrotron X-ray sources, such kind of extended model will provide a very valuable tool to understand and predict specific magnetic interactions in complex solid-state networks<sup>[4,5,6]</sup>. However, it is neither possible to obtain direct information on the fundamental factors causing spin polarization effects nor to distinguish the very subtle exchange/pairing mechanisms using the  $s(\mathbf{r})$  scalar field alone. In general  $s(\mathbf{r})$  can be also obtained from quantum mechanics and do exist a lot of interpretive models, generally rooted in the atomic or molecular orbitals framework, that are used for the purpose of analyze such scalar field. In this thesis, a novel QTAIM based chemical descriptor is introduced, the Source Function for the spin density ( $SF_s$ ). This descriptor is able to gain, in terms of a cause-effect relationship, quantitative insights on the relative capability of different atoms or groups of atoms in a system to determine the spin density at any point within a given molecular system. In this sense, since  $s(\mathbf{r})$  is directly connected to magnetic phenomena in complex systems, a very powerful method to distinguish different spin polarization mechanisms<sup>b</sup>, often in competition to each other, is provided. Magnetism depends on non-local effects and can be exploited through space or through chemical bonds. Magnetic properties will thus depend on how the spin information is propagated from a given paramagnetic centre to its neighbouring atoms. It will be shown in the next subsections that the  $SF_s$  is a tool able to reconstruct  $s(\mathbf{r})$  at any point in terms of atomic contributions, so giving a very clear picture of how the magnetic centre is “magnetically” connected to the ligands within a molecule and of how these ligands may in turn, to various extent and in various ways, influence the magnetic center itself.

---

<sup>b</sup> such as direct exchange, ligand-mediated exchange, superexchange, and so on

## 2.2 Source Function for electron density:

Back in 1998, R. F. W. Bader and C. Gatti showed that the electron density at a point  $\mathbf{r}$  in space may be seen as caused by a local source LS and by its operation at all other points of the space<sup>[7]</sup>, (Eq. 2). The LS is given, Eq. 1, by

$$LS(\mathbf{r}, \mathbf{r}') = -\frac{1}{4\pi} \frac{\nabla^2 \rho(\mathbf{r}')}{|\mathbf{r} - \mathbf{r}'|} \quad \text{eq.1}$$

In this expression  $-(4\pi|\mathbf{r}-\mathbf{r}'|)^{-1}$  is a Green's function or an influence function and represents how effective is the cause, the Laplacian of the density ( $\nabla^2\rho(\mathbf{r}')$ ) at  $\mathbf{r}'$  multiplied by the volume element at  $\mathbf{r}'$ , in determining the effect, the electron density at  $\mathbf{r}$ , ( $\rho(\mathbf{r})$ ). Then if we replace the integration of the LS over the whole space with separate integrations over the disjoint and exhaustive partitioning of  $\mathbf{R}^3$  offered by the basins defined through the zero-flux recipe of the QTAIM<sup>[8]</sup>, the density at  $\mathbf{r}$  may be seen, Eq. 2, as determined by a sum of atomic contributions  $S(\mathbf{r};\Omega)$ , each of which is termed as the *source function* (SF) from the atom  $\Omega$  to  $\rho(\mathbf{r})$ .

$$\rho(\mathbf{r}) = \int_{\mathbf{R}^3} LS(\mathbf{r}, \mathbf{r}') d\mathbf{r}' = \sum_{\Omega} \int_{\Omega} LS(\mathbf{r}, \mathbf{r}') d\mathbf{r}' = \sum_{\Omega} SF(\mathbf{r}, \Omega) \quad \text{eq.2}$$

Eq.1 and 2 are expressions that clearly remind that for the electrostatic potential at  $\mathbf{r}$ ,  $V_{\text{elec}}(\mathbf{r})$ .

$$V_{\text{elec}} = \int \frac{\rho(\mathbf{r}')}{|\mathbf{r} - \mathbf{r}'|} d\mathbf{r}' \quad \text{eq. 3a}$$

Indeed both  $\rho(\mathbf{r})$  and  $V_{\text{elec}}(\mathbf{r})$  are a solution of the Poisson's equation  $\nabla^2\varphi(\mathbf{r}) = -q(\mathbf{r})$

$$\varphi(\mathbf{r}) = \int \frac{q(\mathbf{r}')}{4\pi|\mathbf{r} - \mathbf{r}'|} d\mathbf{r}' \quad \text{eq. 3b}$$

with  $\varphi$  being  $\rho(\mathbf{r})$  or  $V_{\text{elec}}(\mathbf{r})$ ,  $q$  being, respectively,  $\rho(\mathbf{r})$  or  $\nabla^2\rho(\mathbf{r})$ , and exploiting the definition of  $V_{\text{elec}}$  in terms of the Poisson's equation  $\nabla^2V_{\text{elec}}(\mathbf{r}) = 4\pi\rho(\mathbf{r})$ .

Eq. 2 give us an expression which relates  $\rho(\mathbf{r})$  at a point to the behaviour of this scalar (in terms of  $\nabla^2\rho(\mathbf{r}')$ ) in the other points of the space. Decomposition of  $\rho(\mathbf{r})$  in terms of SF atomic contributions enables one to view the properties of the electron density (ED) distribution from a new perspective.



It shows that  $\rho(\mathbf{r})$  is never really local in nature but originates from the cumulative result of the influence of all other parts of the system. This is in agreement with the Density Functional Theory where the ED at a point is known to be a unique functional of the external potential, defined by the positions and nuclear charge of all nuclei in the system. However, through the SF, such non local dependence of the ED is examined using the lenses of chemistry, i.e. in terms of contributions from well defined chemical entities, like atoms or group of atoms within the system. For instance, the SF decomposition may provide a chemically meaningful picture of how a system responds to a perturbation, like chemical substitution, change of environment, by observing the changes on  $\rho$  (or on a given property of  $\rho$ ) and the atomic contribution to such changes at any point  $\mathbf{r}$ . Precious insights on the impact of perturbation on the various parts of a system are provided this way. Finally the SF chemical descriptor is amenable to experimental determination, since, as discussed in Chapter 1, the ED and its Laplacian may be also obtained from experimental structure factors measured through very accurate single crystal X-ray diffraction experiments <sup>[10-14,17-18]</sup>. This is certainly one of the most attractive properties of the SF descriptor, enabling a direct comparison between theory and experiment. <sup>[10]</sup>

## **2.3 Source Function for electron spin density:**

### **2.3.1 Theory:**

The Source Function for the electron spin density ( $SF_s$ ) is obtained through an expression formally similar to that for the electron density <sup>[26]</sup>.

$$s(\mathbf{r}) = \int_{R^3} LS_s(\mathbf{r}, \mathbf{r}') d\mathbf{r}' = \sum_{\Omega} \int_{\Omega} LS_s(\mathbf{r}, \mathbf{r}') d\mathbf{r}' = \sum_{\Omega} SF_s(\mathbf{r}, \Omega) \quad \text{eq.4}$$

In eq.4, however, the decomposition in atomic terms is still done in terms of  $\rho(\mathbf{r})$  and not of  $s(\mathbf{r})$ . Thus the Laplacian of the spin density ( $\nabla^2 s(\mathbf{r})$ ) does not integrate to zero in the atomic basins as it is for the ED Laplacian, because the atomic surface has a net flux of the electron spin density gradient through the surface. The local source and cause for  $s(\mathbf{r})$  at  $\mathbf{r}$  ( $LS_s$ ) is given by

$$LS_s = -\frac{1}{4\pi} \frac{\nabla^2 s(\mathbf{r}')}{|\mathbf{r} - \mathbf{r}'|} = -\frac{\nabla^2 s(\mathbf{r}')}{4\pi|\mathbf{r} - \mathbf{r}'|} = -\frac{\nabla^2 \rho_{\alpha}(\mathbf{r}') - \nabla^2 \rho_{\beta}(\mathbf{r}')}{4\pi|\mathbf{r} - \mathbf{r}'|} \quad \text{eq.5}$$

in terms of  $\nabla^2 s(\mathbf{r})$  rather than  $\nabla^2 \rho(\mathbf{r})$ ; the global effect is  $s(\mathbf{r})$  while the effectiveness of the local cause just remains the same as for electron density because it is a purely geometrical factor that

include the reciprocal of the distance between the  $\mathbf{r}$  (reference point) and  $\mathbf{r}'$  (the local point). Since  $\nabla^2 s(\mathbf{r})$  is different with respect to  $\nabla^2 \rho(\mathbf{r})$ , information on  $\rho(\mathbf{r})$  transmission is different from the information on  $s(\mathbf{r})$  transmission. The reconstruction for the  $s(\mathbf{r})$  has a similar formal expression and  $SF_s$  denote the source function from atom  $\Omega$  to  $s(\mathbf{r})$ . To clarify the differences between information on  $\rho(\mathbf{r})$  and  $s(\mathbf{r})$  transmission, the comparison between the various quantities entering in the definition of the source function for the electron density and spin electron density is necessary.

### 2.3.2 Comparison between the electron density and spin electron density behaviour:

Electron density and electron spin density distribution are defined respectively by

$$\begin{aligned}\rho(\mathbf{r}) &= \rho_\alpha(\mathbf{r}) + \rho_\beta(\mathbf{r}) \\ s(\mathbf{r}) &= \rho_\alpha(\mathbf{r}) - \rho_\beta(\mathbf{r})\end{aligned}$$







with  $\rho_\alpha(\mathbf{r})$  and  $\rho_\beta(\mathbf{r})$  being the spin  $\alpha$  and  $\beta$  contributions to the total ED density. These two scalar fields present very different behaviour and properties. First of all the analysis of  $\rho(\mathbf{r})$  is simpler with respect to  $s(\mathbf{r})$  because  $(LS(\mathbf{r}'))$  will be always positive where  $\nabla^2 \rho(\mathbf{r}')$  is negative ( $\rho(\mathbf{r}')$  concentrated) and viceversa (see Tab.1).

$\rho(\mathbf{r}')$	$\nabla^2 \rho(\mathbf{r}')$	$LS(\mathbf{r}')$	Effect on $\rho(\mathbf{r})$
$> 0$	$> 0$	$< 0$	decreases $\rho$
$> 0$	$< 0$	$> 0$	increases $\rho$

Tab.1: Behaviour of electron density distribution as a function of the sign of the Local Source Function

The situation becomes more complicate and interesting when we analyse the electron spin density field. Regardless of the sign of  $s(\mathbf{r})$ , the local source behaviour depends on the local concentration/dilution of  $\rho_\alpha(\mathbf{r}')$  and  $\rho_\beta(\mathbf{r}')$ . If  $\rho_\alpha(\mathbf{r}')$  is locally diluted ( $\nabla^2 \rho_\alpha(\mathbf{r}')$  positive) and  $\rho_\beta(\mathbf{r}')$  is instead locally concentrated ( $\nabla^2 \rho_\beta(\mathbf{r}')$  negative) then  $\nabla^2 s(\mathbf{r}')$  will be positive (see the 2<sup>nd</sup> row of the Tab.2); the local source will be negative and the infinitesimal region around this point will cause the effect of decreasing  $s(\mathbf{r})$  (denoted as “ $\beta$ ” effect in the last column), making the spin density less positive or more negative with respect to the effect caused by the sum of contributions from the remaining regions of the system. On the contrary if at  $\mathbf{r}'$  the  $\alpha$  distribution is locally concentrated and the  $\beta$  distribution is locally depleted (third row of Tab. 2) there will be an increase of  $s(\mathbf{r})$  (denoted as “ $\alpha$ ” effect in the last column). When  $\rho_\alpha(\mathbf{r}')$  and  $\rho_\beta(\mathbf{r}')$  are both diluted or both

concentrated, the sign of the local source will depend on the relative magnitude of  $\nabla^2\rho_\alpha(\mathbf{r}')$  and  $\nabla^2\rho_\beta(\mathbf{r}')$ .

$s(\mathbf{r}')$	$\nabla^2\rho_\alpha(\mathbf{r}')$	$\nabla^2\rho_\beta(\mathbf{r}')$	Relative magnitude	$\nabla^2s(\mathbf{r}')$	$LS_s(\mathbf{r}')$	Effect on $s(\mathbf{r})$
$\pm$	$> 0$	$> 0$	$\nabla^2\rho_\alpha > \nabla^2\rho_\beta$ $\nabla^2\rho_\alpha < \nabla^2\rho_\beta$	$> 0$ $< 0$	$< 0$ $> 0$	 $\beta$  $\alpha$
$\pm$	$> 0$	$< 0$		$> 0$	$< 0$	 $\beta$
$\pm$	$< 0$	$> 0$		$< 0$	$> 0$	 $\alpha$
$\pm$	$< 0$	$< 0$	$ \nabla^2\rho_\alpha  >  \nabla^2\rho_\beta $ $ \nabla^2\rho_\alpha  <  \nabla^2\rho_\beta $	$< 0$ $> 0$	$> 0$ $< 0$	 $\alpha$  $\beta$

Tab.2: Behaviour of electron density spin distribution as function of the sign of the Local Source Function

For example, the first row of Tab.2 reports the situation where both  $\rho_\alpha(\mathbf{r}')$  and  $\rho_\beta(\mathbf{r}')$  are diluted; in this case  $LS_s(\mathbf{r}')$  will be negative and will generate a “ $\beta$ ” contribution only if  $\rho_\alpha(\mathbf{r}')$  is more diluted than  $\rho_\beta(\mathbf{r}')$ , while it will be positive if  $\rho_\beta(\mathbf{r}')$  is more diluted with respect  $\rho_\alpha(\mathbf{r}')$ . On the contrary, in case they are both concentrated there will be an  $\alpha$  effect if  $\rho_\alpha(\mathbf{r}')$  is more concentrated than  $\rho_\beta(\mathbf{r}')$ ; while if it is  $\rho_\beta(\mathbf{r}')$  that is more concentrated, its Laplacian will be more negative than that of the  $\alpha$  distribution and the local source will be negative causing an effect “ $\beta$ ”. Is very important to stress that, differently from  $\rho(\mathbf{r})$ , it is no longer sufficient to have the  $\alpha$  and  $\beta$  density distributions both concentrated to have a positive source or both diluted to have a negative source. One may obtain a positive or a negative source in both cases. Everything depend on the relative magnitude of concentration or dilution of the  $\alpha$  or  $\beta$  distributions. Let’s see an application of what reported in Tab.1 and 2 on a very simple system, water triplet. Using a simple orbital model, the molecular system is hybridized  $sp^2$  and presents two unpaired electrons in the  $p_x$  orbital perpendicular to the molecular plane (see Figure 1)<sup>c</sup>.

<sup>c</sup> The results for  $^3B_1$   $H_2O$  molecular system here presented are obtained performing quantum mechanical simulations *in vacuo* by means of the Gaussian09 program package, in particular we have optimized the structure at UHF level of theory using 6-311++G(2p,2d) as basis set, detailed description of further QM calculations will be described in the next subsections.

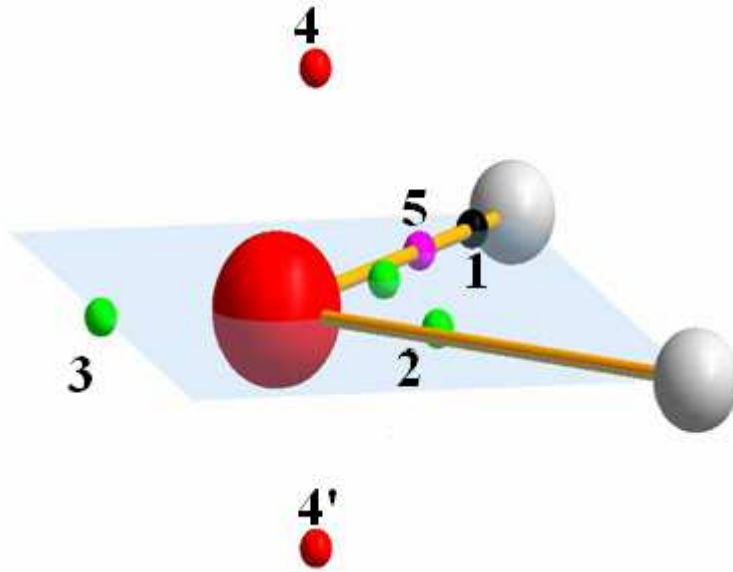


Fig.1: water Triplet  ${}^3B_1$ ;  $\nabla^2\rho(\mathbf{r})$  and  $\rho(\mathbf{r})$  critical points are reported. The  $\nabla^2\rho(\mathbf{r})$  critical points are denoted as follows: green points (3,+3) charge concentration, red points denote (3,-1) saddle points and violet point denote (3,+1) saddle point. The bond critical point is reported in black

CP	$\rho(\mathbf{r})$	$\nabla^2\rho(\mathbf{r})$	$s(\mathbf{r})$	$\nabla^2s(\mathbf{r})$	$\rho_\alpha(\mathbf{r})$	$\nabla^2\rho_\alpha(\mathbf{r})$	$\rho_\beta(\mathbf{r})$	$\nabla^2\rho_\beta(\mathbf{r})$
1	0.288	-2.14	-0.0050	0.21	0.141	-0.96	0.146	-1.18
2	0.888	-5.17	0.0631	1.07	0.475	-2.05	0.412	-3.12
3	1.03	-6.85	0.0051	2.04	0.518	-2.4	0.513	-4.45
4	0.61	-1.18	0.3818	-4.54	0.496	-2.86	0.114	1.68

Tab.3: Values of electron density, electron spin density, Laplacian of total  $\rho(\mathbf{r})$  and in terms of its  $\alpha$  and  $\beta$  counterparts, Laplacian of spin density distribution, at each critical point considered in Fig.1

Let's consider  $\nabla^2s(\mathbf{r})$  and the  $LS_s$  at a number of critical points (CP) in  $\nabla^2\rho(\mathbf{r})$  or in  $\rho(\mathbf{r})$ . At the bond critical point lying on O-H bond (bcp point **1** coloured in black in Fig.1)  $s(\mathbf{r})$  is negative, and both the  $\alpha$  and  $\beta$  distributions are concentrated ( $\nabla^2\rho_\alpha(\mathbf{r})$  and  $\nabla^2\rho_\beta(\mathbf{r}) < 0$ ). Since  $\nabla^2\rho_\beta(\mathbf{r})$  is more negative than its  $\alpha$  counterpart we observe a positive  $\nabla^2s(\mathbf{r})$  at the bcp. The infinitesimal region around this critical point will generate a “ $\beta$ ” transmission effect. At the bond charge concentration (BCC, point **2**, coloured in green in Fig.1)  $s(\mathbf{r})$  is positive, differently from the bcp **1**. Also in this case both  $\rho_\alpha(\mathbf{r})$  and  $\rho_\beta(\mathbf{r})$  are concentrated and  $\nabla^2\rho_\beta(\mathbf{r})$  is more negative than  $\nabla^2\rho_\alpha(\mathbf{r})$ . So again  $\nabla^2s(\mathbf{r}) > 0$  and also this region will have a negative local source generating a beta transmission

effect, regardless that the sign of the spin density was positive in this case. There are three critical points related to the non bonded charge concentrations within the molecular system: the (3,+3) charge concentration corresponding to the lone pair lying in the molecular plane and associated to a  $sp^2$  orbital (CC, point **3**, coloured in green in Fig.1) and two (3,-1) critical points associated to the unpaired electrons in the  $p_z$  orbital (points **4** and **4'** coloured in red in Fig.1) that are very close to the spin density maximum in this plane. Both kind of critical points have positive spin density but differ a lot in their behaviour. In fact at the lone pair charge concentration **3**,  $s(\mathbf{r})$  is marginally positive and the Laplacian of the  $\beta$  distribution is much more negative than the Laplacian of the  $\alpha$  distribution as a reaction to the large concentration of the neighbouring unpaired electrons (this assertion is supported by the fact that  $s(\mathbf{r})$  is close to become negative near CP 3). Hence  $\nabla^2 s(\mathbf{r})$  is greater than zero and the region around the lone pair CC will cause a  $\beta$  effect. If we look at the out of plane (3,-1) CPs **4** and **4'** we find a completely different behaviour. In fact at this CP the spin density is very large, dominated by the  $\alpha$  unpaired electron and, more important, while  $\rho_\alpha(\mathbf{r})$  is concentrated,  $\rho_\beta(\mathbf{r})$  is diluted. As a consequence  $\nabla^2 s(\mathbf{r}) \ll 0$ , leading to a very positive local source from the region around CPs **4** and **4'**. This region will give a large  $\alpha$  effect, hence it will cause an increase of the spin density in the other regions of the system. Though both CC **3** and CP **4,4'** have positive spin density, they have opposite local source effects linked to the chemical difference between the two regions; in fact the first is dominated by a paired lone pair while the second is dominated by unpaired electrons.

### 2.3.3 Total atomic spin population and atomic laplacian of the spin density:

The total spin population of each atom within a molecular system is defined by

$$SP(\Omega) = N_\alpha(\Omega) - N_\beta(\Omega) \text{ eq.6}$$

where

$$N(\Omega) = \int_\Omega \rho(\mathbf{r}) d\mathbf{r} \text{ eq.7}$$

is the atomic population of the atomic basin  $\Omega$ , defined as the portion of  $R^3$  bounded by a surface never crossed by ED gradient lines:

$$\nabla \rho(\mathbf{r}) \bullet \mathbf{n}(\mathbf{r}) = 0 \text{ eq.8}$$

( $\mathbf{n}(\mathbf{r})$  being the unit vector normal to the surface at  $\mathbf{r}$ ). It is clear that, from the definition of electron density and spin electron density, eq.7 can be re-written as sum of the  $\alpha$ -electrons and  $\beta$ -electrons contributions

$$N(\Omega) = \int_{\Omega} (\rho_{\alpha}(\mathbf{r}) + \rho_{\beta}(\mathbf{r})) d\mathbf{r} \quad \text{eq.9}$$

while eq.6 can be written as difference between the two ED counterparts

$$SP(\Omega) = \int_{\Omega} (\rho_{\alpha}(\mathbf{r}) - \rho_{\beta}(\mathbf{r})) d\mathbf{r} \quad \text{eq.10.}$$

Analogously for the atomic spin cause: the atomic Laplacian of the spin density,  $\nabla^2 s(\Omega)$ , is given by:

$$\nabla^2 s(\Omega) = \int_{\Omega} \nabla^2 s(\mathbf{r}) d\mathbf{r} = \int_{\Omega} \nabla^2 (\rho_{\alpha}(\mathbf{r}) - \rho_{\beta}(\mathbf{r})) d\mathbf{r} \quad \text{eq.11}$$

Atomic electron spin density and the atomic laplacian of the spin density reveal us how the lone electron is localized on the oxygen atom in water triplet molecular system. The oxygen spin density population amounts to about 67% of the total unpaired population. The integrated  $\nabla^2 s(\mathbf{r})$  is positive for the hydrogen and negative for the oxygen (see Tab.4); these values of the Laplacian of the electron spin density may be interpreted as the effect of the atoms within the molecular system at very remote points (where the geometric Green's function term<sup>d</sup> may be taken out from the integral), or as an average effect of the atom.

$\Omega$	$q(\Omega)$	$SP(\Omega)$	$\nabla^2 s(\Omega)$
H	0.425	0.288	0.019
O	-0.850	1.422	-0.038

Tab.4: Values of atomic net charge, atomic electron spin density, and atomic Laplacian of spin density

We analyse in the following the reconstruction of the ED and of the spin ED at the CPs displayed in Fig. 1, in terms of the corresponding SF or SF<sub>s</sub> atomic contributions (Table 5). Considering the SF electron density contributions at the bcp 1 (Figure 1) it is possible to note how the contribution from the oxygen atom is larger than that of its bonded hydrogen atomic basin, reflecting the polarity of the bond. In fact at bcp the oxygen atom causes about 60% of the CP ED value, while about 40% of this value comes from the bonded hydrogen and a negligible amount from the remaining non-bonded hydrogen. The reconstruction of  $s(\mathbf{r})$  at the same reference point is completely different. Considering CP 1, the oxygen atom overdetermines its negative spin density while the two hydrogens, that gives a positive spin density contribution, counteract the effect of the oxygen.

Indeed it is possible to see that  $\nabla^2 s(\mathbf{r})$  for the oxygen is almost all positive in the molecular plane, hence its  $LS_s$  value is here negative (Fig.2) and the  $SF_s$  is negative. The bcp **1** is associated to a covalent bond and is therefore normal to find this opposing effect from the two bonded atoms; however it is interesting that at bcp the oxygen contributes a negative spin density despite its unpaired alpha electrons.

CP	H		O		H	
	SF	$SF_s$	SF	$SF_s$	SF	$SF_s$
1	0,1109	0,0063	0,1725	-0,0137	0,0041	0,0024
2	0,0170	0,0042	0,8622	0,0561	0,0073	0,0030
3	0,0061	0,0027	1,0178	-0,0004	0,0061	0,0027
4	0,0082	0,0032	0,5937	0,3740	0,0082	0,0032

Tab.5: Values of SF and  $SF_s$  (atomic units) in  ${}^3B_1$  H<sub>2</sub>O UHF/UHF computational levels

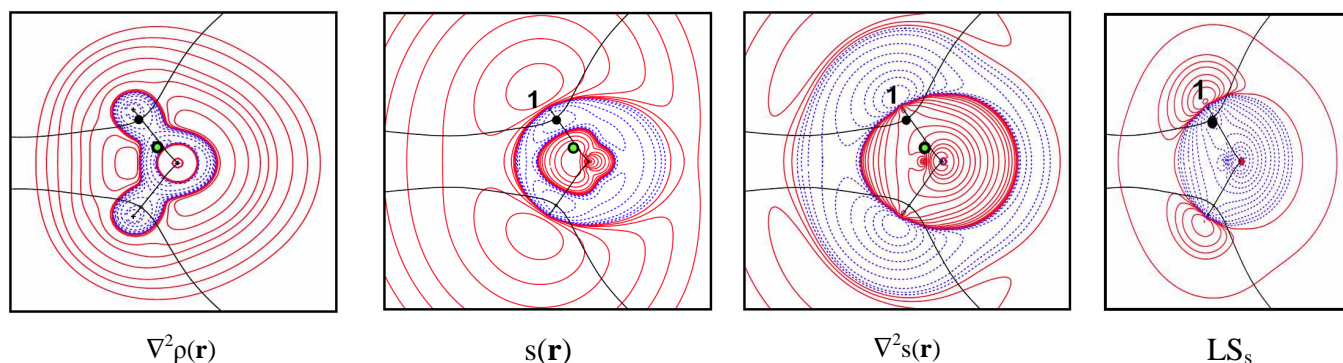


Fig.2: Electron density Laplacian, electron spin density  $s(\mathbf{r})$  and its Laplacian, Local Source for electron spin density in the  $(y,z)$  plane for  ${}^3B_1$  H<sub>2</sub>O, at UHF/UHF spin-contamination annihilated computational levels. Atomic units (a.u.) are used throughout. Contour maps are drawn at interval of  $\pm(2,4,8)\cdot 10^n$ ,  $-4 \leq n \leq 0$  ( $s$ ,  $\nabla^2 s$ ) and  $-3 \leq n \leq 0$  ( $\nabla^2 \rho$ ). Dotted blue (full red) lines indicate negative (positive) values and full black lines mark boundaries of atomic basins. The O–H bond critical point (bcp, 1) and the bonded charge concentration point (BCC, 2) are shown as black and green dots.

Note that, at variance with case of the electron density reconstruction, spin transmission occurs not just through bond, but also through space. Indeed, the other non bonded hydrogen, gives an almost equal contribution to that of the bonded H. This is a fundamental difference with respect to the electron density case, where the contribution to the reconstruction of  $\rho(\mathbf{r})$  at bcp given by the bonded hydrogen atom largely exceeds that of the non-bonded hydrogen.

<sup>d</sup> we remind to the reader that the geometric part of the Green function is the distance between the points  $\mathbf{r}$  and  $\mathbf{r}'$   $|\mathbf{r}-\mathbf{r}'|$

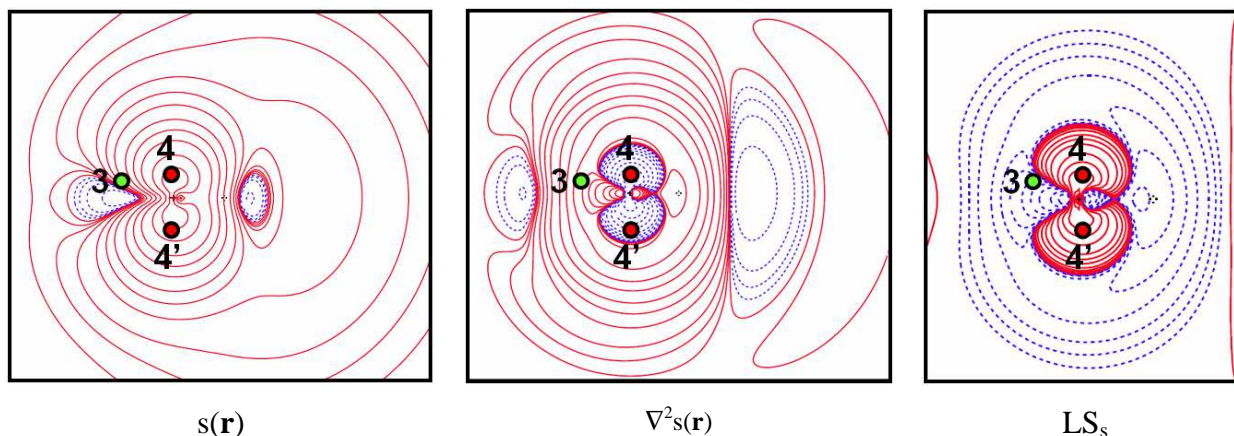


Fig.3: Electron spin density  $s(\mathbf{r})$  and its Laplacian, Local Source function for electron spin density in the  $(x,z)$  plane for  ${}^3B_1$   $H_2O$ , at UHF/UHF spin-contamination annihilated computational levels. Atomic units (a.u.) are used throughout.

Contour maps are drawn as in Figure 2. The CC critical point (CP number 3 coloured green) and the two lone pair electron critical points (CPs number 4 and 4', coloured red) are shown.

The spin reconstruction for the three critical points associated respectively to the non-bonded lone pair (CC **3**) and the two unpaired alpha electrons around the oxygen atom (CP **4** and **4'**), are all characterised by a positive spin density. Nevertheless their reconstructions in terms of atomic contributions, largely differ. In fact at the two (3;-1) CPs the only contribution to  $s(\mathbf{r})$  is given by the oxygen atom (the same is true for the reconstruction of  $\rho(\mathbf{r})$ ) because the point is located inside a region of extremely highly negative  $\nabla^2 s(\mathbf{r})$  (which causes a positive contribution in terms of  $SF_s$ ), see Fig. 3. On the contrary at the lone pair CC  $s(\mathbf{r})$  is marginally positive and the contributions from the two hydrogen atoms dominate, overdetermining  $s(\mathbf{r})$  at the point (Table 5).. The contribution of the oxygen atom is instead negative but very small since the positive contribution due to the unpaired  $\alpha$ -electron regions, is slightly overcompensated by the negative  $LS_s$  contribution due to the  $\beta$ -density region around CP number 3<sup>e</sup> (see the map of  $\nabla^2 s(\mathbf{r})$  in Fig.3). In conclusion the reconstruction of  $s(\mathbf{r})$  at CC **3** is dominated by hydrogen atoms; interestingly, in the case of the reconstruction of the ED it is exactly the opposite. Negative sources have been often seen with some suspicion in the case of the ED reconstruction, being  $\rho(\mathbf{r})$  everywhere positive (or null). The physical and chemical meaning behind their occurrence has, however, been fully and convincingly explained (see in particular Ref. 10). For the electron spin density reconstructions, negative or positive contributions are not surprising and everywhere possible. They also have a clear, immediate physical meaning. In fact negative  $SF_s$  values cause an increase of  $\rho_\beta(\mathbf{r})$  at the reference



point, making  $s(\mathbf{r})$  less positive when  $s(\mathbf{r})$  is positive or more negative when  $s(\mathbf{r})$  is negative.<sup>f</sup>. Negative  $SF_s\%$  values mean that the atom (or group of atoms) in question opposes to the value of  $s(\mathbf{r})$  at reference point due to the remaining atoms, making it less negative (or even positive), by enhancing  $\rho_\alpha(\mathbf{r})$  if  $s(\mathbf{r})$  is negative, or less positive (or even negative) by enhancing  $\rho_\beta(\mathbf{r})$  if  $s(\mathbf{r})$  is positive. Finally at the bonded charge concentration CC number 2 the contribution from the two hydrogen atoms is negligible because of the close proximity of this CP to the oxygen nucleus (the same is true for the electron density SF contributions).

#### 2.3.4 Numerical accuracy of $\rho(\mathbf{r})$ and $s(\mathbf{r})$ reconstruction:

Reconstruction of scalar fields requires particular attention on the accuracy and precision of the process through all the portion of space under analysis. In particular, when reconstructing  $\rho(\mathbf{r})$  and  $s(\mathbf{r})$  through SF and  $SF_s$  contributions it is important to assess whether such reconstructions are accurate enough, that is if they are within few per cent of the value to be reconstructed, and if such an accuracy is reasonably uniform through the molecular space. In general is known that the electron density may be accurately reconstructed provided  $\rho(\mathbf{r})$  is equal to or larger than  $10^{-3}$  a.u. In case of  $\rho(\mathbf{r})$  smaller than  $10^{-3}$  a.u. some problems arise and they become particularly serious if the value of ED that has to be reconstructed is smaller than  $10^{-4}$  a.u. As a consequence one expects to find similar problems in the case of electron spin density reconstruction. Since  $s(\mathbf{r})$  is an electron density difference between the two spin counterparts, its values are generally smaller than  $\rho(\mathbf{r})$  also in regions close to the nuclei and in particular in the covalent bonding regions.<sup>g</sup> For comparing the accuracies of the  $s(\mathbf{r})$  vs  $\rho(\mathbf{r})$  reconstructions, local percentage errors defined as a function of a distance parameter  $t$  along the O-H internuclear axis are introduced; in this way it is possible to explore the different behaviour, if any, of core, valence and bonding regions. The two percentage error ( $f_1$  and  $f_2$ ) are calculated at each point  $\mathbf{r}$  along the O-H axis by

$$f_1 = \frac{\rho(\mathbf{r})_{SF} - \rho(\mathbf{r})_{true}}{\rho(\mathbf{r})_{true}} * 100 \text{ eq.12}$$

and

$$f_2 = \frac{s(\mathbf{r})_{SF} - s(\mathbf{r})_{true}}{s(\mathbf{r})_{true}} * 100 \text{ eq.13}$$

<sup>e</sup> as a reaction to the alpha spin density in the  $p_x$  orbital

<sup>f</sup> or changing its value from positive to negative with respect to the contribution due to the remaining atoms

<sup>g</sup> values as low as  $10^{-3}$  or  $10^{-4}$  a.u. are typical

Since in general the electron spin density has smaller values than the electron density, one may imagine the  $s(\mathbf{r})$  reconstruction to be more difficult. However, the spin density Laplacian has somewhat dampened oscillations with respect to the electron density Laplacian (see Fig.4), so the effect due to the generally lower values for spin densities could be compensated for in some way.

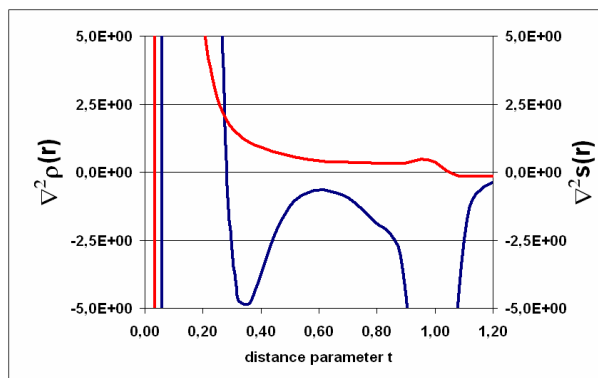


Fig.4: comparison of Laplacian of electron density (blue line) with respect the Laplacian of electron spin density (red line) as a function of a distance parameter  $t$  along the O-H internuclear axis

From the comparison in terms of percentage error functions, the general accuracy for  $s(\mathbf{r})$  results to be worse than for  $\rho(\mathbf{r})$ , and especially in the regions near to the nuclei ( $0.1 < t < 0.35$ ), even for the oxygen atom (see Fig.5a and 5b). This result is quite unexpected since in such regions  $s(\mathbf{r})$  is large enough and so a good accuracy in the reconstruction of both  $\rho(\mathbf{r})$  and  $s(\mathbf{r})$  is expected.

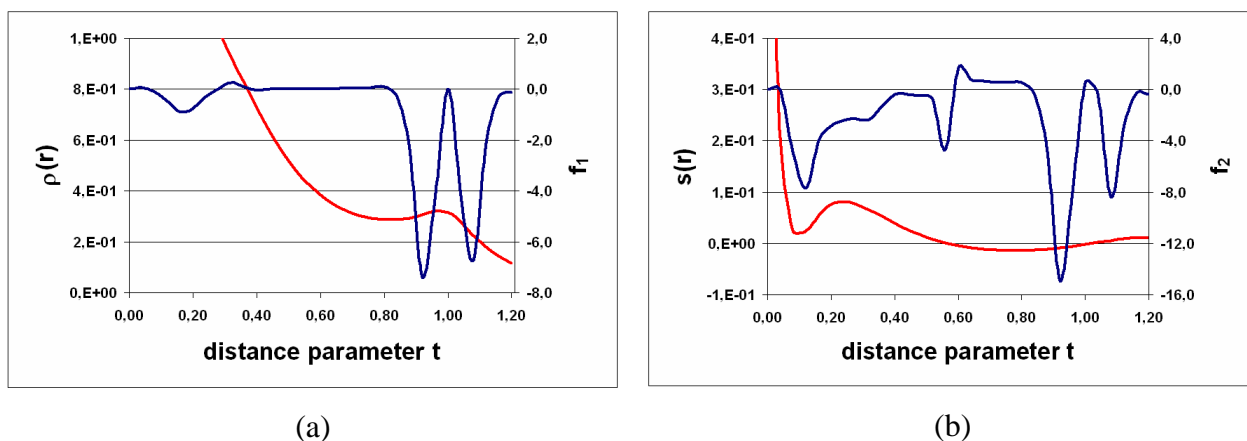


Fig.5: Comparison of the accuracy in reconstruction of electron density with respect the electron spin density using percentage errors defined as a function of a distance parameter  $t$  along O-H internuclear axis. Fig.5a report electron density (red line) vs  $f_1$  percentage error function (blue line); Fig. 5b report electron spin density (red line) vs  $f_2$  percentage error function (blue line). Both  $\rho(\mathbf{r})$  and  $s(\mathbf{r})$  are in a.u.

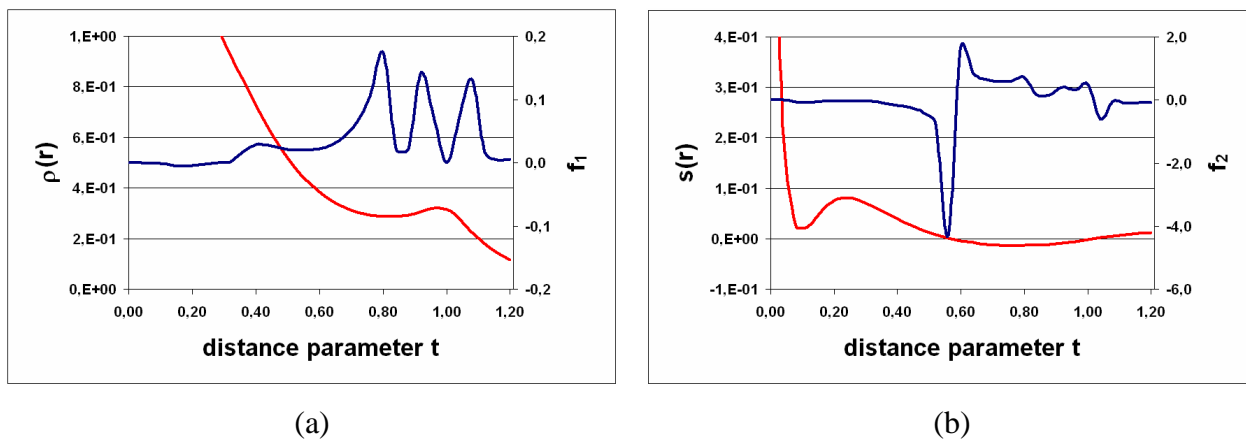


Fig.6: Comparison of the accuracy in reconstruction of electron density with respect to the electron spin density using an improved angular integration. Percentage errors are defined as a function of a distance parameter  $t$  along O-H internuclear axis. Colours and units are the same as in Fig.5a and Fig.5b.

Such kind of behaviour can be explained as follows: at variance with  $\rho(\mathbf{r})$  and  $\nabla^2\rho$ ,  $s(\mathbf{r})$  and  $\nabla^2s(\mathbf{r})$  are far from being spherically symmetric in the atomic cores. In the case of the  $s(\mathbf{r})$  reconstruction, a very accurate angular mesh need to be adopted also when integrating in the core region. By using such an improved grid for the core (the number of point is increased by four times), enabled us to obtain a very much better accuracy in the reconstruction of the electron spin density with errors typically well below 1% and a maximal, almost acceptable, error value of about 4% only for just one very small region, namely the one where the spin density sign changes from positive to negative (see Figure 6b). Adoption of an improved angular grid for the core region had also a positive impact on the errors of the  $\rho(\mathbf{r})$  reconstruction, being all lowered to values very close to 0.1% or so (see Fig.6a).

### 2.3.5 On the interpretation of $s(r)$ information using $SF_s$ QTAIM based descriptor:

The relatively simple case of water in its  ${}^3B_1$  state (Fig.1) is chosen as an example of application of QTAIM based descriptor  $SF_s$  with the aim to analyze whether such tool enables one to gain interesting and valuable insights regarding the transmission of electron spin density information and the magnetic coupling mechanism (ferromagnetic or anti-ferromagnetic coupling between atoms, spin exchange or super-exchange etc.) that are behind such transmission information. The interpretation of the results obtained in water triplet are very encouraging and, of course, pushed us to extend the application of the  $SF_s$  chemical descriptor to molecular systems that are much complicated with respect this first “simpler” case. Nevertheless the results described till now for the water system do not explain in a very exhaustive way, which are the mechanism behind the transmission of electron spin density information. In particular, it is not clear if  $s(\mathbf{r})$  is transmitted

through spin delocalization or spin polarization mechanisms, or also through their in tandem operation. In a very recent work by Deutch et al, the experimental decomposition of the electron density in its spin counterparts is performed for an azido double bridged Cu-Cu molecular system (Figure 7) using an extended version of the well known Hansen&Coppens multipolar model<sup>[5]</sup>, that permits to refine data-set of very good quality obtained combining both polarized X-ray and neutron diffraction techniques.<sup>h</sup>

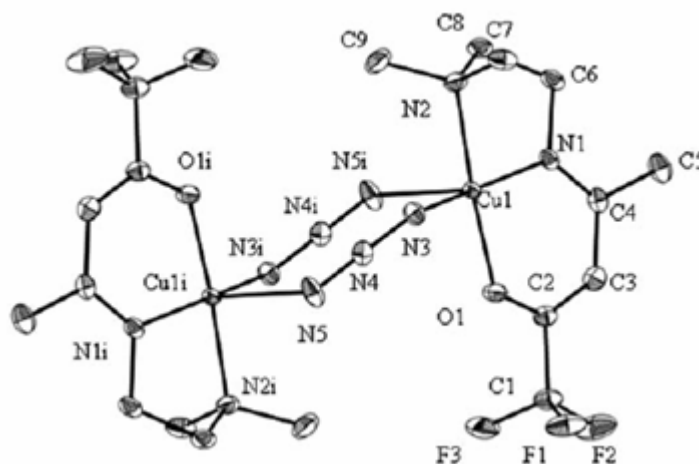


Fig.7: azido double-bridge Copper II di-nuclear complex; the azido groups bridge the two Cu(II) ions through two terminal N atoms ( $\mu$ -1,3), in what is called an END-TO-END coordination mode (EE).

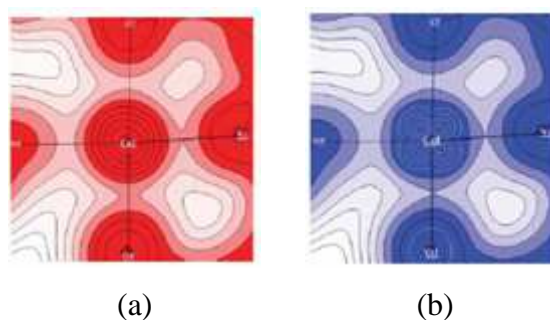


Fig.8: separated  $\alpha$  (a) and  $\beta$  (b) electron density distributions of azido double bridge di-nuclear (Cu-Cu) complex obtained combining Polarized Neutron Diffraction and X-Ray Diffraction experiments, using a spin-split version of the original Hansen&Coppens Multipolar Model refinement

In their work the authors discuss the electron spin density distribution in terms of orbital interactions; in particular they use a fragment orbital approach and consider the interactions between the highest occupied  $d$  orbitals of copper atoms and the two (one for each azido bridge) highest doubly occupied  $\pi_{\text{gerade}}$  azido orbitals. The interpretation of  $s(\mathbf{r})$  distribution was then done through the concept of *spin delocalization* (due to the overlap between the fragment orbitals) and

<sup>h</sup> the application of the topological descriptor  $SF_s$  to this class of complexes will be better described in next sub-sections of this chapter

*spin polarization* (that involve both the  $\pi_{\text{gerade}}$  and the lowest unoccupied  $\pi_{\text{ungerade}}$  molecular orbitals of the  $\text{N}_3^-$  fragment and where the fundamental importance of  $\pi$ - $\pi^*$  excitations to produce the ferromagnetic coupling between the two copper atoms has been emphasized); to this aim the authors have employed either two-electron active orbitals models either more complicated ones, i.e. multi-electron models using more sophisticated multi-configurations wavefunction models.

Mimicking the orbital interpretation adopted by Aronica *et al*, we thought it worth introducing in our SF/SF<sub>s</sub> analysis a physically-rooted partitioning of the values of the observables listed in Tab.1 (and also of their derived SF and SF<sub>s</sub> values) in terms of a sum of two contributions: a *magnetic* one arising from the unpaired  $\alpha$ -electrons orbitals (hereinafter magnetic orbitals) and a *reaction* or *relaxation* contribution due to the remaining orbitals.<sup>[26]</sup>

#### *Computational details:*

The correct analysis of the decomposition of both  $\rho(\mathbf{r})$  and  $s(\mathbf{r})$  in an open shell molecular system as  $^3\text{B}_1$  water triplet requires the use of some particular precaution in the calculation of the wavefunction<sup>i[19]</sup>. For this reason, different levels of theory were employed during all the *in vacuo* quantum mechanical simulation. Thus we performed CASSCF(8,8), UHF (Unrestricted Hartree Fock), ROHF (Restricted Open Hartree Fock) calculations with a 6-311++G(2d,2p) basis set; moreover computations on both spin-contamination annihilated and spin contaminated UHF wavefunctions were performed; such calculations revealed that spin contamination by states of higher multiplicity than the triplet state was very small ( $\langle S^2 \rangle = 2.0069$ ), and becomes almost negligible when annihilation procedure is applied ( $\langle S^2 \rangle = 2.000014$ ). Static electron correlation corrections were considered by performing a CASSCF(8,8) computation. To this aim the starting guess was taken from the UHF spin contamination annihilated Natural Orbitals, obtaining a Slater determinant expansion of the wavefunction which included 3136 configurations of the correct symmetry and spin multiplicity. Thanks to the Natural orbitals analysis<sup>j</sup> magnetic orbitals were very easily singled out, based on their occupation numbers, in all cases. In ROHF calculations, the wavefunction include natural orbitals with occupation numbers equal to one by definition because both  $\beta$ -density and relaxation contribution are equal to zero everywhere; for the other adopted levels of theory the occupation numbers of magnetic orbitals were either one or marginally different from one (highest deviation from one being 0.0003 for CASSCF(8,8) wavefunction). Spin densities were instead

---

<sup>i</sup> in particular we paid particular attention on the problem of spin contamination and static and dynamic electron correlation

<sup>j</sup> pop= no option in G09 program package

calculated from the natural orbitals obtained from separate diagonalizations of the  $\alpha$ - and  $\beta$ -density matrices<sup>k</sup>.

*Results and discussion:*

In the molecular system  $^3B_1$  H<sub>2</sub>O the two magnetic orbitals have B<sub>1</sub> and A<sub>1</sub> symmetry. They are obtained through the diagonalization of the first order density matrix and by taking those natural orbitals with occupation number ( $n$ ) equal to or marginally different from one.

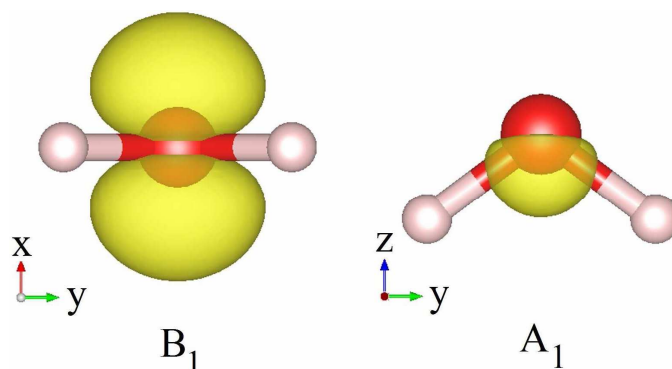


Fig.9: 3D spin density plots in the (x,y) and (z,y) plane, as evaluated just for the B<sub>1</sub> and A<sub>1</sub> symmetry magnetic natural orbitals at the CASSCF(8,8) level of theory. An isosurface value of 0.015 a.u. was selected, with maxima of spin density equal to 0.596 a.u. for B<sub>1</sub> symmetry orbital and 0.250 a.u. for A<sub>1</sub> symmetry orbital.

Figure 9, 10 and 11 report the 3D plot of the two magnetic natural orbitals (NOs) densities, of their sum and of the total spin density, respectively, for the CASSCF(8,8) level of theory wavefunction. For magnetic orbitals,  $\rho(\mathbf{r}) \equiv s(\mathbf{r})$ ,  $\nabla^2\rho(\mathbf{r}) \equiv \nabla^2s(\mathbf{r})$ ,  $\rho_\alpha(\mathbf{r}) \equiv s(\mathbf{r})$ ,  $\nabla^2\rho_\alpha(\mathbf{r}) \equiv \nabla^2s(\mathbf{r})$  while  $\rho_\beta(\mathbf{r})$  and  $\nabla^2\rho_\beta(\mathbf{r})$  are both null, so that only  $s(\mathbf{r})$  and  $\nabla^2s(\mathbf{r})$  values need to be reported (Table 6, values in parentheses). It is very important to stress that  $s(\mathbf{r})$  and  $\nabla^2s(\mathbf{r})$  contributions due to the remaining orbitals are obtained by subtracting those of the magnetic orbitals from the total  $s(\mathbf{r})$  and  $\nabla^2s(\mathbf{r})$  values. Their contributions may differ from zero at a given point, despite they are both null when integrated over the whole space.

<sup>k</sup> pop=noab option G09 program package; For CASSCF method, G09 apparently doesn't calculate and save spin density information. To this aim the IOP(5/72=1) option is mandatory, furthermore at the bottom of input file before the name selected for the .wfn file a "1 1" string needs to be introduced. Finally, SlaterDet option should be used in this case in the CASSCF calculation. In this way is possible to recover a correct  $\alpha$ -density through the pop=noa option (but not the correct spin density through pop=noab, nor the correct  $\beta$ -density through pop=nob). From the total density and the  $\alpha$ -density the electron spin density and electron spin density Laplacian is obtained by difference:  $s(\mathbf{r}) = 2\rho_\alpha(\mathbf{r}) - \rho(\mathbf{r})$ ;  $\nabla^2s(\mathbf{r}) = 2\nabla^2\rho_\alpha(\mathbf{r}) - \nabla^2\rho(\mathbf{r})$ .

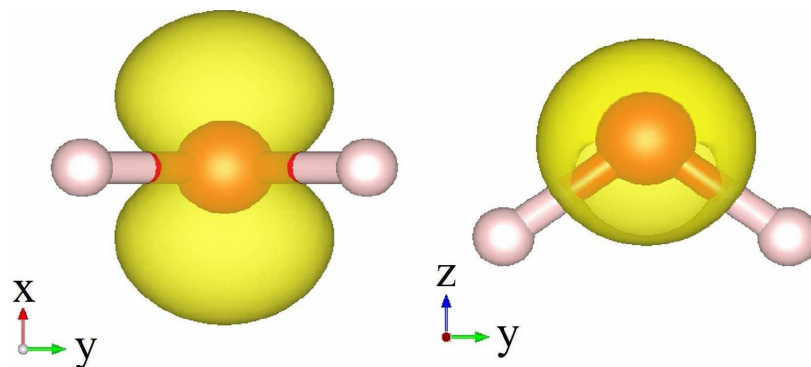


Fig.10: Same as Fig.9 above, but summing up the spin density contributions of the  $B_1$  and  $A_1$  symmetry magnetic natural orbitals. Maxima of spin density fall at 0.603 a.u.

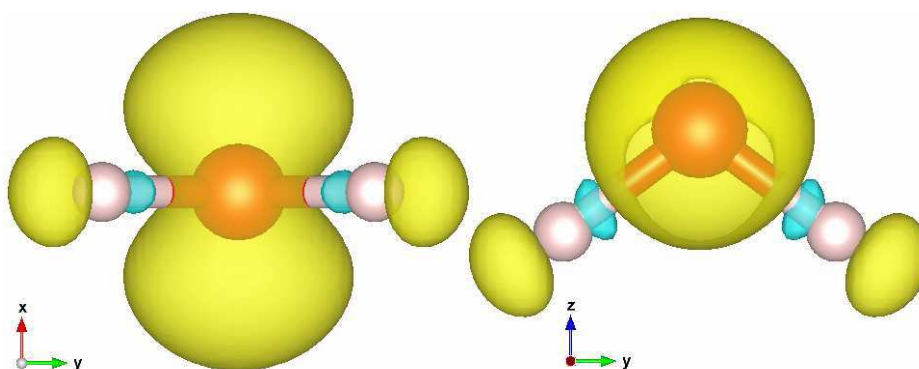


Fig.11: As Figures 9 and 10 above but plotting the total spin density. The maxima and minima of spin density fall at 0.618 a.u and -0.008 a.u. respectively.

As already discussed in the previous paragraph, besides the (3,-1) bond critical point (bcp) of the  $\rho(\mathbf{r})$  distribution (bcp **1**, Fig. 1), suitable reference points (rps) of the  $-\nabla^2\rho(\mathbf{r}) = L(\mathbf{r})$  field for the SF analysis have been selected (Fig. 1).

Table 6 reports the values of  $\rho(\mathbf{r})$ ,  $\rho_\alpha(\mathbf{r})$ ,  $\rho_\beta(\mathbf{r})$ ,  $s(\mathbf{r})$  and the corresponding Laplacians at each reference point mentioned; such results have been obtained using wavefunctions evaluated at a common geometry (the UHF/6-311++G(2d,2p) optimized geometry<sup>1</sup>). The locations of each reference point differ as they correspond to the selected critical point for the considered wavefunction; however since each critical point comes from the analysis of  $\rho(\mathbf{r})$ , they almost coincide for the three computational levels shown in Table 6.

<sup>1</sup> In case of the UHF/6-311++G(2d,2p) level of theory we refer to the spin-contamination annihilated wavefunction

RP	$\rho(\mathbf{r})$	$\nabla^2\rho(\mathbf{r})$	$s(\mathbf{r})$	$\nabla^2s(\mathbf{r})$	$\rho_\alpha(\mathbf{r})$	$\nabla^2\rho_\alpha(\mathbf{r})$	$\rho_\beta(\mathbf{r})$	$\nabla^2\rho_\beta(\mathbf{r})$
<i>CASSCF(8.8)//UHF(6-311++G(2d.2p))</i>								
1	0.291	-2.06	-0.0075 (0.0020)	0.24 (0.13)	0.142	-0.91	0.149	-1.15
2	0.888	-5.08	0.0763 (0.0508)	0.90 (1.21)	0.482	-2.09	0.406	-2.99
3	1.022	-6.64	0.0219 (0.0038)	1.73 (1.97)	0.522	-2.46	0.500	-4.18
4	0.614	-1.23	0.3824 (0.3722)	-4.45 (-4.40)	0.498	-2.84	0.116	1.61
<i>UHF/(6-311++G(2d.2p)) spin contamination annihilated wavefunction</i>								
1	0.288	-2.14	-0.0050 (0.0029)	0.21 (0.11)	0.141	-0.96	0.146	-1.18
2	0.888	-5.17	0.0631 (0.0511)	1.07 (1.18)	0.475	-2.05	0.412	-3.12
3	1.030	-6.85	0.0051 (0.0037)	2.04 (1.95)	0.518	-2.40	0.513	-4.45
4	0.610	-1.18	0.3818 (0.3677)	-4.54 (-4.34)	0.496	-2.86	0.114	1.68
<i>ROHF//UHF(6-311++G(2d.2p))</i>								
1	0.287	-2.14	0.0031	0.11	0.145	-1.01	0.142	-1.13
2	0.890	-5.21	0.0483	1.20	0.469	-2.01	0.421	-3.20
3	1.031	-6.87	0.0032	1.95	0.517	-2.46	0.514	-4.41
4	0.607	-1.13	0.3637	-4.28	0.485	-2.7	0.121	1.57

Tab.6: Values of electron density, electron spin density, Laplacian of total  $\rho(\mathbf{r})$ , Laplacian of the  $\alpha$  and  $\beta$  counterparts of  $\rho(\mathbf{r})$  and Laplacian of spin density distribution (in a.u.) at each critical point considered in Fig.1 for the three adopted computational levels of theory; in parentheses the contributions from the two magnetic NOs are reported. For these NOs  $\rho(\mathbf{r}) \equiv s(\mathbf{r})$ ,  $\nabla^2\rho(\mathbf{r}) \equiv \nabla^2s(\mathbf{r})$ ,  $\rho_\alpha(\mathbf{r}) \equiv s(\mathbf{r})$ ,  $\nabla^2\rho_\alpha(\mathbf{r}) \equiv \nabla^2s(\mathbf{r})$  while  $\rho_\beta(\mathbf{r})$  and  $\nabla^2\rho_\beta(\mathbf{r})$  are both null; in the specific case of the ROHF wavefunction,  $s(\mathbf{r}) \equiv \rho_{\alpha,\text{mag}}(\mathbf{r})$  and  $\nabla^2s(\mathbf{r}) \equiv \nabla^2\rho_{\alpha,\text{mag}}(\mathbf{r})$  where  $\rho_{\alpha,\text{mag}}(\mathbf{r})$  and  $\nabla^2\rho_{\alpha,\text{mag}}(\mathbf{r})$  denote the magnetic contribution to  $\rho_\alpha(\mathbf{r})$  and  $\nabla^2\rho_\alpha(\mathbf{r})$ , respectively.

The decomposition of  $\rho(\mathbf{r})$  and  $s(\mathbf{r})$  in contributions given by the two magnetic orbitals and the reaction orbitals show how the former dominate both the large  $s(\mathbf{r})$  and its largely negative  $\nabla^2s(\mathbf{r})$  at the two symmetric (3,+1) L( $\mathbf{r}$ ) points **4** and **4'** as well as the spin density depletion ( $\nabla^2s > 0$ ) at the in-plane NBCC **3** associated to the lone pair (see Tab.6). At bcp **1** in the case of the CASSCF(8,8) and UHF level of theory, the remaining orbitals overreact to the small positive  $s(\mathbf{r})$  contribution due to the two magnetic orbitals.



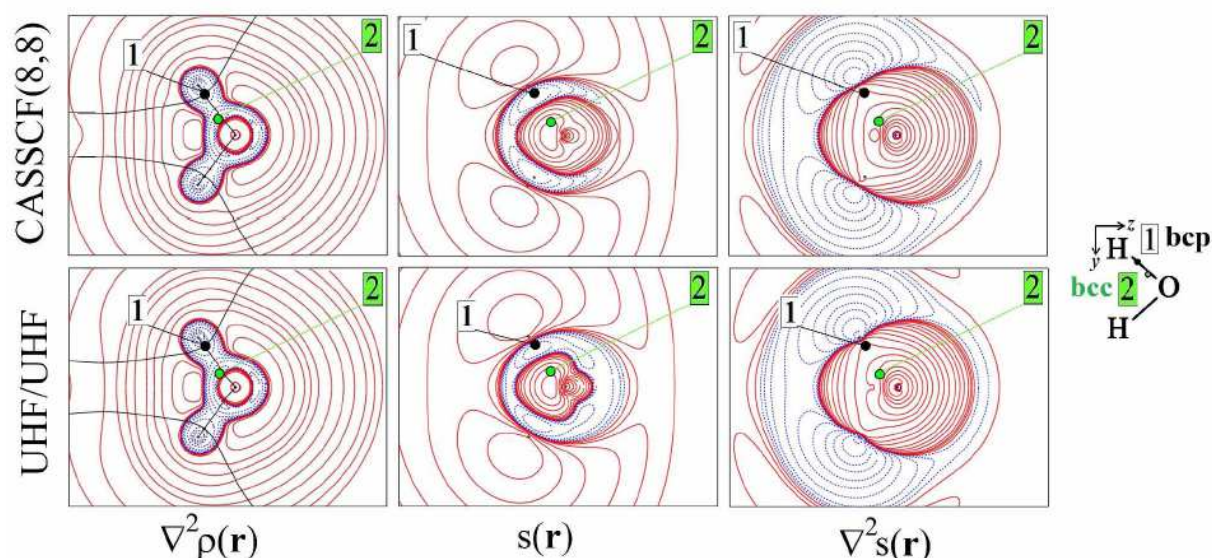


Fig.12: Electron density Laplacian, electron spin density and its Laplacian in the  $(y,z)$  plane for  ${}^3B_1$   $H_2O$ , at (top) CASSCF(8,8) and (bottom) UHF/UHF spin-contamination annihilated computational levels. Atomic units (a.u.) are used throughout. Contour maps are drawn at interval of  $\pm(2,4,8)\cdot 10^n$ ,  $-4 \leq n \leq 0$  ( $s(\mathbf{r})$ ,  $\nabla^2 s(\mathbf{r})$ ) and  $-3 \leq n \leq 0$  ( $\nabla^2 \rho(\mathbf{r})$ ). Dotted blue (full red) lines indicate negative (positive) values and full black lines mark boundaries of atomic basins. The O–H bond critical point (bcp, 1) and the bonded charge concentration point (BCC, 2) are shown as black and green dots, respectively.

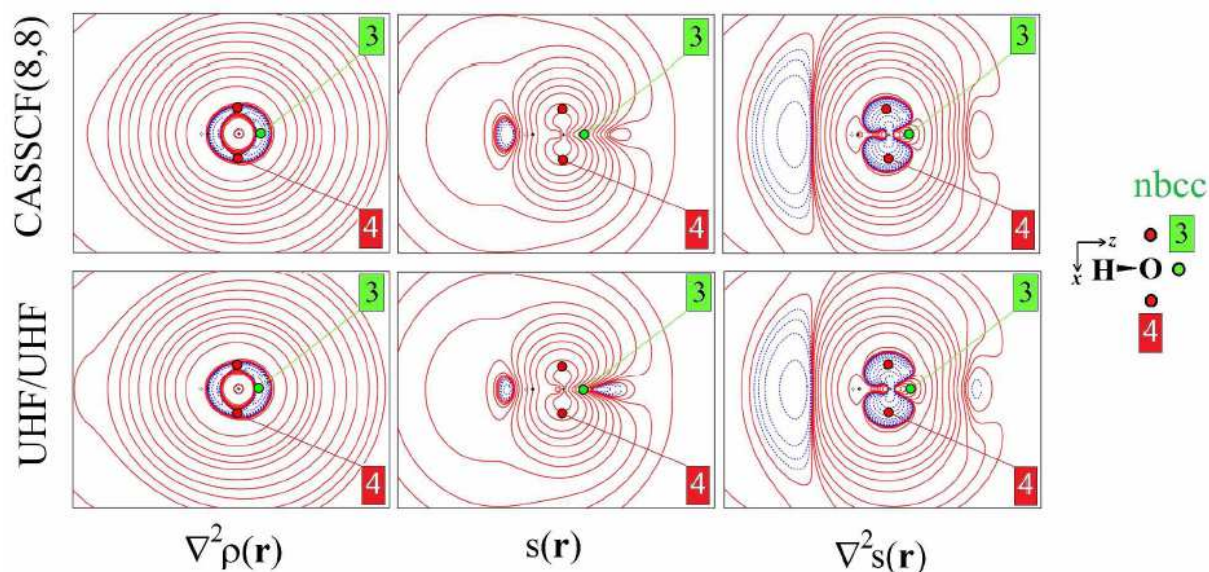


Fig.13: Electron density Laplacian, spin density and its Laplacian in the  $(x,z)$  plane, at (top) CASSCF(8,8) and (bottom) UHF/UHF spin contamination annihilated computational levels. Contour levels as in Figure 12. The non-bonded charge concentration (NBCC, 3) and the  $(3,+1)$   $L(\mathbf{r})$  rcp (4) are shown as green and red dots, respectively.

The last consideration is not true in the case of the ROHF wavefunction, because the reaction mechanism is unattainable and, as a consequence,  $s(\mathbf{r})$  remains positive at this CP. Considering the bonded charge concentration (BCC 2, coloured green), the contributions to  $s(\mathbf{r})$  from the two set of orbitals are equal in sign and definitely larger for the magnetic orbital set, but the  $\nabla^2 s(\mathbf{r})$  value of

the magnetic orbitals is positive ( $\nabla^2 s = 1.2$  au) and larger in magnitude than that of the remaining orbitals which is negative ( $\nabla^2 s = -0.3$  au and  $-0.1$  au for the CASSCF(8,8) and the UHF wavefunctions, respectively). This leads to a global dilution of the spin density at BCC **2**.

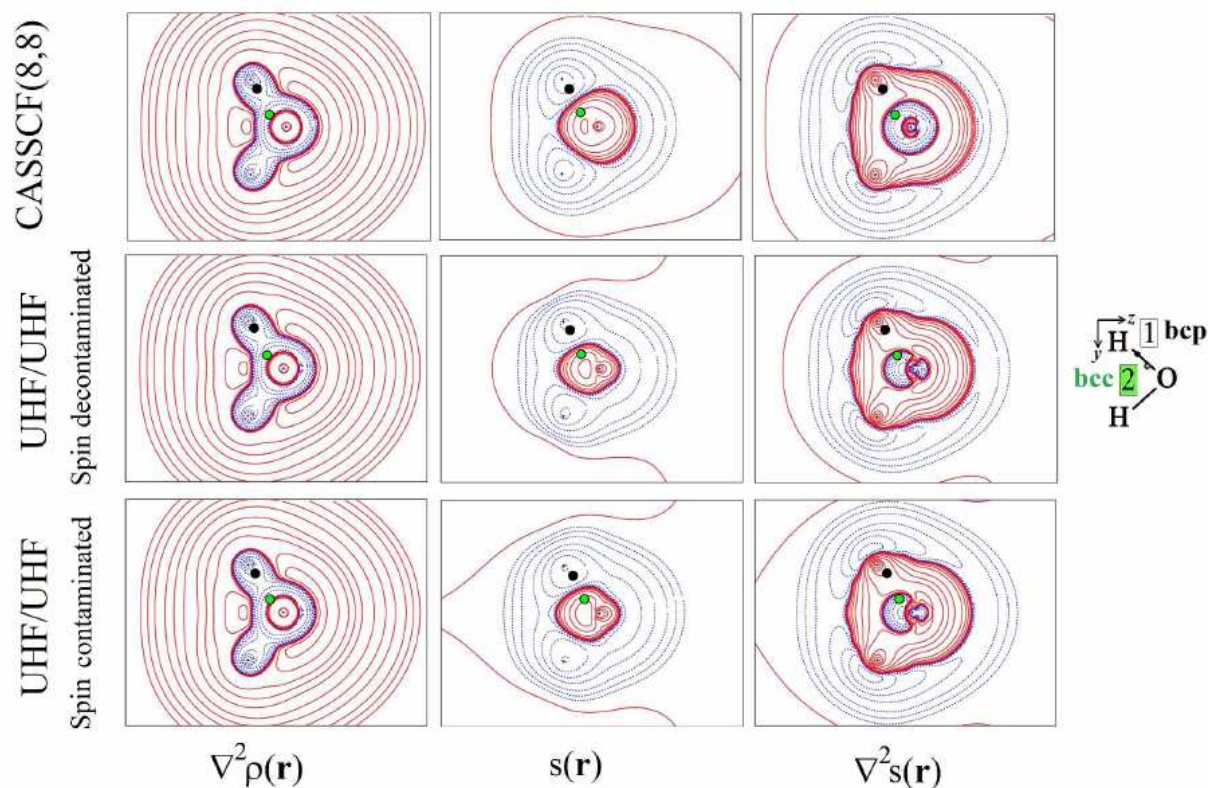


Fig.14: Electron density Laplacian, electron spin density and its Laplacian in the  $(y,z)$  plane for  ${}^3B_1$   $H_2O$  due just to the non-magnetic natural orbitals for the CASSCF(8,8), the UHF spin-contamination annihilated and the UHF spin-contaminated computational levels. Atomic units (a.u.) are used throughout. Contour levels as in Fig.12. The O–H bond critical point (bcp, **1**) and the bonded charge concentration point (BCC, **2**) are shown as black and green dots.

Considering static and dynamic electron correlation at the CASSCF(8,8) level of theory, one may generally observe (Tab. 6, Figures 12-14) a similar qualitative picture relative to that at the UHF spin-contamination annihilated level; this agreement increases a lot when just contributions given by the magnetic orbitals are compared (Tab. 6). The spin density at the in-plane NBCC **3** associated to the lone pair shows a completely different behaviour. In fact the introduction of electron correlation effects raises  $s(\mathbf{r})$  by more than five times, with respect to the value of the spin-contamination annihilated wavefunction; this increase in the  $s(\mathbf{r})$  value is due the reaction or *relaxation* contribution (Tab. 6). This noticeable effect due to electron correlation can be also observed in the  $s(\mathbf{r})$  maps reported in Fig.13, where the small region of negative spin density of the UHF model lying close to the non bonded maximum disappears in the corresponding CASSCF(8,8) plot. The effects of electron correlation are even more evident if the UHF model spin contamination is not annihilated (the plot for this model is not shown, however, in Fig. 13). It is clear that the

electron correlation effects involve the *reaction* orbitals, as it is possible to deduct from Fig. 14 and Fig. 15 where maps of  $s(\mathbf{r})$  and  $\nabla^2 s(\mathbf{r})$  relative to the planes shown in Fig. 12-13 and obtained using only these natural orbitals are reported.

It is now interesting to comment briefly on the different portraits of the ED and of the electron spin density Laplacians. In water,  $\nabla^2 \rho(\mathbf{r})$  implies relatively contracted valence shell charge concentration (VSCC) zones, mainly localized around nuclei and along covalent bonds, while the  $\nabla^2 s(\mathbf{r})$  negative regions are definitely more extended and possibly disjoint (Fig. 12 and 13). Furthermore, a given region of space may occur to be diluted for  $\rho(\mathbf{r})$  and concentrated for  $s(\mathbf{r})$  or vice-versa.

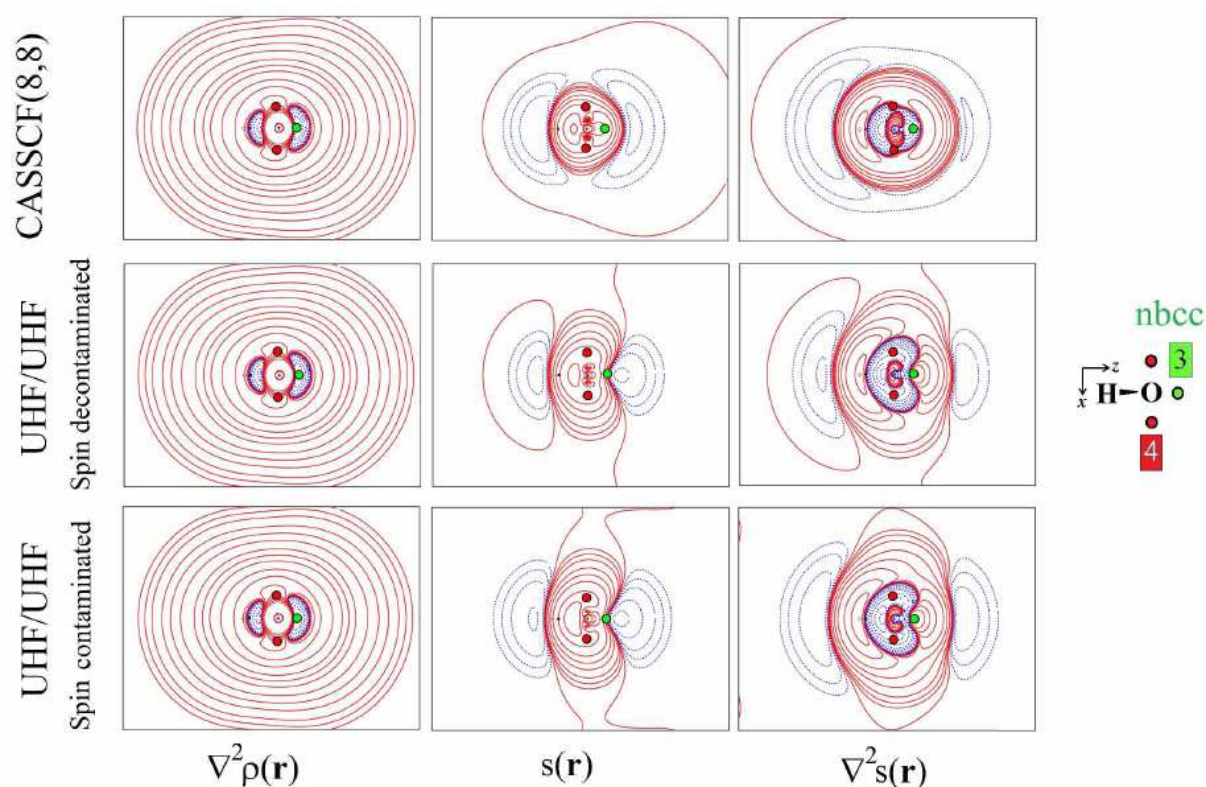


Fig.15: As in Fig.14 above, in the (x,z) plane with same contour levels. The non-bonded charge concentration (NBCC **3**) and the (3,+1)  $L(\mathbf{r})$  critical points (CPs **4** and **4'**) are shown as green and red dots.

### 2.3.6 Electron spin density in terms of its $SF_s$ percentage:

We are now ready to investigate how the spin density is reconstructed in terms of spin density  $SF$  atomic contributions (eq. 4) at the chosen reference points of  ${}^3B_1$   $H_2O$ . We will show that by decomposing the spin density in terms of *non-local* effects precious chemical insight may be retrieved. Table 5 reports the Bader's atomic spin population in water triplet for a wavefunction evaluated using the UHF spin contamination annihilated level of theory. These populations,

however, differ marginally with the level of theory, ranging from 0.29 to 0.31 for the H atom and from 1.42 to 1.39 for the O atom. They also indicate that  $\approx 2/3$  of the unpaired electrons are localized in the oxygen atomic basin ( $\Omega_{(O)}$ ). The Laplacian of the electron spin density distribution integrates to about 0.02 a.u. in the hydrogen atomic basin and to  $-0.04$  a.u. in the oxygen atomic basin, for all adopted levels of theory. The integrated values of  $\nabla^2 s(\mathbf{r})$  reveals the influence exerted by each atom at great distance, i.e. when the Green's factor<sup>m</sup> is small enough to be safely taken out from the integral as a constant. Therefore, H atoms in water triplet will tend to exploit a  $\beta$  effect at large distances, while the O atom is expected to behave opposedly, hence to act as an  $\alpha$  source, at such distances.

In general, regardless of the positive or negative value of the integrated spin density Laplacian, the actual sign of the  $SF_s$  descriptor (eq. 4) will depend on the choice of the reference point which determines, through the Green's factor, the relative weight of the local cause  $\nabla^2 s(\mathbf{r}')$  in the various regions of the integrated atom. In Figure 16 the relative SF and  $SF_s$  percentage contributions from each atomic basins of the  $^3B_1$  H<sub>2</sub>O molecular system and at each previously considered critical points (see Fig. 1 and Tab. 6 and 7) are reported for the CASSCF(8,8) model. Analogous data for the spin-contamination annihilated UHF and for the ROHF wavefunctions are shown in Figures 17 and 18. The corresponding SF and  $SF_s$  absolute values are listed in Table 7 for all investigated models. Considering the bond critical point (bcp **1**), the SF decomposition of the electron density distribution reveals a classical covalent polar bond with the oxygen atom (the more electronegative atom in the bond) providing  $\approx 60\%$  of  $\rho(\mathbf{r})$  at the bcp. The remaining  $\approx 40\%$  is due to the bonded hydrogen, while its symmetry-related H' atom has an almost negligible influence. The reconstruction of the electron spin density transmission information, obtained through the  $SF_s$  chemical descriptor, is completely different. At the bcp **1**, the O atom  $SF_s$  contribution is negative for both the CASSCF(8,8) and the UHF spin contamination annihilated levels of theory, which enable spin relaxation. The corresponding  $SF_s$  percentage contribution is positive (154.6% at the CASSCF (8,8) level and 275.9% at the UHF spin contamination annihilated level), indicating a  $\beta$  effect in this context (red colour code in Fig. 16 and 17), since it concurs to the negative  $s(\mathbf{r})$  value at the bcp (Fig. 16 and 17).

---

<sup>m</sup> i.e. the reciprocal of the distance  $(|\mathbf{r}-\mathbf{r}'|)^{-1}$  in eq.5

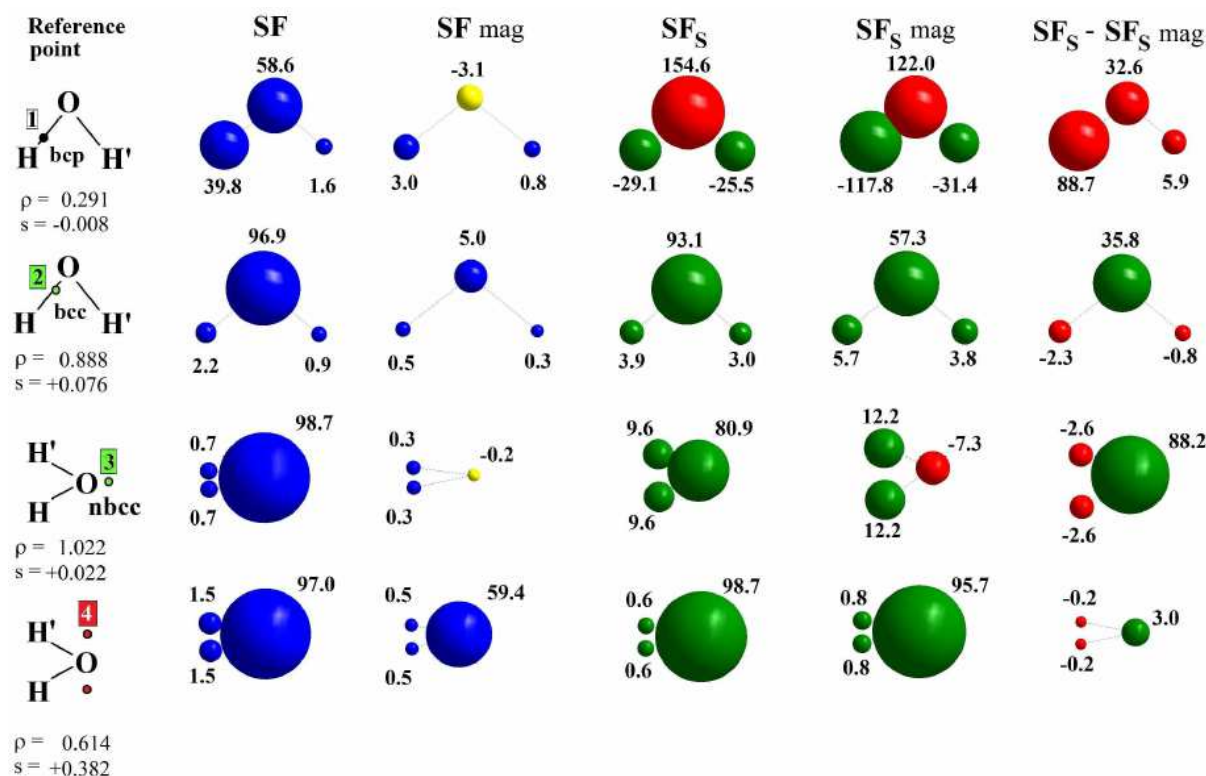


Fig. 16: SF and SF<sub>S</sub> percentage contributions at reference points (rps) for <sup>3</sup>B<sub>1</sub> H<sub>2</sub>O at the CASSCF(8,8) computational level. The separate contributions to SF<sub>S</sub> due to the magnetic (SF<sub>S</sub> mag) and the remaining (SF<sub>S</sub> - SF<sub>S</sub> mag) natural orbitals are also shown (for SF only those due to magnetic orbitals, denoted as SF mag). Each atom is displayed as a sphere, whose volume is proportional to the SF and SF<sub>S</sub> percentage contribution to  $\rho(\mathbf{r})$  or  $s(\mathbf{r})$  values at the rp (first column). Colour codes: blue (yellow) atoms act as positive (negative) sources for  $\rho(\mathbf{r})$  at rp considered; green (red) atoms act as positive (negative) sources for  $s(\mathbf{r})$  at rp, hence yielding a  $\alpha$  ( $\beta$ ) effect (the sign of percentage sources is instead positive or negative whether the atomic source concurs or opposes to electron spin density at rp).

Both hydrogen atomic basins counteract the influence of the O atom through an  $\alpha$  effect; this picture of the  $s(\mathbf{r})$  reconstruction is confirmed by the extended zone of negative  $\nabla^2 s(\mathbf{r})$  in their basins (see Fig. 12 and 13). Such description reflects and quantifies a spin polarization mechanism, where the full pairing of covalent O–H bonds in the X<sup>1</sup>A<sub>1</sub> water ground state is perturbed by the presence of unpaired electrons in the triplet excited state. Interestingly, at the CASSCF(8,8) level of theory the symmetry-related H' atom provides a quite large SF<sub>S</sub> contribution at bcp **1**, very similar to that from H; on the contrary for the UHF model the hydrogen atomic basins give quite different contributions to the  $s(\mathbf{r})$  value at bond critical point; the reported discrepancy is an important effect due to the introduction of electron correlation in wavefunction calculation. In both cases it is however possible to conclude that the spin polarization in the molecular plane takes place both through bond and through space mechanisms. More importantly, both mechanisms imply that the strong  $\beta$  effect at the bcp due to the oxygen atom is partly (in case of CASSCF(8,8) level of theory)

or largely (UHF spin contamination annihilated computational level) counteracted by both hydrogen atoms.

Point	H		O		H'	
	SF	SFs	SF	SFs	SF	SFs
CASSCF(8,8)//UHF/6-311++G(2d,2p)						
<b>1</b>	0.1155	0.0022 (0.0087)	0.1704	-0.0115 (-0.0091)	0.0046	0.0019 (0.0023)
<b>2</b>	0.0192	0.003 (0.0044)	0.8585	0.0713 (0.0439)	0.008	0.0023 (0.0029)
<b>3</b>	0.0068	0.0021 (0.0027)	1.0088	0.0177 (-0.0016)	0.0068	0.0021 (0.0027)
<b>4</b>	0.0091	0.0024 (0.0031)	0.5953	0.3761 (0.3644)	0.0091	0.0024 (0.0031)
UHF/6-311++G(2d,2p) spin-contamination annihilated wavefunction						
<b>1</b>	0.1109	0.0063 (0.0106)	0.1725	-0.0137 (-0.0102)	0.0041	0.0024 (0.0026)
<b>2</b>	0.017	0.0042 (0.0049)	0.8622	0.0561 ( 0.0433)	0.0073	0.003 (0.0033)
<b>3</b>	0.0061	0.0027 (0.0030)	1.0178	-0.0004 (-0.0022)	0.0061	0.0027 (0.0030)
<b>4</b>	0.0082	0.0032 (0.0035)	0.5937	0.374 ( 0.3594)	0.0082	0.0032 (0.0035)
ROHF//UHF/6-311++G(2d,2p)						
<b>1</b>	0.1104	0.0108	0.1724	-0.0102	0.0041	0.0026
<b>2</b>	0.0168	0.0049	0.8643	0.0404	0.0072	0.0033
<b>3</b>	0.0061	0.003	1.0188	-0.0027	0.0061	0.003
<b>4</b>	0.0081	0.0035	0.5901	0.3554	0.0081	0.0035

Tab.7: SF and SFs values (in a.u.) in  $^3B_1$  H<sub>2</sub>O as a function of the computational level and with contribution due to magnetic natural orbitals given in parenthesis. Values reported in this Table for SF and SFs yield the percentage source contributions at the **1–4** reference points shown in Figure 16 for CASSCF(8,8) computational level and in Figures 17 and 18 for UHF and ROHF level of theory respectively. The source contributions of magnetic natural orbitals to SF( $\Omega$ ) equal by definition those to SFs( $\Omega$ ) and are thus not reported in the Table, while their related % source contributions clearly differ; For the ROHF wavefunction,  $s \equiv s$  mag and thus  $SF_s \equiv SF_s$  mag

The comparison between the three considered computational models reveals a qualitatively similar SFs(H') contribution, but the UHF and in particular the ROHF levels of theory give a quite large overestimated counteracting  $\alpha$ -effect of the hydrogen atom involved in the O-H bond.<sup>n</sup> Further insight is provided by examining the separate contributions to SFs due to the magnetic (SFs mag) and the remaining (relaxation) orbitals (SFs - SFs mag) (see Fig. 16, 17 and 18 and Table 6 and 7). Considering the bond critical point (bcp **1**), the relaxation orbitals contributions to  $\rho(\mathbf{r})$  and  $s(\mathbf{r})$  at CASSCF(8,8) level of theory have a magnitude of about 99% and 127% respectively; moreover both the magnetic and the remaining orbitals concur to the strong  $\beta$  effect at bcp 1 due to the oxygen atom (+122.0% by the magnetic orbitals and +32.6% by the remaining orbitals). On the

other side, the two H atoms show a different counteracting  $\alpha$  effect due to the magnetic orbitals, while the remaining orbitals are concurring to the value of the electron spin density at bcp **1** with a  $\beta$ -effect (of quite different magnitude for H and H').

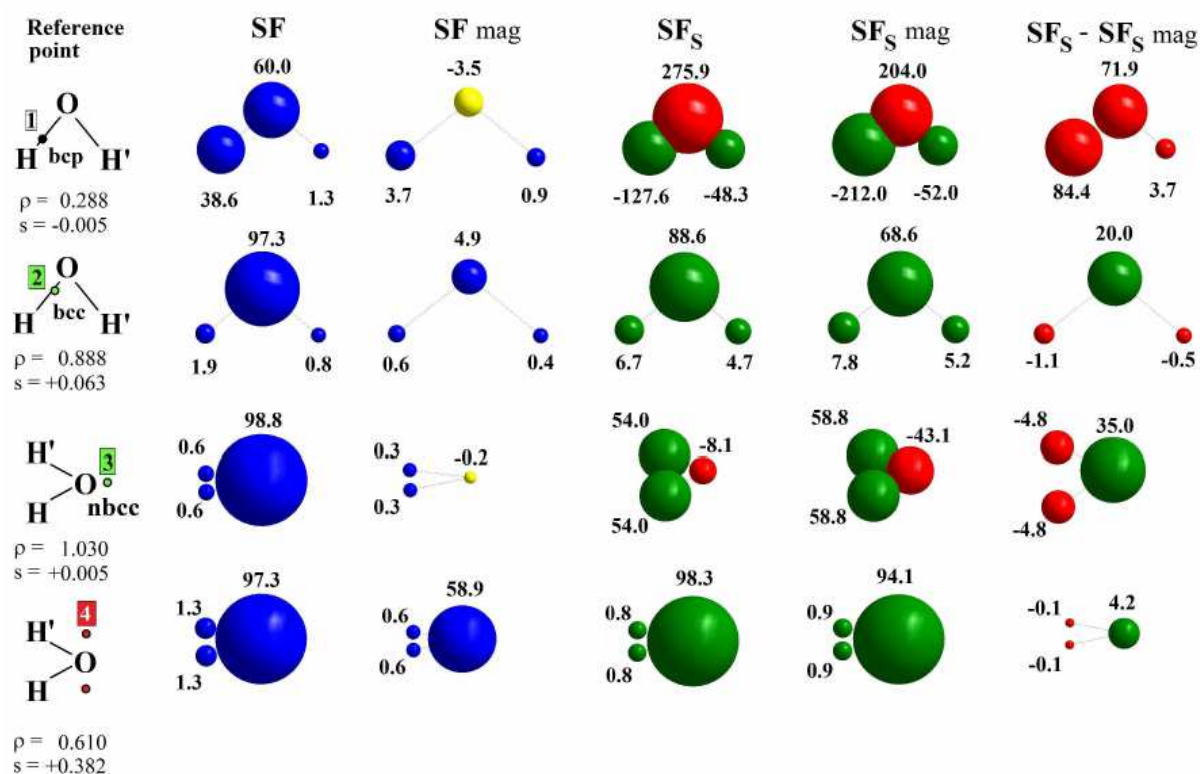


Fig.17: SF and SF<sub>S</sub> percentage contributions at some reference points (rps) for 3B<sub>1</sub> H<sub>2</sub>O at the UHF/UHF spin contamination annihilated level. The separate contributions to SF<sub>S</sub> due to the magnetic (SF<sub>S</sub> mag) and the remaining (SF<sub>S</sub> - SF<sub>S</sub> mag) natural orbitals are also shown (for SF only those due to magnetic natural orbitals, denoted as SF mag). Atoms are displayed as in Fig. 16 with same colour codes.

The decomposition of  $\rho(\mathbf{r})$  and  $s(\mathbf{r})$  in terms of SF and SF<sub>S</sub> reported in Fig.16 gives a clear picture of what are the causes of spin transmission information at the reference point considered, in fact the counteracting  $\alpha$ -effect given by the bonded hydrogen atomic basin is due to the magnetic orbitals (SF<sub>S</sub> mag = -117.8%) but is largely compensated for by the  $\beta$ -effect promoted by the remaining (bonding) orbitals ((SF<sub>S</sub> - SF<sub>S</sub> mag) = + 88.7%). The opposite is true in the case of the hydrogen atomic basin not involved in the O-H bond; in fact the relaxation orbitals have here a very small influence (+5.9 %) while the effect of the magnetic orbitals still remains significant (SFs mag = - 31.4 %)°. Both  $\rho(\mathbf{r})$  and  $s(\mathbf{r})$  are largely dominated by the oxygen atomic basin at the bonded charge concentration (BCC) reference point **2** because of the close proximity of the critical point to this

<sup>n</sup> In particular UHF contamination spin annihilated level of theory provides a contribution three times larger with respect to CASSCF(8,8) computational model while ROHF gives a contribution to  $s(\mathbf{r})$  about five times larger than for the CASSCF(8,8') level of theory.

atom. At BCC 2 the electron spin density is positive, about one order of magnitude larger than at bcp 1 (see Tab. 6), and similarly determined by the magnetic and remaining orbitals, with the former yielding  $\alpha$  contributions for both oxygen and hydrogen atomic basins. At the two symmetric saddle points **4** and **4'**, associated to the unpaired electrons,  $s(\mathbf{r})$  is two order of magnitude larger than at bcp and, like for  $\rho(\mathbf{r})$ , almost all determined by the oxygen atomic basin for all the computational levels considered (Fig. 16, 17, 18). In any case at these reference points  $s(\mathbf{r})$  is dominated by the magnetic orbitals, both for oxygen and hydrogen contributions (UHF = 95.9%; CASSCF(8,8) = 97.3%). In particular, over 93% of them, at CASSCF(8,8) level, comes from the magnetic orbital  $B_1$  since points **4** and **4'** are representative of the  $\alpha$ -spin density described by the  $O[px]$  functions. Considering the SF contributions to  $\rho(\mathbf{r})$  is possible to note the different nature of the two points **2** and **4** as in case of SFs. In fact at the BCC **2** reference point, both UHF and CASSCF(8,8) levels of theory give an almost equal contribution from the magnetic orbitals (UHF = 5.9%; CASSCF = 5.8%) with a marginal influence on the reconstruction of  $\rho(\mathbf{r})$ ; on the contrary at saddle points **4** and **4'** such influence is about ten times larger (UHF = 60.1%; CASSCF = 60.4%), though clearly not as dominant as it is for  $s(\mathbf{r})$ . At the non-bonded charge concentration (NBCC 3)<sup>p</sup>  $s(\mathbf{r})$  is positive, with magnitude largely dependent on the wavefunction model. In fact, at this reference point the value of  $\rho(\mathbf{r})$  is dominated by the oxygen atomic basin for each computational levels of theory, but  $s(\mathbf{r})$  is, at the UHF spin contamination annihilated and ROHF computational models, over-determined by the hydrogen atoms (UHF=108%; ROHF=183.1% see Fig. 17 and 18), despite the NBCC 3 lies on the opposite side of these atoms. The introduction of static and dynamic correlation at the CASSCF(8,8) level of theory, enables one to recover a much less unanticipated result, as the two hydrogen atoms and the oxygen atom contribute, respectively, to 19% and 81% of the  $s(\mathbf{r})$  value. It is possible to explain the behaviour of the different levels of theory by considering the separated orbital contributions. The large  $\alpha$ -effect from the hydrogen atoms results in the UHF model from a dominant  $\alpha$ -contribution due to the magnetic orbitals, slightly opposed by the  $\beta$ -effect due to the remaining orbitals. This is not true for the oxygen atom because these orbital effects are reversed and the  $\beta$ -effect of the magnetic orbitals slightly prevails. More importantly, only the  $A_1$  totally symmetric magnetic orbital is really involved in such mechanisms.

---

<sup>o</sup> Due to the increased distance from the bcp, in this case the influence of the magnetic orbitals is clearly lower with respect to the bonded hydrogen.

<sup>p</sup> This reference point correspond to the oxygen atomic basin's lone pair.



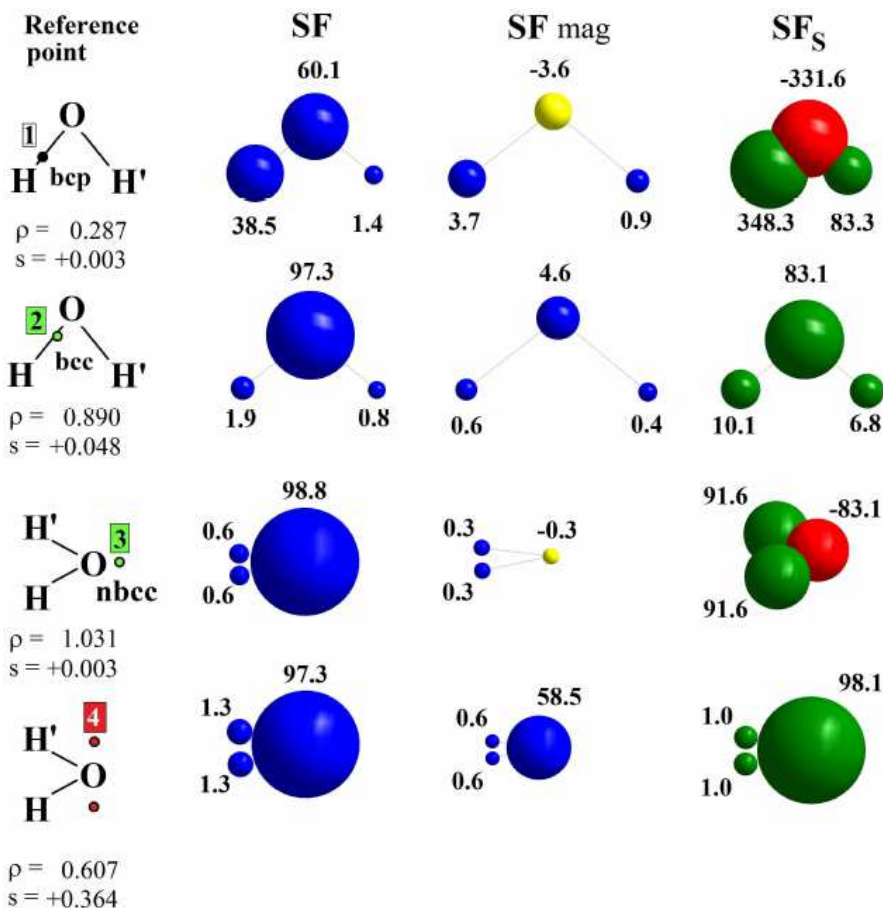


Fig.18: SF and SF<sub>S</sub> percentage contributions at rps for <sup>3</sup>B<sub>1</sub> H<sub>2</sub>O at the ROHF/UHF spin contamination annihilated geometry level. The separate contributions to SF and SF<sub>S</sub> due to the magnetic natural orbitals are also shown (SF mag and SF<sub>S</sub> mag, respectively). Atoms are displayed as in Fig. 16 with same colour codes.

In fact the A<sub>1</sub> magnetic orbital allows the hydrogen atomic basin to exert a direct influence on the positive spin density at the non bonded charge concentration, while causing the oxygen atom to partly oppose to such influence. In the case of the ROHF wavefunction, the SF<sub>S mag</sub><sup>q</sup> contributions from all the atomic basins are very much alike in magnitude to those of the UHF model (see Tab. 7). In any case, because of the lack of the spin relaxation mechanism, the dominance of the hydrogen atoms  $\alpha$ -effect is even largely enhanced for ROHF (compare Fig. 17 and 18). The effect of including a larger amount of electron correlation (CASSCF(8,8) model) is to enhance by one order of magnitude, from 0.0018 (UHF) to 0.0193 a.u., the contribution to SF<sub>S</sub>(O) from the non magnetic orbitals, while that from magnetic orbitals is very similar in the two models, both for O and H atoms. As a consequence the percentage SF<sub>S</sub> sources for the CASSCF(8,8) and the UHF (or ROHF) models at NBCC **3** look very different among each other (Fig. 16, 17 and 18). Finally, it is possible to assess that SF<sub>S</sub> contributions, and in particular their magnetic and non magnetic components, can distinguish the different nature of critical points associated to the unpaired-

<sup>q</sup> It is worth to stress that SF<sub>S mag</sub>  $\equiv$  SF<sub>S</sub> for ROHF level of theory

electrons or to the lone-pair electrons (NBCC **3** and CPs **4** and **4'** respectively), while the corresponding SF values do not (Fig. 16, 17 and 18).

### *Conclusions:*

Analogously to the source function for the electron density (SF), the spin density source function (SF<sub>S</sub>) reconstructs the electron spin density at a reference point in terms of separate atoms or group of atoms contributions. It is clear that the reconstruction of the spin density information transmission from the paramagnetic center to the non-magnetic ones, is strongly dependent on the choice of the reference point because of the large anisotropy of  $s(\mathbf{r})$  and  $\nabla^2s(\mathbf{r})$  within atomic basins. For this reason, the electron spin density at a point can be almost fully determined by the atomic basin to which the point belongs to as it is the case, in the molecular system water triplet ( $^3B_1$  H<sub>2</sub>O), of the saddle points **4** and **4'** associated to the unpaired electrons in the O(p<sub>z</sub>) atomic orbital.<sup>[26]</sup> At the same time, the opposite may also occur, and even in regions within the basin of the paramagnetic center as it is the case of the charge concentration maximum associated to the lone pair, lying 0.33 Å from the oxygen atomic basin and on opposite side with respect to the hydrogen atoms. At this point, the spin density is very low in value and almost fully determined by the two distant H atoms. In particular, if only the limited electron correlation enabled by the UHF model is included, the  $s(\mathbf{r})$  value found at this point is even overestimated (SF<sub>S</sub>(H+H')% = 108) by the contribution brought in by the two hydrogen atomic basins. In water triplet, the dominant oxygen atom contributions and the dominant hydrogen atoms contributions for the different spin density computational levels of theory evaluated at reference points associated to the unpaired and to the lone pair electrons, respectively, have been rationalized in terms of magnetic and relaxation or reaction contributions. Such kind of analysis allows the chemical interpretation of the electron spin density transmission and, in particular, has shown how static and dynamic electron correlation effects should be considered in the reconstruction of  $s(\mathbf{r})$  in terms of atomic (or group of atoms) contributions. In fact, when electron correlation effects are introduced (CASSCF(8,8) level of theory), the oxygen atomic basin contribution becomes dominant also for the spin density at the lone pair position, as expected. It is very important to highlight that the electron correlation leaves almost unaffected both the oxygen and the hydrogen atomic basins magnetic contributions to the spin density at such position, while it increases the oxygen relaxation contribution by one order of magnitude with respect to the UHF spin contamination annihilated computational model. This means that at the uncorrelated (ROHF) or almost uncorrelated (UHF) levels of theory the magnetic orbitals are already very similar to those of the CASSCF(8,8) model where electron correlation is

included<sup>f</sup>. Increasing the wavefunction quality has instead a noticeable effect on the reaction or relaxation component. The magnetic term does not necessarily determine a positive spin density at any reference point, but may instead produce a decrease of the local spin density ( $\beta$ -effect). Furthermore, the relaxation term may either concur or counteract the magnetic term in determining the spin density at a given point, regardless its link to an orbital density integrating to a null spin population over the whole space.

### ***2.3.7 Transferability of $\rho(\mathbf{r})$ and $s(\mathbf{r})$ in n-alkanes and n-alkyl radicals: similarities and differences as viewed through the Source Function descriptors***

Both electron density and electron spin density at a point could be seen as caused by an internal source contribution from the atom where the point is located and by a sum of source contributions from the remaining atoms, or groups of atoms, within a molecule. In chemistry the atomic group transferability paradigm could be deduced from a huge amount of experimental evidences and it is corroborated by QTAIM from a quantitative point of view for a large variety of group properties<sup>[8]</sup>. Using the SF tool one may view chemical transferability from a new and insightful perspective. It is worth to highlight that this topological descriptor enables one to distinguish the case of a) *perfect transferability* which is achieved when the electron density of a piece of matter is fully transferable, from the case of b) *compensatory transferability*, exemplified for instance by the occurrence of a constant electron population for an atomic group, obtained through a compensation of charge transfers within the group, or by the situation of a constant atomic population that, however, realizes, only through significant charge polarizations within the atom itself<sup>[8-10; 20,21]</sup>. Perfect transferability implies that not only the group electron density be transferable but also that the sum of contributions to that density from the remaining atoms, or group of atoms, in the system remains constant. As it is well known<sup>[6]</sup>, the terminal methyl group in n-alkanes, past ethane, is characterized by very transferable atomic properties like energy, electron population, volume and spectroscopic properties, regardless of the length of the chain. The transferability of the electron distribution in the methyl group is so good that a constant value for  $\rho(\mathbf{r})_b$  at its terminal C-H bond is also observed, past ethane (see Tab. 8). Such a transferability realizes because of a constant contribution from the CH<sub>3</sub> group and a constant external contribution from the remaining atoms in the chain, regardless of its length.

---

<sup>f</sup> In terms of both their local properties at the critical points of  $\rho(\mathbf{r})$  or  $\nabla^2\rho(\mathbf{r})$  and of their SF and SF<sub>S</sub> contributions

$SF(\mathbf{r}_b; \Omega\Sigma)$	$\rho(\mathbf{r})_b$ (H-CH <sub>2</sub> )	$SF(\mathbf{r}_b; \text{ext})^s$
ethane		
H-CH <sub>2</sub> -----CH <sub>2</sub> -----H 0.2704 0.0100 0.0026	0.2830	0.0126
propane		
H-CH <sub>2</sub> -----CH <sub>2</sub> -----CH <sub>3</sub> 0.2701 0.0091 0.0035	0.2827	0.0126
butane		
H-CH <sub>2</sub> -----CH <sub>2</sub> -----CH <sub>2</sub> -----CH <sub>3</sub> 0.2701 0.0091 0.0020 0.0016	0.2827	0.0127
pentane		
H-CH <sub>2</sub> -----CH <sub>2</sub> -----CH <sub>2</sub> -----CH <sub>2</sub> -----CH <sub>3</sub> 0.2702 0.0090 0.0019 0.0008 0.0009	0.2827	0.0127

Tab.8: Electron density transferability as viewed through the Source Function, in n-alkyl radicals. The electron densities at a terminal C-H bcp are reported along with their total SF contributions from the various CH<sub>2</sub> and CH<sub>3</sub> groups in each system. All values are given in atomic units (a.u.). Structures of all the molecular systems here presented are obtained performing Gaussian09 QM optimizations *in vacuo* at UPBE1PBE level of theory, using 6-311+G\*\* as basis set.

To study the transferability of the electron spin density, the corresponding series of n-alkyl radicals were chosen; all the wave functions for all the molecular systems were calculated by the UPBE1PBE/6-311+G\*\* level of theory, after optimizing their geometries *in vacuo* at the same theoretical level.<sup>[27]</sup> All the alkyl radicals are characterized by two extended chain conformations, in particular the one we studied is the more stable. In such conformation the radical carbon 2p atomic orbital housing the unpaired electron is eclipsed to a  $\beta$ -CH bond. Tables 8, 9 and 10 report the values of  $\rho(\mathbf{r})$  and  $s(\mathbf{r})$  considering both a terminal CH bond critical point and the  $-\nabla^2\rho(\mathbf{r})$  (3,-1) non bonded charge concentration (NBCC) critical point corresponding to the unpaired electron on the radical terminal methyl group CH<sub>2</sub><sup>•</sup> as reference points. The results (Tables 9 and 10) show how the terminal methyl radical group and the neighboring methylene group produce a significant contributions to the  $s(\mathbf{r})$  to the reference points considered, while this is not true for the remaining group moieties within the molecular system. Interestingly, for the covalently linked atoms SF<sub>S</sub> contributions are opposite in sign denoting a spin polarization along these bonds. More importantly, the analysis of the reconstruction of  $s(\mathbf{r})$  in terms of SF<sub>S</sub> contributions due to all the atomic groups reveals that the transferability is also ensured for the spin electron density and not just for  $\rho(\mathbf{r})$ ; in fact the contribution from the terminal methyl radical is constant throughout the series and this is true also for the contribution from the external groups ( $s(\mathbf{r})_{\text{ext}} = 0.0079$  au). Despite its very low

<sup>s</sup>  $SF(\mathbf{r}_b; \text{ext}) \equiv \Sigma$  of SF contributions to  $\rho(\mathbf{r})_b$  from groups external to the CH<sub>3</sub> group

value, the transferability for  $s(\mathbf{r})$  is also ensured if the CH terminal bond critical point<sup>†</sup> is considered. Also at this reference point, the reconstruction of  $s(\mathbf{r})$  in terms of  $SF_S$  contributions show that the external groups give a negative contribution to the spin density, in clear opposition with respect to the terminal  $CH_2$  radical contribution.

$SF_S(\mathbf{r}_b; \Omega\Sigma)$	$s(\mathbf{r})_b$ (H- $CH_2$ )	$SF_S(\mathbf{r}_b; \text{ext})$
Ethane		
H- $CH_2$ ----- $CH_2$ -----H		
-0.0055 0.0189 -0.0149	-0.0015	-0.0055
Propane		
H- $CH_2$ ----- $CH_2$ ----- $CH_2$		
-0.0001 -0.0054 0.0040	-0.0016	-0.0056
Butane		
H- $CH_2$ ----- $CH_2$ ----- $CH_2$ ----- $CH_2$		
0.0000 -0.0001 -0.0054 0.0041	-0.0016	-0.0055
Pentane		
H- $CH_2$ ----- $CH_2$ ----- $CH_2$ ----- $CH_2$ ----- $CH_2$		
0.0000 0.0000 -0.001 -0.0054 0.0040	-0.0016	-0.0055

Tab.9: Electron spin density transferability, as viewed through the Source Function for the spin density, in n-alkyl radicals. The spin densities at a terminal C-H bcp are reported along with their total  $SF_S$  contributions from the various  $CH_2$  and  $CH_3$  groups in each system. All values are given in atomic units (au). Structures of all the molecular systems are obtained as in Tab.8.

In figure 20 are reported the reconstructions for the electron and the electron spin density in terms of SF and  $SF_S$  percentages, respectively, and considering both the bcp and the (3,-1) reference points in the butyl radical molecular system (Figure 19). Analysing the  $s(\mathbf{r})$  reconstruction at the terminal C-H bcp (Fig.20c), it is clear that if the contributions for the atomic groups decay faster than for  $\rho(\mathbf{r})$  (compare Tables 8 and 9), on the other hand this is not true if we consider the individual atomic contributions since those of the hydrogen atoms always largely oppose those from carbon atoms. In particular, the small positive contribution from the terminal  $CH_2^\bullet$  group is the result of a huge percentage positive contribution from the carbon and an almost compensating percentage negative contribution from the two linked hydrogen atoms. Moreover the reconstruction of  $s(\mathbf{r})$  at the terminal bcp reveal a not negligible positive contribution from the H10 atom of the neighboring methylene group, that is eclipsed to the unpaired electron orbital. Summarizing, at the bcp,  $s(\mathbf{r})$  is due to an almost compensation between a negative and greater in magnitude

<sup>†</sup> $s(\mathbf{r})$  to the bcp is almost two order of magnitude lower with respect (3,-1) saddle critical point of  $-\nabla^2\rho(\mathbf{r})$

contribution from the CH<sub>2</sub> group directly bonded to the methyl radical and a smaller and positive contribution from the terminal CH<sub>2</sub><sup>•</sup>.

SF <sub>S</sub> ( <b>r</b> <sub>b</sub> ;ΩΣ)	s( <b>r</b> ) <sub>b</sub> (H-CH <sub>2</sub> )	SF <sub>S</sub> ( <b>r</b> <sub>b</sub> ;ext)
Ethane		
H-CH <sub>2</sub> -----CH <sub>2</sub> -----H		
-0.0079 0.0924 -0.0054	0.0791	-0.0079
Propane		
H-CH <sub>2</sub> -----CH <sub>2</sub> ----- CH <sub>2</sub>		
-0.0001 -0.0078 0.0870	0.0791	-0.0079
Butane		
H-CH <sub>2</sub> -----CH <sub>2</sub> ----- CH <sub>2</sub> -----CH <sub>2</sub>		
0.0000 -0.0001 -0.0078 0.0864	0.0791	-0.0079
Pentane		
H-CH <sub>2</sub> -----CH <sub>2</sub> ----- CH <sub>2</sub> ----- CH <sub>2</sub> -----CH <sub>2</sub>		
0.0000 0.0000 -0.0001 -0.0078 0.0868	0.0791	-0.0079

Tab.10: Electron spin density transferability as viewed through the Source Function for the spin density, in n-alkyl radicals. The spin densities at (3;-1) saddle point in  $-\nabla^2\rho(\mathbf{r})$  as reference point are reported along with their total SF<sub>S</sub> contributions from the various CH<sub>2</sub> and CH<sub>3</sub> groups in each system. All values are given in atomic units (au). Structures of all the molecular systems are obtained as in Tab.8.

Regarding the NBCC critical point corresponding to the unpaired electron (Fig. 20d), it has a spin density which is larger by two order of magnitude. Again both the hydrogen atoms of the CH<sub>2</sub><sup>•</sup> radical oppose to its carbon atomic contribution, but in a much weaker way in percentage. In this case, the positive contributions from the hydrogens of the neighboring methylene group to s(**r**) are small in percentage but large in value, this because here the reconstructed spin density is two order of magnitude larger. Eventually, it is possible to conclude that SF<sub>S</sub> is able to distinguish very clearly the different nature of different critical points. In fact considering the terminal CH bcp, the spin transmission information follows sigma covalent bonds and it is dominated by the reaction of the external groups to the positive SFs contribution from the terminal methyl radical. The situation is completely different for the (3,-1) saddle critical point in  $-\nabla^2\rho(\mathbf{r})$  associated to the 2p orbital housing the unpaired electron. Here the radical carbon atomic basin gives a SF<sub>S</sub> contribution equal to 120% of the total s(**r**) value. Table 11 report atomic charges, spin density and Laplacian of the spin density in butyl radical molecular system looking at the separate contributions from all atoms. From the results reported it is possible to see that more than 90% of the unpaired electron stays on the terminal methyl radical group and essentially on the carbon atomic basin. This is true in all the alkyl radical molecular systems considered within the series.<sup>[27]</sup>

$\Omega$	$q(\Omega)$	$SP(\Omega)$	$\nabla^2_s(\Omega)$
C1	-0.009	0.001	0.000
H2	-0.001	0.000	0.000
H3	0.004	0.000	0.000
H4	-0.002	0.001	0.000
CH <sub>3</sub>	-0.008	0.002	-0.001
C5	0.042	0.010	0.001
H6	-0.004	0.003	-0.002
H7	-0.008	0.000	-0.001
CH <sub>2</sub>	0.029	0.012	-0.001
C8	0.031	-0.007	-0.066
H9	0.004	0.020	0.004
H10	0.007	0.057	0.011
CH <sub>2</sub>	0.043	0.071	-0.051
C11	-0.114	0.895	0.124
H12	0.029	0.009	-0.035
H13	0.028	0.009	-0.035
CH <sub>2</sub>	-0.057	0.914	0.054

Tab.11: Atomic charge, electron spin population and integrated electron spin density Laplacian for each atom within butyl radical molecular system and for the various CH<sub>2</sub> and CH<sub>3</sub> groups. All values are given in atomic units (au). Structures of all the molecular systems here presented are obtained performing Gaussian09 QM optimizations *in vacuo* at UPBE1PBE level of theory using 6-311+G\*\* as basis set.

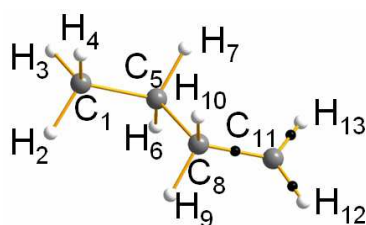


Fig. 19: Molecular scheme for butyl radical molecular system optimized at UPBE1PBE/6-311+G\*\*

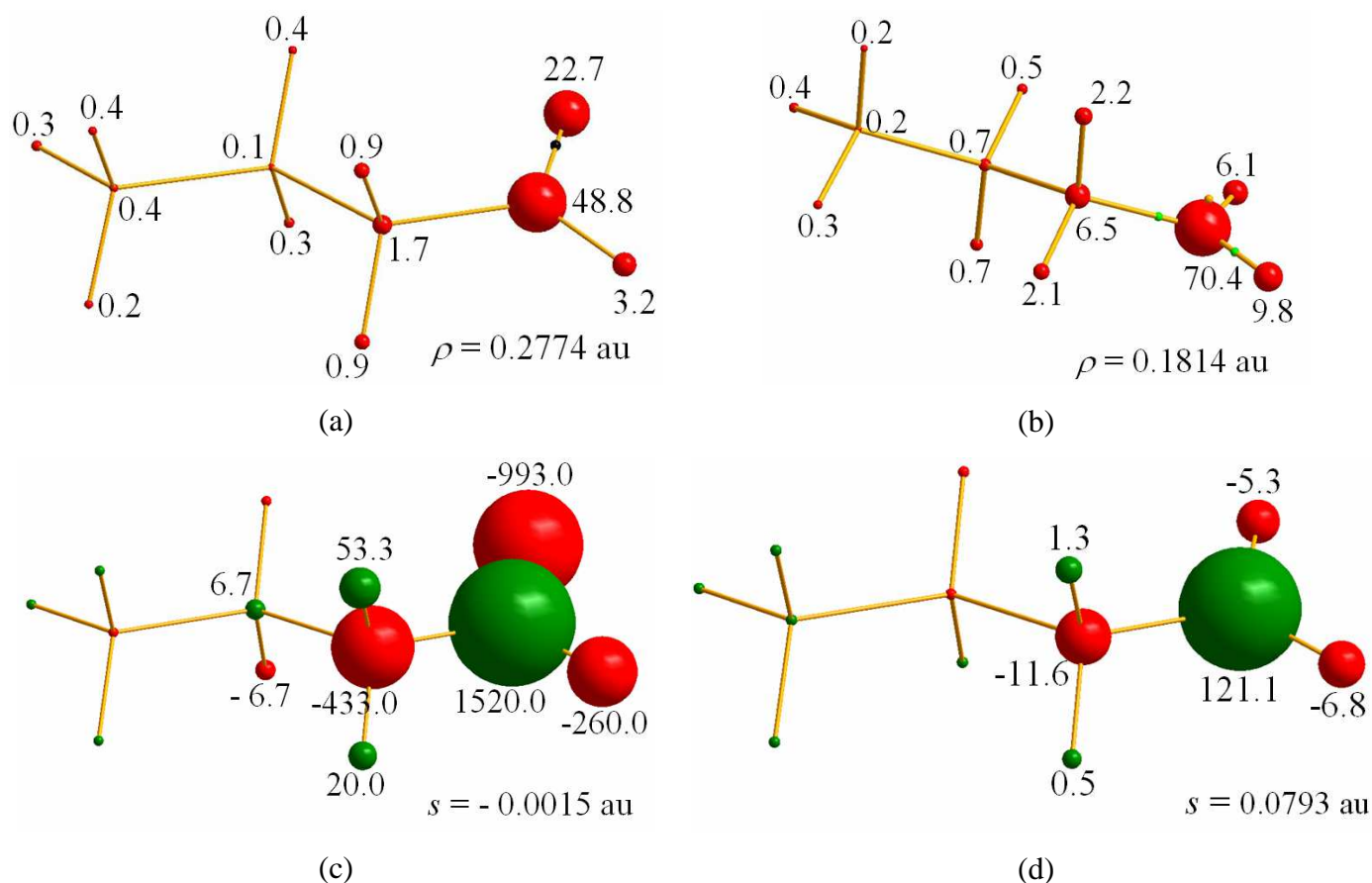


Fig.20: SF and SF<sub>s</sub> percentage contributions at reference points (rps) for butyl radical molecular system at the UPBE1PBEcomputational level. The separate contributions to SF<sub>s</sub> due to each atom is displayed as a sphere, whose volume is proportional to the SF and SF<sub>s</sub> percentage contribution to  $\rho(\mathbf{r})$  or  $s(\mathbf{r})$  values at the rp. Figure 20a and 20b report contributions from all the atomic basins to  $\rho(\mathbf{r})$  at bcp and NBCC as reference points respectively, Fig. 20c and 20d report contributions from atomic basins to  $s(\mathbf{r})$  at the same reference points. Colour codes are the same as in Fig.

16.

**Note:** Here are presented as red balls those atoms bringing a “beta” density contribution and as green balls those atoms bringing an “alpha” density contribution.

In figures 21 and 22  $s(\mathbf{r})$ ,  $\nabla^2 s(\mathbf{r})$  and  $LS_s(\mathbf{r})$  maps are reported. They refer to the plane containing the terminal  $\text{CH}_2^\bullet$  group and perpendicular to the carbon 2p atomic orbital housing the unpaired electron (Fig.21) and the plane containing such orbital (Fig. 22).



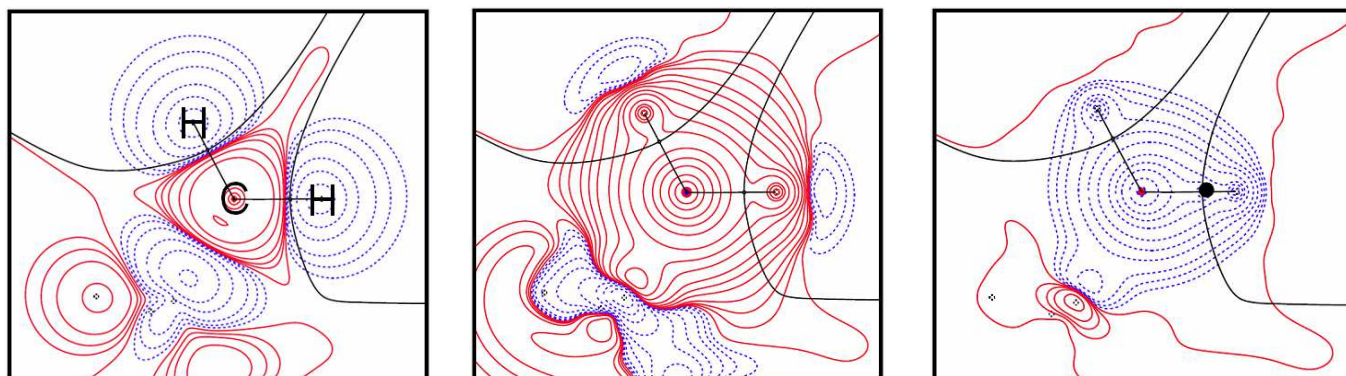


Fig.21:  $s(\mathbf{r})$ ,  $\nabla^2s(\mathbf{r})$  and  $LS_S(\mathbf{r})$  in the terminal  $\text{CH}_2^\bullet$  plane for butane alkyl radical molecular system, geometry is optimized at UPBE1PBE/6-311+G\*\* theoretical level. Atomic units (a.u.) are used throughout. Contour maps are drawn at interval of  $\pm(2,4,8)\cdot 10^n$ ,  $-4 \leq n \leq 0$  ( $s$ ,  $\nabla^2s$ ) and  $-3 \leq n \leq 0$  ( $\nabla^2\rho$ ). Dotted blue (full red) lines indicate negative (positive) values and full black lines mark boundaries of atomic basins. The terminal CH bond critical point is shown as a black dot and it is used as reference point in the evaluation of  $LS_S(\mathbf{r})$  map.

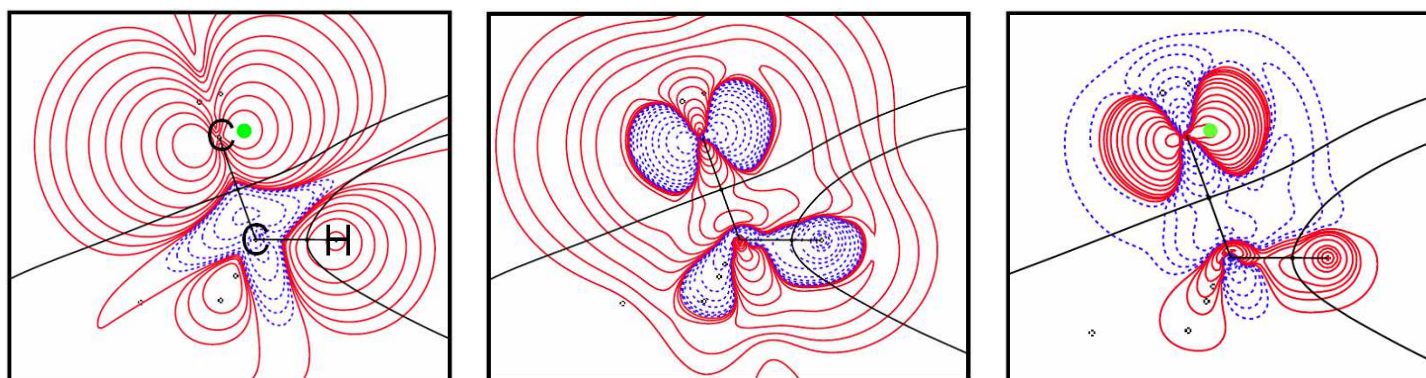


Fig.22:  $s(\mathbf{r})$ ,  $\nabla^2s(\mathbf{r})$  and  $LS_S(\mathbf{r})$  in the unpaired electron plane for butane alkyl radical molecular system, geometry is optimized at UPBE1PBE/6-311+G\*\* theoretical level. Atomic units (a.u.) are used throughout. Contour maps are drawn as in Fig. 21 with the same colour contours. The NBCC critical point associated with the unpaired electron and used as a reference point to evaluate the  $LS_S(\mathbf{r})$  map is shown as a green dot.

The maps in the plane of the unpaired electron located in a singly occupied p-orbital (Fig. 22) show that  $s(\mathbf{r})$  is delocalized on the terminal CH bond and that along this bond the hydrogen atomic basin behaves in part as the unpaired electron on the terminal carbon atom as for its ability to produce  $\alpha$  effect (see the maps of  $\nabla^2s$ ). On the other hand, in the plane of the terminal  $\text{CH}_2^\bullet$ , where spin polarization phenomena between bonded atoms can be observed, a pronounced  $\beta$  effect around terminal carbon atom is reached; this different situation is due to the positive region in  $\nabla^2s(\mathbf{r})$  maps encompassing the carbon and the two hydrogen atomic basins. In conclusion the analyses of the electron spin densities, the Laplacian of the spin density and the  $LS_S$  for a member of the series ( $\text{C}_4\text{H}_9^\bullet$ ) allows us to distinguish the different behaviour of the  $\nabla^2s(\mathbf{r})$  of the terminal carbon atom in the molecular plane and in the perpendicular plane. In both planes  $s(\mathbf{r})$  is positive (or partly positive) in the carbon basin, but  $\nabla^2s(\mathbf{r})$  (and hence the  $LS_S$ ), is totally different. When integrated

over the whole space the behaviour in the perpendicular plane dominates. It is also clear also why the hydrogen atomic basins oppose the terminal carbon contributions.

The results presented above are obtained not considering the problems of spin contamination and not including static and dynamic electron correlation, which can both influence significantly the results of the topological analyses of  $\rho(\mathbf{r})$  and  $s(\mathbf{r})$ . For this reason the calculation of the spin contamination annihilated wavefunction [Gaussian code : IOP(5/14=2), pop = noab] was performed at the same UPBE1PBE/6-311+G(d,p) level of theory, both for the geometry optimization and the SF<sub>S</sub> analysis. Interestingly, but not unexpectedly, significant differences were reached only in the analysis of  $s(\mathbf{r})$ . In fact, considering the bond critical point, a difference of 0,6% in terms of electron density value is reached between the spin-contaminated and the spin contamination annihilated wave functions; on the other hand it is possible to observe a percentage difference as large as 265% for the electron spin density, with  $s(\mathbf{r})$  becoming less negative and decreasing in magnitude upon spin contamination annihilation. The situation change when NBCC is considered: at this critical point the percentage difference between the values of  $s(\mathbf{r})$  is equal to 17,5% and with spin annihilated value increasing in magnitude with respect to that of the spin contaminated wavefunction in this case. The removal of the spin contamination has a large effect on the local evaluation of the electron spin density which is either overestimated or underestimated in magnitude by the contaminated wavefunction, depending on the location (clearly this is an obvious result, since both wavefunctions need to integrate to the same number of unpaired electrons, namely one in this case). Integration of the spin density over the atomic basins of the terminal CH<sub>2</sub><sup>•</sup> group typically shows that more than 91% of the excess  $\alpha$  density lies in this group and essentially on the C atom (90%), the second most important contribution (6%) coming from the eclipsed  $\beta$ -hydrogen atom mentioned above. Tables 12, 13 compare respectively the electron density and the electron spin density transferability at the C-H bcp of the terminal CH<sub>2</sub><sup>•</sup> group for all considered radicals. Perfect transferability is confirmed to occur also for the spin contamination annihilated wave function. The dominant contribution to  $\rho(\mathbf{r})$  at the bcp electron density (0.265 au) comes from the terminal methyl group hosting the bcp, while the remaining methyl and methylene bridge groups adjust their contributions to provide a constant residual density (0.013 au). An almost perfect transferability is recovered also for the very low value of  $s(\mathbf{r})$  (-0.0004 au) for all systems at the bcp. The overall  $\alpha$  SF<sub>S</sub> contribution from the terminal CH<sub>2</sub><sup>•</sup> group,  $s(\mathbf{r}) = 0.0041$ , is more than compensated for by an overall  $\beta$  and constant contribution,  $s = -0.0045$ , arising from the remaining part of the molecule, regardless of the length of the chain. Even in the case of spin contamination annihilated wave function, spin transferability is ensured through a combination of opposing  $\alpha$  and  $\beta$  SF<sub>S</sub> cumulative effects of similar magnitude. An equally remarkable transferability characterizes

the value of the spin density at the (3,-1)  $-\nabla^2\rho$  critical points associated to the non-bonded charge concentrations (NBCC) and largely due to the unpaired electron (see Tab. 14). At the NBCC,  $s(\mathbf{r})$  is large and positive (0.0968 a.u.) and completely dominated by the overall  $\alpha$  effect contribution from the terminal  $\text{CH}_2^\bullet$  group (0.1026 a.u.). The remaining groups of the molecule counteract slightly such contribution through a comparatively modest overall  $\beta$  effect (-0.0058 a.u.). In conclusion, as in case of the spin contaminated wave function, perfect transferability holds true for both the  $\rho(\mathbf{r})$  and  $s(\mathbf{r})$  distributions in n-alkyl radicals. Yet, it realizes in quite different ways, largely dependent on the selected reference point.

SF( $\mathbf{r}_b$ ; $\Omega\Sigma$ )	$\rho(\mathbf{r})_b$ (H-CH <sub>2</sub> )	SF( $\mathbf{r}_b$ ; ext)
Ethane		
H-CH <sub>2</sub> -----CH <sub>2</sub> -----H		
0.2640 0.0104 0.0027	0.2771	0.0125
Propane		
H-CH <sub>2</sub> -----CH <sub>2</sub> ----- CH <sub>3</sub>		
0.2647 0.0091 0.0033	0.2771	0.0125
Butane		
H-CH <sub>2</sub> -----CH <sub>2</sub> ----- CH <sub>2</sub> -----CH <sub>3</sub>		
0.2645 0.0092 0.0011 0.0022	0.2771	0.0125
Pentane		
H-CH <sub>2</sub> -----CH <sub>2</sub> ----- CH <sub>2</sub> ----- CH <sub>2</sub> -----CH <sub>3</sub>		
0.2647 0.0092 0.0013 0.0014 0.0009	0.2771	0.0128

Tab.12: Electron density transferability as viewed through the Source Function, in n-alkyl radicals. For these molecules, the bcp electron densities of the terminal C-H bond, along with their SF contributions from the various CH<sub>2</sub> and CH<sub>3</sub> groups in each molecule, are reported.. All values are given in atomic units (a.u.). Data are obtained from spin contamination annihilated wavafunction, at optimized geometry and using the UPBE1PBE level of theory with 6-311+G\*\* basis set.

In figures 23 and 24 are reported the reconstructions of  $\rho(\mathbf{r})$  and  $s(\mathbf{r})$  in terms of SF and SF<sub>s</sub> atomic components for the *n*-butyl radical at the bcp and the NBCC reference points, respectively. Comparison between figures 20c and 23b reveals that, as in the case of spin contaminated wave function, at the bcp the atoms bonded to each other always oppose themselves in their action, one giving an  $\alpha$  and the other a  $\beta$  effect. This situation is reached in case of through-bond spin transmission between covalently bonded atoms (“antiferromagnetically” coupled).<sup>[27,28]</sup>

$SF_S(\mathbf{r}_b; \Omega\Sigma)$	$s(\mathbf{r})_b$ (H-CH <sub>2</sub> )	$SF_S(\mathbf{r}_b; \text{ext})$
Ethane		
H-CH <sub>2</sub> -----CH <sub>2</sub> -----H		
0.00403 -0.00422 -0.0027	-0.00044	-0.00448
Propane		
H-CH <sub>2</sub> -----CH <sub>2</sub> ----- CH <sub>3</sub>		
0.00403 -0.00422 -0.0027	-0.00044	-0.00448
Butane		
H-CH <sub>2</sub> -----CH <sub>2</sub> ----- CH <sub>2</sub> -----CH <sub>3</sub>		
0.00409 -0.00422 -0.0024 -0.00004	-0.00041	-0.00450
Pentane		
H-CH <sub>2</sub> -----CH <sub>2</sub> ----- CH <sub>2</sub> ----- CH <sub>2</sub> -----CH <sub>3</sub>		
0.00409 -0.00422 -0.0024 -0.00004 -0.00000	-0.00041	-0.00450

Tab.13: Electron spin density transferability as viewed through the Source Function for the spin density, in n-alkyl radicals. For these molecules, the bcp electron spin densities of the terminal C-H bond, along with their SF contributions from the various CH<sub>2</sub> and CH<sub>3</sub> groups in each molecule, are reported.. All values are given in atomic units (a.u.). Molecular systems were computed at the same level of theory indicated in Tab.12.

$SF_S(\mathbf{r}_b; \Omega\Sigma)$	$s(\mathbf{r})_b$ (H-CH <sub>2</sub> )	$SF_S(\mathbf{r}_b; \text{ext})$
Ethane		
H-CH <sub>2</sub> -----CH <sub>2</sub> -----H		
0.10246 -0.0560 -0.0021	0.09665	-0.00581
Propane		
H-CH <sub>2</sub> -----CH <sub>2</sub> ----- CH <sub>3</sub>		
0.10246 -0.0560 -0.0021	0.09665	-0.00581
Butane		
H-CH <sub>2</sub> -----CH <sub>2</sub> ----- CH <sub>2</sub> -----CH <sub>3</sub>		
0.10264 -0.0560 -0.00019 -0.00004	0.09680	-0.00583
Pentane		
H-CH <sub>2</sub> -----CH <sub>2</sub> ----- CH <sub>2</sub> ----- CH <sub>2</sub> -----CH <sub>3</sub>		
0.10263 -0.0560 -0.00019 -0.00004 -0.00000	0.09680	-0.00584

Tab.14: Electron spin density transferability as viewed through the Source Function for the spin density, in n-alkyl radicals. The spin densities at (3;+1) saddle point in  $\nabla^2\rho(\mathbf{r})$  as reference point are reported along with their total SF<sub>S</sub> contributions from the various CH<sub>2</sub> and CH<sub>3</sub> groups in each system. All values are given in atomic units (a.u.). Molecular systems were computed at the same level of theory indicated in Tab.12.

Moreover both the individual atomic SF<sub>S</sub> contributions and the overall contributions from the terminal CH<sub>2</sub><sup>•</sup> or from its neighbouring CH<sub>2</sub> group are very large in magnitude compared to the  $s(\mathbf{r})$  value they concur to reconstruct at reference point considered. Interestingly, while the SF

contributions from the hydrogen atoms of the terminal  $\text{CH}_2^\bullet$  group to the C11-H13 bcp  $\rho(\mathbf{r})$  markedly differ between each other, this is not at all the same for the corresponding  $\text{SF}_s$  contributions which are more comparable in magnitude.<sup>u</sup> For this reason, it is possible to conclude that the spin density at C-H bcp originates from much less local sources than it is for its corresponding electron density. The reconstruction of  $s(\mathbf{r})$  at the NBCC located above the plane of the terminal  $\text{CH}_2^\bullet$  group (Fig. 24b) reveals a different situation: here  $s(\mathbf{r})$  is quite large and positive and it is essentially determined by the carbon atom where the unpaired electron is essentially located ( $\text{SF}_s\%_{(\text{C11})} = 113.4\%$ ); its linked hydrogen and carbon atoms neutralize the slight  $\alpha$ -effect excess arising from the C11 atom. So it is possible to assess that the  $\text{SF}_s\%$  values are able to neatly distinguish the case where the reference point characterizes a covalent bonding interaction, with respect to the case where it is associated to a NBCC largely due to a fairly localised unpaired electron. In fact spin information transmits differently in dependence of the reference point considered. In any case, the magnitude of the overall  $\text{SF}_s$  contributions from the two hydrogen atoms of the terminal  $\text{CH}_2^\bullet$  group and the magnitude of the cumulative  $\text{SF}_s$  contribution from the  $\beta$ - $\text{CH}_2$  group, are similar for both reference points. The large discrepancy on the  $\text{SF}_s$  percentages arises from the three order of magnitude larger  $s(\mathbf{r})$  value at NBCC compared to that at the C-H bcp. Reconstruction of both  $\rho(\mathbf{r})$  and  $s(\mathbf{r})$  in terms of *magnetic* and of *reaction* or *relaxation*  $\text{SF}_s$  contributions, are also reported in Fig. 23 and 24. The magnetic contribution is due only to an  $\alpha$ -density but it does not always lead to an  $\alpha$ -effect. In fact it is possible that it may also result in an overall decrease of  $s(\mathbf{r})$  in dependence of the reference point considered. At the same time the *reaction* contribution may either concur or counteract the magnetic one in determining  $s(\mathbf{r})$  at the reference point. In the case of *n*-alkyl radicals, the situation is very simple as there is only one magnetic natural orbital, whose effects are clearly reported in Figures 23c and 24b for the case of *n*-butyl radical for both bcp and NBCC reference points. The role of the reaction contribution may be assessed from the difference of (b) and (c)  $\text{SF}_s$  values in Figure 23 and, analogously, of (a) and (b)  $\text{SF}_s$  values in Figure 24.

---

<sup>u</sup> In particular the H13 SF contribution to electron density is almost 14 times greater than the one from H12; on the contrary the  $\text{SF}_s$  contribution from H13 to  $s(\mathbf{r})$  is only three times as large as that from H12 atom.

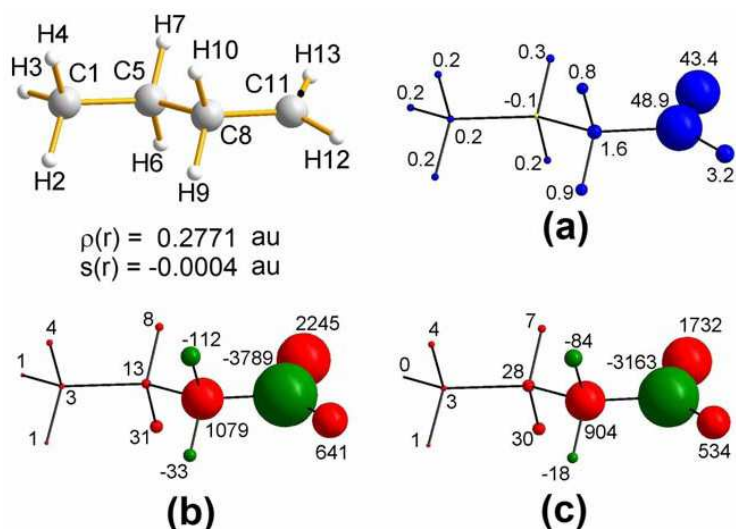


Fig.23: Atomic SF (a) and SF<sub>s</sub> (b) percentages at the C11-H13 bond critical point (shown as a black dot in the molecular scheme) for the *n*-butyl radical. In (c) the SF<sub>s</sub> percentages only due to the *magnetic* orbital density are displayed. The values of  $\rho(\mathbf{r})$  and  $s(\mathbf{r})$  at the bcp are given in a.u. Atoms are portrayed as spheres with volumes proportional to their source percentage contributions to  $\rho(\mathbf{r})$  and  $s(\mathbf{r})$  values at the bcp. Colour codes: (a) blue or yellow whether atoms represent positive or negative sources for  $\rho$  at the bcp; (b) and (c) green or red whether atoms represent positive ( $\alpha$  effect) or negative ( $\beta$  effect) sources for  $s$  at bcp. Note, instead, that in (b) and (c) the sign of percentage atomic sources is positive (negative) when the atom concurs (opposes) to the  $s(\mathbf{r})$  value at the bcp.

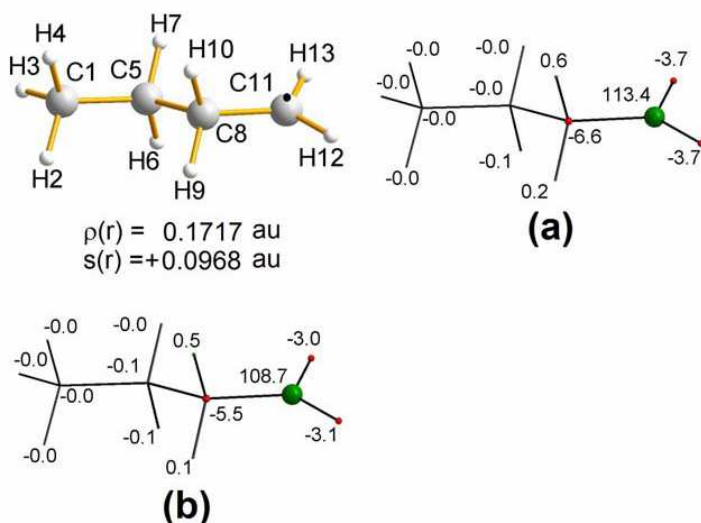


Fig. 24: *n*-butyl radical: (a) atomic SF<sub>s</sub> percentages at the (3,-1)  $-\nabla^2\rho(\mathbf{r})$  critical point, located above the plane of the terminal  $\text{CH}_2^\bullet$  group, highlighted as a black dot in the molecular scheme and associated to non-bonded charge concentrations largely due to the unpaired electron. In (b) the SF<sub>s</sub> percentages only due to the magnetic orbital density are displayed. The values of  $\rho(\mathbf{r})$  and  $s(\mathbf{r})$  at the reference point are shown. Colour codes for atoms and signs of atomic SF<sub>s</sub> percentages as in Fig. 23

One observes that the magnetic orbital density dominates the reconstruction of  $s(\mathbf{r})$  and that the remaining relaxation density moderately (from 5% to 20% in magnitude) concurs to the effects produced by the former density, for both reference points considered. These effects may be either of

$\alpha$  or of  $\beta$  in nature for the two densities, but they always agree in their nature in this case, at least for the more significant contributions.

### *Conclusions:*

Comparison between the electron density and the electron spin density case is illuminating about the different way  $\rho(\mathbf{r})$  and  $s(\mathbf{r})$  information is transmitted and comparison between different reference points allow us to gain information on how such observable are transmitted as a function of the reference point considered. In this subsection the perfect transferability in a series of *n*-alkyl radical through the  $SF_S$  contributions at two different reference points has been examined. The first is a (3,-1) critical point in the  $-\nabla^2\rho(\mathbf{r})$  corresponding roughly to the maximum in the  $s(\mathbf{r})$  above (or below) the plane of the terminal methyl radical group.<sup>v</sup> while the second reference point examined is the C-H bond critical point of the terminal methylene radical group. Wavefunctions for all the molecular systems within the series were calculated at the UPBE1PBE/6-311+G(d,p) level of theory, using the Gaussian-09 code. Both spin contaminated and spin contamination annihilated wavefunctions were used for both geometry optimization and  $SF_S$  analysis. As expected, integration of the spin density over the basin of the terminal  $CH_2^\bullet$  group typically shows that more than 90% of the excess  $\alpha$  density lies in this group and essentially on the carbon atomic basin (90%), the second most important contribution (6%) coming from the eclipsed  $\beta$ -hydrogen atom mentioned above. Perfect transferability of electron density is found to occur also in the *n*-alkyl radicals, and with similar mechanisms to those operative in the corresponding alkanes. Moreover, an almost perfect transferability is also recovered for the very low value of  $s(\mathbf{r})$  (-0.0004 a.u.) at the bcp. At this reference point, the  $\alpha$   $SF_S$  contribution from the terminal  $CH_2^\bullet$  group is compensated for by an overall  $\beta$  and constant contribution arising from the remaining part of the molecule, regardless of the length of the chain. So it is possible to asses that perfect transferability of  $s(\mathbf{r})$  is ensured through a combination of opposing  $\alpha$  and  $\beta$   $SF_S$  cumulative effects of similar magnitude. Quite different is the case for the spin density reconstruction at the non bonded charge concentration located above the plane of the terminal  $CH_2^\bullet$  group, where the very large spin density value is essentially determined by the carbon atom carrying the unpaired electron and where the role of its linked hydrogen and carbon atoms is just that of neutralizing the slight  $\alpha$ -effect excess arising from the radicalic carbon. In summary, though perfect transferability holds true for both the electron and

---

<sup>v</sup> This (3,-1) critical point and the almost symmetric one lying below such plane, but of (3,+1) signature, may be both associated to non-bonded charge concentrations (NBCCs) and are largely due to the unpaired electron, although they do not correspond to electron spin density maxima.

the electron spin density in n-alkyl radicals, it realizes in quite different ways and largely dependent on the selected reference point.

## ***2.4 INTERPRETATION OF FERRO-MAGNETIC INTERACTIONS IN AZIDO Cu(II) DINUCLEAR COMPLEXES USING THE SF<sub>5</sub> BASED TOPOLOGICAL DESCRIPTORS:***

### ***2.4.1 Introduction:***

Applications of SF<sub>5</sub> concerning crystalline systems are now discussed in the remaining part of this chapter. To this purpose an investigation of molecular crystals will be discussed in the next paragraphs, regarding specifically the study of ferromagnetic interactions in two azido double-bridged Copper II dinuclear complexes. Several studies have been previously performed on metal azido complexes and their magneto-structural relationships. In the case of azido double-bridge Copper II dinuclear complexes, the azido groups bridge the Cu(II) ions through one terminal N atom ( $\mu$ -1,1), in the so-called END-ON (EO) coordination mode, or through two terminal N atoms ( $\mu$ -1,3) in the so-called END-TO-END coordination mode (EE) (see Fig. 25). In both EO and EE systems, the bridge may be either symmetric with the two N-Cu bonds being equivalent and short (around 2.0 Å) or asymmetric with one short (about 2.0 Å) and one long (from 2.3 Å to 2.7 Å) Cu-N bond. Generally, EO systems are symmetric while EE systems are asymmetric. In a magnetic perspective, the EO coordination mode mostly provides ferromagnetic Cu-Cu interactions<sup>w</sup>, while the magnetic interactions are zero or generally very small and weakly antiferromagnetic (with a coupling constant J of less than -100 cm<sup>-1</sup>) in the asymmetric EE systems even if it is possible to observe a ferromagnetic interaction in some cases. The few EE symmetric systems showing 6-fold coordination of Cu (II) are instead strong anti-ferromagnetic in nature, with a very large coupling constant and the two bridging azido groups supporting strong overlap between the Cu d<sub>x<sup>2</sup>-y<sup>2</sup></sub> magnetic orbitals (with, in this case, x and y directed approximately along the two Cu-N(azide) bonds). Asymmetric EE molecular systems where the two copper atoms have a square pyramidal geometry, display instead one terminal azido nitrogen (namely that associated to the short Cu-N bond) pointing to the d<sub>x<sup>2</sup>-y<sup>2</sup></sub> magnetic orbital of Cu and the other terminal pointing approximately to the (almost filled) d<sub>z<sup>2</sup></sub> orbital of Cu. The long apical Cu-N<sub>azide</sub> bonds comply with such simple orbital picture.

---

<sup>w</sup> only for large bridging angles Cu-N-Cu >108 degree it turns to antiferromagnetic coupling



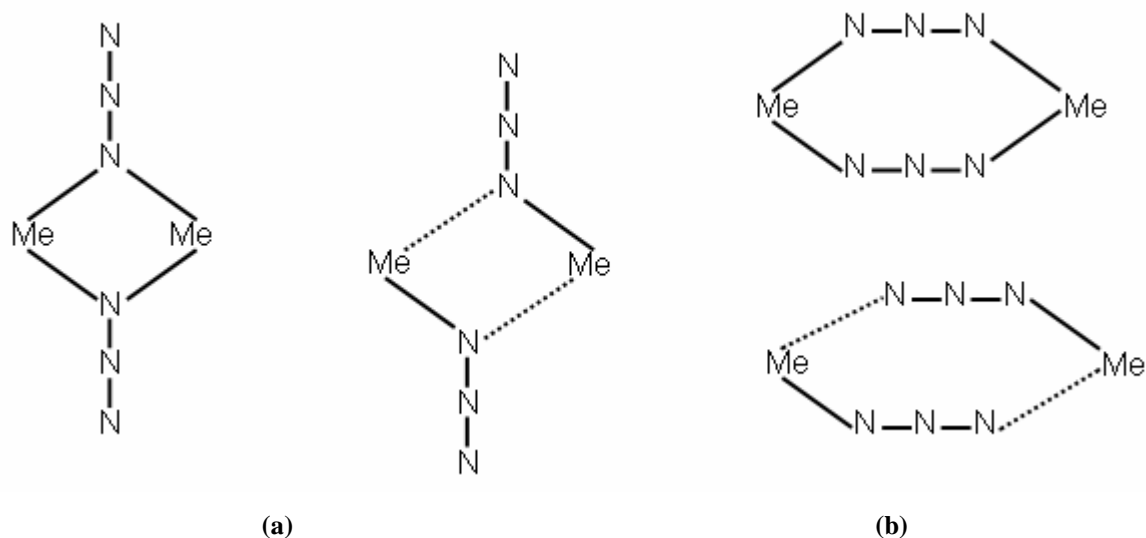


Fig. 25: General structures for azido double-bridge Copper II dinuclear complexes: in 25a symmetric (left) and asymmetric (right) END-ON (EO) coordination modes are reported while in 25b the symmetric (top) and asymmetric (bottom) END-TO-END coordination mode (EE) are shown.

The two cases presented in this subsection have been chosen because their experimental spin density maps from polarized neutron diffraction (PND) studies have been reported in literature, along with remarkable insights based on quantum mechanical approaches. The first case, studied by Aebersold et al<sup>[22]</sup>, involves a symmetric EO di-nuclear copper azido bridged molecular system featuring a short Cu-Cu internuclear distance, a large FM interaction and having four p-terbutylpyridine ligands other than the azido groups and two perchlorate anions to guarantee the complex neutrality (Figure 26).

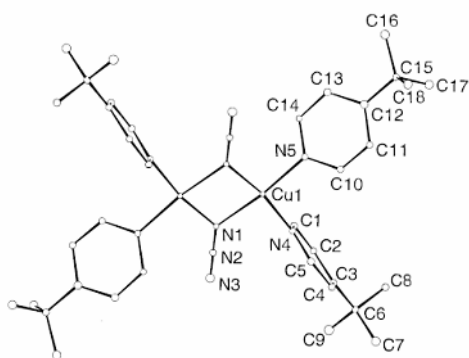


Fig. 26: Symmetric EO di-nuclear copper azido bridged molecular system. The ligands are four p-terbutylpyridine other than the azido groups and two perchlorate anions to guarantee the complex neutrality.

The second case, already introduced in the previous paragraphs, examines an asymmetric EE complex (see Fig. 7), with large Cu-Cu internuclear distance, small FM coupling, having a square pyramidal coordination of the Cu II atoms yielded by the double-bridged azide ligands and the polydentate ligand in its hydrogenated form. Such system has been investigated by polarized neutron diffraction PND and through quantum-mechanical approaches by Aronica et al<sup>[23]</sup>;

moreover, it has been studied very recently also by joint PND and XRD experiments, employing a spin-split version of the original Hans-Coppens Multipolar Model refinement, in order to gain distinct alpha and beta electron density distributions<sup>[5]</sup> (Fig. 8). In EO molecular system the spin distribution has been investigated in terms of orbital language, employing a fragment orbital approach and by considering the interactions between the highest occupied d atomic orbitals on the Cu atoms and the highest doubly occupied  $\pi_{\text{gerade}}$  azido orbitals. The mixing of these 4 orbitals gives four molecular orbitals. The interpretation of the spin distribution was then provided by applying the concepts of spin delocalization (caused by the overlap between the fragment orbitals) and spin polarization (caused by spin interaction within the  $\pi_{\text{gerade}}$  orbital of the  $\text{N}_3^-$  fragment) and also going beyond the active-electron estimate, considering as well the lowest vacant single molecular orbital of the  $\text{N}_3^-$  fragment of  $\pi_{\text{ungerade}}$  symmetry. Essentially, the spin distribution may be read as the result of two mechanisms: first, a spin delocalization from the  $\text{Cu}^{2+}$  ions towards azido bridges and then a spin polarization within the  $\pi$  orbitals of the azido groups (considering also the LUMO of the azido group). In the case of the EE molecular system the spin distribution has been investigated in terms of the shape of the two single occupied molecular orbitals (SOMOs). These orbitals are in-phase and out-of-phase arrangements of the Cu  $d_{x^2-y^2}$  atomic orbitals and show large contributions to the azido bridge. Moreover the spin density distribution has been analysed in terms of the relevance of spin polarization effects. These account for the polarization of the inactive orbitals (those doubly occupied) and, namely, those of the azido groups, in particular those of the bridging azido units concerning typical  $\pi$ - $\pi^*$  (gerade to ungerade) excitations.

#### **2.4.2 Results and discussion:**

The wave functions for both EO and EE molecular systems here presented are obtained performing Gaussian09 QM energy determinations *in vacuo* at UB3LYP level of theory using pob-TVPZ as basis set and the experimental molecular structures reported in references 22 and 23. Considering the EO system, about 60% of unpaired electrons density is localized on the Cu(II) ions, 20% is delocalized over the azido groups and the remaining 20% on the pyridine nitrogen atoms, as displayed by the spin populations (see Tab.15). The central nitrogen of the azido group shows a small negative spin population,  $s(\text{N}_2)$ ; moreover, the integrated  $\nabla^2 s(\mathbf{r})$  is relevant only for the Cu atoms and the azido group atoms. Note that an average positive value for the Laplacian of the spin density, corresponding to a dominating beta-effect, was a bit unexpected for the copper atom. Thus, the attitude of the metal centre in being a source of  $\alpha$ -spin seems to be very directional, very localized and through an  $\alpha$ -spin-delocalization towards the ligands as the  $\nabla^2 s(\mathbf{r})$  map in the plane

containing the two copper atoms plainly displays (see Fig. 27). A further remarkable feature in terms of  $\nabla^2 s(\Omega)$  values is the difference among the azido group nitrogens, with the terminal one performing otherwise than the remaining two and the central one being the atom with the highest  $\alpha$ -spin effect.

$\Omega$	$q(\Omega)$	$s(\Omega)$	$\nabla^2 \rho_\alpha(\Omega)$	$\nabla^2 \rho_\beta(\Omega)$	$\nabla^2 s(\Omega)$
Cu	1.095	+0.617	+0.009	-0.009	+0.018
N1	-0.489	+0.089	-0.004	+0.003	-0.007
N2	-0.138	-0.011	-0.011	+0.011	-0.022
N3	+0.039	+0.110	+0.008	-0.008	+0.016
$(N)_3^-$	-0.588	+0.188	-0.007	+0.006	-0.013
N4	-1.056	+0.095	+0.001	-0.001	+0.002
N5	-1.084	+0.086	+0.001	-0.001	+0.001

Tab. 15: Atomic charges, electron spin populations,, atomic Laplacians of electron spin density divided in  $\alpha$  and  $\beta$  counterparts and Atomic Laplacians of electron spin density in the symmetric EO molecular system and only for the atomic basins (copper and nitrogens) involved in the azido-bridge. All values are given in atomic units (a.u.).

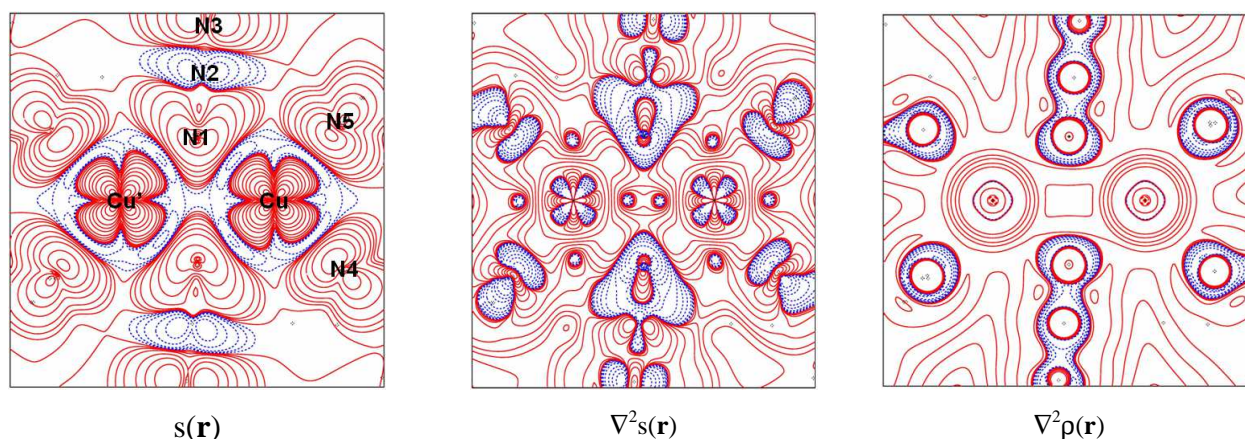


Fig. 27: Electron spin density  $s(\mathbf{r})$  and its Laplacian and Electron density Laplacian in the  $(x,y)$  plane for symmetric EO di-nuclear copper azido bridged molecular system at UB3LYP/pob-TVPZ computational levels. Atomic units (a.u.) are used throughout. Contour maps are drawn at interval of  $\pm(2,4,8)\cdot 10^n$ ,  $-4 \leq n \leq 0$  ( $s$ ,  $\nabla^2 s$ ) and  $-3 \leq n \leq 0$  ( $\nabla^2 \rho$ ). Dotted blue (full red) lines indicate negative (positive) values.

Considering the aspherical  $d$ -electron distribution around the two copper atoms, it is possible to see from the maps of the Laplacian of the spin density how they are fourfold coordinated in an almost square planar arrangement of ligands. According to crystal field theory, and for a  $d^9$  configuration on Cu atom, the  $d_{x^2-y^2}$  orbital is the magnetic singly occupied orbital. By analysing  $\nabla^2 \rho(\mathbf{r})$ , the Charge Depletions (CD) on the Cu atom, related to the singly occupied  $d_{x^2-y^2}$  orbital, are indeed found to be pointing towards the charge concentrations (CC) related to the nitrogen lone pairs, in agreement with a key-lock interaction mechanism between the metal and the ligands. From the map

of  $s(\mathbf{r})$  and  $\nabla^2 s(\mathbf{r})$  reported in Fig. 27, it is possible to note that the spin density surrounding the Cu has the shape of the  $d_{x^2-y^2}$  orbital; the same  $d_{x^2-y^2}$  shape is even more evident considering  $\nabla^2 s(\mathbf{r})$  around the metal centers. Based on the Cu orbital filling related to Cu  $d^9$  in square-planar coordination, the CDs, oriented along the ligands are expected to be characterized by larger spin density values, while the CCs, oriented along the orthogonal direction XY by smaller  $s(\mathbf{r})$  values. In this case, a difference of one order of magnitude indeed occurs in the spin density values of the CCs (0.021 a.u.) relative to those of the CDs (0.282 a.u.). The CC is located in a region of positive  $\nabla^2 s(\mathbf{r})$ , transmitting  $\beta$ -spin density, while the CD behaves as a source of  $\alpha$ -spin density.

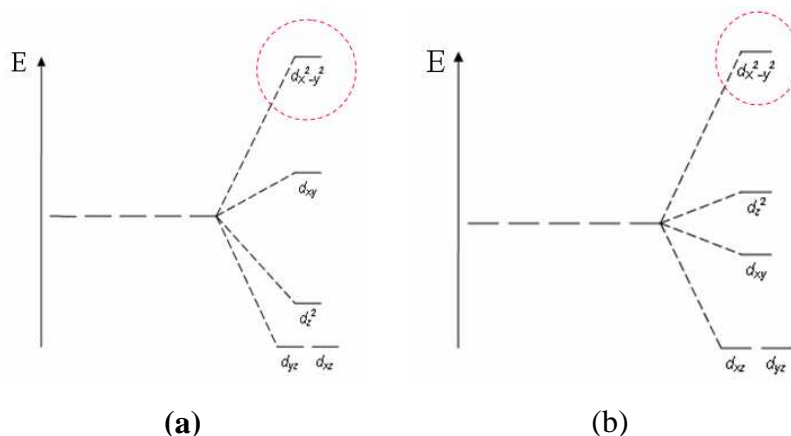


Fig. 28: aspherical  $d$ -electron distribution around the two copper atoms in EO molecular system (a) and EE molecular system (b).

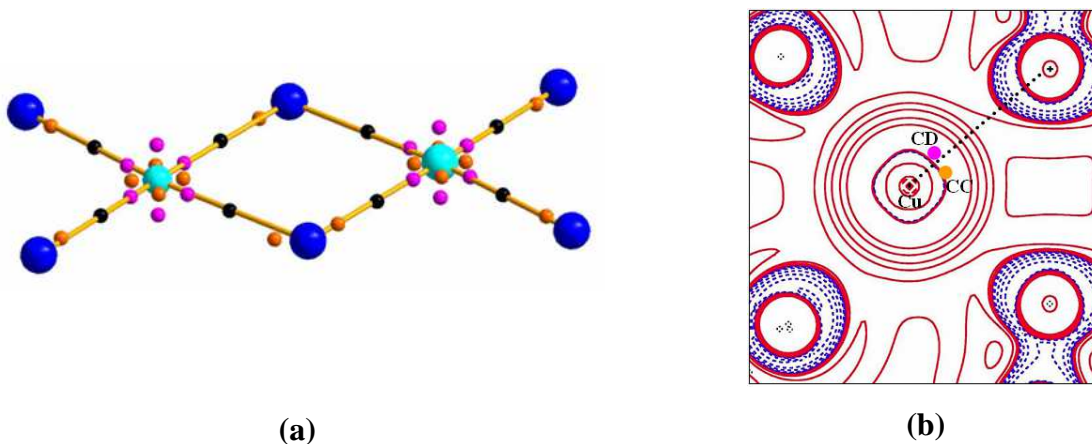


Fig. 29: Electron density Laplacian in the  $(x,y)$  plane for symmetric EO di-nuclear copper azido bridged molecular system at UB3LYP/pob-TVPZ computational levels. Orange dots represent CC while CD are represented by purple dots, eventually bcp are represented by black dots. Atomic units (a.u.) are used throughout and contour maps are drawn as in Fig. 27 with the same colour codes. In the left and right panels, the CC and CD critical points are denoted by orange and by purple dots, respectively, while the bcps by dots coloured in black.

It's worthy to stress that  $\nabla^2 \rho(\mathbf{r})$  and  $s(\mathbf{r})$  perform complementary roles, since the former is concentrated when double occupancy occurs, while the latter is concentrated in case of single

occupancy. Interestingly, the maps of  $s(\mathbf{r})$  and *a fortiori* those of the Laplacian of the spin density, which are both observables, are also visibly showing “physical”, “observable” orbitals in the present case.<sup>x</sup> Considering the SF<sub>S</sub> contributions, the spin density at the CD is almost entirely provided by the contributions from the Cu atom, while the one on the CC pointing towards the azido N receives not negligible and opposing contributions from two of the azido group atoms and a positive “ferromagnetic” coupled contribution from the other Cu atom (see Fig. 30). The SF<sub>S</sub> contributions at the Laplacian CD and CC of the Cu atom are reported in table A2.1 and A.2.2 in appendix A2.

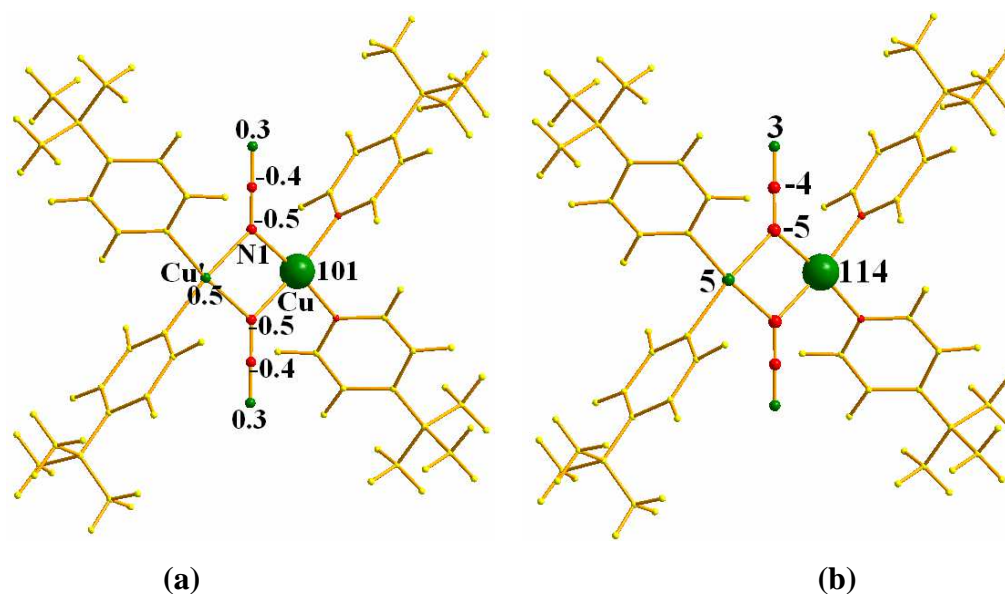


Fig. 30: Atomic SF<sub>S</sub> percentages reconstructing the electron spin density at the CD on the Cu-N1 bond (a) and CC along the Cu-Cu' axis (b) for the EO molecular system. Atoms are portrayed as spheres with volumes proportional to their source percentage contributions to  $s(\mathbf{r})$  values at the critical points considered. Colour codes: green or red whether atoms represent positive ( $\alpha$  effect) or negative ( $\beta$  effect) sources for  $s(\mathbf{r})$  at the critical point considered.

The reconstruction of  $s(\mathbf{r})$  in terms of SF<sub>S</sub> contributions along the Cu-N<sub>bridge</sub> (N1) internuclear axis deserves further consideration, beyond that already illustrated for the CD close to the Cu atom and roughly lying along this axis. Looking at the CC ( $s(\mathbf{r}) = 0.021$  a.u.) associated to the N1 lone pair, pointing towards the CD of the Cu atom, a sign of the spin delocalization mechanism or of the so-called Cu-Cu' super-exchange interaction through the non-magnetic bridging nitrogens (Fig. 31a), is immediately evident. While the SF<sub>S</sub> contribution from the central nitrogen atom of the azidic group opposes to the positive spin density at the CC, the two copper atoms concur to the positive  $s(\mathbf{r})$  CC value with significant contributions from both the metal centers (20.7% in total). Other few reference points are of some interest along the Cu-N<sub>bridge</sub> axis. At the N nucleus, the large positive  $s(\mathbf{r})$  (0.245 a.u.) is entirely due to the nitrogen itself, while the negative spin density at the Cu

<sup>x</sup> except the phase, in practice orbital related densities.

nucleus (Fig. 31c,  $s(\mathbf{r}) = -0.038$  a.u.) – differently from the positive spin density at the CD – is determined by contributions of the same sign from the N1 and N2 atoms of the azide groups and of the opposite sign from the other copper atom. It so appears that the two Cu atoms behave as non “ferromagnetically coupled” when the region of beta spin density around the Cu atom is reconstructed. The spin density at the Cu-N bridge bond critical point is almost zero, though still positive ( $s(\mathbf{r}) = 0.001$  a.u.); it is located close to a wide region of negative spin density separating the copper basin from the region of positive spin density on the bridging nitrogen due to the spin delocalization from the metal center.<sup>y</sup> The region of negative spin density leads to a large negative contribution from the N1 atom at bcp, almost compensating for the positive contribution from the Cu at this point. Eventually, the spin density reconstruction in terms of SF<sub>S</sub> contributions at Cu-N1 bcp (not reported in Fig.31) shows a wide delocalization of sources, typical of reconstructions at bcps.

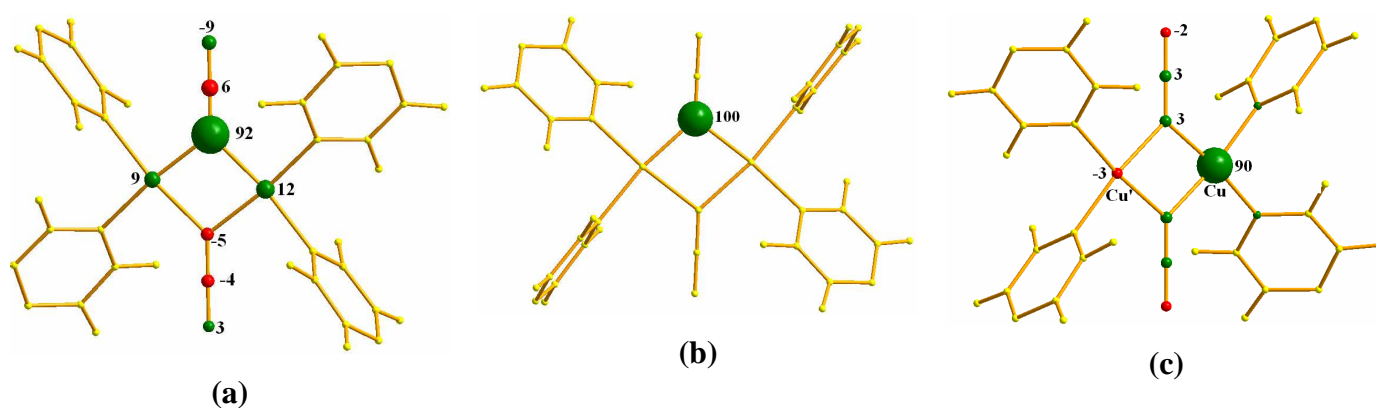


Fig. 31: Atomic SF<sub>S</sub> percentages electron spin density reconstructions along the Cu-N1 bond for the EO molecular system: at the CC on the N1 atomic basin (a), at the N1 nucleus (b) and at the Cu nucleus (c). Atoms are portrayed as in Fig. 30 with same colour codes.

The reconstruction of  $s(\mathbf{r})$  in terms of SF<sub>S</sub> contributions for three reference points along a Cu-N5 bond (that is of Cu with a terminal nitrogen pirydil ligand) reveals that the patterns displayed are similar to those retrieved for Cu-N<sub>azide</sub> bridge. At bcp, the nitrogen of the azido groups appear to be clearly involved in the spin delocalization through copper, because the  $d_{x^2-y^2}$  Cu orbital is connecting all these ligand atoms through the overlap with their fragment double-occupied HOMO orbitals (Fig.32).

<sup>y</sup> in super-exchange terms: the positive spin density is induced close to the N1 atom, but not in the bonding region because the Cu-N1<sub>bridge</sub> is a dative bond

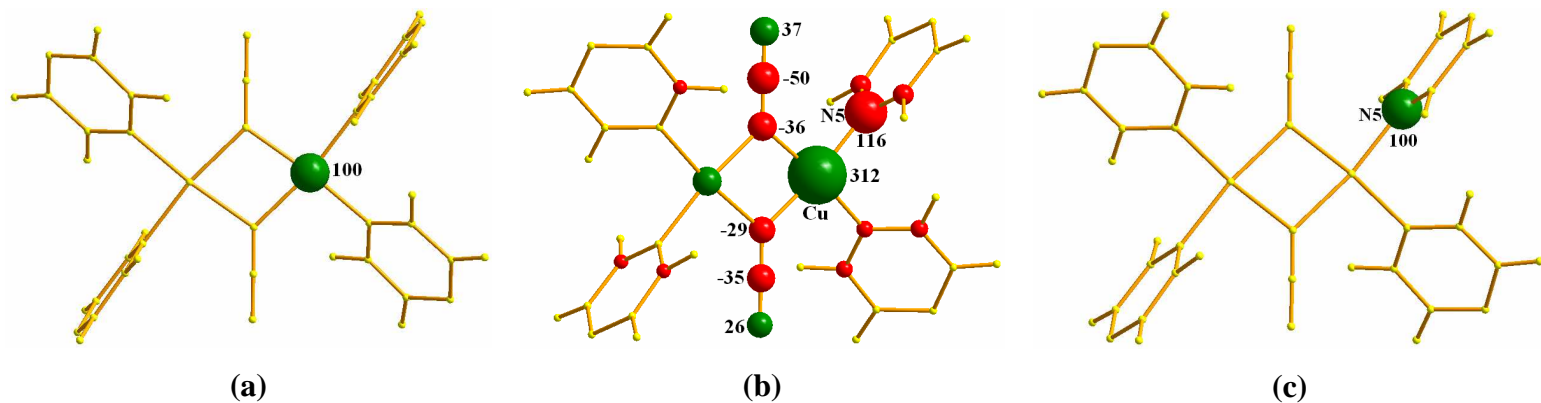


Fig. 32: Atomic  $SF_5$  percentages electron spin density reconstructions along the Cu-N5 bond for the EO molecular system: at the Cu nucleus (a), at the bcp (b) and at the N5 nucleus (c). Atoms are portrayed as in Fig. 30 with same colour codes.

The  $SF_5$  contributions to the spin density along the two N-N bonds of the azido groups are also worth of investigation. The spin density is large on N1 ( $s(\mathbf{r}) = 0.245$  a.u.) but then it decreases and turns out to be about two order smaller along the N1-N2 and N2-N3 internuclear axes. As displayed in the map of  $\nabla^2\rho(\mathbf{r})$  (Fig. 27, right panel), the bridging atom N1 is the only one featured with a  $sp^2$ -like hybridization, hence  $s(\mathbf{r})$  delocalizes through almost pure atomic p-orbitals on N2 and N3 atoms; this clarifies the reason of why the spin density along the N1-N2 and N2-N3 bonds is so low. Note also (figure 33 and 34): a) the large contributions to  $s(\mathbf{r})$ , along these bonds, from quite delocalized sources; b) the different roles of the central and terminal nitrogen atoms<sup>z</sup> and c) the large and almost equal contributions from the two Cu atoms, which always promote the enhancement of the alpha spin density along the two bonds through an electron spin delocalization mechanism.

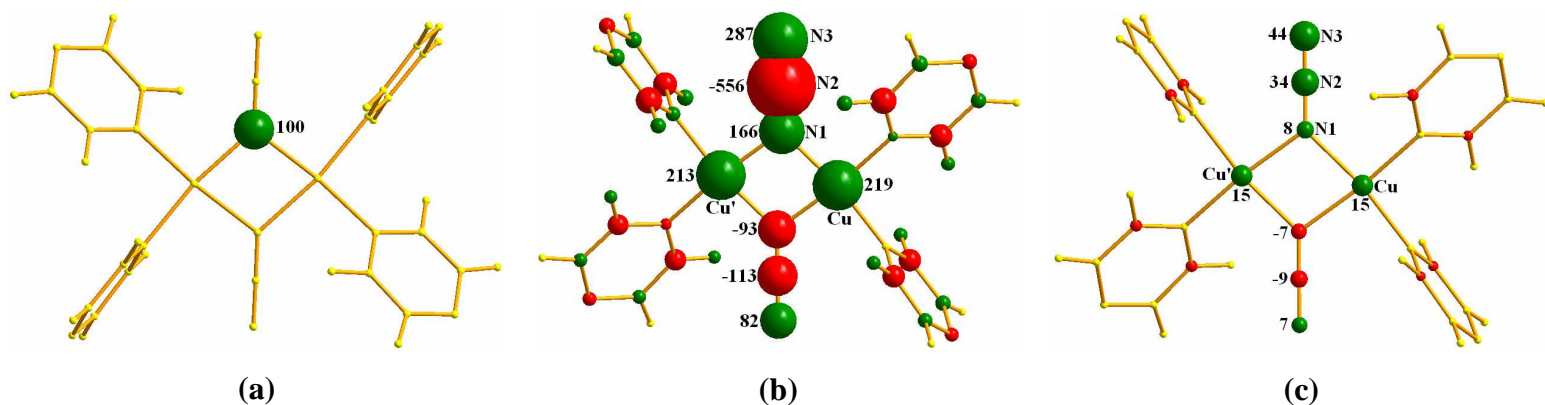


Fig. 33: Atomic  $SF_5$  percentages electron spin density reconstructions along the N1-N2 bond for the EO molecular system: at the N1 nucleus (a), at the bcp (b) and at the N2 nucleus (c). Atoms are portrayed as in Fig. 30 with same colour codes.

<sup>z</sup> the  $\pi^*$  involvement of the central N atom is clear from its spin density, while the  $\pi_{\text{gerade}}$  has no contribution on this atom.

The spin density along the Cu-Cu' inter-nuclear axis, hence along the formally doubly occupied  $d_{xy}$  bond, is negative on the Cu nucleus, then it turns slightly positive and, eventually, it quickly decays to about zero till the mid-point (see Fig. 35). The negative spin density on Cu nucleus (with different in sign  $SF_S$  contributions from the Cu atom considered and from the other Cu atomic basin) is clearly explained by the maps of the Laplacian of the spin density, either in the plane of the azide ligands (Figure 27) and in the plane perpendicular to it and containing the metal centers (Figure 35) and taking into account the specific position of the reference point; then, as  $s(\mathbf{r})$  turns positive, the  $SF_S$  contributions from Cu atoms become the same sign back again. At midpoint, the spin density is negligibly small and the  $s(\mathbf{r})$  reconstruction in terms of  $SF_S$  contributions is very delocalized with positive contributions from the two copper atoms (see Fig. 36).

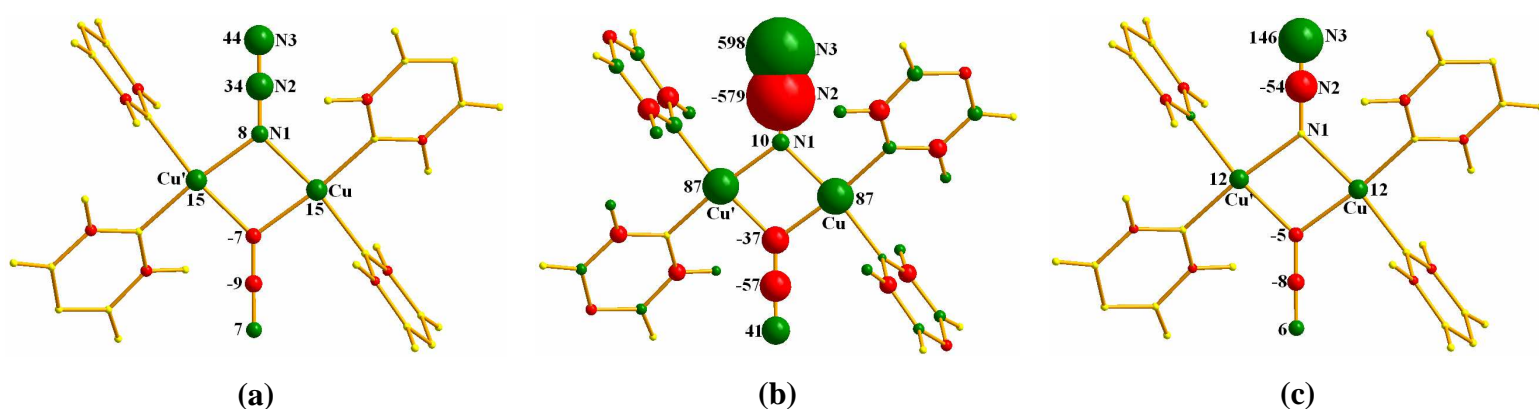


Fig. 34: Atomic  $SF_S$  percentages electron spin density reconstructions along the N2-N3 bond for the EO molecular system. : at the N2 nucleus (a), at the bcp (b) and at the N3 nucleus (c). Atoms are portrayed as in Fig. 30 with same colour codes.

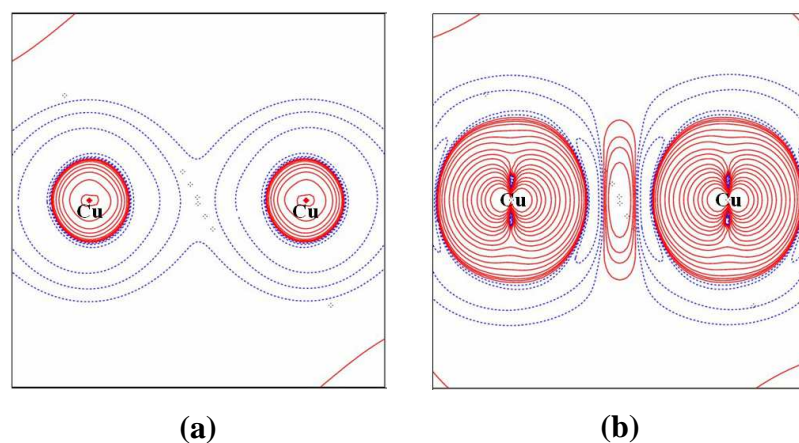


Fig. 35: (a) Electron spin density  $s(\mathbf{r})$  and (b) its Laplacian in the  $(z,y)$  plane for symmetric EO di-nuclear copper azido bridged molecular system at UB3LYP/pob-TVPZ computational level. Atomic units (a.u.) are used throughout. Contour maps are drawn as in Fig. 27 with same colour codes.



Furthermore, it is worthy to note the substantial difference of the  $SF_S$  contributions along this bond and along the one ( $Cu-N_{bridge}$ ) where spin delocalization occurs. Clearly, neither ferromagnetic coupling, nor spin delocalization occur through the  $Cu-Cu'$  internuclear axis and through their direct interaction (compare Fig. 27 with Fig. 35).

Considering the EE molecular system, about 64% of the unpaired electrons density is localized on the  $Cu(II)$  ions, slightly more than for the EO system (see spin atomic populations, Tab.16). The spin density population delocalized on the azide group is almost halved with respect to the EO system, while that on terminal ligands is increased (essentially, because for EE there is one more of them). A small negative spin density population is retrieved for the central nitrogen of the azido group.

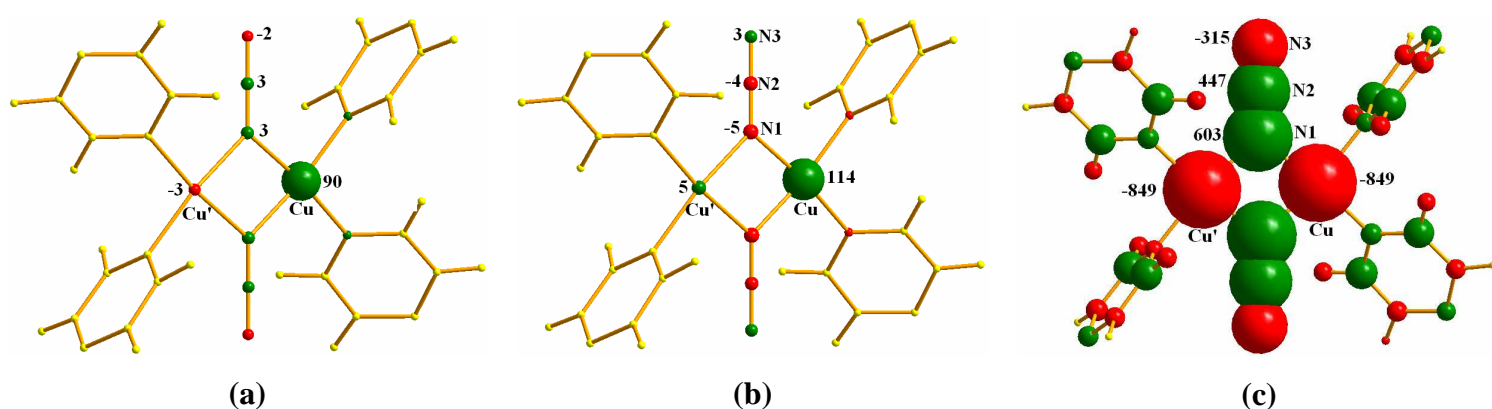


Fig. 36: Atomic  $SF_S$  percentages electron spin density reconstructions along the  $Cu-Cu'$  axis for the EO molecular system.: at the  $Cu$  nucleus (a); at  $0.5 \text{ \AA}$  from the  $Cu$  nucleus (b) and at the middle point along the  $Cu-Cu'$  axis (c).

Atoms are portrayed as in Fig. 30 with same colour codes.

The average beta effect for  $Cu$  atom is confirmed, being the integrated Laplacian of the spin density significantly positive. Such quantity, apart for the  $Cu$  atoms, is relevant only for the  $N3$  and  $N4$  atoms of the azido groups and for  $O1$  (see Figure 40 a for the labels of atoms). The behaviour of the azide group  $N$  atoms closely resembles that of the corresponding  $N$  atoms in the E-O systems, taking into account that the  $N3$  atom in the EE system corresponds to the terminal azide  $N$ , because the shorter  $Cu-N$  bond is formed with  $N5$  and the longer with  $N3$ .

$\Omega$	$q(\Omega)$	$s(\Omega)$	$\nabla^2\rho_\alpha(\Omega)$	$\nabla^2\rho_\beta(\Omega)$	$\nabla^2s(\Omega)$
Cu	1135	+0.640	+0.010	-0.010	+0.020
N1	-0.890	+0.084	+0.000	-0.002	+0.002
N2	-1078	+0.075	+0.000	-0.000	-0.001
N3	-0.227	+0.083	+0.007	-0.007	+0.014
N4	-0.134	-0.004	-0.007	+0.007	-0.013
N5	-0.352	+0.031	-0.002	+0.001	-0.003
$(N)_3^-$	-0.713	+0.110	-0.002	+0.001	-0.003
O1	-1074	+0.070	-0.003	+0.003	-0.006

Tab. 16: Atomic charges, electron spin populations, atomic Laplacians of electron spin density divided in  $\alpha$  and  $\beta$  counterparts and Atomic Laplacians of electron spin density in the EE molecular system and only for the atomic basins (copper and nitrogens) involved in the azido-bridge. All values are given in atomic units (a.u.).

Analogously to the EO system, in order to understand the spin density  $SF_s$  contributions we must consider at first the aspherical  $d$ -electron distribution surrounding metal centers. In the EE system the Cu atom is five-fold coordinated in an almost square pyramidal arrangement of ligands. Once again, as for the EO system, the  $d_{x^2-y^2}$  orbital is the magnetic singly occupied orbital and the base of the pyramid corresponds to bonding with the three external ligand atoms (N1, N2, O1) and the N5 atom of the azide group, in agreement with the crystal field theory and with a  $d^9$  configuration on Cu atom (Fig.28b). The apical ligand N3, connected to the Cu by the longer Cu-N bond is oriented approximatively along  $z$  (local coordinate system on the Cu) and interacts with the almost doubly filled Cu  $d_{z^2}$  orbital (providing so the reason why this bond is actually longer). As expected from orbital model and corroborated by the analysis of the Laplacian electron density, the CDs are found along Cu-dative bonds, with the Cu-ligand dative bonds of the base of the pyramid being greater than those retrieved along the apical bond. Moreover the CCs are accordingly located in between the ligands of the base pyramid. Another expected result was to find a relevant  $s(\mathbf{r})$  at the CD along the shorter Cu-N azide bond (0.286 a.u.) and a definitely smaller  $s(\mathbf{r})$  value ( $s(\mathbf{r}) = 0.005$  a.u.) at the CD of the longer, because of the single occupation of the  $d_{x^2-y^2}$  orbital and the almost double occupation of the  $d_{z^2}$  orbital. Indeed, the spin density at the CD along Cu-N5 bond matches almost perfectly the one found for the bridging bond in the EO system, while the one along Cu-N3 is two order of magnitude lower.

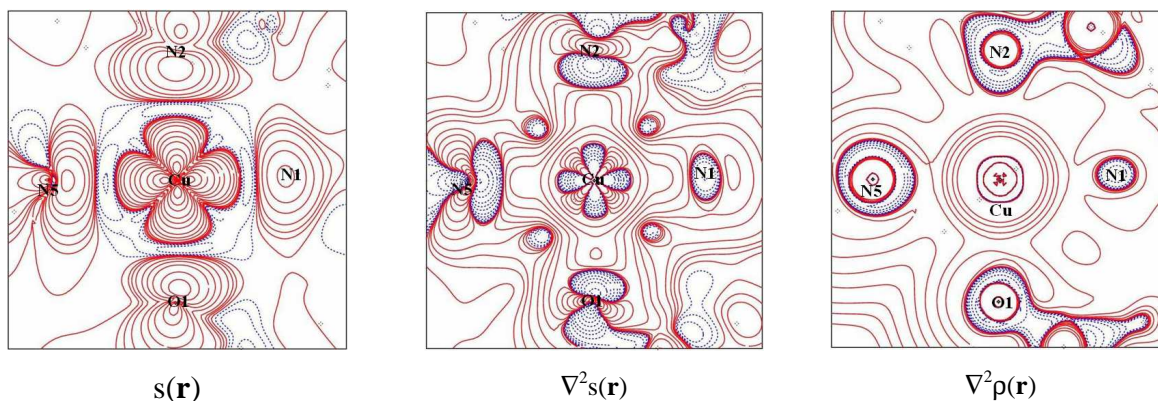


Fig. 37: Electron spin density  $s(\mathbf{r})$  and its Laplacian and Electron density Laplacian in the Cu-N5-O1 plane for the asymmetric EE di-nuclear copper azido bridged molecular system at UB3LYP/pob-TVPZ computational levels. Atomic units (a.u.) are used throughout. Contour maps are drawn as in Fig. 27 with same colour codes.

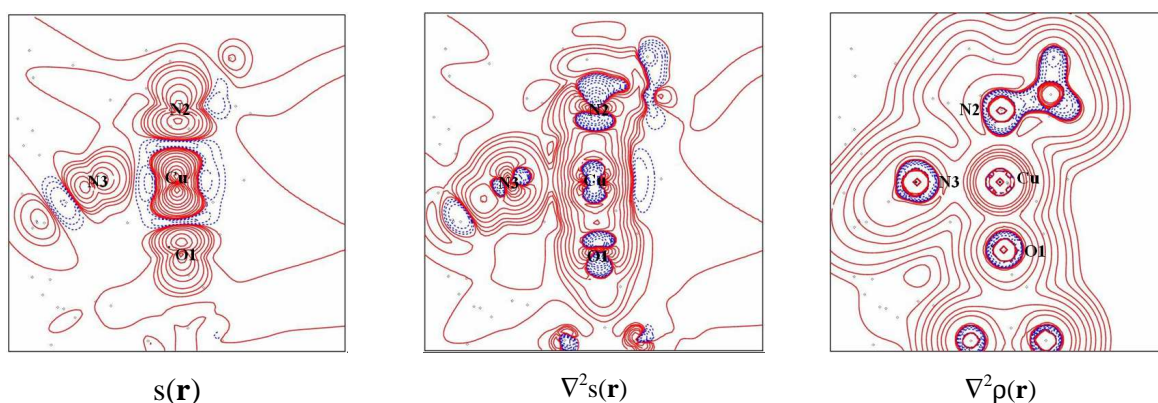


Fig. 38: Electron spin density  $s(\mathbf{r})$  and its Laplacian and Electron density Laplacian in the Cu-N3-O1 plane for the asymmetric EE di-nuclear copper azido bridged molecular system at UB3LYP/pob-TVPZ computational level. Atomic units (a.u.) are used throughout. Contour maps are drawn as in Fig. 27 with same colour codes.

Comparing the spin density  $SF_S$  reconstructions at the CD along these two bonds (Fig. 39) brings further remarkable insights. In fact the  $SF_S$  reconstruction along the Cu-N5 bond is similar to the one of the Cu-N<sub>bridging</sub> bond in the EO system, while that for the Cu-N3 bond is far different and endowed with much more delocalized sources. For both dative bonds, N3 atoms give a relevant contribution, enhancing the  $\alpha$ -spin density and the two metal centers also cooperate in such  $\alpha$ -spin density enhancement (see also the maps reported in Fig.37 and Fig. 38).

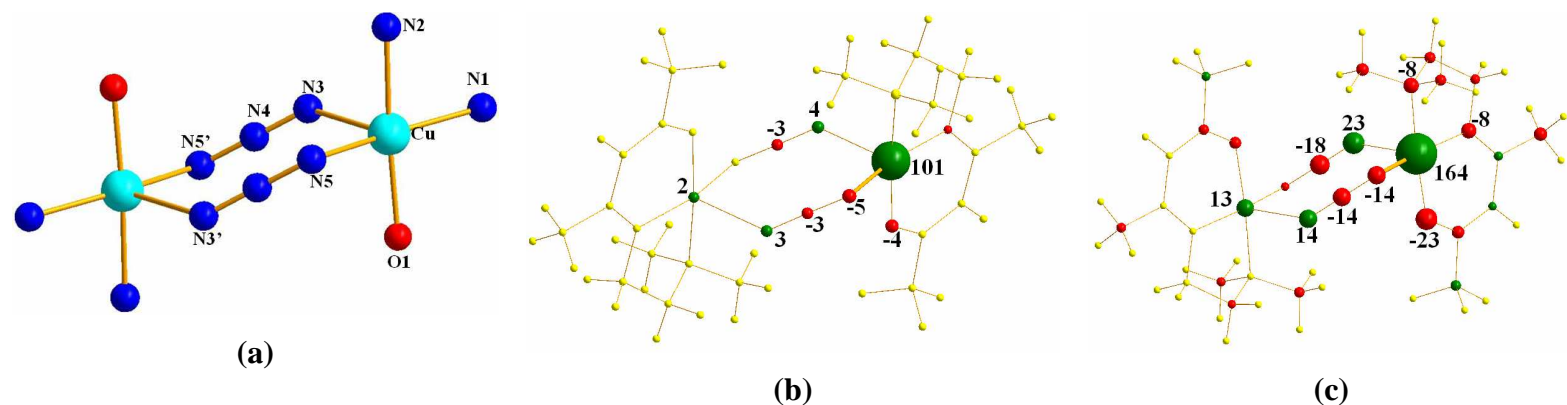


Fig. 39: Atomic  $SF_5$  percentages reconstructing the electron spin density at the (3,+3) CD along the Cu-N5 (b) and the Cu-N3 (c) bonds for the EE molecular system. Atoms are portrayed as in Fig. 30 with same colour codes.

The comparison of the reconstructions of  $s(\mathbf{r})$  in terms of  $SF_5$  contributions for three similar reference points along the shorter and longer Cu- $N_{\text{azide}}$  bonds, with the first point close to the spin density maximum nearby the Cu atom, the second located at the bcp and the third close to the N atom, reveals us that the shorter bond has definitely less delocalized sources (Fig. 40).<sup>aa</sup> This holds true also at bcp but with the important difference that the two bonded atoms concur to enhance the bcp spin density for the longer bond, while have opposed contributions for the shorter Cu-N bond as already found, discussed and interpreted for the Cu-N1 bond in the EO system. .

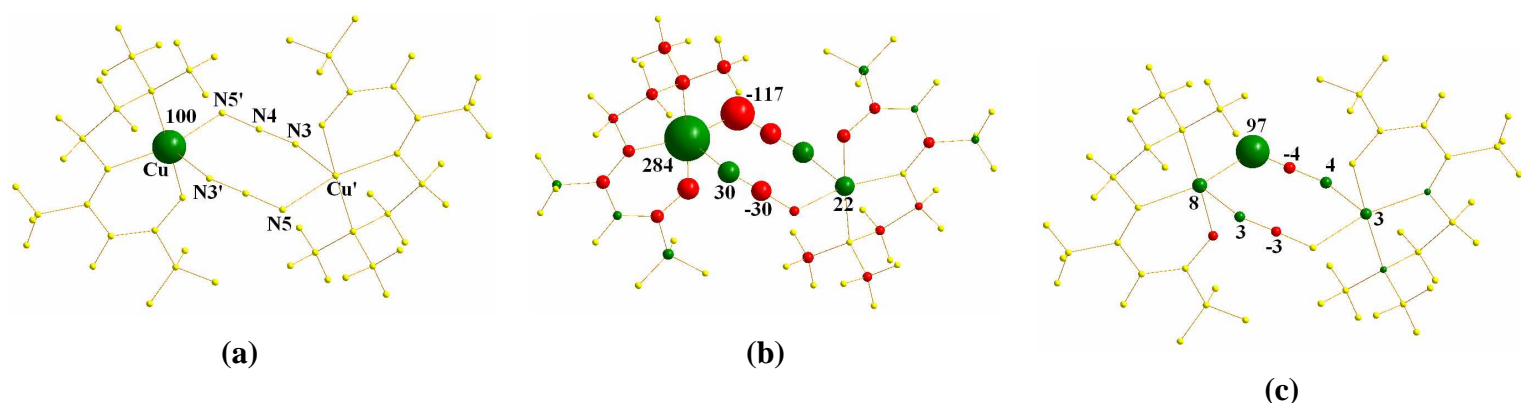


Fig. 40: Atomic  $SF_5$  percentages reconstructing the electron spin density along the Cu-N5 shorter bond of the EE molecular system: at the Cu nucleus (a), at the Cu-N5 bcp (b) and at 0.05 Å from N5 nucleus (c). Atoms are portrayed as in Fig. 30 with same colour codes.

Finally, the analysis of the reconstruction of spin density in terms of  $SF_5$  contributions along the two bonds of the azido group is discussed. Note first that the spin density on the N5 nucleus (Fig 41a) is only 0.063 a.u., to be compared with a value of about 5 times as big for the bridging N, N1, in the EO system. As also shown by the far lower coupling constant, such behaviour denotes that in the EE system spin delocalization is less efficient than in the EO system.

<sup>aa</sup> This observation refers to the percentage, not to the absolute values, as there is a difference of two order of magnitude between the spin density values to be reconstructed

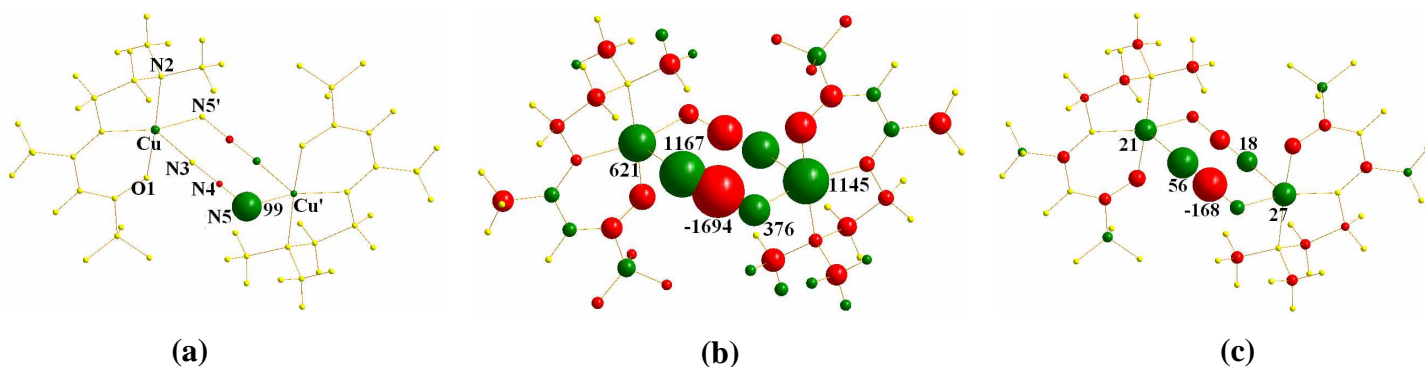


Fig. 41: Atomic  $SF_5$  percentages reconstructing the electron spin density along the N5-N4 bond for the EE molecular system : at the N5 nucleus (a), at the N5-N4 bcp (b) and at the N4 nucleus(c). Atoms are portrayed as in Fig. 30 with same colour codes.

The role of N5 in the super-exchange mechanism is mediated through its influence on N4 and N3 and is thus less proficient. Actually, its spin distribution is shaped differently than the one of the bridging N in the EO system, while those of N4 and N3 atoms resemble more those of the corresponding N atoms in the EO system (compare Fig. 42 with Fig. 27).

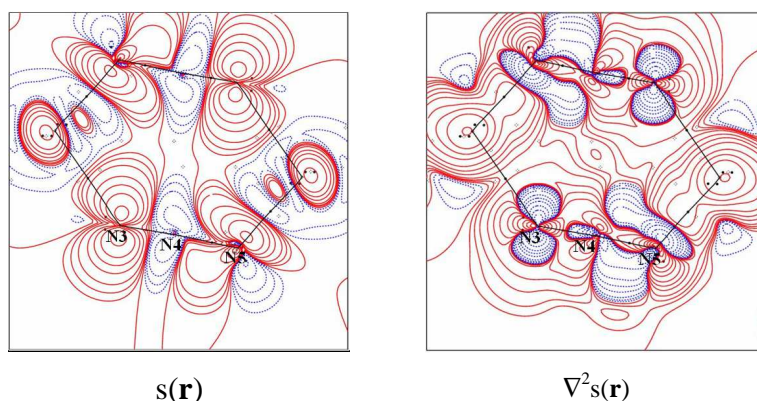


Fig. 42: Electron spin density  $s(\mathbf{r})$  and its Laplacian in the Cu-N3-N5 plane for asymmetric EE di-nuclear copper azido bridged molecular system at UB3LYP/pob-TVPZ computational level. Atomic units (a.u.) are used throughout. Contour maps are drawn as in Fig. 27 with same colour codes.

Looking at the comparison between Fig. 41 (EE: N5-N4 bond) and Fig. 33 (EO: N1-N2 bond) , it is possible to note several common interesting features between the  $SF_5$  reconstructions profiles along these two bonds. One may observe equal reconstructions at the N nucleus connected to Cu (N5 and N1, respectively), similar reconstruction patterns at the bcp but with much larger delocalization for the EE system, and a distinct reconstruction pattern nearby the central N (N4 and N2, respectively). The similar involvement from the two Cu atoms is confirmed, indicating a coupling between them realized through the azide non-innocent linker.. Similar considerations apply to the comparison

between the SF<sub>s</sub> reconstructions profiles along the EE N4-N3 bond (Fig. 43) and the EO N2-N3 bond (Fig. 34)

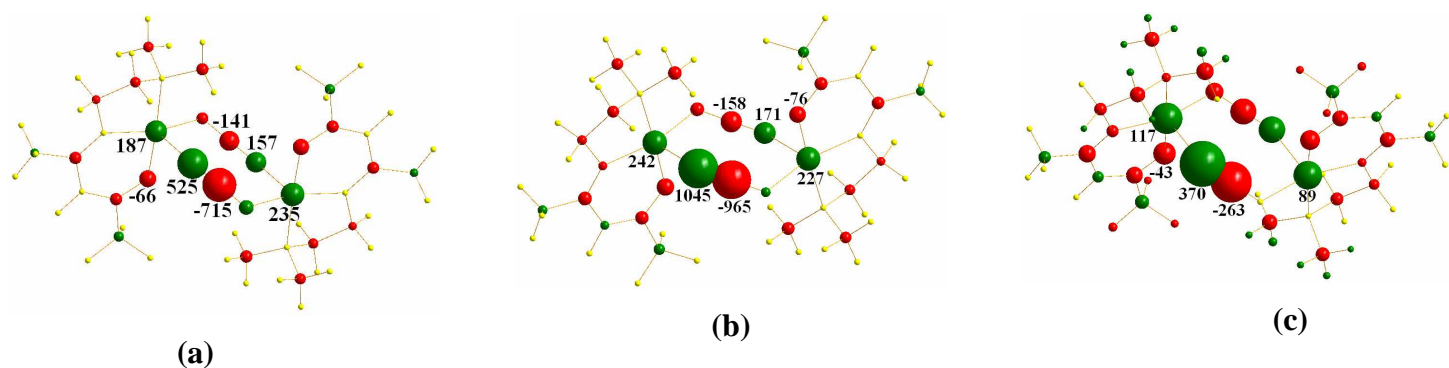


Fig. 43: Atomic SF<sub>s</sub> percentages reconstructing the electron spin density along the N4-N3 bond for the EE molecular system at the N4 nucleus (a), at the N4-N3 bcp (b) and at the N3 nucleus (c). Atoms are portrayed as in Fig. 30 with same colour codes.

### ***Non-Innocent role of ligands in some Ni organometallic complexes as viewed through the Spin Density Source Function***

Non-innocent metal ligand complexes are characterized by the ability to make the oxidation state of the central metal atom and the electronic structure of the ligands not *a priori* and unambiguously determined<sup>[24]</sup>. As showed by Cauchy *et al* in a study on the magnetic properties of a series of neutral CpNi(dithiolene)<sup>•</sup> radical complexes<sup>[25]</sup>, even ligands that are classified as innocent may play a determinant role in the electron spin coupling phenomena. DFT *J* coupling constant calculations showed that spin density is strongly delocalized on the NiS<sub>2</sub> moiety and, more importantly, up to 20% of *s*(**r**) is delocalized on the Cp rings. As a result, the intermolecular Cp...Cp and Cp...dithiolene overlap interactions lead to anti-ferromagnetic couplings mediated by ligands that are commonly classified as innocent. In this subsection preliminary results regarding the reconstruction of spin density in terms of SF<sub>s</sub> applied on CpNi(adt)<sup>•</sup> radical complex (adt=acrylonitrile-2,3-dithiolate) (Fig. 44) are presented, to get insight on the factors that lead to ferro- or anti-ferro magnetic coupling behaviour in crystal and to quantitatively distinguish whether the ligands play a innocent or non-innocent<sup>[25]</sup> role within these metal complexes. In table 17 are reported the values of atomic spin populations for all the atoms within molecular system CpNi(adt)<sup>•</sup>. In table 18, these atomic spin populations are conveniently grouped to evince the contributions of the Ni, the dithiolene and the Cp moieties to the total spin population of the molecule. It is found that almost the 82% of *s*(**r**) is localized on the Ni atomic basin while, differently from the results of Cauchy *et al*, only the 11.5% of the spin density is delocalized on the Cp ligand and just the 6.5% is delocalized onto the dithiolene ligand.

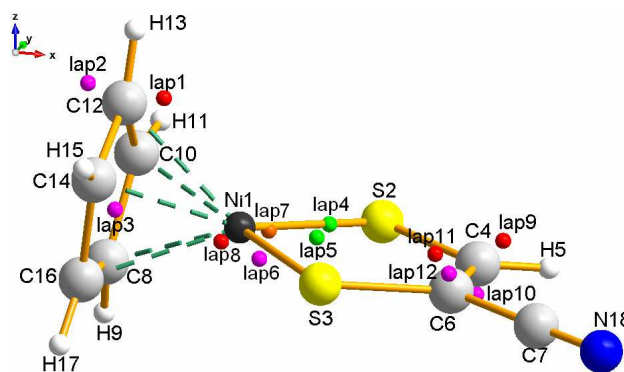


Fig.44: adt CpNi(dithiolene)<sup>•</sup> radical complex;  $\nabla^2\rho(\mathbf{r})$  critical points are reported. The  $\nabla^2\rho(\mathbf{r})$  critical points are denoted as follows: green points (3,+3) charge concentrations (CC), red points denote (3,+1) saddle points, violet point (3,-1) saddle points and orange point denote (3,-3) charge depletions (CD).

$\Omega$	$q(\Omega)$	$s(\Omega)$	$\nabla^2\rho_\alpha(\Omega)$	$\nabla^2\rho_\beta(\Omega)$	$\nabla^2s(\Omega)$
Ni1	1.1245	0.8192	0.0127	-0.0123	0.0250
S2	0.1266	0.0309	-0.0026	0.0019	-0.0046
S3	0.0950	0.0325	-0.0024	0.0020	-0.0044
C4	-0.3280	0.0084	-0.0004	-0.0008	0.0003
H5	-0.1257	0.0003	-0.0003	0.0003	-0.0005
C6	-0.4295	-0.0061	-0.0007	0.0031	-0.0038
C7	1.0990	0.0032	0.0005	-0.0010	0.0015
C8	0.1355	0.0203	-0.0015	0.0023	-0.0038
H9	-0.1352	0.0012	-0.0007	0.0007	-0.0014
C10	0.0670	0.0245	0.0025	-0.0014	0.0039
H11	-0.1263	0.0002	-0.0008	0.0008	-0.0017
C12	0.1659	0.0199	-0.0035	0.0021	-0.0056
H13	-0.1430	0.0016	-0.0007	0.0007	-0.0014
C14	0.0692	0.0240	0.0011	-0.0012	0.0023
H15	-0.1194	0.0003	-0.0008	0.0008	-0.0016
C16	0.1018	0.0223	-0.0004	0.0014	-0.0018
H17	-0.1294	0.0009	-0.0008	0.0008	-0.0016
N18	-1.4463	-0.0036	-0.0004	0.0004	-0.0008

Tab. 17: Atomic charge, electron spin populations, atomic Laplacians of electron spin density divided in  $\alpha$  and  $\beta$  counterparts and atomic Laplacians of electron spin density for each atoms within adt CpNi(dithiolene)<sup>•</sup> radical complex. All values are given in atomic units (a.u.).

The spin population of the two sulfur atoms is slightly different ( almost the 3.3% of the unpaired electron is delocalized on S3 and slightly less, 3.1%, on S2). The difference is not due to a relevant structural difference between Ni-S2 (2.131 Å) and Ni-S3 (2.132 Å) bonds, rather it might be due to a non symmetric delocalization of the spin density on the dithiolene ligand because of the terminal –

CN group or, more likely, to the higher, by about 0.03 e<sup>-</sup>, electron population, of S3 (S3: 31.905 e<sup>-</sup> and S2: 31.873 e<sup>-</sup>). The non negligible spin population on the S atoms reveals the non-innocent nature of the dithiolene ligand and highlights its capability to influence the oxidation state of the metal center in radical metal complexes.

	q( $\Omega$ )	s( $\Omega$ )	%s( $\Omega$ )
Ni1	1,12	0,82	81,92
Dithiolene	-1,01	0,07	6,55
Cp	-0,11	0,12	11,53

Tab. 18: Atomic charge, electron spin population and electron spin population percentage for the Ni metal and both the ligands within adt CpNi(dithiolene)<sup>•</sup> radical complex. All values are given in atomic units (a.u.).

On the other hand, in the case of Cp ligand the rationale behind differences in the spin density delocalization might be different. In fact spin population values show that almost the 2.5% of the unpaired electron distribution is delocalized on the C10 atomic basin, a value quite similar to that delocalized on C14 (2.4%) but larger than that delocalized on the C8 and C12 atoms (both around 2.0%). The behaviour of s(**r**) in this case is mirrored by structural differences in terms of distances. In fact the Ni-C10 distance (2.078 Å) is very similar to the Ni-C14 one (2.076 Å) while it is different from the Ni-C8 and Ni-C12 distances, which are both somewhat longer (respectively 2.107 Å and 2.112 Å). However, one should also note that larger spin populations correspond to larger electron populations (C10: 5.933; C14: 5.931; C8: 5.865; C12: 5.834). So, as in case of adt ligand, also the Cp ligand is non innocent. The analysis of the reconstructions of  $\rho(\mathbf{r})$  and s(**r**) in terms of SF and SF<sub>S</sub> contributions respectively reveals how the latter sources are more delocalized than the former within the whole molecule. The set of analysed reference points, along with their electron density and spin density properties is collected in Table 19, whereas Fig. 44 illustrates pictorially their locations in the molecule. Interestingly, the application of SF<sub>S</sub> permit us to distinguish the mechanism of the transmission of s(**r**) within the molecule; in fact it is possible to observe how s(**r**) is delocalized on the adt ligand through the covalent Ni-S bonds [see the reconstructions of s(**r**) at lap7 and lap4 (Table 19), which are taken as reference points in Fig.46 and 47]; this is not the case of Cp ligand where the spin density appears to be delocalized through space, *via* the  $\pi$  framework of the ligand. Furthermore the application of SF<sub>S</sub> permits us to show in a *quantitative* way how s(**r**) is delocalized onto the Cp ligand; in this sense SF<sub>S</sub> is able to quantify how much a ligand is innocent or not. In the CpNi(adt) complex, the Cp ligand gives a  $\beta$  effect to the delocalization of s(**r**) onto the Ni CD (lap7) and onto the adt ligand CC (lap 4) and a contribution to the spin density at lap7 (which lies onto Ni1-S2 bond) very similar with respect to the adt ligand (SF<sub>S</sub>(Cp)% = 14.1 vs SF<sub>S</sub>(adt)% = 14.6).



	TYPE	$\rho(\mathbf{r})$	$s(\mathbf{r})$	$\nabla^2\rho(\mathbf{r})$	$\nabla^2s(\mathbf{r})$
Lap1	(3, 1)	1,81E-01	2,99E-03	-3,52E-02	-1,63E-02
Lap2	(3,-1)	1,72E-01	2,55E-03	4,31E-02	-1,78E-02
Lap3	(3,-1)	1,76E-01	1,60E-03	6,94E-02	-5,74E-03
Lap4	(3, 3)	1,64E-01	1,81E-03	-3,70E-01	-1,08E-02
Lap5	(3, 3)	1,44E-01	1,27E-03	-3,02E-01	-5,73E-03
Lap6	(3,-1)	1,52E+00	2,97E-01	1,27E+01	-3,64E+00
Lap7	(3,-3)	1,59E+00	-1,16E-02	1,39E+01	1,68E+00
Lap8	(3, 1)	4,59E+00	9,05E-01	-3,18E+01	-4,13E+01
Lap9	(3, 1)	1,97E-01	8,86E-04	-5,08E-02	-5,31E-03
lap10	(3,-1)	1,60E-01	7,28E-04	8,13E-02	-2,85E-03
lap11	(3, 1)	1,97E-01	-9,27E-04	-1,91E-01	5,77E-03
lap12	(3,-1)	1,80E-01	-6,52E-04	-2,30E-02	3,06E-03

Tab. 19: Electron density, electron spin density, Laplacian of  $\rho(\mathbf{r})$  and Laplacian of  $s(\mathbf{r})$  for the selected  $\nabla^2\rho(\mathbf{r})$  reference points in adt CpNi(dithiolene)<sup>•</sup> radical complex (see Fig. 44). All values are given in atomic units (a.u.).

The analysis of the reconstruction of  $s(\mathbf{r})$  at CD along the Ni-S2 bond in terms of SF<sub>3</sub> contributions from the magnetic part of the wave function and from the remaining (relaxation) part of it (relaxation term), allows us to get some more insight on the mechanisms of spin transmission within the molecular system.

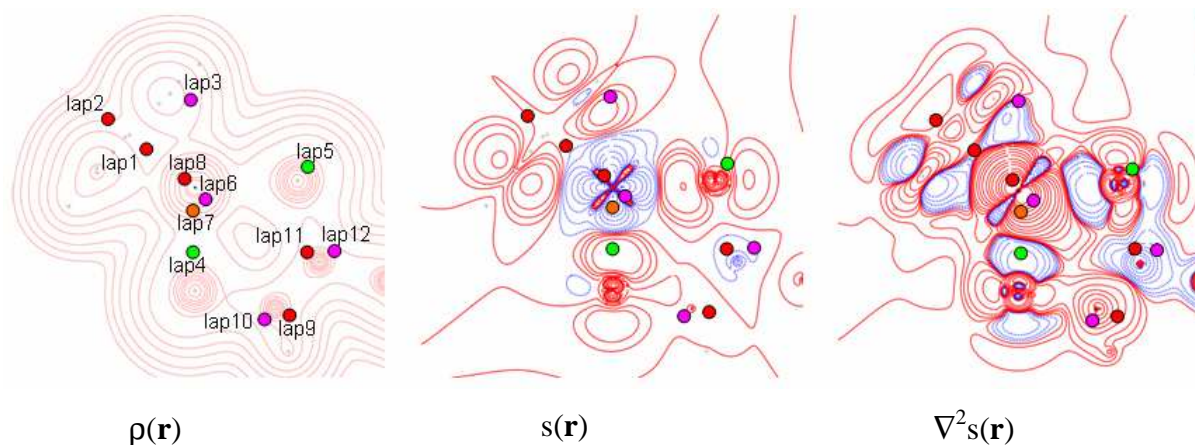


Fig. 45: Electron density, spin density and Laplacian of  $s(\mathbf{r})$  in the Ni-S2-S3 plane for adt CpNi(dithiolene)<sup>•</sup> radical complex at UHF/pob-TVPZ computational levels. Atomic units (a.u.) are used throughout. Contour maps  $\beta$  drawn as in Fig. 27 with same colour codes.

An  $\alpha$ , positive contribution to the spin density is expected and found from the single occupied atomic orbital of the Ni atomic basin (see Fig. 45b), while a negative contribution to the reconstruction of  $s(\mathbf{r})$  is expected from the relaxation molecular orbitals due to polarization effects (see Fig. 45c). In terms of percentage contribution values, SFs%, these contributions from the Ni atom will be instead negative (-136.3%) and positive (210%), respectively, as they oppose and

concur to the negative value of  $s(\mathbf{r})$  at the CP lap 7. The percentage contribution to  $s(\mathbf{r})$  given by the magnetic orbital is negative for the Ni atomic basin ( $\alpha$  effect), while it is positive for the ligands, both giving a  $\beta$  effect. On the contrary, when the relaxation contributions to the spin density are considered, the metal center contributes with a positive value of  $SF_S$  percentage, while both the ligands oppose to the globally negative value of  $s(\mathbf{r})$  at the reference point. This is a clear effect of a spin polarization mechanism driving the electron spin density information transmission at CP lap 7.

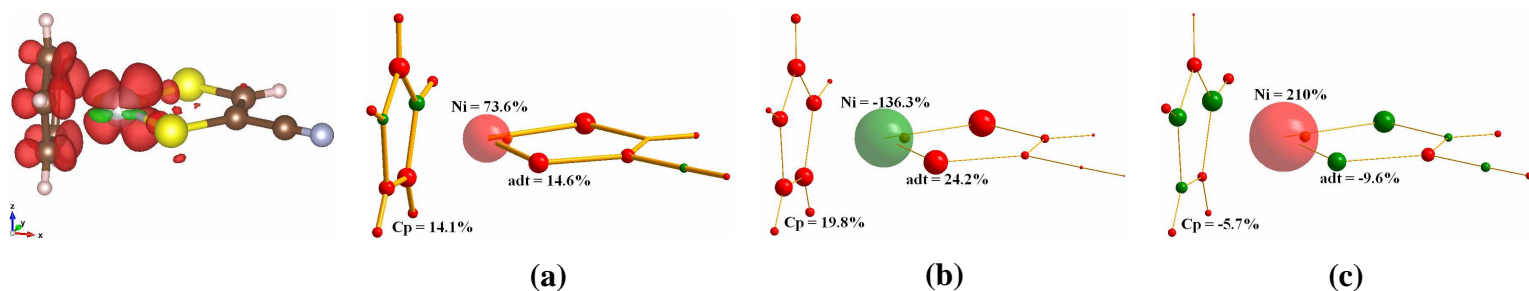


Fig. 46: Atomic  $SF_S$  percentages at the CD lap 7 (Table 17 and Fig. 44) on the Ni1-S2 bond, as evaluated from (a) the total density, (b) the magnetic orbital and (c) the non-magnetic natural orbitals densities for  $\text{adt CpNi(dithiolene)}^\bullet$  radical complex. Atoms are portrayed as spheres with volumes proportional to their source percentage contributions to  $s(\mathbf{r})$  values at the critical points considered. Colour codes: green or red whether atoms represent positive ( $\alpha$  effect) or negative ( $\beta$  effect) sources for  $s(\mathbf{r})$  at critical point considered. On the left is reported 3D isosurface of  $s(\mathbf{r})$  at the value recovered at the CP considered.

The reconstruction of  $s(\mathbf{r})$  in terms of  $SF_S$  contributions given by the magnetic singly occupied natural orbital and by the reaction or relaxation molecular orbitals, highlights how, as in the case of the  ${}^3B_1$  water triplet, the relaxation term essentially counteracts the contributions given by the magnetic orbital to the reconstruction of  $s(\mathbf{r})$  at the CC along the Ni-S2 bond (Fig. 47). At this reference point the spin density is small and positive (0.0018 a.u.) and dominated by the overwhelming  $\alpha$  contribution from Ni. The Cp ligand yields an overall  $\beta$  effect ( $SF_S\% = -57.3$ ), opposing to such positive density with a global contribution which is almost ten times larger in magnitude than that given by the adt ligand ( $SF_S\% = -6.3$ ). In fact, in the case of the adt ligand the contribution from the  $\beta$ -effect due to the magnetic orbital is almost compensated for by the  $\alpha$ -effect brought in by the relaxation natural orbitals, while for the Cp ligand the global  $\beta$ -effect due to the magnetic orbital largely superceeds the small overall  $\alpha$ -effect caused by the relaxation natural orbitals.

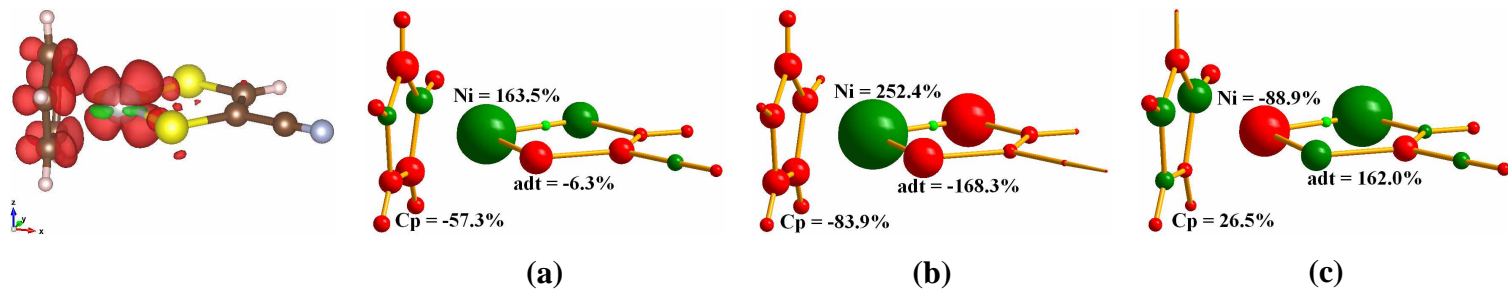


Fig. 47: Atomic  $SF_s$  percentages at the CC lap 4 (table 17 and Fig. 44) on the Ni1-S2 bond as evaluated from (a) the total density, (b) the magnetic natural orbital and (c) the non-magnetic natural orbital densities for adt CpNi(dithiolene) $^{\bullet}$  radical complex. Atoms are portrayed as in Fig.45 with same colour codes. On the left is reported 3D isosurface of  $s(\mathbf{r})$  at the value recovered at the CP considered.

The reconstruction of  $s(\mathbf{r})$  at CP lap7 and CP lap 4 identifies two different mechanisms for spin information transmission. The main and overdetermining contribution to the positive spin density at the CC reference point is given by the Ni atom and by the magnetic natural orbital, localized principally on the Ni  $d^7$  metal, with Cp partly opposing to such density and with adt playing only an almost negligible role. In the case of the negative spin density at the CP lap 7 reference point, it is still the Ni atom which gives the largest dominant contribution, (in this case a  $\beta$ -effect) but this now it is the result of the dominance of the relaxation orbitals contribution over the opposing contribution from the magnetic orbital. The Cp and the adt ligands, in this case, slightly concur to the spin density at the CP, rather than opposing to it as it was in the case of reconstruction of the CP lap4 electron density.

## **REFERENCES:**

- [1] J. A. Duffy and M. J. Cooper, in *Modern Charge Density Analysis*, ed. C. Gatti and P. Macchi. Springer, Dordrecht Heidelberg London New York, 2012, ch. 4, pp. 165-180.
- [2] B. Gillon and P. Becker, in *Modern Charge Density Analysis*, ed. C. Gatti and P. Macchi. Springer, Dordrecht Heidelberg London New York, 2012, ch. 8, pp. 277-302.
- [3] N. K. Hansen and P. Coppens, *Acta Crystallogr., Sect. A: Cryst. Phys., Diffr., Theor. Gen. Crystallogr.*, 1978, **34**, 909–921.
- [4] M. Deutsch, N. Claiser, S. Pillet, Y. Chumakov, P. Becker, J-M. Gillet, B. Gillon, C. Lecomte, M. Souhassou, *Acta Crystallogr., Sect. A: Cryst. Phys., Diffr., Theor. Gen. Crystallogr.*, 2012, **68**, 675-686.
- [5] M. Deutsch, B. Gillon, N. Claiser, J-M. Gillet, C. Lecomte, M. Souhassou, *IUCrJ*, 2014, **1**, 194-199.
- [6] B. Gillon, C. Sangregorio, A. Caneschi, D. Gatteschi, R. Sessoli, E. Ressouche, Y. Pontillon, *Inorganica Chimica Acta*, 2007, **360**, 3802-3806.
- [7] R. F.W. Bader, C. Gatti, *Chem. Phys. Lett.*, 1998, **287**, 233–238.
- [8] R. F.W. Bader, *Atoms in Molecules: A Quantum Theory*; Oxford University Press: Oxford, U.K. 1990.
- [9] C. Gatti, F. Cargnoni, L. Bertini, *J. Comput. Chem.*, 2003, **24**, 422–436.
- [10] C. Gatti, *Struct. Bond.*, 2012, **147**, 193–286.
- [11] L. J. Farrugia, E. Cameron, M. Tegel, *J. Phys. Chem. A*, 2006, **110**, 7952-7961.
- [12] L. J. Farrugia, E. Cameron, D. Lentz, M. Roemer *J. Am. Chem. Soc.*, 2009, **131**, 1251-1268.
- [13] J. Overgaard, B. Schiott, F. K. Larsen, B. B. Iversen, *Chem. Eur. J.*, 2001, **7**, 3756-3767.
- [14] L. Lo Presti and C. Gatti, *Chem. Phys. Lett.*, 2009, **476**, 308-316.
- [15] E. Monza, C. Gatti, L. Lo Presti, E. Ortoleva, *J. Phys. Chem. A*, 2011, **115**, 12864–12878.
- [16] C. Gatti and D. Lasi, *Faraday Discuss.*, 2007, **135**, 55-78.
- [17] L. Lo Presti, A. Ellern, R. Destro, R. Soave, B. Lunelli, *J. Phys. Chem. A*, 2011, **115**, 12695–12707.
- [18] M. Schmokel, S. Cenedese, J. Overgaard, M. R. V. Jorgensen, Y.-S. Cheng, C. Gatti, D. Stalke, B. B. Iversen, *Inorg. Chem.*, 2012, **51**, 8607–8616.
- [19] J. P. Malrieu, R. Caballol, C. J. Calzado, C. De Graaf, N. Guihery, *Chem. Rev.*, 2014, **114**, 429-492.
- [20] C. Gatti, *Phys Scripta* 87, 2013, 048102 (38pp)
- [21] Arfken G (1985) *Mathematical Methods for Physicists*. Academic Press, Orlando, Florida

- [22] M. A. Abersold, B. Gillon, O. Plantevin, L. Pardi, O. Kahn, P. Bergerat, I. von Seggern, F. Tuczeck, L. Öhrström, A. Grand and E. Lelièvre-Berna, *J. Am. Chem. Soc.* 1998, **120**, 5238-5245
- [23] C. Aronica, E. Jeanneau, H. El Moll, D. Luneau, B. Gillon, A. Goujon, A. Cousson, M. A. Carvajal and V. Robert, *Chem. Eur. J.* 2007, **13**, 3666-3674
- [24] K. P. Butin, E. K Beloglazkina and N. V. Zyk, *Russ. Chem. Rev.* 2005, **74**, 531
- [25] T. Cauchy, E. Ruiz, O. Jeannin, M. Nomura, M. Formiguè, *Chem. Eur. J.* 2007, **13**, 8858
- [26] C. Gatti, A. M. Orlando and L. Lo Presti *Chem. Sci.*, 2015,**6**, 3845-3852
- [27] R. Chauvin et al (eds.), Applications of Topological Methods in Molecular Chemistry, Challenges and Advances in Computational Chemistry and Physics 22, DOI 10.1007/978-3-319-29022-5\_5 Springer International Publishing Switzerland 2016
- [28] C. Gatti, A. M. Orlando, L. Lo Presti, *Acta Cryst.*, 2014, **A70**, C281

**GENERAL  
REMARKS AND  
CONCLUSIONS:**

The main purpose of this PhD thesis was the application of novel QTAIM-based chemical descriptors to different chemical problems. In particular, we performed a thorough experimental and theoretical study on a suitable test case to understand how electron delocalization in a conjugated system might be affected by the electric field due to strong crystal field effects (Chapter 1). We also succeeded in disentangling on a quantitative basis the various ways through which spin information is transmitted from one magnetic centre to another (Chapter 2).

In Chapter 1, we showed that local and non-local topological descriptors can be employed to understand which are the correlations between structure, electron delocalization and crystal field polarization effects. To this end, we obtained the charge density distribution of 3-diethylamino-4-(4-methoxyphenyl)-1,1-dioxo-4H-1λ<sup>6</sup>,2-thiazete-4-carbonitrile (DTC) by both single-crystal X-ray diffraction at  $T = 100(2)$  K and quantum mechanical simulations. DTC is a synthetic compound that exhibits a significant similarity with β-sultamic drugs and its core moiety is a very rare 4-membered thiazete-1,1-dioxide heterocycle. Former analysis of DTC and of some structurally analogue compounds revealed that the single C-N bond conjugated to the 4-membered thiazete-1,1-dioxide heterocycle is shorter than the double N=C bond within the ring. We found that this unusual and counterintuitive bond length alternation pattern is the consequence of a significant electronic rearrangement within the molecule. Indeed, there is a significant enhancement of the in-crystal DTC dipole moment with respect to the *in vacuo* relaxed structure. We demonstrated that this enhanced polarization is due to both an increase of the charge transfer and a reduction in the magnitude of the atomic polarization term. However, the charge transfer contribution is the dominating one, *i.e.* the charge separation among bonded atoms significantly increases in the bulk. Since DTC does not show strong directional hydrogen bond networks, its packing is clearly dominated by electrostatics. As a consequence, the high in-crystal electric field due to cooperative alignment of the molecular dipoles enhances the charge separation through the molecule, increasing the importance of quantum states associated to highly polar resonance forms. At the same time, such an enhanced polarity reinforces the crystal field in a sort of positive feedback fashion, influencing the conjugated pattern until the formally N=C double bond of the thiazete ring becomes longer than the adjacent, formally single, C-N one.

DTC represents an interesting test case to understand the subtle interplay between crystal field effects and changes in the molecular structure. Methods that intrinsically neglect quantum effects (such as force fields methods) should be parametrized ad hoc to accurately describe crystalline matrix effects in the presence of strongly polarizable system, especially if the final goal is to predict crystal structures. Finally, it is worth noting that our joint theoretical and experimental approach allowed us to detect and rationalize even subtle and counterintuitive effects, even though it clearly lacks predictability. Anyhow, comparison with accurate single-crystal X-ray structures and

experimentally-derived charge densities is mandatory to improve accuracy and reliability of computational recipes for *in silico* modelling of crystalline materials.

In chapter 2 a new topological tool for the analysis of the electron spin density distribution  $s(\mathbf{r})$  in magnetic molecular systems based on QTAIM is presented. Such chemical descriptor is the Source Function for the spin density ( $SF_s$ ). Analogously to the case of the reconstruction of electron density  $\rho(\mathbf{r})$  in terms of source function (SF) contributions for the electron density, the spin density source function ( $SF_s$ ) reconstructs the electron spin density at a reference point in terms of separate atoms or group of atoms contributions. The large anisotropy of  $s(\mathbf{r})$  and of  $\nabla^2 s(\mathbf{r})$  distributions within atomic basins makes the reconstruction of spin density strongly dependent on the choice of the reference point considered. Hence it may result that the spin density at a determined reference point be almost fully determined by the atomic basin to which the point belongs to as, for example, it occurs in the water triplet molecular system ( ${}^3B_1$  H<sub>2</sub>O) at the saddle points 4 and 4' associated to the unpaired electrons in O( $p_z$ ) atomic orbital. But the opposite situation may also realize and even so in the case of reference points lying within the basin of the paramagnetic center, like for the case of the charge concentration maximum associated to the O atom lone pair in water triplet, when only the limited electron correlation enabled by the UHF model is included. The very low positive spin density value found at this point, lying only 0.33 Å far away from the oxygen and on opposite side with respect to the hydrogen atoms, is even overdetermined ( $SF_s(\text{H}+\text{H}')\% = 108$ ) by the two distant H atoms. The comparison between  $\rho(\mathbf{r})$  and  $s(\mathbf{r})$  reconstructions in terms of SF and  $SF_s$  is illuminating about the different way the information about these scalar functions is transmitted. Furthermore, by comparing the transmission patterns at different reference points, further insight is gained on how such observables are transmitted as a function of the considered reference point.

Chemical interpretation of the  $SF_s$  atomic contributions is largely augmented when they are decomposed in a *magnetic* term due to the magnetic natural orbital(s) density and in a *reaction* or *relaxation* term due to the remaining natural orbitals density. Such a decomposition sheds also light on the causes leading to incorrect spin density distributions from low-level wavefunctions. As mentioned earlier, at the UHF level, the contribution given by the oxygen atomic basin to the spin density at the charge concentration (CC) associated to the lone pair is not dominant; such counterintuitive result disappears when electron correlation effects are introduced (CASSCF(8,8) level of theory). The latter leave almost unaffected the O and H atoms magnetic contributions to the spin density at the lone pair CC, while they selectively increase the O relaxation contribution by one order of magnitude relative to the UHF model. In general, we could show that the magnetic term of the electron density is already well described and similar to that of an adequate CASSCF model, even in the case of UHF or ROHF wavefunctions. The introduction of electron correlation effects in the wavefunction evaluation has instead a noticeable effect on the reaction or relaxation molecular



orbitals, and particularly so in specific molecular regions, where the effect of relaxation is particularly high.

Interestingly it has been shown that the magnetic term can, in some case, cause a decrease of the local spin density ( $\beta$ -effect), rather than determining a positive spin density at any reference point. Considering the relaxation term, it can either concur or counteract the magnetic term in determining the spin density at a given point, regardless its link to an orbital density integrating to a null spin population over the whole space. In fact, the SFs atomic contributions and their magnetic and reaction components, are all obtained through the atomic integration of the corresponding local source functions, which are given in terms of the related spin density Laplacians. We have shown that these latter may be locally positive or negative depending on the local concentration/dilution of the corresponding  $\alpha$ - and  $\beta$ -densities, and independently from the sign of  $s(\mathbf{r})$ .

The perfect transferability of both the electron density and the electron spin density has been demonstrated to occur in a n-alkyl radicals series, as it was shown before for the case of the electron density in the corresponding n-alkanes. An almost perfect transferability for the spin density is also achieved at the terminal C-H bond bcp, despite its very low  $s(\mathbf{r})$  value, and through a combination of opposing  $\alpha$  and  $\beta$  SF<sub>s</sub> cumulative effects of similar magnitude. Perfect transferability for the electron and the electron spin densities realizes in quite different ways and largely dependent on the selected reference point.

The spin density source function has also been applied to molecular systems in crystals, namely the Cu(II) azido and the Ni(II) dithiolene complexes. Concerning the former, we have considered two double azido bridged di-nuclear Cu(II) complexes in different structural configuration (End-End, EE, against End-On, EO, molecular structures). In both EO and EE systems, the bridge may be both symmetric when the two N-Cu bonds are equivalent and short or asymmetric when the two N-Cu bonds differ in distance. In general EO systems are symmetric while EE systems are asymmetric and, from a magnetic point of view, the EO coordination provides ferromagnetic Cu-Cu interactions, while the magnetic interactions are null or weakly antiferromagnetic in the asymmetric EE systems even if it is possible to observe a ferromagnetic interaction in some cases. On the contrary, the few di-nuclear Cu (II) EE symmetric systems are strong anti-ferromagnetic in nature, with a very large coupling constant. The two double azido bridged di-nuclear Cu (II) metal complexes presented as examples in chapter 2, show ferromagnetic coupling between the two metal centers within the molecule and, as revealed by the comparison of atomic spin populations, the unpaired electrons density is slightly more localized on the Cu(II) ions in the EE than the EO molecular system while the delocalization of the unpaired electrons on the azide group is almost

halved in EE, relative to the EO system. In general for both the metal complexes the atomic spin density is relevant only on the metal centers and on the nitrogen atomic basins of the azido groups. More importantly, the corresponding azide nitrogen atoms of both EE and EO structures in the azido group have almost the same behaviour. In fact the spin density at the charge depletion (CD) along the shorter Cu-N5 bond in EE molecular system matches almost perfectly with the corresponding one for the bridging Cu-N bond in the EO system, while the one along the much longer Cu-N3 bond is two order of magnitude lower. Comparing the spin density  $SF_S$  reconstructions at the CD along these two bonds brings further remarkable insights. In fact the  $SF_S$  reconstruction along the Cu-N5 bond is similar to the one of the Cu-N<sub>bridging</sub> bond in the EO system, while that for the Cu-N3 bond is far different and endowed with much more delocalized sources. For both dative bonds, N3 atoms give a relevant contribution, enhancing the  $\alpha$ -spin density and the two metal centers also cooperate in such  $\alpha$ -spin density enhancement. Moreover in case of EE molecular system the Cu spin density is not elongated along Cu-N3 bond. The comparison of the reconstructions of  $s(\mathbf{r})$  in terms of  $SF_S$  contributions for three similar reference points along the shorter Cu-N5 bond in EE and for the Cu-N<sub>azide</sub> bond in EO molecular system shows that the spin density on the N5 nucleus is only 0.063 a.u. to be compared with a value about 5 times as large at the nucleus of the bridging N in the EO system. Such behaviour highlights a stronger magnetic interaction between the two Cu atoms in the EO system relative to the EE system, as also evidenced by the far lower coupling constant in the latter. In the EE system, differently from the N<sub>bridge</sub> in the EO complex, the role of N5 in the super-exchange mechanism is mediated through its influence on N4 and N3 atoms and is thus less efficient. Actually, its spin distribution is shaped differently than the one of the bridging N in the EO system, while those of N4 and N3 atoms resemble more those of the corresponding N atoms in the EO system. The  $SF_S$  reconstructions obtained on the two Cu azide complexes should be considered as preliminary results. Indeed, we expect that the decomposition of  $SF_S$  contributions in magnetic and relaxation terms, as we have successfully proposed for the simpler case of the water triplet, may largely enhance the chemical interpretation of the SF patterns for these complexes.

Finally, in chapter 2, the ability of non-innocent ligands to make the oxidation state of the central metal atom not *a priori* and unambiguously determined is analyzed through the use of the  $SF_S$  topological tool. To this aim the neutral CpNi(adt)<sup>•</sup> (adt=acrylonitrile-2,3-dithiolate) radical complex is chosen. This metal complex is quite interesting since, as showed by Cauchy et al, both its ligands play a determinant role in the electron spin coupling phenomena. DFT  $J$  coupling constant calculations showed that spin density is strongly delocalized on the NiS<sub>2</sub> moiety and, more importantly, up to 20% of  $s(\mathbf{r})$  is delocalized on the Cp rings. As a result, the intermolecular Cp...Cp and Cp...dithiolene overlap interactions in the crystal lead to anti-ferromagnetic couplings mediated

by ligands that are commonly classified as innocent. In chapter 2 preliminary results regarding the reconstruction of spin density in terms of SF<sub>S</sub> applied on CpNi(ad<sup>t</sup>)<sup>•</sup> radical complex are presented. As expected, almost the 81.9% of s(**r**) is localized on the Ni atomic basin while, differently from the results of Cauchy et al, only the 11.5% of the spin density was found to be delocalized on the Cp ligand and just the 6.5% delocalized onto the dithiolene ligand. In the case of the Cp ligand, the spin density is not equally delocalized onto the five carbon atomic basins. Such behaviour of s(**r**) on the Cp ligand is linked to structural differences in terms of distances and electron populations. The analysis of the reconstructions of ρ(**r**) and s(**r**) in terms of SF and SF<sub>S</sub> contributions reveals how s(**r**) sources are much more delocalized within the whole molecule with respect to those for ρ(**r**). The application of the SF<sub>S</sub> analysis allows to distinguish the mechanism of transmission of s(**r**) within the molecule. In particular s(**r**) is delocalized on the ad<sup>t</sup> ligand through the covalent Ni-S bonds, while in the case of Cp ligand it is delocalized through space, by exploiting the π-orbital framework of the Cp ligand (which is an obvious result since the latter interacts with the Ni atom using such framework). Application of SF<sub>S</sub> permits us to show in a *quantitative* way how s(**r**) is delocalized onto the Cp ligand; in this sense SF<sub>S</sub> is able to quantify how much a ligand is innocent or not. The reconstruction of s(**r**) along the bond of Ni with the dithiolene ligand (Ni-S<sub>2</sub> bond) identifies two different mechanisms for spin information transmission, depending on the selected reference point. The main and overdetermining contribution to the positive spin density at the bonded charge concentration (CC) reference point is given by the Ni atom and by the magnetic natural orbital, localized principally on the Ni d<sup>7</sup> metal, with the Cp ligand partly opposing to such density and with ad<sup>t</sup> playing only an almost negligible role. In the case of the negative spin density at the charge depletion (CD) CP, close to the Ni atom, it is again the Ni atom which gives the largest dominant contribution (in this case a β-effect) but this now it is the result of the dominance of the relaxation orbitals contribution over the opposing contribution from the magnetic orbital. The Cp and the ad<sup>t</sup> ligands, in this case, slightly concur to the spin density at the CP, rather than opposing to it as it was in the case of reconstruction at the CC critical point.





# APPENDIX A1

## A1. Experimental procedures: full discussion

**A1.1 Specimens.** We were provided with the original batch of the microcrystalline title compound by prof. F. Clerici, in 2002. The synthetic procedure have been reported in details in another paper.<sup>[1]</sup> The formerly described X-ray analysis was performed with a good-quality selected crystal (hereinafter, sample #1).<sup>[1]</sup> Such crystal had been then preserved within a cupboard in the dark for  $\approx$  6 years, during which no significant deterioration of the diffraction intensities had occurred, as shown by preliminary X-ray data collections performed at RT on sample #1 in 2008. During the same year, new crystallization tests had been also performed, with the purpose of getting higher-quality crystals to employ in the experimental charge density investigation. Several solvents were tested, and slow evaporation from *n*-hexane (8 days) at room temperature provided some fitting specimens: one of them (hereinafter, sample #2) was then elected for the current study (Table A1, Fig. A1).

### A1.2 X-ray diffraction.

The X-ray data collections were all lead in 2008–2009, by graphite-monochromated Mo  $K\alpha$  radiation ( $\lambda = 0.71073 \text{ \AA}$ ) at the same nominal source power of 50 kV x 30 mA, employing a three-circle Bruker SMART APEX II goniometer set with a CCD area detector and an Oxford Cryostream N<sub>2</sub> gas blower. All data reductions were performed by The SAINT program package<sup>[2]</sup>.



Figure A1. Crystals #1 (a) and #2 (b) employed in the present analysis (see text). One small division on the scale corresponds to 0.025 mm.

In the beginning, we selected the larger #1 specimen (Table A1, Figure A1a) for the low- $T$  data collection; namely, it was cooled down to  $T = 100 \text{ K}$  under a 2 K/min temperature gradient. Despite an overall 3.2 % shrinkage of the cell volume, the temperature did not cause any structural changes. A total of 23  $\omega$ -scans (0.5 deg/frame, sweep 180 deg) at fixed  $\phi$  and detector angles were identified at  $T = 100 \text{ K}$ , resulting in a 99.6 % complete sphere of data up to a maximum resolution of  $\sin\theta/\lambda = 0.9 \text{ \AA}^{-1}$ . We carefully screened the recorded frames, so not to include individual measures biased by

the shadows of the beamstop and/or of the cryostat nozzle. Deeply investigating the reciprocal lattice at 100 K, we detected weak off-lattice spots, caused by a minor epitaxial non-merohedral twin component of the same DTC polymorph. The data analysis executed by TWINABS<sup>[3]</sup> revealed that the mass ratio of the parasite crystal was as low as 3.7 % on the basis of several measures of strong reflections having equal indices between the two contrarily directed phases. At the same time, the value of the fraction of overlapped (and possibly problematic) reflections was expected to be as low as  $\approx 15$  %. Despite the accurate molecular structure could be obtained by easily treating the minor twinning of crystal #1 in the beginning, we rather deleted partially overlapped reflections caused by the parasite crystal, since performing high-quality charge density studies requires an unbiased (or the least biased as possible) dataset.<sup>[4]</sup> Note that the quality of the sample (in particular the low-order reflections one) may remarkably influence the point topological descriptors and specific qualities of the charge density distribution in the covalent bonds area.<sup>[4]</sup>



**Table A1** Data collection statistics and relevant refinement details for the three 100 K datasets of the same ‘A’ polymorph of DTC ( $C_{14}H_{17}N_3O_3S$ , molecular weight 307.37 g mol<sup>-1</sup>, space group P2<sub>1</sub>/n,  $\mu = 0.234$  mm<sup>-1</sup>,  $F_{000}=648$  e).

Crystal data	Sample #1	Sample #2	$F_{exp}$	
$a$ (Å)	8.5395(3) <sup>a</sup>	8.5447(2) <sup>b</sup>	8.5421(26) <sup>c</sup>	
$b$ (Å)	13.2383(4) <sup>a</sup>	13.2396(3) <sup>b</sup>	13.2390(6) <sup>c</sup>	
$c$ (Å)	13.0403(4) <sup>a</sup>	13.0483(3) <sup>b</sup>	13.0443(40) <sup>c</sup>	
$\beta$ (deg)	95.105(2) <sup>a</sup>	95.053(1) <sup>b</sup>	95.079(26) <sup>c</sup>	
$V$ (Å <sup>3</sup> )	1468.34(12) <sup>a</sup>	1470.39(7) <sup>b</sup>	1469.37(35) <sup>c</sup>	
Density (g·cm <sup>-3</sup> )	1.390	1.388	1.389	
Crystal size (mm)	0.43 x 0.33 x 0.25	0.23 x 0.20 x 0.13	//	
Data collection ( $\sin\theta/\lambda_{MAX} = 0.65 \text{ \AA}^{-1} / 0.90 \text{ \AA}^{-1}$ )				
Measured reflections	39988 / 110586	46902 / 118397	86720 / 157389	
Unique reflections	3365 / 8940	3376 / 8984	3375 / 8956	
$I > 2\sigma(I)$ reflections	3128 / 7742	2962 / 6917	3117 / 7688	
Completeness (%)	99.7 / 99.6	100.0 / 100.0	100.0 / 99.7	
$R_{int}$	0.0217 / 0.0345	0.0496 / 0.0845	0.0397 / 0.0441	
Refinement				
$R(F)$ , $wR(F^2)$ , Goodness-of-fit <sup>d</sup>	0.0300, 0.992	0.0800, 1.035	0.0355, 1.035	0.0866, 0.0297, 0.0798, 0.999 0.0168, 0.0290, 1.099
$\Delta\rho_{min}$ , $\Delta\rho_{max}$ (eÅ <sup>-3</sup> ), data-to-parameters ratio <sup>e</sup>	-0.340, 11.81	+0.370, 13.80	-0.362, 13.80	+0.383, -0.144, +0.151, 13.37
Experimental ( $F_{exp}$ ) spherical ( $\zeta=\kappa\alpha$ ) and deformation ( $\zeta'=\kappa'\alpha'$ ) exponents <sup>e</sup>	S: $\zeta = 4.306$ , $\zeta' = 4.26(2)$ , 4.54(1) O: $\zeta = 4.345$ , $\zeta' = 4.98(2)$ N: $\zeta = 3.797$ , $\zeta' = 3.28(1)$ C: $\zeta = 3.151$ , $\zeta' = 2.667(3)$ H: $\zeta = 2.436(3)$ , $\zeta' = 3.00(2)$			

<sup>a</sup> Estimated from the least-squares fitting of the orientation matrix against 8501 intense reflections with 6.0 deg < 2 $\theta$  < 114.7 deg.

<sup>b</sup> Estimated from the least-squares fitting of the orientation matrix against 5044 intense reflections with 4.4 deg < 2 $\theta$  < 74.9 deg.

<sup>c</sup> Unweighted average of the two #1 and #2 individual unit cells.

<sup>d</sup> First row: IAM results from shelx, with the thermal motion of H atoms treated as isotropic and  $(\sin\theta/\lambda)_{MAX} = 0.65 \text{ \AA}^{-1}$ . Second row: multipole model (XD2006) on experimental ( $F_{exp}$ ) structure factor amplitudes up to  $\sin\theta/\lambda = 0.9 \text{ \AA}^{-1}$ .

<sup>e</sup> Values in bohr<sup>-1</sup>. Where not reported, least-squares estimated standard deviations are smaller than the last digit.

As shown in Table A1, Figure A1b, Sample #2 was untwinned. Though, it was also remarkably smaller than #1 and - at least with the optics our lab is endowed with (detector, collimator and monochromator) - too small to provide satisfying high-order data ( $2\theta > 55^\circ$ ,  $\lambda = \text{Mo K}\alpha$ ) useful by itself for the accurate charge density estimate. In order to obtain the least biased information as possible from both specimens, we proceeded as follows: (i) first, all the individual measurements of sample #1 undergo to some extent of intensity superposition with the parasite crystal were removed; then (ii), a data collection on sample #2 was performed, namely at the same nominal 100(2) K temperature, employing a similar approach (Table A1). The cell parameters of the two structures were affected by very small variations ( $\approx 0.06\%$ ), although meaningful in terms of expected least-squares standard deviations (esd's): indeed, the unit cell of sample #2 showed a slightly greater volume (+0.1%) than sample #1 (see chapter 1, Table 1). In our opinion, such divergence can be ascribed to slight disparities in the data collection temperatures and so we preferred employing the unweighted average of samples #1 and #2 as the least-biased estimate for the cell parameters of DTC at 100 K (see the third column of table 1 in chapter 1). It is worth stressing that recently Kaminski *et al.*<sup>[5]</sup> analysed the structure and charge density of  $\alpha$ -oxalic acid dehydrate as resulting from a series of 100 K high-resolution datasets. One of their main outcomes was that the variations of topological charge density descriptors for this sole crystal structure occur over quite a small range, even at the same temperature. Thus, we guess the minor incongruity retrieved in the refined cell parameters of the two specimens would not influence the charge density results examined in the current work. (iii) Moreover, the #1 and #2 sets of structure factor amplitudes were independently revised by SADABS<sup>[6]</sup> for beam anisotropy and absorption effects and eventually scaled and merged together by XPREP.<sup>[7]</sup> We also applied an 'instrumental instability' coefficient<sup>[8]</sup> to the final expected standard deviations, according to  $\sigma_{\text{corr}}^2 = \sigma^2 + k_{\text{CPL}} F_{\text{exp}}^2$ , with  $k_{\text{CPL}}$  set to 0.1625 to attain sufficiently coherent probability plot statistics (Figure A3 below). The final dataset (hereinafter:  $F_{\text{exp}}$ ) had a completeness of 99.7 % and an overall internal agreement factor  $R_{\text{int}}$  of 0.0443 (Table A1, third column), and the subsequent multipole analysis was performed throughout by it (see Section A.1.3 below).

### A1.3 Multipole Model.

The observed reflections ( $I > 2\sigma(I)$ ) were the only included in the refinement. Least-squares were performed against  $F_{\text{exp}}^2$  with a statistical  $1/\sigma^2$  weighting scheme, as for the experimental dataset (see above), while the structure factor amplitudes  $F_{\text{theo}}$  were used as observations together with unitary weights concerning synthetic data (see Chapter 1). The core building and valence monopole one-electron density functions were performed by Hartree-Fock atomic neutral functions of Clementi & Roetti<sup>[9]</sup>. We considered radial terms for higher poles as single-exponential forms,  $r^n \exp(-k\alpha r)$ , with  $n$  being 2,2,3,4 for  $l=1,2,3,4$ , respectively, for second-row atoms and hydrogen, while we

selected the  $n = 4,6,6,6$  scheme<sup>[10]</sup> for sulphur<sup>[11]</sup>, since its providing the most fitting outcomes, concerning residual density and statistical agreement factors in preliminary refinements against experimental data. As suitable starting point for the radial exponents  $\alpha$ , we chose slightly adjusted values with respect to the exponents of single-zeta wavefunctions tabulated by Hehre *et al*<sup>[12]</sup>. Nevertheless, in order to portray contractions and expansions of the core and valence shells, a refinement of a couple of radial scaling parameters  $k'$  and  $k$  was also independently performed for each C, N, O and H atomic species during the late phases of the least-squares process. About sulphur, two different deformation scaling factors  $\kappa'$  were allowed to change for the even ( $l = 0, 2, 4$ ) and odd ( $l = 1, 3$ ) poles (Table A1). Dealing with heavy atoms,<sup>[13]</sup> where the different radial extension of the valence and  $4s$  and  $3d$  orbitals are likely to cause problems during the refinement, an efficient strategy is treating even and odd poles with different basis functions. As for the title compound, such strategy is validated by the demand of more adaptable contraction/expansion shells surrounding this atom, since it presents a mixed hybridization state caused by its quite complicated covalent environment (2 oxidic O, 1 C and 1 imminic N, the latter set in a 4-membered cycle). The latter might (and actually) lead to slightly different contraction/expansion effects on the higher-order poles, because of the partial mixing of low-lying virtual  $d$  orbitals with valence  $s$  and  $p$  wavefunctions. However, final  $\kappa'$  revealed to be as large as 1.07(2) for even and 1.14(1) for odd poles, with a total Hansen-Coppens charge of +0.75  $e$  on the oxidized S atom. Nevertheless, we are required to underline that the best assessment of the model against the  $\rho_{\text{EXP}}$  distribution (see also the main text) is provided by the comparison with first-principle charge density. Besides (see Section A1.4 below), thermal motion is fully depicted by the current multipolar model, being the Hirshfeld rigid bond test completely satisfied. Some specific comments are required concerning the treatment of hydrogen atoms, As H atoms are critical for both the molecular electrostatic properties and the chemical reactivity, the model we selected to examine the measured X-ray intensities presents one key-feature in electron density studies of molecular crystals, namely the anisotropic vibrational motion also for H nuclei, In the beginning, the H atoms thermal motion was modelled as isotropic. In due course, i.e. after analyzing the behaviour of some preliminary multipole models, we included anisotropic displacement parameters in the model also for hydrogen atoms (ADPH), as computed by the SHADE2 server<sup>[14]</sup>. Thus, we followed the same method formerly portrayed in A. Ø. Madsen, *J. Appl. Cryst.* **2006**, *39*, 757–758 and in Saleh, G.; Soave, R.; Lo Presti, L.; Destro, R. *Chem. Eur. J.* **2013**, *19*, 3490-3503. Later, we tested other multipole models, changing all the parameters except the ADPH. As we assumed the ultimate multipole model for DTC was found, we ran the SHADE server once more, then the newly computed ADPH added in the model and never refined. Finally, a refinement of multipolar and radial parameters of all the atoms was performed again for some cycles, till convergence fulfillment. The covalent C–H bond distances were arranged to the matching neutron diffraction estimates.<sup>[15]</sup> Besides a general

electroneutrality constraint on the entire asymmetric unit, the monopole populations of all the hydrogen atoms was treated with appropriate chemical constraints, forcing the H atoms in the same –CH<sub>2</sub>, –CH<sub>3</sub> and phenyl groups to assume the same charge. Eventually, the H-centred dipole and quadrupole terms oriented towards the bond direction were the only allowed to be populated.<sup>[16,17]</sup> Reports of the charge density, Laplacian and ellipticity estimates as processed at all the bond and ring critical points (bcp, rcp) retrieved in the asymmetric unit, can be found in Tables A1 and A2.

#### **A1.4. Accuracy of geometric and thermal parameters of DTC in the solid state at T = 100 K.**

A correct treatment of the thermal motion is essential in gaining sensible experimental estimates of the bond distances.<sup>[18,19]</sup> The program THMA14c<sup>[20]</sup> performed the Hirshfeld rigid bond test<sup>[21]</sup> on the thermal parameters deriving from the final multipole model against the  $F_{\text{exp}}$  dataset, so to check the quality of the refined anisotropic displacement parameters (ADP's) at  $T = 100$  K. The test computed the average mean-square displacements amplitude ( $\langle \text{MSDA} \rangle$ ) by the bond vectors being as low as  $4(5) \cdot 10^{-4} \text{ \AA}^2$  for the 22 covalent bonds involving non-H atoms, and thus was fully satisfied. The possible influence of rigid-body motion on the low-temperature geometric parameters in DTC was verified performing the rigid-body TLS analysis by Schomaker and Trueblood.<sup>[21-23]</sup> As a result, we noticed the TLS decomposition conforms with the experimental Debye-Waller factors of non-H atoms, as the variances between experimental and computed  $U_{ij}$  elements of the atomic thermal tensors never exceeded  $\pm 0.003 \text{ \AA}^2$  within the bonded anisole and thiazete moieties. Quite the reverse occurs within those groups far from the two-ring backbone (–CH<sub>2</sub>CH<sub>3</sub>, –CN and sulphonyl oxygen atoms O2 and O3), where stronger incongruities were retrieved, as expected. These evidences lead to the conclusion that the bonded anisole and thiazete groups indeed create a rigid-body system, *i.e.* they collectively vibrate in the crystal, despite the very small amplitudes of their translations and librations. Actually, in the molecular inertial axes reference system the root-mean-square librations are comprised between 1.9 and 1.0 deg, and the related translations between 0.12 and 0.09  $\text{\AA}$ . Hence, rigid-body adjustments<sup>[6]</sup> to covalent bond lengths concerning non-H atoms amount, on average, to  $9.6(3) \cdot 10^{-4} \text{ \AA}$  (corresponding to 0.066(2) %) and thus they can be safely omitted.

#### **A1.5. Statistical assessment of the weighting scheme.**

The normal probability plot<sup>[24]</sup> (Figure A2) resulting from the final multipole model (see Section A1.3 above) displays the slightly left-skewed normal distribution (Figure A3) followed by the deviations among empirical and computed squared structure factor amplitudes. At the same time, we can notice average scale factors are almost constant in  $\sin\vartheta/\lambda$  (Figure A4), showing a maximum deviation not beyond  $\approx 4$  % for high angle data. Such small discrepancies from the ideal results are probably due to slight inaccuracies concerning the merging of the two primary datasets. Actually, every data

manipulations require somehow the loss of a bit of information and thus are likely to systematic miscalculations.<sup>[25]</sup> Moreover, adjusting by twinning during the rebuilding of a full dataset from two different samples is for sure the more awkward stage of the entire data reduction procedure. Nevertheless, the final model seems to be fully satisfactory in physical-chemical perspective. Indeed, the deformation density maps (Figure A5) are perfectly reasonable, showing the charge density mainly set along chemical bonds and N lone pairs well highlighted. The residual maps are essentially featureless, too (Figure A5 and A6). Besides, the thermal motion looks absolutely reasonable, complying with the Hirshfeld rigid bond test for every bonded pair of non-H atoms (see Section A1.4 above). Finally, the good quality of the  $\rho_{\text{EXP}}$  distribution gained through this process is guaranteed by the perfect agreement between the low-order electrostatic moments as processed from the experimental multipole density and those resulting by DFT first-principle simulations in the bulk (see Chapter 1).

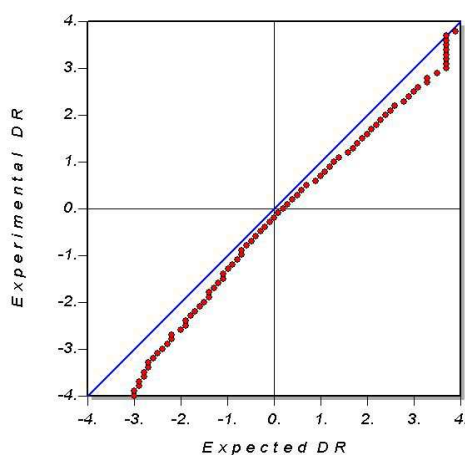


**Figure A2.** Normal probability plot of  $F^2_{\text{exp}}$  dataset against the final multipole model. This picture has been realized with DRKPlot v. 1.00.012, © A. Stash, Moscow, 2007.

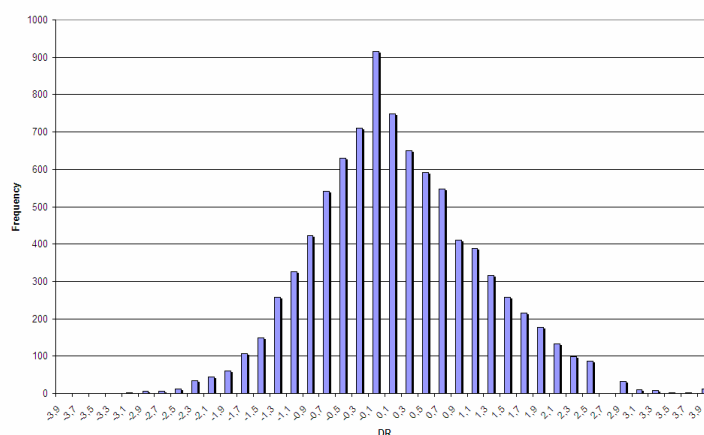


**Figure A3.** Distribution of the residual statistics corresponding to the plot in Figure A2.

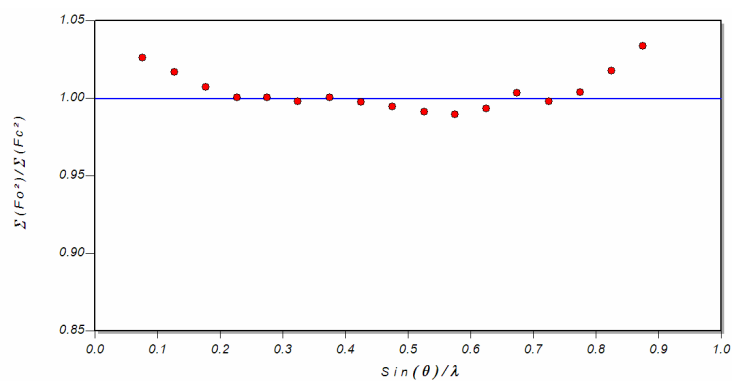


**Figure A4.** Distribution of average scale factors as a function of  $\sin\theta/\lambda$ . This picture has been realized with DRKPlot v. 1.00.012, © A. Stash, Moscow, 2007.

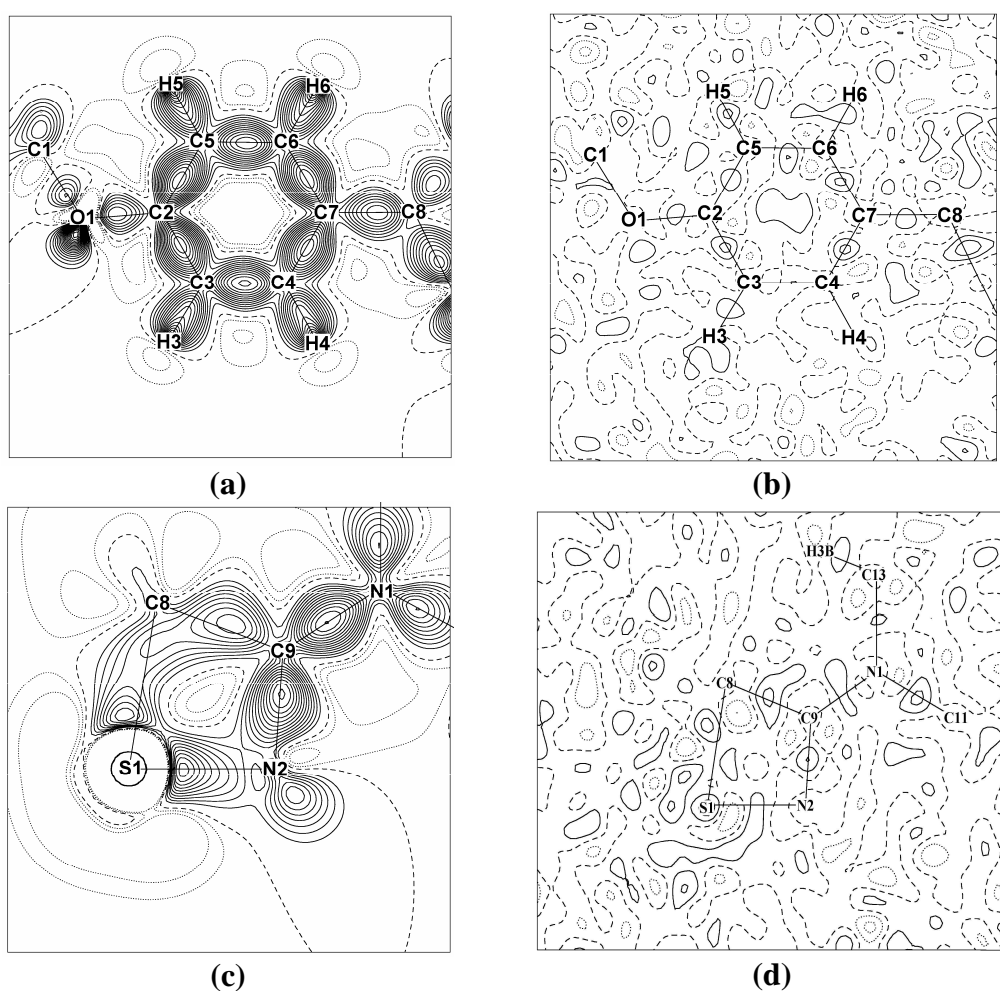


**Figure A5.** Deformation (a), (c) and residual (b), (d) maps plotted in the phenyl (a), (b) and S1-N1-C9 (c), (d) planes. Contour lines are drawn among  $\pm 1.0 \text{ e}\cdot\text{\AA}^{-3}$ , at steps of  $0.05 \text{ e}\cdot\text{\AA}^{-3}$  for deformation density maps while are drawn among  $\pm 0.1 \text{ e}\cdot\text{\AA}^{-3}$ , at steps of  $0.05 \text{ e}\cdot\text{\AA}^{-3}$  for the residual density maps. Solid and dotted curves represent positive and negative values respectively. Dashed lines: zero contour.

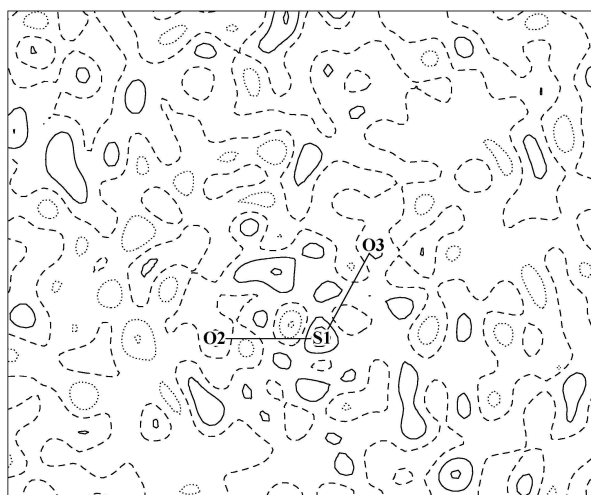


**Figure A6.** 4 Å x 4 Å-wide residual experimental electron density map in the O2-S1-O3 plane of crystalline DTC at T = 100(2) K. See Figure 1 in the main text for the atom numbering. Contour lines are drawn among  $\pm 0.1 \text{ e}\cdot\text{\AA}^{-3}$ , at steps of  $0.05 \text{ e}\cdot\text{\AA}^{-3}$ . Solid lines: positive values. Dashed lines: zero contour. Dotted lines: negative values.

### A1.6 Correlations.

In order to accomplish the current investigation, we are required to wonder whether a maximum resolution of  $0.9 \text{ \AA}^{-1}$  in  $\sin\theta/\lambda$  is enough to prevent the accurate estimate of the experimental charge density to be altered by correspondences among refined parameters.<sup>[26]</sup> Assumed that no ‘magic limits’ could ever guarantee that a certain solution is ‘absolutely’ acceptable, in the case of DTC we found just 17 substantial ( $>0.7$ ) correlation coefficients  $\rho_{ij}$ , in the final model (586 parameters) at the end of the multipole fine-tuning, with an average  $\langle\rho_{ij}\rangle = 0.78(5)$ , basically involving dipoles and quadrupoles of oxygen atoms relating with the matching positional and thermal parameters. Nevertheless, we can safely assess that reliability and accuracy of the multipole model within  $\sin\theta/\lambda \leq 0.9 \text{ \AA}^{-1}$  are satisfactory for the purposes of the present study on the basis of what previously examined, and now recalled: featureless  $\Delta\rho$  maps, reasonable deformation maps, conformity between experimental and theoretical models, fulfilled Hirshfeld test,.

## A2. Gas-phase optimized structures.

### A2.1 Bond polarization and bond strength.

Looking at Figure A7 and Table A2 we can see the dislocation of the bcp from the bond mid-point,  $\Delta_{\text{bcp}} = d/(0.5\cdot R_e)$ , expressed in percentage, for C-N, C=N and S-N bonds (dashed blue lines). Here,  $d$  and  $R_e$ , indicate, respectively, the bcp distance from the bond midpoint and to the X-Y bond distance; the sign of  $d$  is considered as positive (negative) if the bcp is next to Y (X). A measure of the bond polarization can be deduced from the  $\Delta_{\text{bcp}}$  parameter:., equal to zero for a fully homopolar

bond, divergent from zero and increasing in magnitude together with the enhanced polarity of the bond.

**Table A2.** Bond critical point displacement parameter,  $\Delta_{\text{bcp}}$ <sup>a</sup> See Figure 1 and Scheme 2 in the main text for the atom numbering.

System	C9-N1	C9-N2	S1-N2	(S1-O) <sub>avg</sub>
1	-24.8	-25.2	-	-
2	-27.0	-25.4	-10.9	-23.9
3	-26.5	-23.1	-4.7	-21.5
4	-25.9	-22.8	-6.5	-21.4

<sup>a</sup> A negative value for an A-B bond means that the bcp is displaced towards A

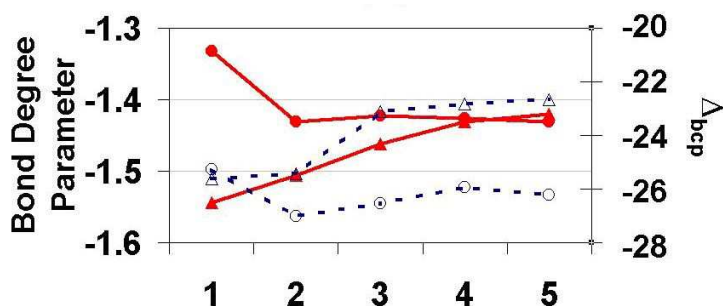


**Figure A7.** As Figure 2 in the main text, showing the Bond Degree parameter (full red lines, left scale) and bond polarization (dotted blue lines, right scale) for the series of compound shown in the Scheme 2 in the main text.

Then, the increasing closeness of bcp to the more electropositive atom with growing bond polarity determines the sign of  $\Delta_{\text{bcp}}$ . In all compounds, both the C–N bonds display a large bond polarity, with the C atom clearly performing as the electropositive partner of every CN pair. Considering the *in vacuo* systems with the sulphonyl group, **2** shows the largest C9–N1 and C9=N2 bond polarities and even the largest S–N polarity. Such features also conform to the largest charge separations in the N1–C9=N2–S1 moiety (**2**: N1–C9, 2.23; C9=N2, 2.35; N2–S1, 3.92; **3**: N1–C9, 2.22; C9=N2, 2.12; N2–S1, 3.70; **4**: N1–C9, 2.19; C9=N2, 2.13; N2–S1, 3.72). The agreement between the largest negative atomic charge of N2 in systems **2–4** (**2**: -1.20; **3**: -1.03, **4**: -1.06) and the largest negative C9=N2 and S1–N2  $\Delta_{\text{bcp}}$  values for compound **2**, implies the relatively higher weight of resonance structures *f-h* and *b* (Scheme 3) in **2**: this may shed light on the causes at the roots of the ellipticity minimum and the lowest Laplacian magnitude at the C9=N2 bcp retrieved in compound **2**. A very



significant polarization increase in the crystal then occurs in the DTC molecule (see QTAIM atomic charges in Fig. 3), Details concerning this point will be discussed in section 3. A further meaningful insight is the gradual and systematic equalization of C9-N1 and C9=N2 bonds along the **1-4** series not being mirrored by the equalization of their  $\Delta_{\text{bcp}}$  values (Table A2). Such values are almost equal in **1**, but then diverge more and more along the series and in a direction opposite and even unexpected, if considering the C9-N1 and C9=N2 bonds respectively growing and reducing their bond order from **2** to **4**. Looking for a possible reason underlying such discrepancy, we sense that also the S-N bond performs so to influence the electron delocalization and polarization in the N-C=N moiety. The remarkable S-N bond polarity reduction during the transition from **2** to **3** (Table A2) clearly affects the N-C=N moiety and it may be the symptom of a variation in the relative importance of the different resonance structures. Finally, the so-called bond degree (BD) parameter<sup>[27]</sup> is portrayed in Figure A7 (full red lines). Described as the ratio  $[H(\mathbf{r}) / \rho(\mathbf{r})]_{\text{bcp}}$ , where  $H(\mathbf{r})$  is the energy density at  $\mathbf{r}$ , such value is meant to measure the bond covalence on absolute footing. Essentially, BD is the expression of the total energy per electron at the bcp; the more negative is BD, the more the bond is covalent and stronger. As predictable, roughly opposite variations occurs for the conjugated C-N bonds:  $\text{BD}_{\text{C9=N2}}$  (full red triangles) turns monotonically less negative, i.e. the double bond fades, while  $\text{BD}_{\text{C9-N1}}$  (full red circles) falls as adding the SO<sub>2</sub> group (from **1** to **2**), but then has no significant variation throughout the series **2-5**, notwithstanding its bond length is more and more decreasing. Considering this parameter, a significant similarity occurs in the two bonds C9=N2 and C9-N1 for compounds **4** (DTC) and **5** (TAYCUR), complying with the performance of the bond length,  $\rho_{\text{bcp}}$ ,  $\epsilon$  and  $\nabla^2\rho_{\text{bcp}}$  parameters (see Figure 2a and 2b in the main text).

## A2.2 Delocalization indices.

The analysis of the delocalization index,  $\delta(\text{A,B})$  represents for sure a useful complement to the current study. Despite the framework of the Kohn-Sham formalism does not strictly define the electron-pair density, in this case *approximate*  $\delta(\text{A,B})$  values were directly drawn from the Kohn-Sham orbitals and by employing an HF-like second order exchange density matrix. Generally, we know that delocalization indices derived by this method are slightly overestimated, as the electronic Coulomb correlation is not entirely considered by common exchange-correlation functionals. However, the current study mainly focuses on trends (not absolute values) of  $\delta(\text{A,B})$ , and this is the reason why we adopted the DFT methods in order to get the most rational and appropriate agreement - in terms of accuracy - among the selected topological descriptors. The delocalization indices among atoms belonging to the conjugated system (N1, C9, N2, S1, plus the sulphonyl

oxygen atoms O2 and O3) are reported in Table A3. At a first glance, we notice that the electronegative atoms directly bonded to sulphur (O2, O3 and N2) always share a remarkable quantity of electrons, yet with no significant variations through the series **2-5**. The  $\delta(N1,N2)$ ,  $\delta(N1,C9)$  and  $\delta(N2,C9)$  descriptors seems to be more intriguing, because of their intimate correlation with the measure of electron delocalization throughout the C–N chain: they are evidently different and far smaller when the conjugation ends, as occurring in the saturated thiazetidine ring **6** (last rows in Table A3). Considering systems **1-5**, the  $\delta$  values performs more constantly and their general trend is systematically decreasing throughout the series for both  $\delta(N1,N2)$  and  $\delta(N2,C9)$  while, an increase occurs for  $\delta(N1,C9)$ .

**Table A3.** Delocalization indices  $\delta(A,B)$  for atom pairs within or near the N–C=N system in compounds 1–6, as evaluated from the gas–phase optimized structures at the B3LYP 6–311G(p,d) level. See Figure 1 and Scheme 2 for the atom numbering

$\delta(A,B)$					
A=N1, B=	C9	N2	S1	O2	O3
1	1.05	0.26	//	//	//
2	1.11	0.26	0.02	0.01	0.00
3	1.10	0.23	0.03	0.01	0.00
4	1.14	0.21	0.02	0.01	0.00
5	1.13	0.21	0.02	0.00	0.00
6	1.02	0.13	0.02	0.00	0.00
A=N2, B=	C9	S1	O2	O3	
1	1.59	//	//	//	
2	1.40	0.89	0.16	0.17	
3	1.42	0.89	0.15	0.15	
4	1.34	0.91	0.14	0.14	
5	1.33	0.92	0.14	0.14	
6	0.89	0.86	0.15	0.17	
A=S1, B=	C9	O2	O3		
2	0.04	1.17	1.15		
3	0.09	1.21	1.21		
4	0.08	1.22	1.21		
5	0.09	1.19	1.19		
6	0.06	1.17	1.15		
A=O2, B=	C9	O3			
2	0.02	0.24			
3	0.03	0.26			
4	0.02	0.25			
5	0.02	0.25			
6	0.02	0.26			

Such values gets even more stable in the conjugated systems, as the sulphonyl group is present (**2-5** series), and display not a prominent  $\delta(\text{N2,C9})$  peak and a shallow  $\delta(\text{N1,C9})$  minimum for compound **3**, i.e. upon insertion of the thiazete ring and before substitution of the H atoms related to N1 by ethyl groups. Actually, the most relevant effects (in the **2-5** series) are due to this latter perturbation, leading to a more similar electron delocalization in the N2=C9 and N1-C9 bonds. The origins of such a performance can be found by inspecting the *localization indices*, or, more meaningfully, the percentage of localized electrons,  $\delta(\Omega,\Omega)/N(\Omega)$  Table S4, which show they are mostly steady for all atoms in systems **2-5**, except quite a remarkable reduction upon H substitution with ethyl groups at this atom, namely from 0.81 to 0.77 of the percentage of electrons localized on N1.

**Table A4.** Percentage of localized electrons,  $\delta(\Omega,\Omega)/N(\Omega)$  in compounds **1-5**, as evaluated from the gas-phase optimized structures at the B3LYP 6-311G(p,d) level. See Figure 1 and Scheme 2 in the main text for the atom numbering.

System	N1	N2	S1	C9	(O) <sub>avg</sub>
<b>1</b>	0.809	0.822	-	0.63	-
<b>2</b>	0.809	0.811	0.840	0.64	0.903
<b>3</b>	0.810	0.809	0.840	0.62	0.903
<b>4</b>	0.772	0.805	0.841	0.62	0.900
<b>4</b> <sup>a</sup>	0.772	0.810	0.843	0.62	0.902
<b>5</b>	0.772	0.806	0.842	0.62	0.901

<sup>a</sup>Crystal geometry

Since having a larger positive inductive (+I) effect than H atoms (their global positive charge in **4** is 0.927 e, compared to a value of only 0.828 for the two H atoms in **3**: see Figure 3 in Chapter 1), ethyl groups spread more electrons than H to the N1 atom that, instead, delocalizes them through the  $\pi$ -system, increasing the relative weight of resonance structure *b*. Actually, from **3** to **4** the negative charge on N1 even slightly reduces by 0.005 e, while the one on N2 grows by six times more. The boost of the  $\delta(\text{N2,S1})$  value transitioning from **3** to **4-5** provides a further validation to our analysis, implying an enhanced weight for resonance structures *c-e*, too.

### A2.3 Source function values.

The rising equalization of N1-C9 and N2=C9 bonds down the **1-4** series is confirmed by the SF data listed in Table A5, as the SF%<sub>C9+N2</sub> value gets closer and closer to SF%<sub>C9+N1</sub> (their discrepancy reduces from 6.8 in **1** to 3.4% in **4**). However, only SF%<sub>C9+N2</sub> is concerned in such variation, complying with the reduction occurring in the value of  $\delta(\text{N2,C9})$ , that is larger than the growth in

$\delta(N1,C9)$ . The reduction rather than the estimated increase of the N1 and N2 SF% contributions at their C-N bond bcps denotes that electron delocalization in the N-C=N moiety does not enhance down the **2-4** series, notwithstanding bond lengths get more similar in value. This occurs either as the reference point is the bcp, either as it is dislocated from the bcp by  $\pm 0.5$  Å along the  $\lambda_2$ -eigenvector to underline the impact of  $\pi$ -electrons. The decrease in SF%<sub>N1</sub> and SF%<sub>N2</sub> values mirrors what observed for  $\delta(N2,N1)$ .

**Table A5.** Percentage Source Function values, SF%( $\Omega$ ,bcp) in compounds 1–4, as evaluated from the gas-phase optimized structures at the B3LYP 6–311G(p,d) level. See Figure 1 and Scheme 2 for the atom numbering.

System	N2 = C9 @bcp				N2 = C9 @bcp $\pm 0.5$ Å					
	C9+N2	N1	N2	C9	C9+N2	N1	N2	C9	C8	C7
<b>1</b>	90.0	4.1	48.9	41.1	82.2	6.9	47.8	34.4	//	//
					82.2	6.7	47.9	34.3		
<b>2</b>	88.2	5.0	48.0	40.2	78.8	8.3	46.5	32.3	0.1	//
					78.8	8.3	46.6	32.2	0.2	
<b>3</b>	87.1	4.7	47.2	39.9	77.2	7.8	45.3	31.9	3.7	//
					77.2	7.8	45.3	31.9	3.7	
<b>4</b>	86.4	4.2	46.7	39.7	75.9	6.7	44.3	31.6	2.5	0.3
					75.9	6.7	44.2	31.7	2.6	0.3

System	C9 – N1 @bcp				C9 – N1 @bcp $\pm 0.5$ Å					
	C9+N1	N2	C9	N1	C9+N1	N2	C9	N1	C8	C7
<b>1</b>	83.2	8.2	38.6	44.6	69.6	14.1	29.1	40.5	//	//
					70.0	14.2	28.6	41.4		
<b>2</b>	84.3	7.3	38.6	45.7	72.3	12.3	29.3	43.0	0.1	//
					72.1	12.3	29.3	42.8	0.1	
<b>3</b>	84.4	6.9	38.5	45.9	71.4	11.9	28.3	43.1	3.6	//
					71.4	11.9	28.3	43.1	3.6	
<b>4</b>	83.0	6.3	38.8	44.2	69.3	10.6	29.7	39.6	2.2	-0.1
					69.5	10.6	29.9	39.6	2.4	0.2

### A3. Crystal field effects.

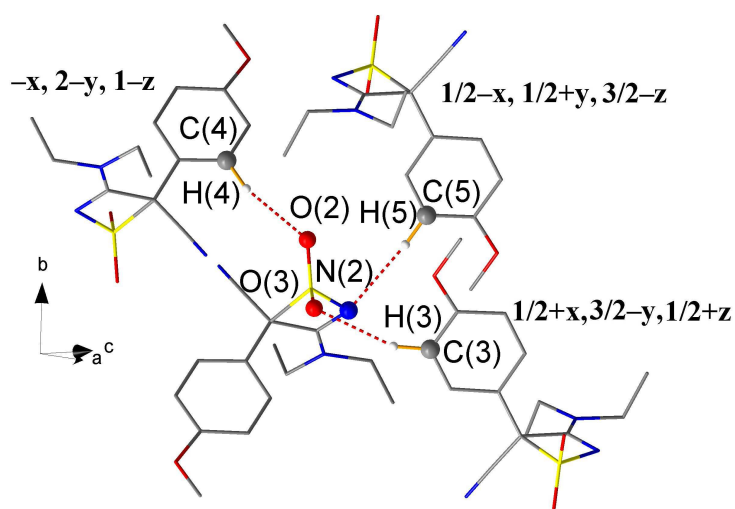


**Figure A8.** Wires diagram of the DTC molecule and part of its crystalline environment, with the relevant  $\text{CH}\cdots\text{X}$ ,  $\text{X}=\text{O},\text{N}$  intermolecular contacts (reported in bold in Table A10 below) highlighted. Other hydrogen atoms are omitted for clarity. The molecule at the centre of the picture corresponds to the DTC asymmetric unit in the solid-state conformation (polymorph A) at  $T = 100$  K.

**Table A6.** Relevant ( $d_{\text{H}\cdots\text{A}} \leq 3.1 \text{ \AA}$ ,  $\alpha_{\text{D-H}\cdots\text{A}} \geq 120.0 \text{ deg}$ ) CH $\cdots$ A, A= N,O hydrogen bonded contacts (in the form Donor–Acceptor $\cdots$ Hydrogen) in solid DTC at  $T = 100 \text{ K}$  (polymorph A, this work), as computed from the final multiple model against measured X–ray structure factor amplitudes. The most significant contacts are highlighted in bold. When meaningful, estimated standard deviations are reported in parentheses.<sup>a,b</sup>

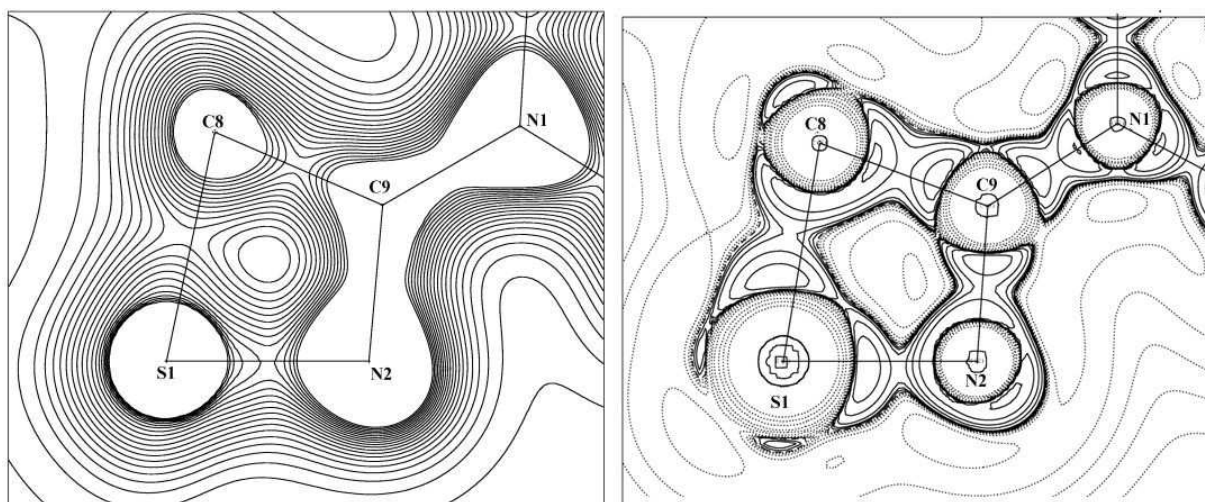
D–H $\cdots$ A	$d_{\text{D-H}} / \text{\AA}^b$	$d_{\text{H}\cdots\text{A}} / \text{\AA}$	$d_{\text{D}\cdots\text{A}} / \text{\AA}$	$\alpha_{\text{D-H}\cdots\text{A}} / \text{deg}$	Symmetry <sup>c</sup>
Involving the thiazete:					
C1–HC1 $\cdots$ N2	1.077	3.053	3.799(1)	126.9	1/2–x, 1/2+y, 3/2–z
<b>C5–H5<math>\cdots</math>N2</b>	<b>1.083</b>	<b>2.538</b>	<b>3.593(1)</b>	<b>164.3</b>	<b>1/2–x, 1/2+y, 3/2–z</b>
C14–H4A $\cdots$ O3	1.077	2.776	3.614(1)	134.6	–1/2+x, 3/2–y, 1/2+z
<b>C3–H3<math>\cdots</math>O3</b>	<b>1.083</b>	<b>2.574</b>	<b>3.604(1)</b>	<b>158.6</b>	<b>1/2+x, 3/2–y, 1/2+z</b>
C1–HA1 $\cdots$ O3	1.077	2.862	3.577(1)	124.0	–1/2–x, 1/2+y, 3/2–z
C6–H6 $\cdots$ O2	1.083	2.654	3.466(1)	131.4	1/2–x, 1/2+y, 3/2–z
<b>C4–H4<math>\cdots</math>O2</b>	<b>1.083</b>	<b>2.407</b>	<b>3.460(1)</b>	<b>163.6</b>	<b>–x, 2–y, 1–z</b>
C14–H4B $\cdots$ O2	1.077	2.838	3.505(1)	120.1	1–x, 2–y, 1–z
Other groups:					
C14–H4C $\cdots$ N3	1.077	2.755	3.686(1)	144.7	x, y, z (intramolecular) <sup>d</sup>
C14–H4B $\cdots$ N3	1.077	2.848	3.746(1)	140.9	1–x, 2–y, 1–z
C12–H2B $\cdots$ O1	1.077	2.887	3.728(1)	135.2	–1+x, y, z
C13–H3A $\cdots$ O1	1.092	3.066	4.129(1)	164.6	–1+x, y, z

<sup>a</sup>See Figure S4 in the Supporting Information for the packing scheme corresponding to this Table.

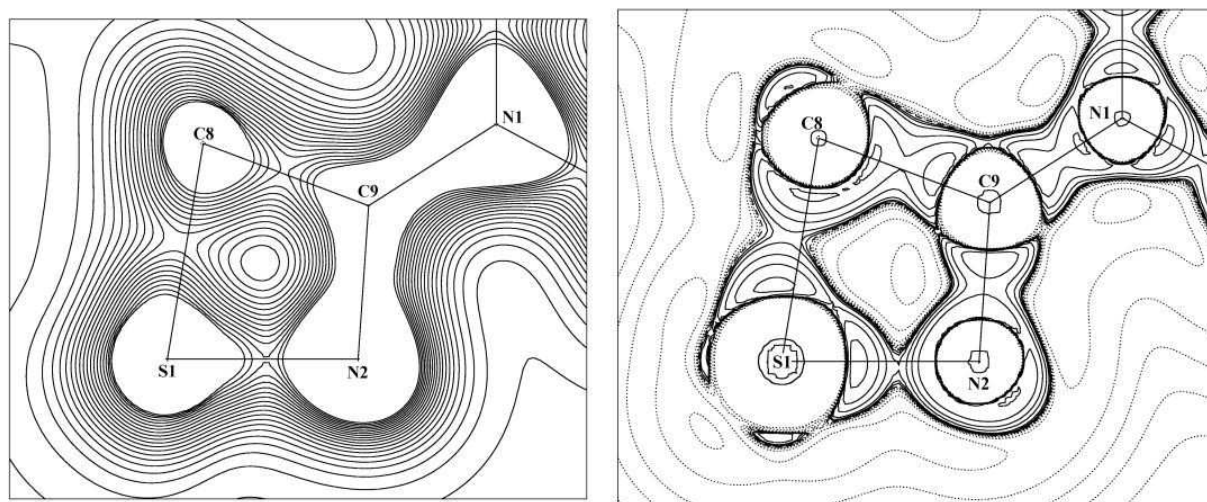
<sup>b</sup>C–H distances have been fixed during the refinement to match neutron estimates (see text).

<sup>c</sup>Symmetry operation, with fractional translations, to localize the Donor D together with its attached hydrogen atom. All the acceptors A belong to the DTC asymmetric unit.

<sup>d</sup>This is a C–H $\cdots$  $\pi$  interaction between the C14 methyl and the localized  $\pi$ -system of the C10 $\equiv$ N3 cyano group. Actually, a bcp is found in the experimental charge density distribution between H14C and C10. See Table S1 above.



(a)



(b)

**Figure A9.** Contour plot of the  $\rho(\mathbf{r})$  (left) and  $-\nabla^2\rho(\mathbf{r})$  (right) functions in the S1–N2–C9 plane within the thiazete ring in DTC. For the charge density, 20 curves are plotted starting from  $0.05 \text{ e}\cdot\text{\AA}^{-3}$ , at steps of  $0.1 \text{ e}\cdot\text{\AA}^{-3}$ . For the negative laplacian, 16 curves are drawn at variable intervals (dotted: negative values, full: positive values, dashed: zero line). (a) Multipole-projected charge density ( $\rho_{\text{MM-PQM}}$ ) of the isolated DTC molecule optimized at the B3LYP 6-311G(p,d) theory level. (b) Multipole charge density ( $\rho_{\text{EXPT}}$ ) of the DTC molecule extracted from the crystal, as refined against experimental structure factor amplitudes

**Table A7.** C-N and C=N distances as obtained for the gas-phase optimized geometries of DTC with different Hamiltonians, in conjunction with the same 6-311G(p,d) basis set.

BOND	C-N, C=N distances		
	PBE0	M06	MP2
N1 – C9	1.3251	1.3266	1.3314
N2 = C9	1.3133	1.3106	1.3255

**Table A8.** Values of various bond descriptors for the DTC molecule from various theoretical models and experiment.<sup>a</sup> See Figure 1 and Scheme 2 in the main text for the atom numbering.

Density	C9-N1			C9-N2			S1-N2		
	R <sub>e</sub>	ρ	Δ <sub>bcp</sub>	R <sub>e</sub>	ρ	Δ <sub>bcp</sub>	R <sub>e</sub>	ρ	Δ <sub>bcp</sub>
ρ <sub>VQM</sub>	1.333	2.274	-25.9	1.316	2.463	-22.8	1.701	1.552	-6.5
ρ <sub>VQM-FRO</sub>	1.314	2.355	-27.3	1.333	2.388	-20.6	1.654	1.674	-18.8
ρ <sub>PQM</sub>	-	2.369	-26.6	-	2.382	-21.4	-	1.680	-17.7
ρ <sub>MM-PQM</sub>	-	2.436	-15.3	-	2.370	-9.8	-	1.663	-3.0
ρ <sub>EXP</sub>	-	2.553	-23.6	-	2.510	-11.5	-	1.752	3.8

<sup>a</sup> Units are Å for distances, e·Å<sup>-3</sup> for electron density ρ; Δ<sub>bcp</sub> is the bcp displacement parameter; a negative value for an A-B bond means that the bcp is displaced towards A

The ρ(**r**) data at bcp's listed in Table A6 confirm that C9-N1 and S1-N2 are strengthened and C9=N2 is weakened upon crystallization, with the larger effect arising from the change of geometry. The displacement of the bcp from the bond mid-point towards the more electropositive atom (C) slightly increases for C9-N1 and similarly decreases for C9=N2, despite the enhancement of the charge separation for C9=N2 upon crystallization would predict an opposite behaviour for such a bond. However, it should be considered that the moderate shift of the bcp towards N2 is but the consequence of the already noticed very large shift of the S1-N2 bcp towards the S atom, due to the great enhancement of the positive charge of S and charge separation between N2 and S1.



**Table A9.** Source contributions at N1–C9, C9=N2 and N2–S1 bcp's for the DTC charge density in the gas-phase and in the solid-state.

ATOM	SOURCE CONTRIBUTIONS AT BCP'S DTC CHARGE DENSITY					
	N1 – C9		C9 = N2		N2 – S1	
	gas-ph.	solid-st.	gas-ph.	solid-st.	gas-ph.	solid-st.
S1	0.20	0.21	0.81	1.10	35.93	34.27
O1	0.15	0.12	0.14	0.12	0.21	0.17
O3	0.71	0.71	1.19	1.37	6.93	6.22
O2	0.70	0.67	1.20	1.33	6.98	6.02
N1	44.16	45.01	4.22	3.84	1.23	1.21
N2	6.31	5.04	46.70	47.83	40.79	43.73
N3	1.16	1.04	1.07	1.04	1.50	1.34
C1	0.01	-0.02	0.01	-0.02	0.02	-0.03
C2	0.06	0.12	0.06	0.13	0.09	0.16
C5	0.19	0.18	0.18	0.18	0.25	0.22
C6	-0.04	-0.02	0.01	0.02	-0.02	-0.01
C3	0.13	0.14	0.12	0.14	0.18	0.19
C4	0.17	0.21	0.17	0.21	0.21	0.25
C7	0.04	0.18	0.16	0.28	0.14	0.30
C8	1.43	1.22	1.62	1.44	0.87	0.95
C9	38.80	39.27	39.71	39.05	2.90	3.19
C10	-0.11	-0.10	0.02	0.01	-0.05	-0.02
C11	0.66	0.57	0.09	-0.03	0.03	-0.07
C12	0.13	0.13	0.07	0.06	0.07	0.05
C13	0.66	0.74	0.19	0.22	0.10	0.12
C14	0.13	0.16	0.05	0.07	0.04	0.06
HB1	0.01	-0.01	0.00	-0.02	-0.02	-0.05
HC1	-0.02	0.00	-0.01	0.00	0.01	0.02
HA1	0.09	0.07	0.08	0.07	0.12	0.10
H5	0.14	0.12	0.12	0.12	0.18	0.16
H6	-0.11	-0.12	-0.17	-0.19	-0.21	-0.18
H3	0.15	0.13	0.13	0.13	0.20	0.18
H4	0.14	0.13	0.12	0.12	0.17	0.16
H1A	0.67	0.60	0.45	0.43	0.40	0.36
H1B	0.56	0.55	0.17	0.17	-0.06	-0.03
H2C	0.12	0.08	-0.06	-0.11	-0.23	-0.23
H2A	0.39	0.35	0.30	0.29	0.29	0.27
H2B	0.28	0.23	0.25	0.22	0.25	0.21
H3B	0.52	0.48	0.18	0.17	0.07	0.06
H3A	0.64	0.60	0.32	0.31	0.28	0.27
H4B	0.26	0.23	0.14	0.13	0.14	0.12
H4C	0.12	0.10	0.01	0.00	-0.06	-0.06
H4A	0.36	0.33	0.23	0.22	0.23	0.22

**Table A10.** Structural and topological point descriptors at the bond critical points for the  $\rho_{\text{EXPT}}$  charge density distribution of DTC at  $T = 100(2)$  K. Units are Å,  $\text{e}\cdot\text{Å}^{-3}$  and  $\text{e}\cdot\text{Å}^{-5}$ . Least-squares estimated standard deviations are reported in parentheses.

Bond	$d$	$\rho(r)_{\text{bcp}}$	$\nabla^2\rho(r)_{\text{bcp}}$	$\epsilon$
S(1) -N(2)	1.6539(4)	1.752( 22)	-5.998( 66)	0.05
S(1) -O(2)	1.4367(5)	2.462( 30)	-18.082(143)	0.23
S(1) -O(3)	1.4318(6)	2.566( 30)	-19.711(145)	0.09
S(1) -C(8)	1.8960(6)	1.116( 15)	-1.498( 29)	0.13
O(1) -C(1)	1.4271(8)	1.703( 17)	-8.116( 66)	0.09
O(1) -C(2)	1.3551(7)	2.092( 16)	-20.338( 79)	0.05
N(1) -C(9)	1.3144(5)	2.553( 16)	-34.390( 75)	0.17
N(1) -C(11)	1.4741(7)	1.698( 14)	-9.159( 47)	0.02
N(1) -C(13)	1.4693(5)	1.755( 14)	-10.508( 45)	0.04
N(2) -C(9)	1.3325(5)	2.510( 15)	-23.784( 50)	0.17
N(3) -C(10)	1.1569(5)	3.356( 21)	-0.511(145)	0.02
C(1) -H(A1)	1.0770(5)	1.782( 27)	-14.831( 80)	0.03
C(1) -H(B1)	1.0770(5)	1.823( 28)	-16.666( 76)	0.10
C(1) -H(C1)	1.0770(5)	1.828( 25)	-16.951( 65)	0.06
C(2) -C(3)	1.4009(5)	2.200( 13)	-21.167( 33)	0.21
C(2) -C(5)	1.3996(5)	2.208( 13)	-21.192( 33)	0.20
C(3) -C(4)	1.3861(5)	2.172( 13)	-19.754( 32)	0.18
C(3) -H(3)	1.0830(4)	1.857( 24)	-17.768( 74)	0.04
C(4) -C(7)	1.4009(5)	2.156( 13)	-19.559( 31)	0.18
C(4) -H(4)	1.0830(4)	1.858( 24)	-17.462( 74)	0.04
C(5) -C(6)	1.3940(5)	2.126( 13)	-18.711( 33)	0.17
C(5) -H(5)	1.0830(4)	1.856( 23)	-17.647( 66)	0.05
C(6) -C(7)	1.3972(5)	2.173( 13)	-20.098( 32)	0.17
C(6) -H(6)	1.0830(4)	1.848( 23)	-17.558( 72)	0.06
C(7) -C(8)	1.5032(5)	1.724( 11)	-12.179( 27)	0.12
C(8) -C(9)	1.5343(5)	1.648( 11)	-10.027( 25)	0.03
C(8) -C(10)	1.4548(5)	1.826( 13)	-12.624( 32)	0.04
C(11) -C(12)	1.5173(6)	1.696( 13)	-10.758( 27)	0.04
C(11) -H(1A)	1.0920(4)	1.847( 23)	-16.494( 64)	0.04
C(11) -H(1B)	1.0920(4)	1.840( 24)	-16.289( 68)	0.07
C(12) -H(2A)	1.0770(5)	1.792( 27)	-14.802( 75)	0.03
C(12) -H(2B)	1.0770(5)	1.733( 29)	-13.990( 77)	0.06
C(12) -H(2C)	1.0770(7)	1.780( 25)	-14.903( 67)	0.02
C(13) -C(14)	1.5211(6)	1.667( 12)	-10.502( 25)	0.04
C(13) -H(3A)	1.0920(4)	1.838( 23)	-15.858( 62)	0.03
C(13) -H(3B)	1.0920(4)	1.861( 23)	-16.189( 62)	0.04
C(14) -H(4A)	1.0770(4)	1.810( 24)	-15.363( 59)	0.03
C(14) -H(4B)	1.0770(5)	1.838( 24)	-16.013( 65)	0.03
C(14) -H(4C)	1.0770(4)	1.821( 26)	-15.546( 69)	0.04
C(10) -H(4C)	2.8247	0.044(2)	0.525(1)	0.33

**Table A11.** Topological point descriptors at the ring critical points for the  $\rho_{\text{EXPT}}$  charge density distribution of DTC at  $T = 100(2)$  K. Units are  $\text{e}\cdot\text{\AA}^{-3}$  and  $\text{e}\cdot\text{\AA}^{-5}$ .

Ring	$\rho(\mathbf{r})_{\text{bcp}}$	$\nabla^2\rho(\mathbf{r})_{\text{bcp}}$
S(1)-N(2)-C(9)-C(8)	0.5767	8.5
C(2)-C(3)-C(4)-C(5)-C(6)-C(7)	0.0816	4.5
H(4C)-C(14)-C(13)-N(1)-C(9)-C(8)-C(10)	0.0280	0.5

**Table A12.** Relevant bond distances ( $\text{\AA}$ ) as obtained for DTC and related compounds from B3LYP 6-311G(p,d) calculations in the gas-phase, compared with multipole-derived experimental estimates at  $T = 100(2)$  K (last column). See Scheme 2 in the main text for the meaning of the various labels. 5A and 5B refer to the two independent molecules in the asymmetric unit of TAYCUR, whereas ‘4-froz.’ refers to gas-phase DTC at frozen solid-state geometry.

BOND	BOND LENGTH								
	1	2	3	4	5A	5B	6	4-froz.	Expt.
S1 - N2	//	1.6916	1.7277	1.7013	1.6965	1.6960	1.7149	1.6539	1.6539(4)
N2 - C9	1.2721	1.2896	1.3048	1.3159	1.3209	1.3215	1.5109	1.3325	1.3325(5)
C9 - C8	//	//	1.5125	1.5407	1.5352	1.5346	1.5486	1.5343	1.5343(5)
C8 - S1	//	1.7992	1.8577	1.9686	1.9468	1.9461	1.8251	1.8960	1.8960(6)
C9 - N1	1.3799	1.3434	1.3401	1.3330	1.3329	1.3325	1.4312	1.3144	1.3144(5)
C8 - C10	//	//	//	1.4466	1.4997	1.4984	//	1.4548	1.4548(5)
C10 - N3	//	//	//	1.1539	1.2701	1.2707	//	1.1569	1.3144(5)
C8 - C7	//	//	//	1.5031	1.5065	1.5042	//	1.5032	1.5032(5)
S1 - O2	//	1.4585	1.4538	1.4542	1.4599	1.4618	1.4535	1.4367	1.4367(5)
S1 - O3	//	1.4693	1.4538	1.4555	1.4611	1.4600	1.4625	1.4318	1.4318(6)

**Table A13.** Same as Table A12 above, for charge density estimates at the bcp’s ( $\text{e}\text{\AA}^{-3}$ ).

BOND	ELECTRON DENSITY AT BCP								
	1	2	3	4	5A	5B	6	4-froz.	Expt.
S1 - N2	//	1.53	1.49	1.55	1.57	1.57	1.48	1.67	1.75(2)
N2 - C9	2.63	2.52	2.53	2.46	2.44	2.43	1.62	2.39	2.51(2)
C9 - C8	//	//	1.72	1.63	1.65	1.65	1.63	1.65	1.65(1)
C8 - S1	//	1.36	1.22	0.97	1.02	1.02	1.30	1.12	1.12(2)
C9 - N1	2.05	2.21	2.22	2.27	2.27	2.27	1.94	2.35	2.55(2)
C8 - C10	//	//	//	1.83	1.74	1.75	//	1.80	1.83(1)
C10 - N3	//	//	//	3.23	2.57	2.57	//	3.21	3.36(2)
C8 - C7	//	//	//	1.69	1.68	1.69	//	1.69	1.72(1)
S1 - O2	//	1.98	1.98	1.97	1.95	1.94	1.98	2.03	2.46(3)
S1 - O3	//	1.94	1.98	1.96	1.95	1.95	1.95	2.04	2.57(3)
rcp <sub>(S1-N2-C9-C8)</sub>	//	//	0.54	0.49	0.50	0.50	0.46	0.53	0.58

**Table A14.** Same as Table A12 above, for the charge density laplacian at the bcp's ( $e\text{\AA}^{-5}$ ).

BOND	CHARGE DENSITY LAPLACIAN AT BCP								
	1	2	3	4	5A	5B	6	4-froz.	Expt.
S1 - N2	//	-14.2	-11.5	-13.3	-13.8	-13.8	-12.8	-14.6	-6.00(7)
N2 - C9	-27.0	-25.4	-27.8	-26.9	-26.6	-26.6	-13.0	-25.8	-23.78(5)
C9 - C8	//	//	-14.3	-12.7	-13.0	-13.1	-13.0	-13.0	-10.03(3)
C8 - S1	//	-9.2	-6.6	-2.9	-3.5	-3.5	-8.1	-5.0	-1.50(3)
C9 - N1	-20.7	-21.6	-22.3	-22.7	-22.6	-22.6	-19.4	-22.3	-34.39(8)
C8 - C10	//	//	//	-17.0	-15.0	-15.0	//	-16.4	-12.62(3)
C10 - N3	//	//	//	-5.8	-19.6	-19.8	//	-6.1	-0.5(1)
C8 - C7	//	//	//	-13.9	-13.8	-13.9	//	-13.9	-12.18(3)
S1 - O2	//	22.2	23.6	23.8	22.6	22.1	23.7	28.5	-18.1(1)
S1 - O3	//	20.1	23.6	23.6	22.3	22.6	21.4	30.0	-19.7(1)
rcp <sub>(S1-N2-C9-C8)</sub>	//	//	9.3	8.5	8.7	8.7	8.7	9.2	8.5

**Table A15.** Same as Table A12 above, for the ellipticity estimates at the bcp's (dimensionless).

BOND	ELLIPTICITY								
	1	2	3	4	5A	5B	6	4-froz.	Expt.
S1 - N2	//	0.04	0.04	0.03	0.04	0.04	0.08	0.04	0.05
N2 - C9	0.25	0.15	0.23	0.22	0.20	0.20	0.03	0.21	0.17
C9 - C8	//	//	0.01	0.01	0.02	0.02	0.01	0.01	0.03
C8 - S1	//	0.00	0.02	0.03	0.02	0.02	0.01	0.03	0.13
C9 - N1	0.07	0.09	0.11	0.19	0.17	0.17	0.04	0.19	0.17
C8 - C10	//	//	//	0.03	0.07	0.07	//	0.03	0.04
C10 - N3	//	//	//	0.01	0.23	0.23	//	0.01	0.02
C8 - C7	//	//	//	0.10	0.07	0.07	//	0.09	0.12
S1 - O2	//	0.03	0.07	0.09	0.08	0.08	0.07	0.08	0.23
S1 - O3	//	0.05	0.07	0.09	0.09	0.09	0.08	0.08	0.09
rcp <sub>(S1-N2-C9-C8)</sub>	//	//	0.16	0.18	0.20	0.20	0.17	0.15	0.33

**Table A16.** Same as Table A12 above, for the bond degree parameter at the bcp (atomic units).

BOND	BOND DEGREE PARAMETER							
	1	2	3	4	5A	5B	6	4-froz.
S1 - N2	//	-1.10	-0.93	-1.01	-1.02	-1.02	-1.03	-1.32
N2 - C9	-1.54	-1.51	-1.46	-1.43	-1.42	-1.42	-0.97	-1.36
C9 - C8	//	//	-0.84	-0.79	-0.80	-0.80	-0.79	-0.80
C8 - S1	//	-0.71	-0.64	-0.50	-0.52	-0.52	-0.68	-0.59
C9 - N1	-1.33	-1.43	-1.42	-1.43	-1.43	-1.43	-1.10	-1.48
C8 - C10	//	//	//	-0.94	-0.84	-0.84	//	-0.93
C10 - N3	//	//	//	-1.80	-1.58	-1.58	//	-1.80
C8 - C7	//	//	//	-0.83	-0.82	-0.83	//	-0.83
S1 - O2	//	-1.22	-1.21	-1.20	-1.20	-1.20	-1.21	-1.19
S1 - O3	//	-1.22	-1.21	-1.20	-1.20	-1.20	-1.21	-1.18

**Table A17.** Distance of the bcp's of the N1-C9, N2=C9 and N2-S1 bonds from the corresponding N atoms for the compounds described in the caption of Table A8.

BOND	N-BCP DISTANCES								Expt.
	1	2	3	4	5A	5B	6	4-froz.	
N1 - C9	0.86370	0.85315	0.84779	0.83925	0.84107	0.84093	0.83767	0.83623	0.8120
N2 - C9	0.79762	0.80859	0.80308	0.80803	0.81005	0.81008	0.88361	0.80376	0.7428
N2 - S1	//	0.93920	0.90337	0.90577	0.90659	0.90564	0.93759	0.98213	0.7959



## **REFERENCES**

- [1] Clerici, F. ; Gelmi, M. L. ; Soave, R. ; Lo Presti, L. *Tetrahedron* **2002**, 58, 5173-5178
- [2] Bruker. SMART and SAINT. Bruker AXS Inc., **1999** Madison, Wisconsin, USA
- [3] Sheldrick, G. M. *TWINABS*. **2008**, University of Göttingen, Germany.
- [4] Destro, R.; Loconte, L.; Lo Presti, L.; Roversi, P.; Soave, R., *Acta Cryst.* **2004**, A60, 365–370
- [5] Kaminski, R., Domagała, S., Jarzemska, K. N.; Hoser, A. A.W.; Sanjuan-Szklarz, F.; Gutmann, M. J.; Makal, A.; Malinska, M.; Bak, J. M.; Wozniak, K. *Acta Crystallogr., Sect. A* **2014** 70, 72–91.
- [6] Bruker *SADABS*. **2007**, Bruker AXS Inc., Madison, Wisconsin, USA.
- [7] Bruker *XPREP*. **2004**, Bruker AXS Inc., Madison, Wisconsin, USA.
- [8] Peterson, S. W.; Levy, H. A., *Acta Cryst.* **1957**, 10, 70–76.
- [9] Clementi, E.; Roetti, C. *At. Data Nucl. Data Tables* **1974**, 14, 177-478
- [10] Lo Presti, L.; Destro, R. *J. Chem. Phys.*, **2008**, 128, 044710, 9 pages.
- [11] Dominiak, P.; Coppens, P. *Acta Cryst.* **2006**, A62, 224–227
- [12] Hehre, W. J.; Ditchfield, R. ; Stewart, R. F. ; Pople, J. A. *J. Chem. Phys.* **1970**, 52, 2769-2773.
- [13] Farrugia, L. J.; Mallinson, P. R.; Stewart, B. *Acta Crystallogr. Sect. B* **2003**, 59, 234–247.
- [14] Østergaard Madsen, A. *J. Appl. Crystallogr.* **2006**, 39, 757 –758.
- [15] Allen, F. H. ; Bruno, I. J. *Acta Crystallogr. Sect. B* **2010**, 66, 380 – 386.
- [16] Hathwar, V. R. ; Thakur, T. S. ; Dubey, R.; Pavan, M. S. ; Guru Row, T. N. ; Desiraju, G. R. *J. Phys. Chem. A* **2011**, 115, 12852–12863.
- [17] A. A. Hoser, P. M. Dominiak, K. Wozniak *Acta Cryst.* **2009**, A65, 300-311
- [18] R. Destro, L. Lo Presti, R. Soave, A. E. Goeta, *Multi-Temperature Electron Density Studies*, in *Modern Charge Density Analysis*, Editors: C. Gatti & P. Macchi, **2012**, Springer, Dordrecht (D)
- [19] B. T. M. Willis, A. W. Pryor, *Thermal Vibrations in Crystallography*, Cambridge University Press, Cambridge (UK), **1975**.
- [20] Schomaker, V.; Trueblood, K. N. *Acta Crystallogr., Sect. B* **1998**, 54, 507-514.
- [21] Hirshfeld, F. L. *Acta Crystallogr., Sect. A* **1976**, 32, 239-244.
- [22] Schomaker, V.; Trueblood, K. N. *Acta Crystallogr., Sect. B* **1968**, 24, 63-76.
- [23] Dunitz, J. D.; Schomaker, V.; Trueblood, K. N. *J. Phys. Chem.* **1988**, 92, 856-867.
- [24] Abrahams, S. C.; Keve, E.T., *Acta Crystallogr. Sect. A* **1971**, 27, 157-165.
- [25] Henn, J.; Meindl, K., *Acta Crystallogr. Sect. A* **2010**, 66, 676–684.
- [26] B. Dittrich, C.B Hubschle, J. J. Holstein, F. P. A. Fabbiani, *J. Appl. Cryst.* **2009**, 42, 1110-1121
- [27] Espinosa, E.; Alkorta, I.; Elguero, J.; Molins, E. *J. Chem. Phys.* **2002**, 117, 5529-5542.

# **APPENDIX A2**



$\Omega$	LS	SF%	$LS_{\alpha}$	$LS_{\beta}$	LSs	SFs%	$R_{SF}$	$R_{FSs}$
Cu1	1.899	98.291	1.093	0.806	0.286	101.430	0.497	0.502
N1	0.000	0.013	-0.001	0.001	-0.001	-0.458	0.026	-0.083
N2	0.002	0.120	0.001	0.002	-0.001	-0.376	0.053	-0.078
N3	0.003	0.158	0.002	0.001	0.001	0.269	0.058	0.070
N5	0.000	-0.002	0.000	0.000	0.000	-0.102	-0.014	-0.050
N4	-0.001	-0.026	0.000	0.000	0.000	-0.067	-0.032	-0.044
C14	0.001	0.054	0.000	0.001	0.000	-0.084	0.041	-0.047
C13	0.001	0.046	0.000	0.000	0.000	0.021	0.039	0.030
C12	0.000	0.025	0.000	0.000	0.000	-0.019	0.031	-0.029
C11	0.001	0.043	0.000	0.000	0.000	0.024	0.038	0.031
C10	0.001	0.056	0.000	0.001	0.000	-0.089	0.041	-0.048
C15	0.000	0.000	0.000	0.000	0.000	0.003	0.005	0.016
C17	0.000	0.004	0.000	0.000	0.000	0.000	0.017	-0.007
C16	0.000	0.006	0.000	0.000	0.000	0.000	0.019	-0.006
C16	0.000	0.006	0.000	0.000	0.000	0.000	0.020	-0.005
C1	0.001	0.031	0.000	0.000	0.000	-0.064	0.034	-0.043
C2	0.001	0.039	0.000	0.000	0.000	0.018	0.036	0.028
C3	0.000	0.020	0.000	0.000	0.000	-0.015	0.029	-0.026
C4	0.001	0.038	0.000	0.000	0.000	0.017	0.036	0.028
C5	0.001	0.040	0.000	0.000	0.000	-0.069	0.037	-0.044
C6	0.000	0.001	0.000	0.000	0.000	0.003	0.009	0.015
C9	0.000	0.006	0.000	0.000	0.000	0.000	0.019	-0.006
C8	0.000	0.004	0.000	0.000	0.000	0.000	0.017	-0.006
C7	0.000	0.004	0.000	0.000	0.000	0.000	0.017	-0.006
Cu1'	0.001	0.053	0.001	0.000	0.001	0.449	0.040	0.083
N1'	0.005	0.233	0.001	0.003	-0.002	-0.728	0.066	-0.097
N2'	0.003	0.178	0.001	0.002	-0.001	-0.463	0.061	-0.083
N3'	0.004	0.223	0.003	0.002	0.001	0.331	0.065	0.075
N5'	-0.001	-0.034	0.000	0.000	0.000	0.003	-0.035	0.016
N4'	-0.001	-0.034	0.000	0.000	0.000	0.000	-0.035	-0.008
C14'	0.000	0.005	0.000	0.000	0.000	-0.047	0.018	-0.039
C13'	0.000	0.013	0.000	0.000	0.000	0.013	0.026	0.026
C12'	0.000	0.010	0.000	0.000	0.000	-0.013	0.023	-0.025
C11'	0.000	0.013	0.000	0.000	0.000	0.015	0.025	0.027
C10'	0.000	0.005	0.000	0.000	0.000	-0.050	0.019	-0.040
C15'	0.000	-0.001	0.000	0.000	0.000	0.002	-0.010	0.014
C17'	0.000	0.003	0.000	0.000	0.000	0.000	0.016	-0.007
C16'	0.000	0.005	0.000	0.000	0.000	0.000	0.018	-0.005
C16'	0.000	0.004	0.000	0.000	0.000	0.000	0.018	-0.005
C1'	0.000	0.008	0.000	0.000	0.000	-0.039	0.021	-0.037
C2'	0.000	0.015	0.000	0.000	0.000	0.012	0.027	0.025
C3'	0.000	0.010	0.000	0.000	0.000	-0.011	0.023	-0.024
C4'	0.000	0.016	0.000	0.000	0.000	0.013	0.027	0.025
C5'	0.000	0.003	0.000	0.000	0.000	-0.049	0.015	-0.039
C6'	0.000	-0.001	0.000	0.000	0.000	0.002	-0.009	0.014
C9'	0.000	0.004	0.000	0.000	0.000	0.000	0.017	-0.006

C8'	0.000	0.003	0.000	0.000	0.000	0.000	0.016	-0.005
C7'	0.000	0.003	0.000	0.000	0.000	0.000	0.016	-0.005
H1	0.000	0.015	0.000	0.000	0.000	0.000	0.026	0.003
H2	0.000	0.001	0.000	0.000	0.000	0.000	0.010	-0.005
H3	0.000	-0.002	0.000	0.000	0.000	0.000	-0.012	-0.006
H4	0.000	0.015	0.000	0.000	0.000	0.000	0.027	-0.004
H5	0.000	-0.002	0.000	0.000	0.000	0.000	-0.014	-0.006
H6	0.000	0.001	0.000	0.000	0.000	0.000	0.009	0.005
H7	0.000	0.016	0.000	0.000	0.000	0.000	0.027	-0.004
H8	0.000	-0.002	0.000	0.000	0.000	0.000	-0.014	-0.005
H9	0.000	-0.003	0.000	0.000	0.000	0.000	-0.015	0.006
H10	0.000	0.017	0.000	0.000	0.000	0.000	0.027	0.003
H11	0.000	0.000	0.000	0.000	0.000	0.000	0.007	-0.006
H12	0.000	0.000	0.000	0.000	0.000	0.000	-0.007	-0.006
H13	0.000	0.017	0.000	0.000	0.000	0.000	0.028	-0.004
H14	0.000	-0.001	0.000	0.000	0.000	0.000	-0.009	0.006
H15	0.000	-0.001	0.000	0.000	0.000	0.000	-0.010	-0.006
H16	0.000	0.017	0.000	0.000	0.000	0.000	0.028	-0.005
H17	0.000	-0.002	0.000	0.000	0.000	0.000	-0.013	-0.006
H18	0.000	-0.004	0.000	0.000	0.000	0.000	-0.016	0.005
H19	0.000	0.019	0.000	0.000	0.000	0.021	0.029	0.030
H20	0.001	0.033	0.000	0.000	0.000	0.001	0.035	0.009
H21	0.001	0.032	0.000	0.000	0.000	0.001	0.034	0.011
H22	0.000	0.018	0.000	0.000	0.000	0.020	0.028	0.029
H23	0.000	0.012	0.000	0.000	0.000	0.016	0.025	0.027
H24	0.001	0.027	0.000	0.000	0.000	0.001	0.032	0.009
H25	0.001	0.027	0.000	0.000	0.000	0.001	0.032	0.011
H26	0.000	0.007	0.000	0.000	0.000	0.014	0.021	0.026
H1'	0.000	0.011	0.000	0.000	0.000	0.000	0.024	0.002
H2'	0.000	0.001	0.000	0.000	0.000	0.000	0.010	-0.005
H3'	0.000	-0.006	0.000	0.000	0.000	0.000	-0.019	-0.006
H4'	0.000	0.010	0.000	0.000	0.000	0.000	0.023	-0.004
H5'	0.000	0.001	0.000	0.000	0.000	0.000	0.010	-0.005
H6'	0.000	0.001	0.000	0.000	0.000	0.000	0.009	0.004
H7'	0.000	0.011	0.000	0.000	0.000	0.000	0.024	-0.004
H8'	0.000	0.000	0.000	0.000	0.000	0.000	0.006	-0.005
H9'	0.000	-0.006	0.000	0.000	0.000	0.000	-0.020	0.005
H10'	0.000	0.010	0.000	0.000	0.000	0.000	0.023	0.003
H11'	0.000	0.001	0.000	0.000	0.000	0.000	0.011	-0.006
H12'	0.000	-0.002	0.000	0.000	0.000	0.000	-0.014	-0.005
H13'	0.000	0.010	0.000	0.000	0.000	0.000	0.023	-0.004
H14'	0.000	0.000	0.000	0.000	0.000	0.000	0.008	0.005
H15'	0.000	-0.001	0.000	0.000	0.000	0.000	-0.011	-0.005
H16'	0.000	0.011	0.000	0.000	0.000	0.000	0.024	-0.004
H17'	0.000	-0.002	0.000	0.000	0.000	0.000	-0.014	-0.006
H18'	0.000	-0.005	0.000	0.000	0.000	0.000	-0.018	0.004
H19'	0.000	-0.006	0.000	0.000	0.000	0.012	-0.019	0.025
H20'	0.000	0.014	0.000	0.000	0.000	0.000	0.026	0.008
H21'	0.000	0.013	0.000	0.000	0.000	0.001	0.025	0.010

H22'	0.000	-0.007	0.000	0.000	0.000	0.011	-0.020	0.024
H23'	0.000	0.007	0.000	0.000	0.000	0.009	0.021	0.023
H24'	0.000	0.016	0.000	0.000	0.000	0.000	0.027	0.008
H25'	0.000	0.012	0.000	0.000	0.000	0.001	0.024	0.011
H26'	0.000	-0.023	0.000	0.000	0.000	0.011	-0.030	0.024

**Table A2.1:** Contributions at the CD near to the Cu1 atomic basin along on the Cu-N1 bond for the EO molecular system; LS, SF%, LS<sub>α</sub>, LS<sub>β</sub>, LS<sub>s</sub>, SF<sub>s</sub>% are respectively the Local source, the Source Function atomic percentage for ρ(**r**), the Local source alpha and beta, the Local Source for s(**r**) and the Source Function atomic percentage for s(**r**).

R<sub>SF</sub> (R<sub>FS<sub>s</sub></sub>) are the ray of the sphere that are proportional to the atomic contribution to ρ(**r**) (s(**r**)) evaluated as

$$R_{SF} = 0.5 \cdot (SF\%/100)^{1/3}$$

$$R_{FS_s} = 0.5 \cdot (SF_s\%/100)^{1/3}$$

All the reported quantity are reported in a.u.

Ω	LS	SF%	LS <sub>α</sub>	LS <sub>β</sub>	LS <sub>s</sub>	SF <sub>s</sub> %	R <sub>SF</sub>	R <sub>FS<sub>s</sub></sub>
Cu1	6,473	99,509	3,249	3,224	0,025	118,959	0,499	0,530
N1	0,002	0,025	0,000	0,002	-0,002	-7,676	0,031	-0,212
N2	0,003	0,043	0,001	0,002	-0,001	-5,454	0,038	-0,190
N3	0,003	0,054	0,002	0,001	0,001	3,890	0,041	0,169
N5	0,000	-0,004	0,000	0,000	0,000	-1,161	-0,017	-0,113
N4	0,000	-0,002	0,000	0,000	0,000	-1,213	-0,014	-0,115
C14	0,001	0,014	0,000	0,001	0,000	-1,063	0,026	-0,110
C13	0,001	0,013	0,000	0,000	0,000	0,273	0,025	0,070
C12	0,000	0,007	0,000	0,000	0,000	-0,240	0,020	-0,067
C11	0,001	0,012	0,000	0,000	0,000	0,312	0,024	0,073
C10	0,001	0,014	0,000	0,001	0,000	-1,125	0,026	-0,112
C15	0,000	0,000	0,000	0,000	0,000	0,039	-0,003	0,036
C17	0,000	0,001	0,000	0,000	0,000	-0,004	0,011	-0,017
C16	0,000	0,002	0,000	0,000	0,000	-0,002	0,012	-0,013
C16	0,000	0,002	0,000	0,000	0,000	-0,002	0,013	-0,013
C1	0,001	0,012	0,000	0,000	0,000	-0,909	0,025	-0,104
C2	0,001	0,013	0,000	0,000	0,000	0,251	0,025	0,068
C3	0,000	0,007	0,000	0,000	0,000	-0,206	0,020	-0,064
C4	0,001	0,013	0,000	0,000	0,000	0,247	0,025	0,068
C5	0,001	0,015	0,000	0,001	0,000	-1,005	0,026	-0,108
C6	0,000	0,000	0,000	0,000	0,000	0,036	0,007	0,036
C9	0,000	0,002	0,000	0,000	0,000	-0,003	0,013	-0,015
C8	0,000	0,001	0,000	0,000	0,000	-0,002	0,011	-0,014
C7	0,000	0,001	0,000	0,000	0,000	-0,002	0,011	-0,014
Cu1'	0,001	0,015	0,001	0,000	0,001	5,954	0,027	0,195
N1'	0,002	0,029	0,000	0,002	-0,002	-7,305	0,033	-0,209
N2'	0,003	0,041	0,001	0,002	-0,001	-5,626	0,037	-0,192
N3'	0,004	0,056	0,002	0,001	0,001	4,036	0,041	0,172
N5'	-0,001	-0,011	0,000	0,000	0,000	0,051	-0,024	0,040
N4'	-0,001	-0,010	0,000	0,000	0,000	-0,012	-0,023	-0,025
C14'	0,000	0,001	0,000	0,000	0,000	-0,639	0,012	-0,093
C13'	0,000	0,004	0,000	0,000	0,000	0,182	0,017	0,061

C12'	0,000	0,003	0,000	0,000	0,000	-0,172	0,016	-0,060
C11'	0,000	0,004	0,000	0,000	0,000	0,210	0,017	0,064
C10'	0,000	0,001	0,000	0,000	0,000	-0,685	0,012	-0,095
C15'	0,000	0,000	0,000	0,000	0,000	0,030	-0,007	0,033
C17'	0,000	0,001	0,000	0,000	0,000	-0,003	0,010	-0,016
C16'	0,000	0,001	0,000	0,000	0,000	-0,002	0,012	-0,012
C16'	0,000	0,001	0,000	0,000	0,000	-0,001	0,012	-0,012
C1'	0,000	0,002	0,000	0,000	0,000	-0,518	0,014	-0,087
C2'	0,000	0,004	0,000	0,000	0,000	0,160	0,018	0,059
C3'	0,000	0,003	0,000	0,000	0,000	-0,146	0,015	-0,057
C4'	0,000	0,005	0,000	0,000	0,000	0,169	0,018	0,060
C5'	0,000	0,001	0,000	0,000	0,000	-0,633	0,011	-0,092
C6'	0,000	0,000	0,000	0,000	0,000	0,028	-0,006	0,033
C9'	0,000	0,001	0,000	0,000	0,000	-0,002	0,011	-0,014
C8'	0,000	0,001	0,000	0,000	0,000	-0,001	0,010	-0,012
C7'	0,000	0,001	0,000	0,000	0,000	-0,002	0,011	-0,013
H1	0,000	0,005	0,000	0,000	0,000	0,000	0,018	0,006
H2	0,000	0,000	0,000	0,000	0,000	-0,002	0,007	-0,013
H3	0,000	-0,001	0,000	0,000	0,000	-0,002	-0,009	-0,014
H4	0,000	0,005	0,000	0,000	0,000	-0,001	0,018	-0,010
H5	0,000	0,000	0,000	0,000	0,000	-0,002	-0,008	-0,013
H6	0,000	0,000	0,000	0,000	0,000	0,001	0,007	0,012
H7	0,000	0,005	0,000	0,000	0,000	-0,001	0,018	-0,011
H8	0,000	-0,001	0,000	0,000	0,000	-0,002	-0,009	-0,013
H9	0,000	-0,001	0,000	0,000	0,000	0,002	-0,010	0,013
H10	0,000	0,005	0,000	0,000	0,000	0,000	0,018	0,008
H11	0,000	0,000	0,000	0,000	0,000	-0,003	-0,006	-0,015
H12	0,000	0,000	0,000	0,000	0,000	-0,002	0,004	-0,014
H13	0,000	0,005	0,000	0,000	0,000	-0,001	0,018	-0,011
H14	0,000	0,000	0,000	0,000	0,000	0,002	-0,008	0,014
H15	0,000	0,000	0,000	0,000	0,000	-0,002	-0,007	-0,013
H16	0,000	0,005	0,000	0,000	0,000	-0,001	0,018	-0,011
H17	0,000	-0,001	0,000	0,000	0,000	-0,002	-0,009	-0,015
H18	0,000	-0,001	0,000	0,000	0,000	0,001	-0,010	0,012
H19	0,000	0,004	0,000	0,000	0,000	0,273	0,016	0,070
H20	0,001	0,009	0,000	0,000	0,000	0,008	0,022	0,021
H21	0,001	0,009	0,000	0,000	0,000	0,015	0,022	0,027
H22	0,000	0,004	0,000	0,000	0,000	0,252	0,016	0,068
H23	0,000	0,006	0,000	0,000	0,000	0,219	0,020	0,065
H24	0,001	0,009	0,000	0,000	0,000	0,008	0,022	0,022
H25	0,001	0,009	0,000	0,000	0,000	0,017	0,022	0,028
H26	0,000	0,003	0,000	0,000	0,000	0,206	0,016	0,064
H1'	0,000	0,003	0,000	0,000	0,000	0,000	0,016	0,006
H2'	0,000	0,000	0,000	0,000	0,000	-0,001	0,006	-0,012
H3'	0,000	-0,001	0,000	0,000	0,000	-0,002	-0,012	-0,013
H4'	0,000	0,003	0,000	0,000	0,000	-0,001	0,015	-0,010
H5'	0,000	0,000	0,000	0,000	0,000	-0,001	0,006	-0,012
H6'	0,000	0,000	0,000	0,000	0,000	0,001	0,006	0,011
H7'	0,000	0,003	0,000	0,000	0,000	-0,001	0,016	-0,010

H8'	0,000	0,000	0,000	0,000	0,000	-0,001	-0,004	-0,012
H9'	0,000	-0,002	0,000	0,000	0,000	0,002	-0,013	0,012
H10'	0,000	0,003	0,000	0,000	0,000	0,000	0,016	0,007
H11'	0,000	0,000	0,000	0,000	0,000	-0,002	0,008	-0,013
H12'	0,000	-0,001	0,000	0,000	0,000	-0,002	-0,010	-0,013
H13'	0,000	0,003	0,000	0,000	0,000	-0,001	0,015	-0,010
H14'	0,000	0,000	0,000	0,000	0,000	0,001	0,007	0,012
H15'	0,000	0,000	0,000	0,000	0,000	-0,001	-0,007	-0,012
H16'	0,000	0,003	0,000	0,000	0,000	-0,001	0,016	-0,010
H17'	0,000	-0,001	0,000	0,000	0,000	-0,002	-0,009	-0,013
H18'	0,000	-0,002	0,000	0,000	0,000	0,001	-0,013	0,011
H19'	0,000	-0,001	0,000	0,000	0,000	0,162	-0,012	0,059
H20'	0,000	0,004	0,000	0,000	0,000	0,006	0,017	0,019
H21'	0,000	0,004	0,000	0,000	0,000	0,011	0,017	0,024
H22'	0,000	-0,002	0,000	0,000	0,000	0,155	-0,013	0,058
H23'	0,000	0,002	0,000	0,000	0,000	0,122	0,013	0,053
H24'	0,000	0,004	0,000	0,000	0,000	0,006	0,018	0,019
H25'	0,000	0,003	0,000	0,000	0,000	0,012	0,016	0,025
H26'	0,000	-0,006	0,000	0,000	0,000	0,137	-0,020	0,056

**Table A2.2:** Contributions at the CC near to the Cu1 atomic basin along on the Cu1-Cu1' internuclear axis for the EO molecular system; LS, SF%, LS $_{\alpha}$ , LS $_{\beta}$ , LS $_s$ , SF $_s$ % are respectively the Local source, the Source Function atomic percentage for  $\rho(\mathbf{r})$ , the Local source alpha and beta, the Local Source for  $s(\mathbf{r})$  and the Source Function atomic percentage for  $s(\mathbf{r})$ . R $_{SF}$  (R $_{FSs}$ ) are evaluated as in tab A2.1.

$\Omega$	LS	SF%	LS $_{\alpha}$	LS $_{\beta}$	LS $_s$	SF $_s$ %	R $_{SF}$	R $_{FSs}$
Cu1	79.040	0.489	89.503	89.537	-0.034	90.425	0.085	0.484
N1	0.001	0.000	0.000	0.001	-0.001	3.504	0.002	0.164
N2	0.002	0.000	0.000	0.002	-0.001	2.910	0.003	0.154
N3	0.003	0.000	0.002	0.001	0.001	-2.085	0.003	-0.138
N5	0.000	0.000	0.000	0.000	0.000	0.935	0.001	0.105
N4	0.001	0.000	0.000	0.000	0.000	0.958	0.002	0.106
C14	0.001	0.000	0.000	0.001	0.000	0.629	0.002	0.092
C13	0.001	0.000	0.000	0.000	0.000	-0.159	0.002	-0.058
C12	0.000	0.000	0.000	0.000	0.000	0.139	0.002	0.056
C11	0.001	0.000	0.000	0.000	0.000	-0.181	0.002	-0.061
C10	0.001	0.000	0.000	0.001	0.000	0.662	0.002	0.094
C15	0.000	0.000	0.000	0.000	0.000	-0.022	0.000	-0.030
C17	0.000	0.000	0.000	0.000	0.000	0.002	0.001	0.014
C16	0.000	0.000	0.000	0.000	0.000	0.001	0.001	0.011
C16	0.000	0.000	0.000	0.000	0.000	0.001	0.001	0.011
C1	0.001	0.000	0.000	0.001	0.000	0.547	0.002	0.088
C2	0.001	0.000	0.001	0.000	0.000	-0.148	0.002	-0.057
C3	0.000	0.000	0.000	0.000	0.000	0.119	0.002	0.053
C4	0.001	0.000	0.000	0.000	0.000	-0.142	0.002	-0.056
C5	0.001	0.000	0.000	0.001	0.000	0.581	0.002	0.090
C6	0.000	0.000	0.000	0.000	0.000	-0.021	0.001	-0.030
C9	0.000	0.000	0.000	0.000	0.000	0.001	0.001	0.012

C8	0.000	0.000	0.000	0.000	0.000	0.001	0.001	0.010
C7	0.000	0.000	0.000	0.000	0.000	0.001	0.001	0.012
Cu1'	0.001	0.000	0.001	0.000	0.001	-2.975	0.002	-0.155
N1'	0.001	0.000	0.000	0.001	-0.001	3.333	0.002	0.161
N2'	0.002	0.000	0.000	0.002	-0.001	3.028	0.002	0.156
N3'	0.003	0.000	0.002	0.001	0.001	-2.183	0.003	-0.140
N5'	-0.001	0.000	0.000	0.000	0.000	-0.039	-0.002	-0.037
N4'	-0.001	0.000	0.000	0.000	0.000	-0.005	-0.002	-0.018
C14'	0.000	0.000	0.000	0.000	0.000	0.338	0.001	0.075
C13'	0.000	0.000	0.000	0.000	0.000	-0.097	0.001	-0.050
C12'	0.000	0.000	0.000	0.000	0.000	0.092	0.001	0.049
C11'	0.000	0.000	0.000	0.000	0.000	-0.112	0.001	-0.052
C10'	0.000	0.000	0.000	0.000	0.000	0.363	0.001	0.077
C15'	0.000	0.000	0.000	0.000	0.000	-0.016	0.000	-0.027
C17'	0.000	0.000	0.000	0.000	0.000	0.002	0.001	0.013
C16'	0.000	0.000	0.000	0.000	0.000	0.001	0.001	0.010
C16'	0.000	0.000	0.000	0.000	0.000	0.001	0.001	0.010
C1'	0.000	0.000	0.000	0.000	0.000	0.274	0.001	0.070
C2'	0.000	0.000	0.000	0.000	0.000	-0.085	0.001	-0.047
C3'	0.000	0.000	0.000	0.000	0.000	0.078	0.001	0.046
C4'	0.000	0.000	0.000	0.000	0.000	-0.090	0.001	-0.048
C5'	0.000	0.000	0.000	0.000	0.000	0.335	0.001	0.075
C6'	0.000	0.000	0.000	0.000	0.000	-0.015	0.000	-0.026
C9'	0.000	0.000	0.000	0.000	0.000	0.001	0.001	0.011
C8'	0.000	0.000	0.000	0.000	0.000	0.001	0.001	0.009
C7'	0.000	0.000	0.000	0.000	0.000	0.001	0.001	0.011
H1	0.000	0.000	0.000	0.000	0.000	0.000	0.001	-0.005
H2	0.000	0.000	0.000	0.000	0.000	0.001	0.001	0.010
H3	0.000	0.000	0.000	0.000	0.000	0.001	-0.001	0.012
H4	0.000	0.000	0.000	0.000	0.000	0.001	0.001	0.009
H5	0.000	0.000	0.000	0.000	0.000	0.001	-0.001	0.011
H6	0.000	0.000	0.000	0.000	0.000	-0.001	0.001	-0.010
H7	0.000	0.000	0.000	0.000	0.000	0.001	0.001	0.009
H8	0.000	0.000	0.000	0.000	0.000	0.001	-0.001	0.011
H9	0.000	0.000	0.000	0.000	0.000	-0.001	-0.001	-0.011
H10	0.000	0.000	0.000	0.000	0.000	0.000	0.001	-0.007
H11	0.000	0.000	0.000	0.000	0.000	0.001	-0.001	0.012
H12	0.000	0.000	0.000	0.000	0.000	0.001	0.000	0.012
H13	0.000	0.000	0.000	0.000	0.000	0.001	0.001	0.009
H14	0.000	0.000	0.000	0.000	0.000	-0.001	-0.001	-0.011
H15	0.000	0.000	0.000	0.000	0.000	0.001	-0.001	0.011
H16	0.000	0.000	0.000	0.000	0.000	0.001	0.001	0.009
H17	0.000	0.000	0.000	0.000	0.000	0.001	-0.001	0.012
H18	0.000	0.000	0.000	0.000	0.000	-0.001	-0.001	-0.010
H19	0.000	0.000	0.000	0.000	0.000	-0.160	0.001	-0.059
H20	0.001	0.000	0.000	0.000	0.000	-0.004	0.002	-0.018
H21	0.001	0.000	0.000	0.000	0.000	-0.009	0.002	-0.022
H22	0.000	0.000	0.000	0.000	0.000	-0.147	0.001	-0.057
H23	0.000	0.000	0.000	0.000	0.000	-0.133	0.002	-0.055

H24	0.001	0.000	0.000	0.000	0.000	-0.005	0.002	-0.018
H25	0.001	0.000	0.000	0.000	0.000	-0.010	0.002	-0.023
H26	0.000	0.000	0.000	0.000	0.000	-0.117	0.001	-0.053
H1'	0.000	0.000	0.000	0.000	0.000	0.000	0.001	-0.005
H2'	0.000	0.000	0.000	0.000	0.000	0.001	0.000	0.009
H3'	0.000	0.000	0.000	0.000	0.000	0.001	-0.001	0.011
H4'	0.000	0.000	0.000	0.000	0.000	0.000	0.001	0.008
H5'	0.000	0.000	0.000	0.000	0.000	0.001	0.000	0.010
H6'	0.000	0.000	0.000	0.000	0.000	-0.001	0.000	-0.009
H7'	0.000	0.000	0.000	0.000	0.000	0.000	0.001	0.008
H8'	0.000	0.000	0.000	0.000	0.000	0.001	0.000	0.010
H9'	0.000	0.000	0.000	0.000	0.000	-0.001	-0.001	-0.010
H10'	0.000	0.000	0.000	0.000	0.000	0.000	0.001	-0.006
H11'	0.000	0.000	0.000	0.000	0.000	0.001	0.001	0.011
H12'	0.000	0.000	0.000	0.000	0.000	0.001	-0.001	0.011
H13'	0.000	0.000	0.000	0.000	0.000	0.000	0.001	0.008
H14'	0.000	0.000	0.000	0.000	0.000	-0.001	0.001	-0.010
H15'	0.000	0.000	0.000	0.000	0.000	0.001	-0.001	0.010
H16'	0.000	0.000	0.000	0.000	0.000	0.001	0.001	0.009
H17'	0.000	0.000	0.000	0.000	0.000	0.001	-0.001	0.011
H18'	0.000	0.000	0.000	0.000	0.000	-0.001	-0.001	-0.009
H19'	0.000	0.000	0.000	0.000	0.000	-0.085	-0.001	-0.047
H20'	0.000	0.000	0.000	0.000	0.000	-0.003	0.001	-0.016
H21'	0.000	0.000	0.000	0.000	0.000	-0.006	0.001	-0.019
H22'	0.000	0.000	0.000	0.000	0.000	-0.082	-0.001	-0.047
H23'	0.000	0.000	0.000	0.000	0.000	-0.064	0.001	-0.043
H24'	0.000	0.000	0.000	0.000	0.000	-0.003	0.001	-0.016
H25'	0.000	0.000	0.000	0.000	0.000	-0.007	0.001	-0.020
H26'	0.000	0.000	0.000	0.000	0.000	-0.072	-0.001	-0.045

**Table A2.3:** Contributions at the Cu1 atomic basin along on the Cu-N1 bond for the EO molecular system; LS, SF%,  $LS_{\alpha}$ ,  $LS_{\beta}$ ,  $LS_s$ ,  $SF_s\%$  are respectively the Local source, the Source Function atomic percentage for  $\rho(\mathbf{r})$ , the Local source alpha and beta, the Local Source for  $s(\mathbf{r})$  and the Source Function atomic percentage for  $s(\mathbf{r})$ .  $R_{SF}$  ( $R_{FSs}$ ) are evaluated as in tab A2.1.

$\Omega$	LS	SF%	$LS_{\alpha}$	$LS_{\beta}$	$LS_s$	$SF_s\%$	$R_{SF}$	$R_{FSs}$
Cu1	0.003	0.002	0.003	0.001	0.002	0.797	0.013	0.100
N1	98.301	49.554	99.272	99.028	0.244	99.532	0.396	0.499
N2	0.044	0.022	0.021	0.023	-0.002	-0.915	0.030	-0.105
N3	0.011	0.006	0.006	0.005	0.001	0.602	0.019	0.091
N5	-0.001	0.000	0.000	0.000	0.000	-0.006	-0.008	-0.019
N4	-0.001	-0.001	-0.001	-0.001	0.000	-0.006	-0.009	-0.019
C14	0.000	0.000	0.000	0.000	0.000	-0.058	0.005	-0.042
C13	0.000	0.000	0.000	0.000	0.000	0.016	0.006	0.027
C12	0.000	0.000	0.000	0.000	0.000	-0.015	0.005	-0.027
C11	0.000	0.000	0.000	0.000	0.000	0.019	0.006	0.029
C10	0.000	0.000	0.000	0.000	0.000	-0.062	0.005	-0.043
C15	0.000	0.000	0.000	0.000	0.000	0.003	-0.002	0.015

C17	0.000	0.000	0.000	0.000	0.000	0.000	0.003	-0.007
C16	0.000	0.000	0.000	0.000	0.000	0.000	0.004	-0.005
C16	0.000	0.000	0.000	0.000	0.000	0.000	0.004	-0.005
C1	0.000	0.000	0.000	0.000	0.000	-0.061	0.007	-0.042
C2	0.000	0.000	0.000	0.000	0.000	0.018	0.007	0.028
C3	0.000	0.000	0.000	0.000	0.000	-0.017	0.006	-0.028
C4	0.001	0.000	0.000	0.000	0.000	0.021	0.007	0.030
C5	0.000	0.000	0.000	0.000	0.000	-0.084	-0.002	-0.047
C6	0.000	0.000	0.000	0.000	0.000	0.003	0.001	0.016
C9	0.000	0.000	0.000	0.000	0.000	0.000	0.004	-0.007
C8	0.000	0.000	0.000	0.000	0.000	0.000	0.004	-0.005
C7	0.000	0.000	0.000	0.000	0.000	0.000	0.003	-0.006
Cu1'	0.003	0.002	0.003	0.001	0.002	0.748	0.013	0.098
N1'	-0.001	-0.001	-0.001	0.000	-0.001	-0.332	-0.009	-0.075
N2'	0.002	0.001	0.000	0.001	-0.001	-0.360	0.010	-0.077
N3'	0.002	0.001	0.001	0.001	0.001	0.259	0.011	0.069
N5'	-0.002	-0.001	-0.001	-0.001	0.000	0.002	-0.010	0.014
N4'	-0.001	0.000	0.000	0.000	0.000	-0.011	-0.008	-0.024
C14'	0.000	0.000	0.000	0.000	0.000	-0.079	0.004	-0.046
C13'	0.000	0.000	0.000	0.000	0.000	0.021	0.007	0.030
C12'	0.000	0.000	0.000	0.000	0.000	-0.020	0.006	-0.029
C11'	0.000	0.000	0.000	0.000	0.000	0.025	0.007	0.031
C10'	0.000	0.000	0.000	0.000	0.000	-0.084	0.005	-0.047
C15'	0.000	0.000	0.000	0.000	0.000	0.003	-0.002	0.016
C17'	0.000	0.000	0.000	0.000	0.000	0.000	0.004	-0.007
C16'	0.000	0.000	0.000	0.000	0.000	0.000	0.004	-0.006
C16'	0.000	0.000	0.000	0.000	0.000	0.000	0.004	-0.006
C1'	0.000	0.000	0.000	0.000	0.000	-0.050	0.004	-0.040
C2'	0.000	0.000	0.000	0.000	0.000	0.015	0.006	0.027
C3'	0.000	0.000	0.000	0.000	0.000	-0.013	0.005	-0.025
C4'	0.000	0.000	0.000	0.000	0.000	0.015	0.006	0.026
C5'	0.000	0.000	0.000	0.000	0.000	-0.055	0.005	-0.041
C6'	0.000	0.000	0.000	0.000	0.000	0.002	-0.002	0.014
C9'	0.000	0.000	0.000	0.000	0.000	0.000	0.004	-0.006
C8'	0.000	0.000	0.000	0.000	0.000	0.000	0.003	-0.005
C7'	0.000	0.000	0.000	0.000	0.000	0.000	0.003	-0.006
H1	0.000	0.000	0.000	0.000	0.000	0.000	0.006	0.003
H2	0.000	0.000	0.000	0.000	0.000	0.000	0.003	-0.006
H3	0.000	0.000	0.000	0.000	0.000	0.000	-0.005	-0.006
H4	0.000	0.000	0.000	0.000	0.000	0.000	0.005	-0.004
H5	0.000	0.000	0.000	0.000	0.000	0.000	0.003	-0.006
H6	0.000	0.000	0.000	0.000	0.000	0.000	0.003	0.005
H7	0.000	0.000	0.000	0.000	0.000	0.000	0.006	-0.005
H8	0.000	0.000	0.000	0.000	0.000	0.000	0.003	-0.006
H9	0.000	0.000	0.000	0.000	0.000	0.000	-0.005	0.006
H10	0.000	0.000	0.000	0.000	0.000	0.000	0.005	0.003
H11	0.000	0.000	0.000	0.000	0.000	0.000	-0.002	-0.006
H12	0.000	0.000	0.000	0.000	0.000	0.000	-0.002	-0.006
H13	0.000	0.000	0.000	0.000	0.000	0.000	0.005	-0.004



H14	0.000	0.000	0.000	0.000	0.000	0.000	-0.003	0.006
H15	0.000	0.000	0.000	0.000	0.000	0.000	-0.002	-0.005
H16	0.000	0.000	0.000	0.000	0.000	0.000	0.005	-0.005
H17	0.000	0.000	0.000	0.000	0.000	0.000	-0.003	-0.006
H18	0.000	0.000	0.000	0.000	0.000	0.000	-0.003	0.005
H19	0.000	0.000	0.000	0.000	0.000	0.015	-0.004	0.027
H20	0.000	0.000	0.000	0.000	0.000	0.000	0.006	0.008
H21	0.000	0.000	0.000	0.000	0.000	0.001	0.006	0.011
H22	0.000	0.000	0.000	0.000	0.000	0.014	-0.005	0.026
H23	0.000	0.000	0.000	0.000	0.000	0.013	0.006	0.026
H24	0.000	0.000	0.000	0.000	0.000	0.001	0.007	0.009
H25	0.000	0.000	0.000	0.000	0.000	0.001	0.006	0.012
H26	-0.001	0.000	0.000	0.000	0.000	0.019	-0.007	0.029
H1'	0.000	0.000	0.000	0.000	0.000	0.000	0.005	0.002
H2'	0.000	0.000	0.000	0.000	0.000	0.000	0.001	-0.005
H3'	0.000	0.000	0.000	0.000	0.000	0.000	-0.003	-0.006
H4'	0.000	0.000	0.000	0.000	0.000	0.000	0.005	-0.004
H5'	0.000	0.000	0.000	0.000	0.000	0.000	-0.003	-0.005
H6'	0.000	0.000	0.000	0.000	0.000	0.000	-0.002	0.005
H7'	0.000	0.000	0.000	0.000	0.000	0.000	0.005	-0.004
H8'	0.000	0.000	0.000	0.000	0.000	0.000	-0.003	-0.005
H9'	0.000	0.000	0.000	0.000	0.000	0.000	-0.003	0.005
H10'	0.000	0.000	0.000	0.000	0.000	0.000	0.006	0.003
H11'	0.000	0.000	0.000	0.000	0.000	0.000	0.004	-0.006
H12'	0.000	0.000	0.000	0.000	0.000	0.000	-0.004	-0.006
H13'	0.000	0.000	0.000	0.000	0.000	0.000	0.006	-0.005
H14'	0.000	0.000	0.000	0.000	0.000	0.000	0.003	0.006
H15'	0.000	0.000	0.000	0.000	0.000	0.000	-0.002	-0.006
H16'	0.000	0.000	0.000	0.000	0.000	0.000	0.006	-0.005
H17'	0.000	0.000	0.000	0.000	0.000	0.000	-0.003	-0.006
H18'	0.000	0.000	0.000	0.000	0.000	0.000	-0.005	0.005
H19'	0.000	0.000	0.000	0.000	0.000	0.019	0.005	0.029
H20'	0.001	0.000	0.000	0.000	0.000	0.001	0.007	0.009
H21'	0.000	0.000	0.000	0.000	0.000	0.001	0.007	0.012
H22'	0.000	0.000	0.000	0.000	0.000	0.019	0.005	0.029
H23'	0.000	0.000	0.000	0.000	0.000	0.012	-0.002	0.025
H24'	0.000	0.000	0.000	0.000	0.000	0.001	0.006	0.009
H25'	0.000	0.000	0.000	0.000	0.000	0.001	0.006	0.011
H26'	0.000	0.000	0.000	0.000	0.000	0.012	-0.005	0.024

**Table A2.4:** Contributions at the N1 atomic basin along on the Cu-N1 bond for the EO molecular system; LS, SF%,  $LS_{\alpha}$ ,  $LS_{\beta}$ ,  $LS_s$ ,  $SF_s\%$  are respectively the Local source, the Source Function atomic percentage for  $\rho(\mathbf{r})$ , the Local source alpha and beta, the Local Source for  $s(\mathbf{r})$  and the Source Function atomic percentage for  $s(\mathbf{r})$ .  $R_{SF}$  ( $R_{FS_s}$ ) are evaluated as in tab A2.1.

$\Omega$	LS	SF%	$LS_{\alpha}$	$LS_{\beta}$	LSs	SFs%	$R_{SF}$	$R_{SFs}$
Cu1	87.346	99.962	44.070	43.275	0.795	100.377	0.500	0.501
N1	0.000	0.000	0.000	0.001	-0.001	-0.154	0.008	-0.058
N2	0.002	0.002	0.000	0.001	-0.001	-0.135	0.014	-0.055
N3	0.003	0.003	0.002	0.001	0.001	0.097	0.016	0.050
N5	0.001	0.001	0.000	0.001	0.000	-0.053	0.011	-0.041
N4	0.001	0.001	0.000	0.000	0.000	-0.045	0.009	-0.038
C14	0.001	0.001	0.000	0.001	0.000	-0.031	0.012	-0.034
C13	0.001	0.001	0.001	0.000	0.000	0.008	0.011	0.021
C12	0.001	0.001	0.000	0.000	0.000	-0.007	0.009	-0.020
C11	0.001	0.001	0.000	0.000	0.000	0.009	0.011	0.022
C10	0.001	0.001	0.001	0.001	0.000	-0.033	0.012	-0.034
C15	0.000	0.000	0.000	0.000	0.000	0.001	0.002	0.011
C17	0.000	0.000	0.000	0.000	0.000	0.000	0.005	-0.005
C16	0.000	0.000	0.000	0.000	0.000	0.000	0.005	-0.004
C16	0.000	0.000	0.000	0.000	0.000	0.000	0.006	-0.004
C1	0.001	0.001	0.000	0.001	0.000	-0.026	0.011	-0.032
C2	0.001	0.001	0.001	0.000	0.000	0.007	0.011	0.021
C3	0.000	0.001	0.000	0.000	0.000	-0.006	0.009	-0.019
C4	0.001	0.001	0.000	0.000	0.000	0.007	0.011	0.020
C5	0.001	0.001	0.000	0.001	0.000	-0.027	0.012	-0.032
C6	0.000	0.000	0.000	0.000	0.000	0.001	0.003	0.011
C9	0.000	0.000	0.000	0.000	0.000	0.000	0.006	-0.004
C8	0.000	0.000	0.000	0.000	0.000	0.000	0.005	-0.004
C7	0.000	0.000	0.000	0.000	0.000	0.000	0.005	-0.004
Cu1'	0.001	0.001	0.001	0.000	0.001	0.139	0.010	0.056
N1'	0.001	0.001	0.000	0.001	-0.001	-0.158	0.011	-0.058
N2'	0.002	0.002	0.000	0.001	-0.001	-0.147	0.014	-0.057
N3'	0.003	0.004	0.002	0.001	0.001	0.106	0.017	0.051
N5'	-0.001	-0.001	0.000	0.000	0.000	0.002	-0.010	0.013
N4'	-0.001	-0.001	0.000	0.000	0.000	0.000	-0.009	0.008
C14'	0.000	0.000	0.000	0.000	0.000	-0.016	0.004	-0.027
C13'	0.000	0.000	0.000	0.000	0.000	0.005	0.007	0.018
C12'	0.000	0.000	0.000	0.000	0.000	-0.004	0.006	-0.018
C11'	0.000	0.000	0.000	0.000	0.000	0.005	0.007	0.019
C10'	0.000	0.000	0.000	0.000	0.000	-0.017	0.005	-0.028
C15'	0.000	0.000	0.000	0.000	0.000	0.001	-0.003	0.010
C17'	0.000	0.000	0.000	0.000	0.000	0.000	0.004	-0.005
C16'	0.000	0.000	0.000	0.000	0.000	0.000	0.005	-0.004
C16'	0.000	0.000	0.000	0.000	0.000	0.000	0.005	-0.003
C1'	0.000	0.000	0.000	0.000	0.000	-0.013	0.005	-0.025
C2'	0.000	0.000	0.000	0.000	0.000	0.004	0.007	0.017
C3'	0.000	0.000	0.000	0.000	0.000	-0.004	0.006	-0.017
C4'	0.000	0.000	0.000	0.000	0.000	0.004	0.007	0.018
C5'	0.000	0.000	0.000	0.000	0.000	-0.016	0.004	-0.027
C6'	0.000	0.000	0.000	0.000	0.000	0.001	-0.003	0.010
C9'	0.000	0.000	0.000	0.000	0.000	0.000	0.005	-0.004
C8'	0.000	0.000	0.000	0.000	0.000	0.000	0.004	-0.003
C7'	0.000	0.000	0.000	0.000	0.000	0.000	0.004	-0.004

H1	0.000	0.000	0.000	0.000	0.000	0.000	0.008	0.002
H2	0.000	0.000	0.000	0.000	0.000	0.000	0.003	-0.004
H3	0.000	0.000	0.000	0.000	0.000	0.000	-0.003	-0.004
H4	0.000	0.000	0.000	0.000	0.000	0.000	0.008	-0.003
H5	0.000	0.000	0.000	0.000	0.000	0.000	-0.004	-0.004
H6	0.000	0.000	0.000	0.000	0.000	0.000	0.003	0.004
H7	0.000	0.000	0.000	0.000	0.000	0.000	0.008	-0.003
H8	0.000	0.000	0.000	0.000	0.000	0.000	-0.004	-0.004
H9	0.000	0.000	0.000	0.000	0.000	0.000	-0.004	0.004
H10	0.000	0.000	0.000	0.000	0.000	0.000	0.008	0.002
H11	0.000	0.000	0.000	0.000	0.000	0.000	-0.003	-0.004
H12	0.000	0.000	0.000	0.000	0.000	0.000	0.003	-0.004
H13	0.000	0.000	0.000	0.000	0.000	0.000	0.008	-0.003
H14	0.000	0.000	0.000	0.000	0.000	0.000	-0.004	0.004
H15	0.000	0.000	0.000	0.000	0.000	0.000	-0.003	-0.004
H16	0.000	0.000	0.000	0.000	0.000	0.000	0.008	-0.003
H17	0.000	0.000	0.000	0.000	0.000	0.000	-0.004	-0.004
H18	0.000	0.000	0.000	0.000	0.000	0.000	-0.004	0.004
H19	0.000	0.001	0.000	0.000	0.000	0.008	0.009	0.021
H20	0.001	0.001	0.000	0.000	0.000	0.000	0.010	0.006
H21	0.001	0.001	0.000	0.000	0.000	0.000	0.010	0.008
H22	0.000	0.001	0.000	0.000	0.000	0.007	0.009	0.021
H23	0.000	0.001	0.000	0.000	0.000	0.006	0.009	0.020
H24	0.001	0.001	0.000	0.000	0.000	0.000	0.010	0.007
H25	0.001	0.001	0.000	0.000	0.000	0.000	0.010	0.008
H26	0.000	0.000	0.000	0.000	0.000	0.005	0.008	0.019
H1'	0.000	0.000	0.000	0.000	0.000	0.000	0.007	0.002
H2'	0.000	0.000	0.000	0.000	0.000	0.000	0.003	-0.003
H3'	0.000	0.000	0.000	0.000	0.000	0.000	-0.005	-0.004
H4'	0.000	0.000	0.000	0.000	0.000	0.000	0.006	-0.003
H5'	0.000	0.000	0.000	0.000	0.000	0.000	0.003	-0.004
H6'	0.000	0.000	0.000	0.000	0.000	0.000	0.002	0.003
H7'	0.000	0.000	0.000	0.000	0.000	0.000	0.007	-0.003
H8'	0.000	0.000	0.000	0.000	0.000	0.000	0.001	-0.003
H9'	0.000	0.000	0.000	0.000	0.000	0.000	-0.005	0.004
H10'	0.000	0.000	0.000	0.000	0.000	0.000	0.006	0.002
H11'	0.000	0.000	0.000	0.000	0.000	0.000	0.003	-0.004
H12'	0.000	0.000	0.000	0.000	0.000	0.000	-0.004	-0.004
H13'	0.000	0.000	0.000	0.000	0.000	0.000	0.006	-0.003
H14'	0.000	0.000	0.000	0.000	0.000	0.000	0.003	0.004
H15'	0.000	0.000	0.000	0.000	0.000	0.000	-0.003	-0.004
H16'	0.000	0.000	0.000	0.000	0.000	0.000	0.007	-0.003
H17'	0.000	0.000	0.000	0.000	0.000	0.000	-0.004	-0.004
H18'	0.000	0.000	0.000	0.000	0.000	0.000	-0.005	0.003
H19'	0.000	0.000	0.000	0.000	0.000	0.004	-0.005	0.017
H20'	0.000	0.000	0.000	0.000	0.000	0.000	0.007	0.006
H21'	0.000	0.000	0.000	0.000	0.000	0.000	0.007	0.007
H22'	0.000	0.000	0.000	0.000	0.000	0.004	-0.006	0.017
H23'	0.000	0.000	0.000	0.000	0.000	0.003	0.005	0.016

H24'	0.000	0.000	0.000	0.000	0.000	0.000	0.007	0.006
H25'	0.000	0.000	0.000	0.000	0.000	0.000	0.006	0.007
H26'	0.000	0.000	0.000	0.000	0.000	0.003	-0.008	0.016

**Table A2.5:** Contributions at the Cu atomic basin along on the Cu-N5 bond for the EO molecular system; LS, SF%,  $LS_{\alpha}$ ,  $LS_{\beta}$ ,  $LS_s$ ,  $SF_s\%$  are respectively the Local source, the Source Function atomic percentage for  $\rho(\mathbf{r})$ , the Local source alpha and beta, the Local Source for  $s(\mathbf{r})$  and the Source Function atomic percentage for  $s(\mathbf{r})$ .  $R_{SF}$  ( $R_{FS_s}$ ) are evaluated as in tab A2.1.

$\Omega$	LS	SF%	$LS_{\alpha}$	$LS_{\beta}$	$LS_s$	$SF_s\%$	$R_{SF}$	$R_{FS_s}$
Cu1	0.047	47.486	0.027	0.020	0.008	311.676	0.390	0.730
N1	-0.001	-0.638	-0.001	0.000	-0.001	-29.112	-0.093	-0.331
N2	0.001	0.848	0.000	0.001	-0.001	-35.386	0.102	-0.354
N3	0.002	2.039	0.001	0.001	0.001	25.636	0.137	0.318
N5	0.022	22.416	0.010	0.013	-0.003	-116.287	0.304	-0.526
N4	-0.001	-0.980	-0.001	0.000	0.000	-7.826	-0.107	-0.214
C14	0.003	3.481	0.002	0.002	0.000	-13.328	0.163	-0.255
C13	0.002	1.620	0.001	0.001	0.000	3.124	0.127	0.157
C12	0.001	0.743	0.000	0.000	0.000	-2.625	0.098	-0.149
C11	0.001	1.503	0.001	0.001	0.000	3.572	0.123	0.165
C10	0.003	3.510	0.002	0.002	0.000	-13.873	0.164	-0.259
C15	0.000	0.025	0.000	0.000	0.000	0.402	0.031	0.080
C17	0.000	0.082	0.000	0.000	0.000	-0.040	0.047	-0.037
C16	0.000	0.117	0.000	0.000	0.000	-0.019	0.053	-0.029
C16	0.000	0.152	0.000	0.000	0.000	-0.017	0.057	-0.028
C1	0.000	0.482	0.000	0.000	0.000	-8.462	0.084	-0.220
C2	0.001	0.951	0.001	0.000	0.000	2.284	0.106	0.142
C3	0.000	0.440	0.000	0.000	0.000	-1.761	0.082	-0.130
C4	0.001	0.750	0.000	0.000	0.000	1.980	0.098	0.135
C5	0.001	0.986	0.000	0.001	0.000	-7.717	0.107	-0.213
C6	0.000	0.019	0.000	0.000	0.000	0.311	0.029	0.073
C9	0.000	0.120	0.000	0.000	0.000	-0.022	0.053	-0.030
C8	0.000	0.069	0.000	0.000	0.000	-0.013	0.044	-0.025
C7	0.000	0.084	0.000	0.000	0.000	-0.019	0.047	-0.029
Cu1'	0.000	0.451	0.001	0.000	0.001	37.058	0.083	0.359
N1'	0.000	0.308	0.000	0.001	-0.001	-36.146	0.073	-0.356
N2'	0.000	0.208	-0.001	0.001	-0.001	-50.432	0.064	-0.398
N3'	0.003	3.359	0.002	0.001	0.001	36.779	0.161	0.358
N5'	0.000	-0.466	0.000	0.000	0.000	0.706	-0.084	0.096
N4'	0.000	-0.480	0.000	0.000	0.000	0.470	-0.084	0.084
C14'	0.000	0.047	0.000	0.000	0.000	-4.505	0.039	-0.178
C13'	0.000	0.179	0.000	0.000	0.000	1.317	0.061	0.118
C12'	0.000	0.151	0.000	0.000	0.000	-1.259	0.057	-0.116
C11'	0.000	0.169	0.000	0.000	0.000	1.512	0.060	0.124
C10'	0.000	0.051	0.000	0.000	0.000	-4.830	0.040	-0.182
C15'	0.000	-0.016	0.000	0.000	0.000	0.222	-0.027	0.065
C17'	0.000	0.053	0.000	0.000	0.000	-0.023	0.040	-0.031
C16'	0.000	0.084	0.000	0.000	0.000	-0.012	0.047	-0.024
C16'	0.000	0.074	0.000	0.000	0.000	-0.010	0.045	-0.023

C1'	0.000	0.096	0.000	0.000	0.000	-3.900	0.049	-0.170
C2'	0.000	0.221	0.000	0.000	0.000	1.234	0.065	0.116
C3'	0.000	0.151	0.000	0.000	0.000	-1.164	0.057	-0.113
C4'	0.000	0.202	0.000	0.000	0.000	1.337	0.063	0.119
C5'	0.000	-0.027	0.000	0.000	0.000	-4.899	-0.032	-0.183
C6'	0.000	-0.016	0.000	0.000	0.000	0.223	-0.027	0.065
C9'	0.000	0.071	0.000	0.000	0.000	-0.017	0.045	-0.028
C8'	0.000	0.059	0.000	0.000	0.000	-0.010	0.042	-0.023
C7'	0.000	0.057	0.000	0.000	0.000	-0.014	0.041	-0.026
H1	0.000	0.292	0.000	0.000	0.000	0.001	0.071	0.012
H2	0.000	0.011	0.000	0.000	0.000	-0.013	0.024	-0.025
H3	0.000	0.020	0.000	0.000	0.000	-0.018	0.029	-0.028
H4	0.000	0.329	0.000	0.000	0.000	-0.008	0.074	-0.021
H5	0.000	-0.088	0.000	0.000	0.000	-0.018	-0.048	-0.028
H6	0.000	0.002	0.000	0.000	0.000	0.011	0.014	0.024
H7	0.000	0.320	0.000	0.000	0.000	-0.008	0.074	-0.022
H8	0.000	-0.082	0.000	0.000	0.000	-0.016	-0.047	-0.027
H9	0.000	0.006	0.000	0.000	0.000	0.016	0.020	0.027
H10	0.000	0.407	0.000	0.000	0.000	0.004	0.080	0.017
H11	0.000	-0.004	0.000	0.000	0.000	-0.026	-0.018	-0.032
H12	0.000	0.040	0.000	0.000	0.000	-0.022	0.037	-0.030
H13	0.000	0.419	0.000	0.000	0.000	-0.009	0.081	-0.023
H14	0.000	-0.026	0.000	0.000	0.000	0.020	-0.032	0.029
H15	0.000	0.001	0.000	0.000	0.000	-0.019	0.012	-0.029
H16	0.000	0.416	0.000	0.000	0.000	-0.011	0.080	-0.024
H17	0.000	-0.019	0.000	0.000	0.000	-0.025	-0.029	-0.031
H18	0.000	-0.030	0.000	0.000	0.000	0.013	-0.034	0.025
H19	0.002	1.628	0.001	0.001	0.000	3.049	0.127	0.156
H20	0.001	0.974	0.000	0.000	0.000	0.085	0.107	0.047
H21	0.001	0.942	0.000	0.000	0.000	0.162	0.106	0.059
H22	0.002	1.577	0.001	0.001	0.000	2.836	0.125	0.152
H23	0.000	0.037	0.000	0.000	0.000	2.260	0.036	0.141
H24	0.001	0.585	0.000	0.000	0.000	0.070	0.090	0.044
H25	0.001	0.572	0.000	0.000	0.000	0.139	0.089	0.056
H26	0.000	0.457	0.000	0.000	0.000	1.497	0.083	0.123
H1'	0.000	0.195	0.000	0.000	0.000	0.001	0.063	0.011
H2'	0.000	0.016	0.000	0.000	0.000	-0.010	0.027	-0.024
H3'	0.000	-0.123	0.000	0.000	0.000	-0.015	-0.054	-0.027
H4'	0.000	0.167	0.000	0.000	0.000	-0.006	0.059	-0.019
H5'	0.000	0.025	0.000	0.000	0.000	-0.011	0.031	-0.024
H6'	0.000	0.014	0.000	0.000	0.000	0.008	0.026	0.021
H7'	0.000	0.197	0.000	0.000	0.000	-0.006	0.063	-0.020
H8'	0.000	0.014	0.000	0.000	0.000	-0.011	0.026	-0.024
H9'	0.000	-0.132	0.000	0.000	0.000	0.013	-0.055	0.025
H10'	0.000	0.165	0.000	0.000	0.000	0.002	0.059	0.015
H11'	0.000	0.017	0.000	0.000	0.000	-0.015	0.028	-0.026
H12'	0.000	-0.046	0.000	0.000	0.000	-0.013	-0.039	-0.026
H13'	0.000	0.159	0.000	0.000	0.000	-0.006	0.058	-0.019
H14'	0.000	0.008	0.000	0.000	0.000	0.011	0.021	0.024

H15'	0.000	-0.019	0.000	0.000	0.000	-0.011	-0.029	-0.024
H16'	0.000	0.179	0.000	0.000	0.000	-0.007	0.061	-0.021
H17'	0.000	-0.039	0.000	0.000	0.000	-0.015	-0.036	-0.026
H18'	0.000	-0.089	0.000	0.000	0.000	0.007	-0.048	0.021
H19'	0.000	-0.116	0.000	0.000	0.000	1.136	-0.053	0.112
H20'	0.000	0.200	0.000	0.000	0.000	0.041	0.063	0.037
H21'	0.000	0.189	0.000	0.000	0.000	0.081	0.062	0.047
H22'	0.000	-0.131	0.000	0.000	0.000	1.090	-0.055	0.111
H23'	0.000	0.121	0.000	0.000	0.000	0.894	0.053	0.104
H24'	0.000	0.257	0.000	0.000	0.000	0.045	0.068	0.038
H25'	0.000	0.150	0.000	0.000	0.000	0.101	0.057	0.050
H26'	0.000	-0.427	0.000	0.000	0.000	1.063	-0.081	0.110

**Table A2.6:** Contributions at bcp along on the Cu-N5 bond for the EO molecular system; LS, SF%,  $LS_{\alpha}$ ,  $LS_{\beta}$ ,  $LS_s$ ,  $SF_s\%$  are respectively the Local source, the Source Function atomic percentage for  $\rho(\mathbf{r})$ , the Local source alpha and beta, the Local Source for  $s(\mathbf{r})$  and the Source Function atomic percentage for  $s(\mathbf{r})$ .  $R_{SF}$  ( $R_{FSs}$ ) are evaluated as in tab A2.1.

$\Omega$	LS	SF%	$LS_{\alpha}$	$LS_{\beta}$	$LS_s$	$SF_s\%$	$R_{SF}$	$R_{FSs}$
Cu1	0.004	0.002	0.003	0.001	0.001	1.032	0.013	0.109
N1	-0.001	0.000	-0.001	0.000	0.000	-0.314	-0.007	-0.073
N2	0.000	0.000	0.000	0.001	-0.001	-0.482	0.006	-0.084
N3	0.001	0.001	0.001	0.000	0.001	0.352	0.009	0.076
N5	98.174	49.524	99.159	99.014	0.145	100.197	0.396	0.500
N4	-0.001	-0.001	-0.001	-0.001	0.000	-0.023	-0.009	-0.031
C14	0.015	0.008	0.007	0.008	0.000	-0.343	0.021	-0.075
C13	0.003	0.002	0.002	0.002	0.000	0.077	0.013	0.046
C12	0.001	0.001	0.001	0.001	0.000	-0.063	0.010	-0.043
C11	0.003	0.002	0.002	0.002	0.000	0.089	0.013	0.048
C10	0.016	0.008	0.008	0.008	-0.001	-0.349	0.021	-0.076
C15	0.000	0.000	0.000	0.000	0.000	0.009	0.004	0.022
C17	0.000	0.000	0.000	0.000	0.000	-0.001	0.004	-0.010
C16	0.000	0.000	0.000	0.000	0.000	0.000	0.004	-0.008
C16	0.000	0.000	0.000	0.000	0.000	0.000	0.005	-0.008
C1	0.000	0.000	0.000	0.000	0.000	-0.129	-0.005	-0.054
C2	0.001	0.000	0.000	0.000	0.000	0.037	0.008	0.036
C3	0.000	0.000	0.000	0.000	0.000	-0.028	0.006	-0.033
C4	0.001	0.000	0.000	0.000	0.000	0.029	0.007	0.033
C5	0.001	0.000	0.000	0.000	0.000	-0.108	0.007	-0.051
C6	0.000	0.000	0.000	0.000	0.000	0.005	0.002	0.018
C9	0.000	0.000	0.000	0.000	0.000	0.000	0.004	-0.008
C8	0.000	0.000	0.000	0.000	0.000	0.000	0.003	-0.006
C7	0.000	0.000	0.000	0.000	0.000	0.000	0.004	-0.007
Cu1'	0.000	0.000	0.000	0.000	0.001	0.500	0.005	0.086
N1'	0.000	0.000	0.000	0.000	0.000	-0.317	0.006	-0.073
N2'	-0.001	-0.001	-0.001	0.000	-0.001	-0.854	-0.010	-0.102
N3'	0.002	0.001	0.002	0.001	0.001	0.638	0.011	0.093
N5'	0.000	0.000	0.000	0.000	0.000	0.013	-0.006	0.026
N4'	0.000	0.000	0.000	0.000	0.000	0.013	-0.006	0.025

C14'	0.000	0.000	0.000	0.000	0.000	-0.066	0.003	-0.044
C13'	0.000	0.000	0.000	0.000	0.000	0.020	0.004	0.029
C12'	0.000	0.000	0.000	0.000	0.000	-0.019	0.004	-0.029
C11'	0.000	0.000	0.000	0.000	0.000	0.023	0.004	0.030
C10'	0.000	0.000	0.000	0.000	0.000	-0.071	0.003	-0.045
C15'	0.000	0.000	0.000	0.000	0.000	0.003	-0.002	0.016
C17'	0.000	0.000	0.000	0.000	0.000	0.000	0.003	-0.008
C16'	0.000	0.000	0.000	0.000	0.000	0.000	0.004	-0.006
C16'	0.000	0.000	0.000	0.000	0.000	0.000	0.003	-0.006
C1'	0.000	0.000	0.000	0.000	0.000	-0.060	0.004	-0.042
C2'	0.000	0.000	0.000	0.000	0.000	0.019	0.005	0.029
C3'	0.000	0.000	0.000	0.000	0.000	-0.019	0.004	-0.029
C4'	0.000	0.000	0.000	0.000	0.000	0.021	0.004	0.030
C5'	0.000	0.000	0.000	0.000	0.000	-0.077	-0.004	-0.046
C6'	0.000	0.000	0.000	0.000	0.000	0.004	-0.002	0.017
C9'	0.000	0.000	0.000	0.000	0.000	0.000	0.003	-0.007
C8'	0.000	0.000	0.000	0.000	0.000	0.000	0.003	-0.006
C7'	0.000	0.000	0.000	0.000	0.000	0.000	0.003	-0.007
H1	0.000	0.000	0.000	0.000	0.000	0.000	0.005	0.003
H2	0.000	0.000	0.000	0.000	0.000	0.000	0.000	-0.006
H3	0.000	0.000	0.000	0.000	0.000	0.000	0.003	-0.007
H4	0.000	0.000	0.000	0.000	0.000	0.000	0.006	-0.005
H5	0.000	0.000	0.000	0.000	0.000	0.000	-0.005	-0.007
H6	0.000	0.000	0.000	0.000	0.000	0.000	-0.002	0.006
H7	0.000	0.000	0.000	0.000	0.000	0.000	0.006	-0.005
H8	0.000	0.000	0.000	0.000	0.000	0.000	-0.004	-0.007
H9	0.000	0.000	0.000	0.000	0.000	0.000	0.003	0.007
H10	0.001	0.000	0.000	0.000	0.000	0.000	0.007	0.005
H11	0.000	0.000	0.000	0.000	0.000	-0.001	0.003	-0.009
H12	0.000	0.000	0.000	0.000	0.000	0.000	0.004	-0.008
H13	0.001	0.000	0.000	0.000	0.000	0.000	0.007	-0.006
H14	0.000	0.000	0.000	0.000	0.000	0.000	0.002	0.008
H15	0.000	0.000	0.000	0.000	0.000	0.000	0.003	-0.008
H16	0.001	0.000	0.000	0.000	0.000	0.000	0.007	-0.007
H17	0.000	0.000	0.000	0.000	0.000	-0.001	0.003	-0.009
H18	0.000	0.000	0.000	0.000	0.000	0.000	0.002	0.007
H19	0.004	0.002	0.002	0.002	0.000	0.058	0.014	0.042
H20	0.002	0.001	0.001	0.001	0.000	0.002	0.010	0.014
H21	0.002	0.001	0.001	0.001	0.000	0.004	0.010	0.017
H22	0.004	0.002	0.002	0.002	0.000	0.058	0.014	0.042
H23	-0.001	0.000	0.000	0.000	0.000	0.037	-0.007	0.036
H24	0.000	0.000	0.000	0.000	0.000	0.001	0.006	0.011
H25	0.000	0.000	0.000	0.000	0.000	0.002	0.007	0.014
H26	0.000	0.000	0.000	0.000	0.000	0.020	0.006	0.029
H1'	0.000	0.000	0.000	0.000	0.000	0.000	0.005	0.003
H2'	0.000	0.000	0.000	0.000	0.000	0.000	0.002	-0.006
H3'	0.000	0.000	0.000	0.000	0.000	0.000	-0.005	-0.007
H4'	0.000	0.000	0.000	0.000	0.000	0.000	0.005	-0.005
H5'	0.000	0.000	0.000	0.000	0.000	0.000	0.003	-0.006

H6'	0.000	0.000	0.000	0.000	0.000	0.000	0.002	0.005
H7'	0.000	0.000	0.000	0.000	0.000	0.000	0.005	-0.005
H8'	0.000	0.000	0.000	0.000	0.000	0.000	0.003	-0.006
H9'	0.000	0.000	0.000	0.000	0.000	0.000	-0.005	0.006
H10'	0.000	0.000	0.000	0.000	0.000	0.000	0.004	0.004
H11'	0.000	0.000	0.000	0.000	0.000	0.000	0.002	-0.007
H12'	0.000	0.000	0.000	0.000	0.000	0.000	-0.003	-0.006
H13'	0.000	0.000	0.000	0.000	0.000	0.000	0.004	-0.005
H14'	0.000	0.000	0.000	0.000	0.000	0.000	0.001	0.006
H15'	0.000	0.000	0.000	0.000	0.000	0.000	-0.002	-0.006
H16'	0.000	0.000	0.000	0.000	0.000	0.000	0.005	-0.005
H17'	0.000	0.000	0.000	0.000	0.000	0.000	-0.003	-0.007
H18'	0.000	0.000	0.000	0.000	0.000	0.000	-0.004	0.005
H19'	0.000	0.000	0.000	0.000	0.000	0.017	-0.004	0.027
H20'	0.000	0.000	0.000	0.000	0.000	0.001	0.005	0.009
H21'	0.000	0.000	0.000	0.000	0.000	0.001	0.004	0.012
H22'	0.000	0.000	0.000	0.000	0.000	0.016	-0.004	0.027
H23'	0.000	0.000	0.000	0.000	0.000	0.014	0.004	0.026
H24'	0.000	0.000	0.000	0.000	0.000	0.001	0.005	0.010
H25'	0.000	0.000	0.000	0.000	0.000	0.002	0.004	0.013
H26'	0.000	0.000	0.000	0.000	0.000	0.017	-0.006	0.027

**Table A2.7:** Contributions at the N5 atomic basin along on the Cu-N5 bond for the EO molecular system; LS, SF%,  $LS_{\alpha}$ ,  $LS_{\beta}$ ,  $LS_s$ ,  $SF_s\%$  are respectively the Local source, the Source Function atomic percentage for  $\rho(\mathbf{r})$ , the Local source alfa and beta, the Local Source for  $s(\mathbf{r})$  and the Source Function atomic percentage for  $s(\mathbf{r})$ .  $R_{SF}$  ( $R_{FSs}$ ) are evaluated as in tab A2.1.

$\Omega$	LS	SF%	$LS_{\alpha}$	$LS_{\beta}$	$LS_s$	$SF_s\%$	$R_{SF}$	$R_{FSs}$
Cu1	0.002	0.364	0.002	0.000	0.002	219.550	0.077	0.650
N1	0.233	50.306	0.117	0.116	0.001	166.644	0.398	0.593
N2	0.199	43.000	0.097	0.101	-0.004	-555.920	0.377	-0.886
N3	0.020	4.331	0.011	0.009	0.002	286.863	0.176	0.710
N5	-0.001	-0.130	0.000	0.000	0.000	-0.551	-0.055	-0.088
N4	-0.001	-0.292	-0.001	-0.001	0.000	1.705	-0.071	0.129
C14	0.000	0.035	0.000	0.000	0.000	-18.887	0.035	-0.287
C13	0.000	0.064	0.000	0.000	0.000	5.375	0.043	0.189
C12	0.000	0.045	0.000	0.000	0.000	-5.007	0.038	-0.184
C11	0.000	0.058	0.000	0.000	0.000	6.162	0.042	0.197
C10	0.000	0.034	0.000	0.000	0.000	-20.360	0.035	-0.294
C15	0.000	-0.003	0.000	0.000	0.000	0.865	-0.016	0.103
C17	0.000	0.011	0.000	0.000	0.000	-0.089	0.024	-0.048
C16	0.000	0.016	0.000	0.000	0.000	-0.044	0.027	-0.038
C16	0.000	0.019	0.000	0.000	0.000	-0.039	0.029	-0.037
C1	0.000	0.095	0.000	0.000	0.000	-21.177	0.049	-0.298
C2	0.000	0.100	0.000	0.000	0.000	6.423	0.050	0.200
C3	0.000	0.068	0.000	0.000	0.000	-6.059	0.044	-0.196
C4	0.001	0.124	0.000	0.000	0.000	7.667	0.054	0.212
C5	0.000	-0.075	0.000	0.000	0.000	-30.455	-0.045	-0.336



C6	0.000	-0.001	0.000	0.000	0.000	1.098	-0.010	0.111
C9	0.000	0.022	0.000	0.000	0.000	-0.084	0.030	-0.047
C8	0.000	0.021	0.000	0.000	0.000	-0.049	0.030	-0.039
C7	0.000	0.015	0.000	0.000	0.000	-0.065	0.026	-0.043
Cu1'	0.002	0.421	0.002	0.000	0.001	212.758	0.081	0.643
N1'	-0.001	-0.232	-0.001	0.000	-0.001	-92.506	-0.066	-0.487
N2'	0.001	0.222	0.000	0.001	-0.001	-112.821	0.065	-0.521
N3'	0.002	0.389	0.001	0.001	0.001	81.723	0.079	0.467
N5'	-0.002	-0.471	-0.001	-0.001	0.000	5.143	-0.084	0.186
N4'	-0.001	-0.140	0.000	0.000	0.000	-2.534	-0.056	-0.147
C14'	0.000	-0.012	0.000	0.000	0.000	-29.178	-0.025	-0.332
C13'	0.000	0.094	0.000	0.000	0.000	7.937	0.049	0.215
C12'	0.000	0.064	0.000	0.000	0.000	-7.301	0.043	-0.209
C11'	0.000	0.092	0.000	0.000	0.000	9.148	0.049	0.225
C10'	0.000	0.007	0.000	0.000	0.000	-30.607	0.021	-0.337
C15'	0.000	-0.002	0.000	0.000	0.000	1.203	-0.013	0.115
C17'	0.000	0.016	0.000	0.000	0.000	-0.120	0.027	-0.053
C16'	0.000	0.030	0.000	0.000	0.000	-0.061	0.034	-0.042
C16'	0.000	0.023	0.000	0.000	0.000	-0.049	0.031	-0.039
C1'	0.000	0.014	0.000	0.000	0.000	-16.634	0.026	-0.275
C2'	0.000	0.069	0.000	0.000	0.000	5.046	0.044	0.185
C3'	0.000	0.043	0.000	0.000	0.000	-4.346	0.038	-0.176
C4'	0.000	0.069	0.000	0.000	0.000	4.825	0.044	0.182
C5'	0.000	0.042	0.000	0.000	0.000	-17.919	0.037	-0.282
C6'	0.000	-0.002	0.000	0.000	0.000	0.816	-0.013	0.101
C9'	0.000	0.017	0.000	0.000	0.000	-0.060	0.028	-0.042
C8'	0.000	0.011	0.000	0.000	0.000	-0.035	0.024	-0.035
C7'	0.000	0.014	0.000	0.000	0.000	-0.052	0.026	-0.040
H1	0.000	0.070	0.000	0.000	0.000	0.006	0.044	0.019
H2	0.000	0.013	0.000	0.000	0.000	-0.050	0.025	-0.040
H3	0.000	-0.043	0.000	0.000	0.000	-0.075	-0.038	-0.046
H4	0.000	0.057	0.000	0.000	0.000	-0.026	0.042	-0.032
H5	0.000	0.012	0.000	0.000	0.000	-0.052	0.025	-0.040
H6	0.000	0.012	0.000	0.000	0.000	0.036	0.025	0.035
H7	0.000	0.072	0.000	0.000	0.000	-0.030	0.045	-0.033
H8	0.000	0.010	0.000	0.000	0.000	-0.051	0.024	-0.040
H9	0.000	-0.047	0.000	0.000	0.000	0.063	-0.039	0.043
H10	0.000	0.042	0.000	0.000	0.000	0.009	0.037	0.023
H11	0.000	-0.006	0.000	0.000	0.000	-0.058	-0.019	-0.042
H12	0.000	-0.002	0.000	0.000	0.000	-0.051	-0.013	-0.040
H13	0.000	0.042	0.000	0.000	0.000	-0.022	0.038	-0.030
H14	0.000	-0.008	0.000	0.000	0.000	0.045	-0.021	0.038
H15	0.000	-0.005	0.000	0.000	0.000	-0.043	-0.018	-0.038
H16	0.000	0.042	0.000	0.000	0.000	-0.026	0.037	-0.032
H17	0.000	-0.007	0.000	0.000	0.000	-0.055	-0.020	-0.041
H18	0.000	-0.009	0.000	0.000	0.000	0.028	-0.022	0.033
H19	0.000	-0.031	0.000	0.000	0.000	4.872	-0.034	0.183
H20	0.000	0.057	0.000	0.000	0.000	0.161	0.042	0.059
H21	0.000	0.054	0.000	0.000	0.000	0.321	0.041	0.074

H22	0.000	-0.037	0.000	0.000	0.000	4.660	-0.036	0.180
H23	0.000	0.100	0.000	0.000	0.000	4.549	0.050	0.178
H24	0.001	0.110	0.000	0.000	0.000	0.226	0.052	0.066
H25	0.000	0.094	0.000	0.000	0.000	0.534	0.049	0.087
H26	-0.001	-0.146	0.000	0.000	0.000	6.757	-0.057	0.204
H1'	0.000	0.041	0.000	0.000	0.000	0.004	0.037	0.017
H2'	0.000	-0.001	0.000	0.000	0.000	-0.036	-0.010	-0.036
H3'	0.000	-0.006	0.000	0.000	0.000	-0.050	-0.019	-0.040
H4'	0.000	0.043	0.000	0.000	0.000	-0.021	0.038	-0.030
H5'	0.000	-0.008	0.000	0.000	0.000	-0.045	-0.022	-0.038
H6'	0.000	-0.003	0.000	0.000	0.000	0.029	-0.016	0.033
H7'	0.000	0.044	0.000	0.000	0.000	-0.022	0.038	-0.030
H8'	0.000	-0.009	0.000	0.000	0.000	-0.040	-0.023	-0.037
H9'	0.000	-0.008	0.000	0.000	0.000	0.043	-0.022	0.038
H10'	0.000	0.067	0.000	0.000	0.000	0.012	0.044	0.025
H11'	0.000	0.021	0.000	0.000	0.000	-0.074	0.030	-0.045
H12'	0.000	-0.019	0.000	0.000	0.000	-0.070	-0.029	-0.044
H13'	0.000	0.061	0.000	0.000	0.000	-0.028	0.042	-0.033
H14'	0.000	0.017	0.000	0.000	0.000	0.056	0.028	0.041
H15'	0.000	-0.002	0.000	0.000	0.000	-0.056	-0.013	-0.041
H16'	0.000	0.079	0.000	0.000	0.000	-0.036	0.046	-0.036
H17'	0.000	-0.012	0.000	0.000	0.000	-0.080	-0.025	-0.046
H18'	0.000	-0.047	0.000	0.000	0.000	0.041	-0.039	0.037
H19'	0.000	0.064	0.000	0.000	0.000	6.970	0.043	0.206
H20'	0.001	0.118	0.000	0.000	0.000	0.244	0.053	0.067
H21'	0.001	0.113	0.000	0.000	0.000	0.452	0.052	0.083
H22'	0.000	0.064	0.000	0.000	0.000	6.584	0.043	0.202
H23'	0.000	-0.016	0.000	0.000	0.000	4.185	-0.027	0.174
H24'	0.000	0.057	0.000	0.000	0.000	0.170	0.042	0.060
H25'	0.000	0.055	0.000	0.000	0.000	0.358	0.041	0.077
H26'	0.000	-0.027	0.000	0.000	0.000	3.722	-0.032	0.167

**Table A2.8:** Contributions at the bcp along on the N1-N2 bond for the EO molecular system; LS, SF%,  $LS_{\alpha}$ ,  $LS_{\beta}$ ,  $LS_s$ ,  $SF_s\%$  are respectively the Local source, the Source Function atomic percentage for  $p(\mathbf{r})$ , the Local source alpha and beta, the Local Source for  $s(\mathbf{r})$  and the Source Function atomic percentage for  $s(\mathbf{r})$ .  $R_{SF}$  ( $R_{FS_s}$ ) are evaluated as in tab

A2.1.

$\Omega$	LS	SF%	$LS_{\alpha}$	$LS_{\beta}$	$LS_s$	$SF_s\%$	$R_{SF}$	$R_{FS_s}$
Cu1	0.001	0.000	0.001	0.000	0.001	15.280	0.008	0.267
N1	0.044	0.022	0.022	0.022	0.001	8.058	0.030	0.216
N2	98.305	49.547	99.154	99.151	0.003	34.376	0.396	0.350
N3	0.054	0.027	0.029	0.025	0.003	44.342	0.032	0.381
N5	-0.001	0.000	0.000	0.000	0.000	0.075	-0.007	0.045
N4	-0.001	-0.001	-0.001	-0.001	0.000	0.491	-0.009	0.085
C14	0.000	0.000	0.000	0.000	0.000	-1.551	0.004	-0.125
C13	0.000	0.000	0.000	0.000	0.000	0.449	0.005	0.082
C12	0.000	0.000	0.000	0.000	0.000	-0.423	0.005	-0.081
C11	0.000	0.000	0.000	0.000	0.000	0.515	0.005	0.086

C10	0.000	0.000	0.000	0.000	0.000	-1.681	0.004	-0.128
C15	0.000	0.000	0.000	0.000	0.000	0.074	-0.002	0.045
C17	0.000	0.000	0.000	0.000	0.000	-0.008	0.003	-0.021
C16	0.000	0.000	0.000	0.000	0.000	-0.004	0.004	-0.017
C16	0.000	0.000	0.000	0.000	0.000	-0.003	0.004	-0.016
C1	0.000	0.000	0.000	0.000	0.000	-1.855	0.006	-0.132
C2	0.000	0.000	0.000	0.000	0.000	0.577	0.006	0.090
C3	0.000	0.000	0.000	0.000	0.000	-0.564	0.006	-0.089
C4	0.000	0.000	0.000	0.000	0.000	0.714	0.006	0.096
C5	-0.001	0.000	-0.001	0.000	0.000	-2.759	-0.008	-0.151
C6	0.000	0.000	0.000	0.000	0.000	0.103	-0.002	0.050
C9	0.000	0.000	0.000	0.000	0.000	-0.008	0.004	-0.022
C8	0.000	0.000	0.000	0.000	0.000	-0.005	0.004	-0.018
C7	0.000	0.000	0.000	0.000	0.000	-0.006	0.004	-0.020
Cu1'	0.001	0.000	0.001	0.000	0.001	15.083	0.008	0.266
N1'	-0.001	0.000	-0.001	0.000	-0.001	-6.549	-0.008	-0.202
N2'	0.001	0.000	0.000	0.001	-0.001	-8.985	0.007	-0.224
N3'	0.001	0.001	0.001	0.000	0.001	6.543	0.010	0.201
N5'	-0.002	-0.001	-0.001	-0.001	0.000	0.897	-0.011	0.104
N4'	-0.001	0.000	0.000	0.000	0.000	-0.097	-0.007	-0.050
C14'	0.000	0.000	0.000	0.000	0.000	-2.705	-0.006	-0.150
C13'	0.000	0.000	0.000	0.000	0.000	0.751	0.006	0.098
C12'	0.000	0.000	0.000	0.000	0.000	-0.700	0.005	-0.096
C11'	0.000	0.000	0.000	0.000	0.000	0.857	0.006	0.102
C10'	0.000	0.000	0.000	0.000	0.000	-2.792	-0.005	-0.152
C15'	0.000	0.000	0.000	0.000	0.000	0.115	-0.002	0.052
C17'	0.000	0.000	0.000	0.000	0.000	-0.011	0.004	-0.024
C16'	0.000	0.000	0.000	0.000	0.000	-0.006	0.005	-0.019
C16'	0.000	0.000	0.000	0.000	0.000	-0.005	0.004	-0.018
C1'	0.000	0.000	0.000	0.000	0.000	-1.398	0.002	-0.120
C2'	0.000	0.000	0.000	0.000	0.000	0.429	0.006	0.081
C3'	0.000	0.000	0.000	0.000	0.000	-0.370	0.005	-0.077
C4'	0.000	0.000	0.000	0.000	0.000	0.404	0.006	0.080
C5'	0.000	0.000	0.000	0.000	0.000	-1.477	0.005	-0.123
C6'	0.000	0.000	0.000	0.000	0.000	0.070	-0.002	0.044
C9'	0.000	0.000	0.000	0.000	0.000	-0.005	0.004	-0.019
C8'	0.000	0.000	0.000	0.000	0.000	-0.003	0.003	-0.016
C7'	0.000	0.000	0.000	0.000	0.000	-0.005	0.003	-0.018
H1	0.000	0.000	0.000	0.000	0.000	0.001	0.006	0.009
H2	0.000	0.000	0.000	0.000	0.000	-0.005	0.004	-0.018
H3	0.000	0.000	0.000	0.000	0.000	-0.007	-0.006	-0.021
H4	0.000	0.000	0.000	0.000	0.000	-0.002	0.006	-0.014
H5	0.000	0.000	0.000	0.000	0.000	-0.005	0.004	-0.018
H6	0.000	0.000	0.000	0.000	0.000	0.003	0.004	0.016
H7	0.000	0.000	0.000	0.000	0.000	-0.003	0.006	-0.015
H8	0.000	0.000	0.000	0.000	0.000	-0.005	0.004	-0.018
H9	0.000	0.000	0.000	0.000	0.000	0.006	-0.006	0.020
H10	0.000	0.000	0.000	0.000	0.000	0.001	0.005	0.010
H11	0.000	0.000	0.000	0.000	0.000	-0.005	-0.003	-0.018

H12	0.000	0.000	0.000	0.000	0.000	-0.004	-0.001	-0.018
H13	0.000	0.000	0.000	0.000	0.000	-0.002	0.005	-0.013
H14	0.000	0.000	0.000	0.000	0.000	0.004	-0.003	0.017
H15	0.000	0.000	0.000	0.000	0.000	-0.004	-0.002	-0.017
H16	0.000	0.000	0.000	0.000	0.000	-0.002	0.005	-0.014
H17	0.000	0.000	0.000	0.000	0.000	-0.005	-0.003	-0.018
H18	0.000	0.000	0.000	0.000	0.000	0.002	-0.003	0.014
H19	0.000	0.000	0.000	0.000	0.000	0.397	-0.004	0.079
H20	0.000	0.000	0.000	0.000	0.000	0.014	0.005	0.026
H21	0.000	0.000	0.000	0.000	0.000	0.027	0.005	0.032
H22	0.000	0.000	0.000	0.000	0.000	0.384	-0.005	0.078
H23	0.000	0.000	0.000	0.000	0.000	0.389	0.007	0.079
H24	0.001	0.000	0.000	0.000	0.000	0.021	0.007	0.030
H25	0.000	0.000	0.000	0.000	0.000	0.051	0.006	0.040
H26	-0.001	0.000	0.000	0.000	0.000	0.603	-0.008	0.091
H1'	0.000	0.000	0.000	0.000	0.000	0.000	0.005	0.008
H2'	0.000	0.000	0.000	0.000	0.000	-0.003	-0.002	-0.016
H3'	0.000	0.000	0.000	0.000	0.000	-0.004	-0.002	-0.017
H4'	0.000	0.000	0.000	0.000	0.000	-0.002	0.005	-0.013
H5'	0.000	0.000	0.000	0.000	0.000	-0.004	-0.003	-0.017
H6'	0.000	0.000	0.000	0.000	0.000	0.003	-0.002	0.015
H7'	0.000	0.000	0.000	0.000	0.000	-0.002	0.005	-0.013
H8'	0.000	0.000	0.000	0.000	0.000	-0.003	-0.003	-0.016
H9'	0.000	0.000	0.000	0.000	0.000	0.004	-0.002	0.017
H10'	0.000	0.000	0.000	0.000	0.000	0.001	0.006	0.011
H11'	0.000	0.000	0.000	0.000	0.000	-0.007	0.004	-0.021
H12'	0.000	0.000	0.000	0.000	0.000	-0.007	-0.004	-0.020
H13'	0.000	0.000	0.000	0.000	0.000	-0.003	0.006	-0.015
H14'	0.000	0.000	0.000	0.000	0.000	0.005	0.004	0.019
H15'	0.000	0.000	0.000	0.000	0.000	-0.005	-0.001	-0.019
H16'	0.000	0.000	0.000	0.000	0.000	-0.004	0.006	-0.016
H17'	0.000	0.000	0.000	0.000	0.000	-0.008	-0.003	-0.021
H18'	0.000	0.000	0.000	0.000	0.000	0.004	-0.006	0.017
H19'	0.000	0.000	0.000	0.000	0.000	0.623	0.006	0.092
H20'	0.001	0.000	0.000	0.000	0.000	0.024	0.007	0.031
H21'	0.001	0.000	0.000	0.000	0.000	0.043	0.007	0.038
H22'	0.000	0.000	0.000	0.000	0.000	0.579	0.006	0.090
H23'	0.000	0.000	0.000	0.000	0.000	0.354	-0.004	0.076
H24'	0.000	0.000	0.000	0.000	0.000	0.015	0.005	0.026
H25'	0.000	0.000	0.000	0.000	0.000	0.030	0.005	0.034
H26'	0.000	0.000	0.000	0.000	0.000	0.304	-0.004	0.072

**Table A2.9:** Contributions at the N2 atomic basin along on the N1-N2 bond for the EO molecular system; LS, SF%,  $LS_{\alpha}$ ,  $LS_{\beta}$ ,  $LS_s$ ,  $SF_s\%$  are respectively the Local source, the Source Function atomic percentage for  $\rho(\mathbf{r})$ , the Local source alpha and beta, the Local Source for  $s(\mathbf{r})$  and the Source Function atomic percentage for  $s(\mathbf{r})$ .  $R_{SF}$  ( $R_{FS_s}$ ) are evaluated as in tab A2.1.

$\Omega$	LS	SF%	$LS_{\alpha}$	$LS_{\beta}$	LSs	SFs%	$R_{SF}$	$R_{FSs}$
Cu1	0.000	0.081	0.001	0.000	0.001	87.276	0.047	0.478
N1	0.016	3.094	0.008	0.008	0.000	9.512	0.157	0.228
N2	0.232	45.300	0.113	0.119	-0.006	-579.053	0.384	-0.898
N3	0.260	50.777	0.133	0.127	0.006	598.104	0.399	0.908
N5	0.000	-0.086	0.000	0.000	0.000	1.082	-0.048	0.111
N4	-0.001	-0.137	0.000	0.000	0.000	4.736	-0.056	0.181
C14	0.000	0.016	0.000	0.000	0.000	-9.963	0.027	-0.232
C13	0.000	0.039	0.000	0.000	0.000	2.921	0.037	0.154
C12	0.000	0.030	0.000	0.000	0.000	-2.779	0.033	-0.151
C11	0.000	0.034	0.000	0.000	0.000	3.360	0.035	0.161
C10	0.000	0.014	0.000	0.000	0.000	-10.833	0.026	-0.238
C15	0.000	-0.003	0.000	0.000	0.000	0.490	-0.016	0.085
C17	0.000	0.009	0.000	0.000	0.000	-0.051	0.023	-0.040
C16	0.000	0.012	0.000	0.000	0.000	-0.025	0.025	-0.032
C16	0.000	0.015	0.000	0.000	0.000	-0.023	0.027	-0.030
C1	0.000	0.055	0.000	0.000	0.000	-12.356	0.041	-0.249
C2	0.000	0.063	0.000	0.000	0.000	3.945	0.043	0.170
C3	0.000	0.044	0.000	0.000	0.000	-3.994	0.038	-0.171
C4	0.000	0.023	0.000	0.000	0.000	4.972	0.030	0.184
C5	-0.001	-0.208	-0.001	0.000	0.000	-18.511	-0.064	-0.285
C6	0.000	-0.004	0.000	0.000	0.000	0.739	-0.018	0.097
C9	0.000	0.022	0.000	0.000	0.000	-0.058	0.030	-0.042
C8	0.000	0.014	0.000	0.000	0.000	-0.043	0.026	-0.038
C7	0.000	0.014	0.000	0.000	0.000	-0.043	0.026	-0.038
Cu1'	0.001	0.104	0.001	0.000	0.001	87.037	0.051	0.477
N1'	-0.001	-0.138	-0.001	0.000	0.000	-37.742	-0.056	-0.361
N2'	0.000	0.087	0.000	0.001	-0.001	-56.554	0.048	-0.413
N3'	0.001	0.221	0.001	0.000	0.000	41.353	0.065	0.373
N5'	-0.002	-0.351	-0.001	-0.001	0.000	8.029	-0.076	0.216
N4'	-0.001	-0.098	0.000	0.000	0.000	-0.020	-0.050	-0.029
C14'	-0.001	-0.131	0.000	0.000	0.000	-18.760	-0.055	-0.286
C13'	0.000	0.009	0.000	0.000	0.000	5.372	0.022	0.189
C12'	0.000	0.022	0.000	0.000	0.000	-5.121	0.030	-0.186
C11'	0.000	0.025	0.000	0.000	0.000	6.075	0.031	0.197
C10'	0.000	-0.072	0.000	0.000	0.000	-19.119	-0.045	-0.288
C15'	0.000	-0.003	0.000	0.000	0.000	0.852	-0.015	0.102
C17'	0.000	0.015	0.000	0.000	0.000	-0.083	0.026	-0.047
C16'	0.000	0.033	0.000	0.000	0.000	-0.044	0.035	-0.038
C16'	0.000	0.021	0.000	0.000	0.000	-0.032	0.030	-0.034
C1'	0.000	-0.003	0.000	0.000	0.000	-9.121	-0.015	-0.225
C2'	0.000	0.044	0.000	0.000	0.000	2.836	0.038	0.152
C3'	0.000	0.030	0.000	0.000	0.000	-2.453	0.033	-0.145
C4'	0.000	0.044	0.000	0.000	0.000	2.636	0.038	0.149
C5'	0.000	0.024	0.000	0.000	0.000	-9.519	0.031	-0.228
C6'	0.000	-0.002	0.000	0.000	0.000	0.469	-0.013	0.084
C9'	0.000	0.014	0.000	0.000	0.000	-0.034	0.026	-0.035
C8'	0.000	0.009	0.000	0.000	0.000	-0.020	0.022	-0.029
C7'	0.000	0.012	0.000	0.000	0.000	-0.030	0.024	-0.034

H1	0.000	0.071	0.000	0.000	0.000	0.004	0.045	0.017
H2	0.000	0.022	0.000	0.000	0.000	-0.034	0.030	-0.035
H3	0.000	-0.067	0.000	0.000	0.000	-0.055	-0.044	-0.041
H4	0.000	0.051	0.000	0.000	0.000	-0.017	0.040	-0.028
H5	0.000	0.020	0.000	0.000	0.000	-0.033	0.029	-0.035
H6	0.000	0.017	0.000	0.000	0.000	0.023	0.028	0.031
H7	0.000	0.071	0.000	0.000	0.000	-0.020	0.045	-0.029
H8	0.000	0.022	0.000	0.000	0.000	-0.033	0.030	-0.035
H9	0.000	-0.069	0.000	0.000	0.000	0.044	-0.044	0.038
H10	0.000	0.031	0.000	0.000	0.000	0.005	0.034	0.019
H11	0.000	-0.008	0.000	0.000	0.000	-0.034	-0.021	-0.035
H12	0.000	0.000	0.000	0.000	0.000	-0.029	-0.007	-0.033
H13	0.000	0.032	0.000	0.000	0.000	-0.013	0.034	-0.025
H14	0.000	-0.010	0.000	0.000	0.000	0.026	-0.023	0.032
H15	0.000	-0.004	0.000	0.000	0.000	-0.025	-0.017	-0.031
H16	0.000	0.031	0.000	0.000	0.000	-0.015	0.034	-0.027
H17	0.000	-0.005	0.000	0.000	0.000	-0.031	-0.018	-0.034
H18	0.000	-0.005	0.000	0.000	0.000	0.016	-0.018	0.027
H19	0.000	-0.023	0.000	0.000	0.000	2.530	-0.031	0.147
H20	0.000	0.038	0.000	0.000	0.000	0.089	0.036	0.048
H21	0.000	0.034	0.000	0.000	0.000	0.180	0.035	0.061
H22	0.000	-0.033	0.000	0.000	0.000	2.464	-0.035	0.145
H23	0.000	0.091	0.000	0.000	0.000	2.552	0.048	0.147
H24	0.000	0.096	0.000	0.000	0.000	0.146	0.049	0.057
H25	0.000	0.063	0.000	0.000	0.000	0.363	0.043	0.077
H26	-0.001	-0.111	0.000	0.000	0.000	3.943	-0.052	0.170
H1'	0.000	0.031	0.000	0.000	0.000	0.002	0.034	0.015
H2'	0.000	-0.002	0.000	0.000	0.000	-0.021	-0.015	-0.030
H3'	0.000	-0.001	0.000	0.000	0.000	-0.028	-0.011	-0.033
H4'	0.000	0.033	0.000	0.000	0.000	-0.013	0.035	-0.025
H5'	0.000	-0.010	0.000	0.000	0.000	-0.027	-0.023	-0.032
H6'	0.000	-0.005	0.000	0.000	0.000	0.017	-0.019	0.028
H7'	0.000	0.032	0.000	0.000	0.000	-0.013	0.034	-0.025
H8'	0.000	-0.009	0.000	0.000	0.000	-0.023	-0.023	-0.031
H9'	0.000	-0.003	0.000	0.000	0.000	0.025	-0.015	0.031
H10'	0.000	0.067	0.000	0.000	0.000	0.009	0.044	0.022
H11'	0.000	0.036	0.000	0.000	0.000	-0.050	0.036	-0.040
H12'	0.000	-0.028	0.000	0.000	0.000	-0.050	-0.033	-0.040
H13'	0.000	0.059	0.000	0.000	0.000	-0.019	0.042	-0.029
H14'	0.000	0.029	0.000	0.000	0.000	0.037	0.033	0.036
H15'	0.000	0.000	0.000	0.000	0.000	-0.039	-0.006	-0.036
H16'	0.000	0.089	0.000	0.000	0.000	-0.027	0.048	-0.032
H17'	0.000	-0.015	0.000	0.000	0.000	-0.059	-0.027	-0.042
H18'	0.000	-0.078	0.000	0.000	0.000	0.029	-0.046	0.033
H19'	0.000	0.092	0.000	0.000	0.000	4.180	0.049	0.174
H20'	0.001	0.114	0.000	0.000	0.000	0.176	0.052	0.060
H21'	0.001	0.110	0.000	0.000	0.000	0.311	0.052	0.073
H22'	0.000	0.097	0.000	0.000	0.000	3.849	0.049	0.169
H23'	0.000	-0.027	0.000	0.000	0.000	2.319	-0.032	0.143

H24'	0.000	0.037	0.000	0.000	0.000	0.097	0.036	0.049
H25'	0.000	0.039	0.000	0.000	0.000	0.201	0.037	0.063
H26'	0.000	-0.014	0.000	0.000	0.000	1.944	-0.026	0.134

**Table A2.10:** Contributions at the bcp along on the N2-N3 bond for the EO molecular system; LS, SF%,  $LS_{\alpha}$ ,  $LS_{\beta}$ ,  $LS_s$ ,  $SF_s\%$  are respectively the Local source, the Source Function atomic percentage for  $\rho(\mathbf{r})$ , the Local source alpha and beta, the Local Source for  $s(\mathbf{r})$  and the Source Function atomic percentage for  $s(\mathbf{r})$ .  $R_{SF}$  ( $R_{FSs}$ ) are evaluated as in tab A2.1.

$\Omega$	LS	SF%	$LS_{\alpha}$	$LS_{\beta}$	$LS_s$	$SF_s\%$	$R_{SF}$	$R_{FSs}$
Cu1	0.000	0.000	0.001	0.000	0.001	11.902	0.006	0.246
N1	0.009	0.004	0.004	0.004	0.000	-0.596	0.018	-0.091
N2	0.055	0.027	0.026	0.029	-0.004	-54.314	0.033	-0.408
N3	99.204	49.784	99.607	99.597	0.010	145.460	0.396	0.567
N5	0.000	0.000	0.000	0.000	0.000	0.216	-0.006	0.065
N4	0.000	0.000	0.000	0.000	0.000	0.815	-0.007	0.101
C14	0.000	0.000	0.000	0.000	0.000	-1.460	0.003	-0.122
C13	0.000	0.000	0.000	0.000	0.000	0.432	0.005	0.081
C12	0.000	0.000	0.000	0.000	0.000	-0.414	0.004	-0.080
C11	0.000	0.000	0.000	0.000	0.000	0.497	0.005	0.085
C10	0.000	0.000	0.000	0.000	0.000	-1.590	0.003	-0.126
C15	0.000	0.000	0.000	0.000	0.000	0.073	-0.002	0.045
C17	0.000	0.000	0.000	0.000	0.000	-0.008	0.003	-0.021
C16	0.000	0.000	0.000	0.000	0.000	-0.004	0.003	-0.017
C16	0.000	0.000	0.000	0.000	0.000	-0.003	0.004	-0.016
C1	0.000	0.000	0.000	0.000	0.000	-1.838	0.005	-0.132
C2	0.000	0.000	0.000	0.000	0.000	0.599	0.006	0.091
C3	0.000	0.000	0.000	0.000	0.000	-0.622	0.005	-0.092
C4	0.000	0.000	0.000	0.000	0.000	0.757	-0.004	0.098
C5	-0.001	-0.001	-0.001	0.000	0.000	-2.733	-0.009	-0.151
C6	0.000	0.000	0.000	0.000	0.000	0.117	-0.003	0.053
C9	0.000	0.000	0.000	0.000	0.000	-0.009	0.004	-0.023
C8	0.000	0.000	0.000	0.000	0.000	-0.005	0.004	-0.019
C7	0.000	0.000	0.000	0.000	0.000	-0.007	0.004	-0.020
Cu1'	0.000	0.000	0.001	0.000	0.001	11.921	0.006	0.246
N1'	-0.001	0.000	0.000	0.000	0.000	-5.161	-0.007	-0.186
N2'	0.000	0.000	0.000	0.000	-0.001	-8.188	0.006	-0.217
N3'	0.001	0.000	0.001	0.000	0.000	6.003	0.008	0.196
N5'	-0.001	-0.001	-0.001	-0.001	0.000	1.350	-0.009	0.119
N4'	0.000	0.000	0.000	0.000	0.000	0.057	-0.007	0.042
C14'	-0.001	0.000	0.000	0.000	0.000	-2.838	-0.008	-0.153
C13'	0.000	0.000	0.000	0.000	0.000	0.838	-0.005	0.102
C12'	0.000	0.000	0.000	0.000	0.000	-0.817	-0.002	-0.101
C11'	0.000	0.000	0.000	0.000	0.000	0.940	-0.002	0.106
C10'	0.000	0.000	0.000	0.000	0.000	-2.875	-0.006	-0.153
C15'	0.000	0.000	0.000	0.000	0.000	0.138	-0.002	0.056
C17'	0.000	0.000	0.000	0.000	0.000	-0.013	0.004	-0.026
C16'	0.000	0.000	0.000	0.000	0.000	-0.007	0.005	-0.021

C16'	0.000	0.000	0.000	0.000	0.000	-0.005	0.004	-0.019
C1'	0.000	0.000	0.000	0.000	0.000	-1.348	-0.003	-0.119
C2'	0.000	0.000	0.000	0.000	0.000	0.423	0.005	0.081
C3'	0.000	0.000	0.000	0.000	0.000	-0.367	0.004	-0.077
C4'	0.000	0.000	0.000	0.000	0.000	0.390	0.005	0.079
C5'	0.000	0.000	0.000	0.000	0.000	-1.397	0.004	-0.120
C6'	0.000	0.000	0.000	0.000	0.000	0.071	-0.002	0.045
C9'	0.000	0.000	0.000	0.000	0.000	-0.005	0.003	-0.019
C8'	0.000	0.000	0.000	0.000	0.000	-0.003	0.003	-0.016
C7'	0.000	0.000	0.000	0.000	0.000	-0.005	0.003	-0.018
H1	0.000	0.000	0.000	0.000	0.000	0.001	0.006	0.009
H2	0.000	0.000	0.000	0.000	0.000	-0.005	0.004	-0.019
H3	0.000	0.000	0.000	0.000	0.000	-0.009	-0.006	-0.022
H4	0.000	0.000	0.000	0.000	0.000	-0.003	0.005	-0.015
H5	0.000	0.000	0.000	0.000	0.000	-0.005	0.004	-0.019
H6	0.000	0.000	0.000	0.000	0.000	0.004	0.004	0.016
H7	0.000	0.000	0.000	0.000	0.000	-0.003	0.006	-0.016
H8	0.000	0.000	0.000	0.000	0.000	-0.005	0.004	-0.019
H9	0.000	0.000	0.000	0.000	0.000	0.007	-0.006	0.021
H10	0.000	0.000	0.000	0.000	0.000	0.001	0.005	0.010
H11	0.000	0.000	0.000	0.000	0.000	-0.005	-0.003	-0.018
H12	0.000	0.000	0.000	0.000	0.000	-0.004	0.000	-0.018
H13	0.000	0.000	0.000	0.000	0.000	-0.002	0.005	-0.013
H14	0.000	0.000	0.000	0.000	0.000	0.004	-0.003	0.017
H15	0.000	0.000	0.000	0.000	0.000	-0.004	-0.002	-0.017
H16	0.000	0.000	0.000	0.000	0.000	-0.002	0.004	-0.014
H17	0.000	0.000	0.000	0.000	0.000	-0.005	-0.002	-0.018
H18	0.000	0.000	0.000	0.000	0.000	0.002	-0.002	0.014
H19	0.000	0.000	0.000	0.000	0.000	0.369	-0.004	0.077
H20	0.000	0.000	0.000	0.000	0.000	0.013	0.005	0.026
H21	0.000	0.000	0.000	0.000	0.000	0.027	0.005	0.032
H22	0.000	0.000	0.000	0.000	0.000	0.360	-0.005	0.077
H23	0.000	0.000	0.000	0.000	0.000	0.377	0.007	0.078
H24	0.000	0.000	0.000	0.000	0.000	0.023	0.007	0.031
H25	0.000	0.000	0.000	0.000	0.000	0.057	0.005	0.041
H26	0.000	0.000	0.000	0.000	0.000	0.569	-0.007	0.089
H1'	0.000	0.000	0.000	0.000	0.000	0.000	0.005	0.008
H2'	0.000	0.000	0.000	0.000	0.000	-0.003	-0.002	-0.016
H3'	0.000	0.000	0.000	0.000	0.000	-0.004	-0.001	-0.017
H4'	0.000	0.000	0.000	0.000	0.000	-0.002	0.005	-0.013
H5'	0.000	0.000	0.000	0.000	0.000	-0.004	-0.003	-0.017
H6'	0.000	0.000	0.000	0.000	0.000	0.003	-0.003	0.015
H7'	0.000	0.000	0.000	0.000	0.000	-0.002	0.005	-0.014
H8'	0.000	0.000	0.000	0.000	0.000	-0.004	-0.003	-0.016
H9'	0.000	0.000	0.000	0.000	0.000	0.004	-0.002	0.017
H10'	0.000	0.000	0.000	0.000	0.000	0.001	0.006	0.012
H11'	0.000	0.000	0.000	0.000	0.000	-0.008	0.005	-0.021
H12'	0.000	0.000	0.000	0.000	0.000	-0.008	-0.005	-0.022
H13'	0.000	0.000	0.000	0.000	0.000	-0.003	0.006	-0.016



H14'	0.000	0.000	0.000	0.000	0.000	0.006	0.005	0.019
H15'	0.000	0.000	0.000	0.000	0.000	-0.006	0.001	-0.020
H16'	0.000	0.000	0.000	0.000	0.000	-0.004	0.007	-0.018
H17'	0.000	0.000	0.000	0.000	0.000	-0.010	-0.004	-0.023
H18'	0.000	0.000	0.000	0.000	0.000	0.005	-0.007	0.018
H19'	0.000	0.000	0.000	0.000	0.000	0.620	0.007	0.092
H20'	0.001	0.000	0.000	0.000	0.000	0.028	0.007	0.033
H21'	0.001	0.000	0.000	0.000	0.000	0.049	0.007	0.040
H22'	0.001	0.000	0.000	0.000	0.000	0.568	0.007	0.089
H23'	0.000	0.000	0.000	0.000	0.000	0.343	-0.005	0.075
H24'	0.000	0.000	0.000	0.000	0.000	0.014	0.005	0.026
H25'	0.000	0.000	0.000	0.000	0.000	0.030	0.005	0.033
H26'	0.000	0.000	0.000	0.000	0.000	0.284	-0.003	0.071

**Table A2.11:** Contributions at the N3 atomic basin along on the N2-N3 bond for the EO molecular system; LS, SF%,  $LS_{\alpha}$ ,  $LS_{\beta}$ ,  $LS_s$ ,  $SF_s\%$  are respectively the Local source, the Source Function atomic percentage for  $\rho(\mathbf{r})$ , the Local source alpha and beta, the Local Source for  $s(\mathbf{r})$  and the Source Function atomic percentage for  $s(\mathbf{r})$ .  $R_{SF}$  ( $R_{FSs}$ ) are evaluated as in tab A2.1.

$\Omega$	LS	SF%	$LS_{\alpha}$	$LS_{\beta}$	$LS_s$	$SF_s\%$	$R_{SF}$	$R_{FSs}$
Cu1	0.001	0.004	0.001	0.000	0.001	4.510	0.017	0.178
N1	0.001	0.007	0.000	0.001	-0.001	-5.339	0.020	-0.188
N2	0.002	0.010	0.001	0.002	-0.001	-4.420	0.023	-0.177
N3	0.003	0.016	0.002	0.001	0.001	3.178	0.027	0.158
N5	-0.001	-0.003	0.000	0.000	0.000	0.048	-0.015	0.039
N4	-0.001	-0.003	0.000	0.000	0.000	-0.002	-0.015	-0.013
C14	0.000	0.000	0.000	0.000	0.000	-0.497	0.008	-0.085
C13	0.000	0.001	0.000	0.000	0.000	0.142	0.011	0.056
C12	0.000	0.001	0.000	0.000	0.000	-0.134	0.010	-0.055
C11	0.000	0.001	0.000	0.000	0.000	0.164	0.011	0.059
C10	0.000	0.000	0.000	0.000	0.000	-0.533	0.007	-0.087
C15	0.000	0.000	0.000	0.000	0.000	0.023	-0.004	0.031
C17	0.000	0.000	0.000	0.000	0.000	-0.002	0.007	-0.014
C16	0.000	0.000	0.000	0.000	0.000	-0.001	0.008	-0.011
C16	0.000	0.000	0.000	0.000	0.000	-0.001	0.008	-0.011
C1	0.000	0.001	0.000	0.000	0.000	-0.404	0.010	-0.080
C2	0.000	0.001	0.000	0.000	0.000	0.125	0.012	0.054
C3	0.000	0.001	0.000	0.000	0.000	-0.115	0.010	-0.052
C4	0.000	0.001	0.000	0.000	0.000	0.132	0.012	0.055
C5	0.000	0.000	0.000	0.000	0.000	-0.493	0.007	-0.085
C6	0.000	0.000	0.000	0.000	0.000	0.022	-0.003	0.030
C9	0.000	0.000	0.000	0.000	0.000	-0.002	0.008	-0.013
C8	0.000	0.000	0.000	0.000	0.000	-0.001	0.007	-0.011
C7	0.000	0.000	0.000	0.000	0.000	-0.001	0.007	-0.012
Cu1'	22.414	99.866	11.222	11.192	0.030	114.287	0.500	0.523
N1'	0.001	0.005	0.000	0.001	-0.001	-5.586	0.019	-0.191
N2'	0.002	0.011	0.001	0.002	-0.001	-4.260	0.024	-0.175

N3'	0.003	0.015	0.002	0.001	0.001	3.045	0.027	0.156
N5'	0.000	0.000	0.000	0.000	0.000	-1.101	0.006	-0.111
N4'	0.000	0.001	0.000	0.000	0.000	-1.132	0.009	-0.112
C14'	0.001	0.004	0.000	0.001	0.000	-0.871	0.018	-0.103
C13'	0.001	0.004	0.000	0.000	0.000	0.223	0.017	0.065
C12'	0.000	0.002	0.000	0.000	0.000	-0.194	0.014	-0.062
C11'	0.001	0.004	0.000	0.000	0.000	0.254	0.016	0.068
C10'	0.001	0.005	0.000	0.001	0.000	-0.919	0.018	-0.105
C15'	0.000	0.000	0.000	0.000	0.000	0.031	-0.001	0.034
C17'	0.000	0.000	0.000	0.000	0.000	-0.003	0.008	-0.016
C16'	0.000	0.001	0.000	0.000	0.000	-0.002	0.009	-0.012
C16'	0.000	0.001	0.000	0.000	0.000	-0.001	0.009	-0.012
C1'	0.001	0.004	0.000	0.000	0.000	-0.747	0.016	-0.098
C2'	0.001	0.004	0.000	0.000	0.000	0.205	0.017	0.063
C3'	0.000	0.002	0.000	0.000	0.000	-0.167	0.014	-0.059
C4'	0.001	0.004	0.000	0.000	0.000	0.200	0.017	0.063
C5'	0.001	0.005	0.000	0.001	0.000	-0.814	0.018	-0.101
C6'	0.000	0.000	0.000	0.000	0.000	0.029	0.003	0.033
C9'	0.000	0.000	0.000	0.000	0.000	-0.002	0.009	-0.014
C8'	0.000	0.000	0.000	0.000	0.000	-0.001	0.007	-0.012
C7'	0.000	0.000	0.000	0.000	0.000	-0.002	0.008	-0.013
H1	0.000	0.001	0.000	0.000	0.000	0.000	0.010	0.005
H2	0.000	0.000	0.000	0.000	0.000	-0.001	0.004	-0.011
H3	0.000	0.000	0.000	0.000	0.000	-0.001	-0.008	-0.012
H4	0.000	0.001	0.000	0.000	0.000	-0.001	0.010	-0.009
H5	0.000	0.000	0.000	0.000	0.000	-0.001	0.003	-0.011
H6	0.000	0.000	0.000	0.000	0.000	0.001	0.004	0.010
H7	0.000	0.001	0.000	0.000	0.000	-0.001	0.011	-0.009
H8	0.000	0.000	0.000	0.000	0.000	-0.001	-0.002	-0.011
H9	0.000	0.000	0.000	0.000	0.000	0.001	-0.008	0.011
H10	0.000	0.001	0.000	0.000	0.000	0.000	0.010	0.007
H11	0.000	0.000	0.000	0.000	0.000	-0.002	0.005	-0.012
H12	0.000	0.000	0.000	0.000	0.000	-0.001	-0.007	-0.012
H13	0.000	0.001	0.000	0.000	0.000	-0.001	0.010	-0.009
H14	0.000	0.000	0.000	0.000	0.000	0.001	0.005	0.011
H15	0.000	0.000	0.000	0.000	0.000	-0.001	-0.005	-0.011
H16	0.000	0.001	0.000	0.000	0.000	-0.001	0.011	-0.010
H17	0.000	0.000	0.000	0.000	0.000	-0.002	-0.006	-0.012
H18	0.000	0.000	0.000	0.000	0.000	0.001	-0.008	0.010
H19	0.000	0.000	0.000	0.000	0.000	0.126	-0.008	0.054
H20	0.000	0.001	0.000	0.000	0.000	0.004	0.011	0.018
H21	0.000	0.001	0.000	0.000	0.000	0.009	0.011	0.022
H22	0.000	-0.001	0.000	0.000	0.000	0.121	-0.009	0.053
H23	0.000	0.000	0.000	0.000	0.000	0.095	0.008	0.049
H24	0.000	0.001	0.000	0.000	0.000	0.004	0.012	0.018
H25	0.000	0.001	0.000	0.000	0.000	0.010	0.011	0.023
H26	0.000	-0.002	0.000	0.000	0.000	0.107	-0.013	0.051
H1'	0.000	0.001	0.000	0.000	0.000	0.000	0.012	0.006
H2'	0.000	0.000	0.000	0.000	0.000	-0.001	0.005	-0.012

H3'	0.000	0.000	0.000	0.000	0.000	-0.002	-0.006	-0.013
H4'	0.000	0.001	0.000	0.000	0.000	-0.001	0.012	-0.010
H5'	0.000	0.000	0.000	0.000	0.000	-0.002	-0.005	-0.012
H6'	0.000	0.000	0.000	0.000	0.000	0.001	0.004	0.011
H7'	0.000	0.001	0.000	0.000	0.000	-0.001	0.012	-0.010
H8'	0.000	0.000	0.000	0.000	0.000	-0.001	-0.006	-0.012
H9'	0.000	0.000	0.000	0.000	0.000	0.002	-0.007	0.012
H10'	0.000	0.001	0.000	0.000	0.000	0.000	0.012	0.007
H11'	0.000	0.000	0.000	0.000	0.000	-0.002	-0.004	-0.014
H12'	0.000	0.000	0.000	0.000	0.000	-0.002	0.004	-0.013
H13'	0.000	0.001	0.000	0.000	0.000	-0.001	0.012	-0.010
H14'	0.000	0.000	0.000	0.000	0.000	0.002	-0.006	0.013
H15'	0.000	0.000	0.000	0.000	0.000	-0.002	-0.005	-0.012
H16'	0.000	0.001	0.000	0.000	0.000	-0.001	0.012	-0.010
H17'	0.000	0.000	0.000	0.000	0.000	-0.002	-0.006	-0.014
H18'	0.000	0.000	0.000	0.000	0.000	0.001	-0.006	0.011
H19'	0.000	0.001	0.000	0.000	0.000	0.223	0.012	0.065
H20'	0.001	0.003	0.000	0.000	0.000	0.006	0.015	0.020
H21'	0.001	0.003	0.000	0.000	0.000	0.012	0.015	0.025
H22'	0.000	0.001	0.000	0.000	0.000	0.205	0.012	0.064
H23'	0.000	0.002	0.000	0.000	0.000	0.181	0.013	0.061
H24'	0.001	0.003	0.000	0.000	0.000	0.006	0.015	0.020
H25'	0.001	0.003	0.000	0.000	0.000	0.014	0.015	0.026
H26'	0.000	0.001	0.000	0.000	0.000	0.166	0.012	0.059

**Table A2.12:** Contributions at 0.5 Å to Cu1 atomic basin along the Cu-Cu internuclear axis for the EO molecular system; LS, SF%,  $LS_{\alpha}$ ,  $LS_{\beta}$ ,  $LS_s$ ,  $SF_s\%$  are respectively the Local source, the Source Function atomic percentage for  $\rho(\mathbf{r})$ , the Local source alfa and beta, the Local Source for  $s(\mathbf{r})$  and the Source Function atomic percentage for  $s(\mathbf{r})$ .  $R_{SF}$  ( $R_{FS_s}$ ) are evaluated as in tab A2.1.

$\Omega$	LS	SF%	$LS_{\alpha}$	$LS_{\beta}$	$LS_s$	$SF_s\%$	$R_{SF}$	$R_{FS_s}$
Cu1	0.004	13.236	0.003	0.001	0.002	-849.522	0.255	-1.020
N1	-0.004	-12.259	-0.003	-0.001	-0.002	602.638	-0.248	0.910
N2	0.005	18.984	0.002	0.003	-0.001	446.862	0.287	0.824
N3	0.004	15.102	0.003	0.002	0.001	-315.074	0.266	-0.733
N5	-0.001	-3.401	-0.001	0.000	0.000	12.023	-0.162	0.247
N4	-0.001	-3.122	0.000	0.000	0.000	16.992	-0.157	0.277
C14	0.000	1.017	0.000	0.000	0.000	60.319	0.108	0.422
C13	0.000	1.606	0.000	0.000	0.000	-16.442	0.126	-0.274
C12	0.000	1.022	0.000	0.000	0.000	14.992	0.109	0.266
C11	0.000	1.503	0.000	0.000	0.000	-18.907	0.123	-0.287
C10	0.000	1.063	0.000	0.000	0.000	64.390	0.110	0.432
C15	0.000	-0.035	0.000	0.000	0.000	-2.514	-0.035	-0.146
C17	0.000	0.203	0.000	0.000	0.000	0.255	0.063	0.068
C16	0.000	0.333	0.000	0.000	0.000	0.127	0.075	0.054
C16	0.000	0.345	0.000	0.000	0.000	0.108	0.076	0.051
C1	0.000	1.189	0.000	0.000	0.000	49.395	0.114	0.395
C2	0.000	1.611	0.000	0.000	0.000	-14.596	0.126	-0.263

C3	0.000	0.973	0.000	0.000	0.000	12.815	0.107	0.252
C4	0.001	1.815	0.000	0.000	0.000	-15.196	0.131	-0.267
C5	0.000	0.986	0.000	0.000	0.000	59.336	0.107	0.420
C6	0.000	0.008	0.000	0.000	0.000	-2.344	0.022	-0.143
C9	0.000	0.324	0.000	0.000	0.000	0.174	0.074	0.060
C8	0.000	0.260	0.000	0.000	0.000	0.103	0.069	0.050
C7	0.000	0.226	0.000	0.000	0.000	0.143	0.066	0.056
Cu1'	0.004	13.258	0.003	0.001	0.002	-849.472	0.255	-1.020
N1'	-0.004	-12.211	-0.003	-0.001	-0.002	602.633	-0.248	0.910
N2'	0.005	18.961	0.002	0.003	-0.001	446.879	0.287	0.824
N3'	0.004	15.101	0.003	0.002	0.001	-315.073	0.266	-0.733
N5'	-0.001	-3.409	-0.001	0.000	0.000	12.023	-0.162	0.247
N4'	-0.001	-3.123	0.000	0.000	0.000	16.995	-0.157	0.277
C14'	0.000	1.010	0.000	0.000	0.000	60.318	0.108	0.422
C13'	0.000	1.590	0.000	0.000	0.000	-16.440	0.126	-0.274
C12'	0.000	1.025	0.000	0.000	0.000	14.991	0.109	0.266
C11'	0.000	1.505	0.000	0.000	0.000	-18.907	0.123	-0.287
C10'	0.000	1.094	0.000	0.000	0.000	64.381	0.111	0.432
C15'	0.000	-0.036	0.000	0.000	0.000	-2.514	-0.036	-0.146
C17'	0.000	0.236	0.000	0.000	0.000	0.254	0.067	0.068
C16'	0.000	0.367	0.000	0.000	0.000	0.126	0.077	0.054
C16'	0.000	0.348	0.000	0.000	0.000	0.108	0.076	0.051
C1'	0.000	1.004	0.000	0.000	0.000	49.294	0.108	0.395
C2'	0.000	1.613	0.000	0.000	0.000	-14.597	0.126	-0.263
C3'	0.000	0.975	0.000	0.000	0.000	12.815	0.107	0.252
C4'	0.001	1.790	0.000	0.000	0.000	-15.196	0.131	-0.267
C5'	0.000	0.977	0.000	0.000	0.000	59.324	0.107	0.420
C6'	0.000	-0.024	0.000	0.000	0.000	-2.346	-0.031	-0.143
C9'	0.000	0.313	0.000	0.000	0.000	0.174	0.073	0.060
C8'	0.000	0.221	0.000	0.000	0.000	0.101	0.065	0.050
C7'	0.000	0.241	0.000	0.000	0.000	0.143	0.067	0.056
H1	0.000	0.879	0.000	0.000	0.000	-0.012	0.103	-0.025
H2	0.000	0.057	0.000	0.000	0.000	0.105	0.041	0.051
H3	0.000	-0.276	0.000	0.000	0.000	0.149	-0.070	0.057
H4	0.000	0.826	0.000	0.000	0.000	0.058	0.101	0.042
H5	0.000	-0.013	0.000	0.000	0.000	0.121	-0.026	0.053
H6	0.000	0.062	0.000	0.000	0.000	-0.081	0.043	-0.047
H7	0.000	0.917	0.000	0.000	0.000	0.063	0.105	0.043
H8	0.000	-0.056	0.000	0.000	0.000	0.113	-0.041	0.052
H9	0.000	-0.337	0.000	0.000	0.000	-0.128	-0.075	-0.054
H10	0.000	0.866	0.000	0.000	0.000	-0.027	0.103	-0.032
H11	0.000	0.056	0.000	0.000	0.000	0.164	0.041	0.059
H12	0.000	-0.122	0.000	0.000	0.000	0.147	-0.053	0.057
H13	0.000	0.846	0.000	0.000	0.000	0.061	0.102	0.043
H14	0.000	0.017	0.000	0.000	0.000	-0.125	0.028	-0.054
H15	0.000	-0.066	0.000	0.000	0.000	0.122	-0.044	0.053
H16	0.000	0.927	0.000	0.000	0.000	0.075	0.105	0.045
H17	0.000	-0.147	0.000	0.000	0.000	0.162	-0.057	0.059
H18	0.000	-0.324	0.000	0.000	0.000	-0.083	-0.074	-0.047

H19	0.000	-0.154	0.000	0.000	0.000	-15.502	-0.058	-0.269
H20	0.000	1.395	0.000	0.000	0.000	-0.488	0.120	-0.085
H21	0.000	1.331	0.000	0.000	0.000	-0.947	0.118	-0.106
H22	0.000	-0.235	0.000	0.000	0.000	-14.684	-0.066	-0.264
H23	0.000	0.663	0.000	0.000	0.000	-11.675	0.094	-0.244
H24	0.000	1.405	0.000	0.000	0.000	-0.493	0.121	-0.085
H25	0.000	1.263	0.000	0.000	0.000	-1.081	0.116	-0.111
H26	0.000	-1.088	0.000	0.000	0.000	-12.792	-0.111	-0.252
H1'	0.000	0.878	0.000	0.000	0.000	-0.012	0.103	-0.025
H2'	0.000	0.058	0.000	0.000	0.000	0.105	0.042	0.051
H3'	0.000	-0.275	0.000	0.000	0.000	0.149	-0.070	0.057
H4'	0.000	0.826	0.000	0.000	0.000	0.058	0.101	0.042
H5'	0.000	-0.003	0.000	0.000	0.000	0.121	-0.015	0.053
H6'	0.000	0.037	0.000	0.000	0.000	-0.081	0.036	-0.047
H7'	0.000	0.917	0.000	0.000	0.000	0.063	0.105	0.043
H8'	0.000	-0.056	0.000	0.000	0.000	0.113	-0.041	0.052
H9'	0.000	-0.338	0.000	0.000	0.000	-0.128	-0.075	-0.054
H10'	0.000	0.866	0.000	0.000	0.000	-0.027	0.103	-0.032
H11'	0.000	0.057	0.000	0.000	0.000	0.164	0.041	0.059
H12'	0.000	-0.122	0.000	0.000	0.000	0.147	-0.053	0.057
H13'	0.000	0.846	0.000	0.000	0.000	0.061	0.102	0.043
H14'	0.000	0.008	0.000	0.000	0.000	-0.125	0.022	-0.054
H15'	0.000	-0.066	0.000	0.000	0.000	0.122	-0.043	0.053
H16'	0.000	0.926	0.000	0.000	0.000	0.075	0.105	0.045
H17'	0.000	-0.147	0.000	0.000	0.000	0.162	-0.057	0.059
H18'	0.000	-0.323	0.000	0.000	0.000	-0.083	-0.074	-0.047
H19'	0.000	-0.154	0.000	0.000	0.000	-15.501	-0.058	-0.269
H20'	0.000	1.395	0.000	0.000	0.000	-0.488	0.120	-0.085
H21'	0.000	1.331	0.000	0.000	0.000	-0.947	0.118	-0.106
H22'	0.000	-0.233	0.000	0.000	0.000	-14.684	-0.066	-0.264
H23'	0.000	0.663	0.000	0.000	0.000	-11.675	0.094	-0.244
H24'	0.000	1.408	0.000	0.000	0.000	-0.493	0.121	-0.085
H25'	0.000	1.257	0.000	0.000	0.000	-1.081	0.116	-0.111
H26'	0.000	-1.088	0.000	0.000	0.000	-12.792	-0.111	-0.252

**Table A2.13:** Contributions at the middle point between the two copper atoms along the Cu-Cu internuclear axis for the EO molecular system; LS, SF%,  $LS_{\alpha}$ ,  $LS_{\beta}$ ,  $LS_s$ ,  $SF_s\%$  are respectively the Local source, the Source Function atomic percentage for  $\rho(\mathbf{r})$ , the Local source alpha and beta, the Local Source for  $s(\mathbf{r})$  and the Source Function atomic percentage for  $s(\mathbf{r})$ .  $R_{SF}$  ( $R_{FSs}$ ) are evaluated as in tab A2.1.

$\Omega$	LS	SF%	$LS_{\alpha}$	$LS_{\beta}$	$LS_s$	$SF_s\%$	$R_{SF}$	$R_{FSs}$
Cu1	1.895	98.268	1.093	0.803	0.290	101.355	0.497	0.502
N1	0.000	-0.010	0.000	0.000	0.000	-0.995	-0.023	-0.108
N2	-0.002	-0.092	-0.001	-0.001	0.000	-1.607	-0.049	-0.126
N5'	-0.002	-0.086	0.000	-0.001	0.001	3.551	-0.047	0.164
N4'	0.001	0.077	0.000	0.001	-0.001	-2.768	0.046	-0.151
N3	0.005	0.279	0.002	0.003	-0.001	-4.927	0.070	-0.183
O1	0.002	0.128	0.001	0.002	-0.001	-4.147	0.054	-0.173

F1	0.000	0.022	0.000	0.000	0.000	-0.078	0.030	-0.046
F2	0.001	0.051	0.000	0.001	0.000	-0.118	0.040	-0.053
F3	0.000	0.018	0.000	0.000	0.000	-0.075	0.028	-0.045
C1	0.000	0.001	0.000	0.000	0.000	0.448	0.012	0.082
C2	0.001	0.063	0.000	0.001	0.000	-0.832	0.043	-0.101
C3	0.001	0.041	0.000	0.000	0.000	0.252	0.037	0.068
C4	0.000	0.014	0.000	0.000	0.000	0.303	0.026	0.072
C5	0.001	0.058	0.000	0.001	0.000	-0.915	0.042	-0.105
C6	0.001	0.029	0.000	0.000	0.000	-0.338	0.033	-0.075
C7	0.000	0.022	0.000	0.000	0.000	-0.594	0.030	-0.091
C8	0.000	0.017	0.000	0.000	0.000	-0.705	0.028	-0.096
C9	0.000	0.011	0.000	0.000	0.000	-0.856	0.024	-0.102
H1	0.001	0.029	0.000	0.000	0.000	0.072	0.033	0.045
H2	0.001	0.074	0.001	0.001	0.000	0.147	0.045	0.057
H3	0.001	0.036	0.000	0.000	0.000	0.006	0.036	0.019
H4	0.000	0.024	0.000	0.000	0.000	0.086	0.031	0.048
H5	0.001	0.073	0.001	0.001	0.000	0.092	0.045	0.049
H6	0.001	0.034	0.000	0.000	0.000	0.078	0.035	0.046
H7	0.000	0.019	0.000	0.000	0.000	-0.034	0.029	-0.035
H8	0.000	0.016	0.000	0.000	0.000	-0.034	0.027	-0.035
H9	0.001	0.028	0.000	0.000	0.000	-0.007	0.033	-0.021
H10	0.001	0.065	0.001	0.001	0.000	0.064	0.043	0.043
H11	0.001	0.037	0.000	0.000	0.000	0.035	0.036	0.035
H12	0.001	0.045	0.000	0.000	0.000	0.007	0.038	0.020
H13	0.001	0.055	0.001	0.001	0.000	0.037	0.041	0.036
H14	0.001	0.051	0.000	0.000	0.000	-0.014	0.040	-0.026
Cu1'	0.000	-0.005	0.000	0.000	0.001	2.350	-0.019	0.143
N1'	0.000	-0.018	0.000	0.000	0.000	-0.050	-0.028	-0.040
N2'	0.000	-0.018	0.000	0.000	0.000	0.065	-0.028	0.043
N5	0.004	0.215	0.002	0.002	0.001	2.751	0.065	0.151
N4	0.003	0.170	0.001	0.002	-0.001	-2.711	0.060	-0.150
N3'	0.002	0.116	0.001	0.001	0.000	-0.284	0.053	-0.071
O1'	-0.001	-0.040	0.000	0.000	0.000	-0.769	-0.037	-0.099
F1'	0.000	0.012	0.000	0.000	0.000	-0.052	0.025	-0.040
F2'	0.000	0.026	0.000	0.000	0.000	-0.081	0.032	-0.047
F3'	0.000	-0.024	0.000	0.000	0.000	-0.056	-0.031	-0.041
C1'	0.000	0.001	0.000	0.000	0.000	0.289	0.011	0.071
C2'	0.000	0.006	0.000	0.000	0.000	-0.451	0.019	-0.083
C3'	0.000	0.009	0.000	0.000	0.000	0.127	0.022	0.054
C4'	0.000	0.003	0.000	0.000	0.000	0.161	0.016	0.059
C5'	0.000	0.008	0.000	0.000	0.000	-0.430	0.022	-0.081
C6'	0.000	0.007	0.000	0.000	0.000	-0.149	0.021	-0.057
C7'	0.000	0.005	0.000	0.000	0.000	-0.270	0.018	-0.070
C8'	0.000	0.007	0.000	0.000	0.000	-0.295	0.021	-0.072
C9'	0.000	-0.001	0.000	0.000	0.000	-0.442	-0.011	-0.082
H1'	0.000	-0.007	0.000	0.000	0.000	0.040	-0.021	0.037
H2'	0.001	0.026	0.000	0.000	0.000	0.095	0.032	0.049
H3'	-0.001	-0.028	0.000	0.000	0.000	0.001	-0.033	0.010
H4'	0.000	-0.003	0.000	0.000	0.000	0.036	-0.016	0.036

H5'	0.000	0.014	0.000	0.000	0.000	0.045	0.026	0.038
H6'	0.000	0.012	0.000	0.000	0.000	0.029	0.024	0.033
H7'	0.000	0.002	0.000	0.000	0.000	-0.020	0.014	-0.029
H8'	0.000	0.008	0.000	0.000	0.000	-0.019	0.022	-0.029
H9'	0.000	0.008	0.000	0.000	0.000	-0.004	0.021	-0.018
H10'	0.000	0.016	0.000	0.000	0.000	0.034	0.027	0.035
H11'	0.000	-0.011	0.000	0.000	0.000	0.017	-0.024	0.028
H12'	0.000	0.014	0.000	0.000	0.000	0.003	0.026	0.015
H13'	0.000	0.009	0.000	0.000	0.000	0.019	0.022	0.029
H14'	0.000	0.015	0.000	0.000	0.000	-0.008	0.026	-0.022

**Table A2.14:** Contributions at the CD along the Cu-N5 bond for the EE molecular system; LS, SF%,  $LS_{\alpha}$ ,  $LS_{\beta}$ ,  $LS_s$ ,  $SF_s\%$  are respectively the Local source, the Source Function atomic percentage for  $\rho(\mathbf{r})$ , the Local source alfa and beta, the Local Source for  $s(\mathbf{r})$  and the Source Function atomic percentage for  $s(\mathbf{r})$ .  $R_{SF}$  ( $R_{FSs}$ ) are evaluated as in tab A2.1.

$\Omega$	LS	SF%	$LS_{\alpha}$	$LS_{\beta}$	$LS_s$	$SF_s\%$	$R_{SF}$	$R_{FSs}$
Cu1	1.893	98.467	0.951	0.942	0.009	164.093	0.497	0.590
N1	0.000	0.008	0.000	0.000	0.000	-8.227	0.022	-0.217
N2	-0.002	-0.092	-0.001	-0.001	0.000	-8.396	-0.049	-0.219
N5'	-0.002	-0.086	0.000	-0.001	0.001	23.366	-0.048	0.308
N4'	0.003	0.153	0.001	0.002	-0.001	-17.452	0.058	-0.279
N3	0.002	0.080	0.000	0.001	-0.001	-13.663	0.046	-0.258
O1	0.002	0.129	0.001	0.002	-0.001	-22.979	0.054	-0.306
F1	0.001	0.031	0.000	0.000	0.000	-0.423	0.034	-0.081
F2	0.001	0.050	0.000	0.001	0.000	-0.666	0.040	-0.094
F3	0.000	0.016	0.000	0.000	0.000	-0.423	0.027	-0.081
C1	0.000	0.002	0.000	0.000	0.000	2.535	0.014	0.147
C2	0.001	0.058	0.000	0.001	0.000	-4.739	0.042	-0.181
C3	0.001	0.043	0.000	0.000	0.000	1.491	0.038	0.123
C4	0.000	0.018	0.000	0.000	0.000	1.794	0.028	0.131
C5	0.001	0.075	0.001	0.001	0.000	-5.524	0.045	-0.190
C6	0.001	0.038	0.000	0.000	0.000	-2.066	0.036	-0.137
C7	0.000	0.007	0.000	0.000	0.000	-3.481	0.020	-0.163
C8	0.001	0.028	0.000	0.000	0.000	-3.583	0.033	-0.165
C9	0.000	0.012	0.000	0.000	0.000	-4.622	0.025	-0.179
H1	0.001	0.041	0.000	0.000	0.000	0.362	0.037	0.077
H2	0.001	0.072	0.001	0.001	0.000	0.799	0.045	0.100
H3	0.000	0.021	0.000	0.000	0.000	0.023	0.030	0.031
H4	0.001	0.032	0.000	0.000	0.000	0.402	0.034	0.079
H5	0.001	0.063	0.001	0.001	0.000	0.472	0.043	0.084
H6	0.001	0.027	0.000	0.000	0.000	0.391	0.032	0.079
H7	0.000	0.019	0.000	0.000	0.000	-0.200	0.029	-0.063
H8	0.000	0.022	0.000	0.000	0.000	-0.194	0.030	-0.062
H9	0.001	0.031	0.000	0.000	0.000	-0.042	0.034	-0.038
H10	0.001	0.075	0.001	0.001	0.000	0.378	0.045	0.078
H11	0.001	0.032	0.000	0.000	0.000	0.219	0.034	0.065
H12	0.001	0.059	0.001	0.001	0.000	0.037	0.042	0.036
H13	0.001	0.061	0.001	0.001	0.000	0.225	0.042	0.066

H14	0.001	0.057	0.001	0.001	0.000	-0.084	0.042	-0.047
Cu1'	0.000	-0.004	0.000	0.000	0.001	13.047	-0.017	0.254
N1'	0.000	-0.017	0.000	0.000	0.000	-0.291	-0.028	-0.071
N2'	0.000	-0.019	0.000	0.000	0.000	0.356	-0.029	0.076
N5	0.003	0.164	0.002	0.001	0.001	13.974	0.059	0.259
N4	0.001	0.042	0.000	0.001	-0.001	-13.674	0.038	-0.258
N3'	0.003	0.144	0.001	0.001	0.000	-1.419	0.056	-0.121
O1'	-0.001	-0.043	-0.001	0.000	0.000	-4.255	-0.038	-0.175
F1'	0.000	0.009	0.000	0.000	0.000	-0.287	0.023	-0.071
F2'	0.001	0.027	0.000	0.000	0.000	-0.440	0.032	-0.082
F3'	0.000	-0.022	0.000	0.000	0.000	-0.307	-0.030	-0.073
C1'	0.000	0.001	0.000	0.000	0.000	1.572	0.011	0.125
C2'	0.000	0.008	0.000	0.000	0.000	-2.463	0.021	-0.145
C3'	0.000	0.010	0.000	0.000	0.000	0.687	0.023	0.095
C4'	0.000	0.003	0.000	0.000	0.000	0.868	0.016	0.103
C5'	0.000	0.009	0.000	0.000	0.000	-2.324	0.022	-0.143
C6'	0.000	0.007	0.000	0.000	0.000	-0.804	0.021	-0.100
C7'	0.000	0.005	0.000	0.000	0.000	-1.467	0.018	-0.122
C8'	0.000	0.007	0.000	0.000	0.000	-1.651	0.020	-0.127
C9'	0.000	-0.002	0.000	0.000	0.000	-2.448	-0.013	-0.145
H1'	0.000	-0.013	0.000	0.000	0.000	0.225	-0.026	0.066
H2'	0.001	0.027	0.000	0.000	0.000	0.527	0.032	0.087
H3'	0.000	-0.023	0.000	0.000	0.000	0.006	-0.031	0.020
H4'	0.000	-0.006	0.000	0.000	0.000	0.204	-0.019	0.063
H5'	0.000	0.015	0.000	0.000	0.000	0.250	0.026	0.068
H6'	0.000	0.012	0.000	0.000	0.000	0.160	0.025	0.059
H7'	0.000	0.003	0.000	0.000	0.000	-0.107	0.015	-0.051
H8'	0.000	0.008	0.000	0.000	0.000	-0.101	0.021	-0.050
H9'	0.000	0.007	0.000	0.000	0.000	-0.023	0.021	-0.031
H10'	0.000	0.016	0.000	0.000	0.000	0.181	0.027	0.061
H11'	0.000	-0.008	0.000	0.000	0.000	0.093	-0.021	0.049
H12'	0.000	0.013	0.000	0.000	0.000	0.016	0.025	0.027
H13'	0.000	0.010	0.000	0.000	0.000	0.105	0.023	0.051
H14'	0.000	0.015	0.000	0.000	0.000	-0.046	0.026	-0.039

**Table A2.15:** Contributions at the CD along the Cu-N3 bond for the EE molecular system; LS, SF%,  $LS_{\alpha}$ ,  $LS_{\beta}$ ,  $LS_s$ ,  $SF_s\%$  are respectively the Local source, the Source Function atomic percentage for  $\rho(\mathbf{r})$ , the Local source alfa and beta, the Local Source for  $s(\mathbf{r})$  and the Source Function atomic percentage for  $s(\mathbf{r})$ .  $R_{SF}$  ( $R_{FSs}$ ) are evaluated as in tab A2.1.

$\Omega$	LS	SF%	$LS_{\alpha}$	$LS_{\beta}$	$LS_s$	$SF_s\%$	$R_{SF}$	$R_{FSs}$
Cu1	9.135	99.711	5.114	4.021	1.093	100.271	0.500	0.500
N1	0.000	0.003	0.000	0.000	0.000	-0.035	0.016	-0.035
N2	-0.001	-0.016	-0.001	0.000	-0.001	-0.048	-0.027	-0.039
N5'	-0.002	-0.019	0.000	-0.001	0.001	0.091	-0.029	0.048
N4'	0.002	0.018	0.000	0.001	-0.001	-0.071	0.028	-0.045
N3	0.003	0.033	0.001	0.002	-0.001	-0.093	0.034	-0.049
O1	0.003	0.033	0.001	0.002	-0.001	-0.115	0.034	-0.052
F1	0.000	0.005	0.000	0.000	0.000	-0.002	0.019	-0.014



F2	0.001	0.011	0.000	0.001	0.000	-0.003	0.024	-0.016
F3	0.000	0.004	0.000	0.000	0.000	-0.002	0.018	-0.014
C1	0.000	0.000	0.000	0.000	0.000	0.012	0.008	0.025
C2	0.001	0.013	0.000	0.001	0.000	-0.022	0.026	-0.030
C3	0.001	0.009	0.000	0.000	0.000	0.007	0.023	0.021
C4	0.001	0.015	0.001	0.001	0.000	-0.026	0.026	-0.032
C5	0.000	0.003	0.000	0.000	0.000	0.008	0.016	0.022
C6	0.001	0.007	0.000	0.000	0.000	-0.010	0.021	-0.023
C7	0.000	0.004	0.000	0.000	0.000	-0.016	0.018	-0.027
C8	0.000	0.004	0.000	0.000	0.000	-0.019	0.017	-0.029
C9	0.000	0.004	0.000	0.000	0.000	-0.022	0.017	-0.030
H1	0.001	0.007	0.000	0.000	0.000	0.002	0.021	0.013
H2	0.001	0.015	0.001	0.001	0.000	0.004	0.027	0.017
H3	0.001	0.007	0.000	0.000	0.000	0.000	0.021	0.006
H4	0.001	0.007	0.000	0.000	0.000	0.002	0.020	0.014
H5	0.001	0.016	0.001	0.001	0.000	0.002	0.027	0.015
H6	0.001	0.006	0.000	0.000	0.000	0.002	0.020	0.014
H7	0.000	0.004	0.000	0.000	0.000	-0.001	0.018	-0.011
H8	0.000	0.004	0.000	0.000	0.000	-0.001	0.017	-0.011
H9	0.001	0.006	0.000	0.000	0.000	0.000	0.020	-0.006
H10	0.001	0.015	0.001	0.001	0.000	0.002	0.026	0.013
H11	0.001	0.009	0.000	0.000	0.000	0.001	0.022	0.011
H12	0.001	0.011	0.000	0.000	0.000	0.000	0.024	0.006
H13	0.001	0.013	0.001	0.001	0.000	0.001	0.025	0.011
H14	0.001	0.012	0.001	0.001	0.000	0.000	0.024	-0.008
Cu1'	0.000	-0.001	0.000	0.000	0.001	0.060	-0.011	0.042
N1'	0.000	-0.004	0.000	0.000	0.000	-0.001	-0.016	-0.011
N2'	0.000	-0.004	0.000	0.000	0.000	0.002	-0.017	0.013
N5	0.004	0.039	0.002	0.001	0.001	0.067	0.036	0.044
N4	0.002	0.025	0.001	0.002	-0.001	-0.066	0.032	-0.044
N3'	0.002	0.024	0.001	0.001	0.000	-0.007	0.031	-0.021
O1'	-0.001	-0.008	0.000	0.000	0.000	-0.019	-0.022	-0.029
F1'	0.000	0.002	0.000	0.000	0.000	-0.001	0.014	-0.012
F2'	0.000	0.005	0.000	0.000	0.000	-0.002	0.019	-0.014
F3'	0.000	-0.005	0.000	0.000	0.000	-0.001	-0.018	-0.012
C1'	0.000	0.000	0.000	0.000	0.000	0.007	0.007	0.021
C2'	0.000	0.001	0.000	0.000	0.000	-0.011	0.011	-0.024
C3'	0.000	0.002	0.000	0.000	0.000	0.003	0.013	0.016
C4'	0.000	0.002	0.000	0.000	0.000	-0.011	0.013	-0.024
C5'	0.000	0.001	0.000	0.000	0.000	0.004	0.009	0.017
C6'	0.000	0.001	0.000	0.000	0.000	-0.004	0.012	-0.017
C7'	0.000	0.001	0.000	0.000	0.000	-0.007	0.011	-0.020
C8'	0.000	0.001	0.000	0.000	0.000	-0.008	0.012	-0.021
C9'	0.000	0.000	0.000	0.000	0.000	-0.011	-0.006	-0.024
H1'	0.000	-0.002	0.000	0.000	0.000	0.001	-0.013	0.011
H2'	0.000	0.005	0.000	0.000	0.000	0.002	0.019	0.015
H3'	-0.001	-0.005	0.000	0.000	0.000	0.000	-0.019	0.003
H4'	0.000	-0.001	0.000	0.000	0.000	0.001	-0.010	0.010
H5'	0.000	0.003	0.000	0.000	0.000	0.001	0.015	0.011

H6'	0.000	0.002	0.000	0.000	0.000	0.001	0.014	0.010
H7'	0.000	0.000	0.000	0.000	0.000	-0.001	0.008	-0.009
H8'	0.000	0.002	0.000	0.000	0.000	0.000	0.013	-0.008
H9'	0.000	0.002	0.000	0.000	0.000	0.000	0.012	-0.005
H10'	0.000	0.003	0.000	0.000	0.000	0.001	0.016	0.010
H11'	0.000	-0.002	0.000	0.000	0.000	0.000	-0.014	0.008
H12'	0.000	0.003	0.000	0.000	0.000	0.000	0.015	0.004
H13'	0.000	0.002	0.000	0.000	0.000	0.000	0.013	0.009
H14'	0.000	0.003	0.000	0.000	0.000	0.000	0.015	-0.006

**Table A2.16:** Contributions at the Cu1 atomic basin along the Cu-N5 bond for the EE molecular system; LS, SF%,  $LS_{\alpha}$ ,  $LS_{\beta}$ ,  $LS_s$ ,  $SF_s\%$  are respectively the Local source, the Source Function atomic percentage for  $\rho(\mathbf{r})$ , the Local source alpha and beta, the Local Source for  $s(\mathbf{r})$  and the Source Function atomic percentage for  $s(\mathbf{r})$ .  $R_{SF}$  ( $R_{FSs}$ ) are evaluated as in tab A2.1.

$\Omega$	LS	SF%	$LS_{\alpha}$	$LS_{\beta}$	$LS_s$	$SF_s\%$	$R_{SF}$	$R_{FSs}$
Cu1	0.044	46.746	0.026	0.017	0.009	284.129	0.388	0.708
N1	-0.001	-0.598	0.000	0.000	0.000	-5.577	-0.091	-0.191
N2	-0.002	-2.512	-0.001	-0.001	0.000	-10.157	-0.146	-0.233
N5'	-0.001	-1.537	0.000	-0.001	0.001	30.306	-0.124	0.336
N4'	0.001	0.870	0.000	0.001	-0.001	-24.220	0.103	-0.312
N3	0.021	22.961	0.009	0.013	-0.004	-117.241	0.306	-0.527
O1	0.001	0.938	0.000	0.001	-0.001	-30.361	0.105	-0.336
F1	0.000	0.309	0.000	0.000	0.000	-0.705	0.073	-0.096
F2	0.001	1.017	0.000	0.000	0.000	-1.035	0.108	-0.109
F3	0.000	0.301	0.000	0.000	0.000	-0.672	0.072	-0.094
C1	0.000	0.002	0.000	0.000	0.000	3.909	0.012	0.170
C2	0.001	1.158	0.000	0.001	0.000	-7.127	0.113	-0.207
C3	0.001	0.734	0.000	0.000	0.000	2.089	0.097	0.138
C4	0.001	0.877	0.000	0.001	0.000	-7.455	0.103	-0.210
C5	0.000	0.231	0.000	0.000	0.000	2.526	0.066	0.147
C6	0.000	0.450	0.000	0.000	0.000	-2.740	0.083	-0.151
C7	0.000	0.499	0.000	0.000	0.000	-5.002	0.085	-0.184
C8	0.000	0.208	0.000	0.000	0.000	-6.427	0.064	-0.200
C9	0.000	0.066	0.000	0.000	0.000	-7.863	0.044	-0.214
H1	0.000	0.250	0.000	0.000	0.000	0.712	0.068	0.096
H2	0.001	1.548	0.001	0.001	0.000	1.365	0.125	0.119
H3	0.001	0.847	0.000	0.000	0.000	0.053	0.102	0.040
H4	0.000	0.110	0.000	0.000	0.000	0.853	0.052	0.102
H5	0.001	1.510	0.001	0.001	0.000	0.851	0.124	0.102
H6	0.001	0.823	0.000	0.000	0.000	0.686	0.101	0.095
H7	0.000	0.350	0.000	0.000	0.000	-0.284	0.076	-0.071
H8	0.000	0.258	0.000	0.000	0.000	-0.286	0.069	-0.071
H9	0.000	0.482	0.000	0.000	0.000	-0.062	0.084	-0.043
H10	0.001	1.134	0.001	0.001	0.000	0.542	0.112	0.088
H11	0.001	0.648	0.000	0.000	0.000	0.285	0.093	0.071
H12	0.001	0.703	0.000	0.000	0.000	0.055	0.096	0.041
H13	0.001	0.948	0.000	0.000	0.000	0.311	0.106	0.073

H14	0.001	0.906	0.000	0.000	0.000	-0.123	0.104	-0.054
Cu1'	0.000	-0.145	0.000	0.000	0.001	22.218	-0.057	0.303
N1'	0.000	-0.412	0.000	0.000	0.000	-0.489	-0.080	-0.085
N2'	0.000	-0.409	0.000	0.000	0.000	0.550	-0.080	0.088
N5	0.006	5.947	0.003	0.002	0.001	28.234	0.195	0.328
N4	0.008	8.191	0.003	0.004	-0.001	-27.972	0.217	-0.327
N3'	0.002	2.214	0.001	0.001	0.000	-2.838	0.140	-0.153
O1'	-0.001	-0.859	-0.001	0.000	0.000	-7.328	-0.102	-0.209
F1'	0.000	0.319	0.000	0.000	0.000	-0.486	0.074	-0.085
F2'	0.001	0.548	0.000	0.000	0.000	-0.770	0.088	-0.099
F3'	0.000	-0.535	0.000	0.000	0.000	-0.535	-0.087	-0.087
C1'	0.000	0.017	0.000	0.000	0.000	2.747	0.028	0.151
C2'	0.000	0.096	0.000	0.000	0.000	-4.299	0.049	-0.175
C3'	0.000	0.183	0.000	0.000	0.000	1.215	0.061	0.115
C4'	0.000	0.172	0.000	0.000	0.000	-4.116	0.060	-0.173
C5'	0.000	0.071	0.000	0.000	0.000	1.537	0.045	0.124
C6'	0.000	0.153	0.000	0.000	0.000	-1.420	0.058	-0.121
C7'	0.000	0.095	0.000	0.000	0.000	-2.555	0.049	-0.147
C8'	0.000	0.156	0.000	0.000	0.000	-2.747	0.058	-0.151
C9'	0.000	-0.007	0.000	0.000	0.000	-4.128	-0.021	-0.173
H1'	0.000	-0.069	0.000	0.000	0.000	0.364	-0.044	0.077
H2'	0.001	0.553	0.000	0.000	0.000	0.884	0.088	0.103
H3'	-0.001	-0.667	0.000	0.000	0.000	0.003	-0.094	0.016
H4'	0.000	-0.032	0.000	0.000	0.000	0.328	-0.034	0.074
H5'	0.000	0.299	0.000	0.000	0.000	0.413	0.072	0.080
H6'	0.000	0.239	0.000	0.000	0.000	0.268	0.067	0.069
H7'	0.000	0.040	0.000	0.000	0.000	-0.191	0.037	-0.062
H8'	0.000	0.193	0.000	0.000	0.000	-0.177	0.062	-0.061
H9'	0.000	0.167	0.000	0.000	0.000	-0.041	0.059	-0.037
H10'	0.000	0.368	0.000	0.000	0.000	0.320	0.077	0.074
H11'	0.000	-0.271	0.000	0.000	0.000	0.168	-0.070	0.059
H12'	0.000	0.310	0.000	0.000	0.000	0.027	0.073	0.032
H13'	0.000	0.186	0.000	0.000	0.000	0.186	0.061	0.061
H14'	0.000	0.321	0.000	0.000	0.000	-0.081	0.074	-0.047

**Table A2.17:** Contributions at the bcp along the Cu-N5 bond for the EE molecular system; LS, SF%,  $LS_{\alpha}$ ,  $LS_{\beta}$ ,  $LS_s$ ,  $SF_s\%$  are respectively the Local source, the Source Function atomic percentage for  $\rho(\mathbf{r})$ , the Local source alfa and beta, the Local Source for  $s(\mathbf{r})$  and the Source Function atomic percentage for  $s(\mathbf{r})$ .  $R_{SF}$  ( $R_{FSS}$ ) are evaluated as in tab A2.1

$\Omega$	LS	SF%	$LS_{\alpha}$	$LS_{\beta}$	$LS_s$	$SF_s\%$	$R_{SF}$	$R_{FSS}$
Cu1	0.005	0.725	0.003	0.001	0.002	8.424	0.097	0.219
N1	-0.001	-0.094	0.000	0.000	0.000	-0.340	-0.049	-0.075
N2	-0.002	-0.335	-0.001	-0.001	0.000	-0.426	-0.075	-0.081
N5'	-0.001	-0.133	0.000	-0.001	0.001	3.190	-0.055	0.159
N4'	0.000	-0.007	0.000	0.000	-0.001	-2.674	-0.020	-0.150
N3	0.597	92.021	0.311	0.286	0.025	96.902	0.486	0.495
O1	-0.001	-0.123	-0.001	0.000	-0.001	-2.395	-0.054	-0.144
F1	0.000	0.016	0.000	0.000	0.000	-0.081	0.027	-0.047

F2	0.001	0.133	0.000	0.000	0.000	-0.115	0.055	-0.052
F3	0.000	0.025	0.000	0.000	0.000	-0.076	0.031	-0.046
C1	0.000	-0.003	0.000	0.000	0.000	0.429	-0.015	0.081
C2	0.001	0.121	0.000	0.000	0.000	-0.754	0.053	-0.098
C3	0.001	0.080	0.000	0.000	0.000	0.214	0.046	0.064
C4	0.001	0.079	0.000	0.000	0.000	-0.750	0.046	-0.098
C5	0.000	0.023	0.000	0.000	0.000	0.262	0.031	0.069
C6	0.000	0.045	0.000	0.000	0.000	-0.272	0.038	-0.070
C7	0.000	0.060	0.000	0.000	0.000	-0.514	0.042	-0.086
C8	0.000	0.026	0.000	0.000	0.000	-0.706	0.032	-0.096
C9	0.000	-0.006	0.000	0.000	0.000	-0.889	-0.019	-0.104
H1	-0.001	-0.087	0.000	0.000	0.000	0.091	-0.048	0.049
H2	0.001	0.207	0.001	0.001	0.000	0.162	0.064	0.059
H3	0.001	0.117	0.000	0.000	0.000	0.006	0.053	0.020
H4	-0.001	-0.096	0.000	0.000	0.000	0.105	-0.049	0.051
H5	0.001	0.188	0.001	0.001	0.000	0.098	0.062	0.050
H6	0.001	0.120	0.000	0.000	0.000	0.072	0.053	0.045
H7	0.000	0.040	0.000	0.000	0.000	-0.030	0.037	-0.034
H8	0.000	0.025	0.000	0.000	0.000	-0.030	0.032	-0.034
H9	0.000	0.053	0.000	0.000	0.000	-0.007	0.040	-0.020
H10	0.001	0.118	0.000	0.000	0.000	0.057	0.053	0.041
H11	0.000	0.066	0.000	0.000	0.000	0.029	0.043	0.033
H12	0.000	0.065	0.000	0.000	0.000	0.006	0.043	0.019
H13	0.001	0.101	0.000	0.000	0.000	0.032	0.050	0.034
H14	0.001	0.100	0.000	0.000	0.000	-0.013	0.050	-0.025
Cu1'	0.000	-0.029	0.000	0.000	0.001	2.835	-0.033	0.152
N1'	0.000	-0.072	0.000	0.000	0.000	-0.065	-0.045	-0.043
N2'	0.000	-0.066	0.000	0.000	0.000	0.056	-0.044	0.041
N5	0.009	1.406	0.005	0.004	0.001	4.215	0.121	0.174
N4	0.030	4.682	0.015	0.016	-0.001	-4.233	0.180	-0.174
N3'	0.002	0.265	0.001	0.001	0.000	-0.394	0.069	-0.079
O1'	-0.001	-0.127	-0.001	0.000	0.000	-0.948	-0.054	-0.106
F1'	0.000	0.062	0.000	0.000	0.000	-0.061	0.043	-0.042
F2'	0.001	0.082	0.000	0.000	0.000	-0.099	0.047	-0.050
F3'	-0.001	-0.084	0.000	0.000	0.000	-0.068	-0.047	-0.044
C1'	0.000	0.001	0.000	0.000	0.000	0.354	0.010	0.076
C2'	0.000	0.005	0.000	0.000	0.000	-0.556	0.019	-0.089
C3'	0.000	0.024	0.000	0.000	0.000	0.159	0.031	0.058
C4'	0.000	0.025	0.000	0.000	0.000	-0.538	0.031	-0.088
C5'	0.000	0.012	0.000	0.000	0.000	0.200	0.024	0.063
C6'	0.000	0.023	0.000	0.000	0.000	-0.185	0.031	-0.061
C7'	0.000	0.013	0.000	0.000	0.000	-0.328	0.026	-0.074
C8'	0.000	0.025	0.000	0.000	0.000	-0.341	0.031	-0.075
C9'	0.000	0.004	0.000	0.000	0.000	-0.514	0.017	-0.086
H1'	0.000	0.010	0.000	0.000	0.000	0.044	0.024	0.038
H2'	0.001	0.083	0.000	0.000	0.000	0.109	0.047	0.051
H3'	-0.001	-0.112	0.000	0.000	0.000	0.000	-0.052	-0.005
H4'	0.000	0.004	0.000	0.000	0.000	0.040	0.017	0.037
H5'	0.000	0.045	0.000	0.000	0.000	0.051	0.038	0.040

H6'	0.000	0.033	0.000	0.000	0.000	0.033	0.035	0.035
H7'	0.000	0.004	0.000	0.000	0.000	-0.025	0.017	-0.031
H8'	0.000	0.033	0.000	0.000	0.000	-0.023	0.035	-0.031
H9'	0.000	0.027	0.000	0.000	0.000	-0.005	0.032	-0.019
H10'	0.000	0.061	0.000	0.000	0.000	0.041	0.042	0.037
H11'	0.000	-0.054	0.000	0.000	0.000	0.022	-0.041	0.030
H12'	0.000	0.053	0.000	0.000	0.000	0.003	0.040	0.016
H13'	0.000	0.026	0.000	0.000	0.000	0.024	0.032	0.031
H14'	0.000	0.052	0.000	0.000	0.000	-0.011	0.040	-0.024

**Table A2.18:** Contributions at 0.05 Å to the N5 atomic basin along the Cu-N5 bond for the EE molecular system; LS, SF%, LS<sub>α</sub>, LS<sub>β</sub>, LS<sub>s</sub>, SF<sub>s</sub>% are respectively the Local source, the Source Function atomic percentage for ρ(**r**), the Local source alpha and beta, the Local Source for s(**r**) and the Source Function atomic percentage for s(**r**). R<sub>SF</sub> (R<sub>FSS</sub>) are evaluated as in tab A2.1

Ω	LS	SF%	LS <sub>α</sub>	LS <sub>β</sub>	LS <sub>s</sub>	SF <sub>s</sub> %	R <sub>SF</sub>	R <sub>FSS</sub>
Cu1	0.003	0.001	0.002	0.000	0.002	2.792	0.012	0.152
N1	-0.001	0.000	0.000	0.000	0.000	-0.111	-0.007	-0.052
N2	-0.002	-0.001	-0.001	-0.001	0.000	-0.104	-0.011	-0.051
N5'	-0.001	0.000	0.000	-0.001	0.001	1.219	-0.007	0.115
N4'	0.000	0.000	0.000	0.000	-0.001	-1.039	-0.005	-0.109
N3	98.616	49.635	99.340	99.277	0.063	99.148	0.396	0.499
O1	-0.001	-0.001	-0.001	0.000	-0.001	-0.842	-0.009	-0.102
F1	0.000	0.000	0.000	0.000	0.000	-0.032	0.003	-0.034
F2	0.001	0.000	0.000	0.000	0.000	-0.045	0.008	-0.038
F3	0.000	0.000	0.000	0.000	0.000	-0.030	0.004	-0.033
C1	0.000	0.000	0.000	0.000	0.000	0.168	-0.002	0.059
C2	0.001	0.000	0.000	0.000	0.000	-0.291	0.008	-0.071
C3	0.000	0.000	0.000	0.000	0.000	0.082	0.007	0.047
C4	0.000	0.000	0.000	0.000	0.000	-0.287	0.007	-0.071
C5	0.000	0.000	0.000	0.000	0.000	0.101	0.004	0.050
C6	0.000	0.000	0.000	0.000	0.000	-0.104	0.005	-0.051
C7	0.000	0.000	0.000	0.000	0.000	-0.197	0.006	-0.063
C8	0.000	0.000	0.000	0.000	0.000	-0.273	0.005	-0.070
C9	0.000	0.000	0.000	0.000	0.000	-0.347	0.002	-0.076
H1	-0.001	0.000	0.000	0.000	0.000	0.037	-0.008	0.036
H2	0.001	0.001	0.001	0.001	0.000	0.064	0.009	0.043
H3	0.001	0.000	0.000	0.000	0.000	0.003	0.008	0.015
H4	-0.001	0.000	0.000	0.000	0.000	0.042	-0.008	0.037
H5	0.001	0.001	0.001	0.001	0.000	0.039	0.009	0.036
H6	0.001	0.000	0.000	0.000	0.000	0.027	0.008	0.032
H7	0.000	0.000	0.000	0.000	0.000	-0.012	0.005	-0.024
H8	0.000	0.000	0.000	0.000	0.000	-0.012	0.004	-0.025
H9	0.000	0.000	0.000	0.000	0.000	-0.003	0.006	-0.015
H10	0.001	0.000	0.000	0.000	0.000	0.022	0.008	0.030
H11	0.000	0.000	0.000	0.000	0.000	0.011	0.006	0.024
H12	0.000	0.000	0.000	0.000	0.000	0.002	0.006	0.014

H13	0.001	0.000	0.000	0.000	0.000	0.012	0.007	0.025
H14	0.001	0.000	0.000	0.000	0.000	-0.005	0.007	-0.019
Cu1'	0.000	0.000	0.000	0.000	0.001	1.168	-0.005	0.113
N1'	-0.001	0.000	0.000	0.000	0.000	-0.026	-0.007	-0.032
N2'	0.000	0.000	0.000	0.000	0.000	0.022	-0.007	0.030
N5	0.011	0.005	0.006	0.005	0.001	1.842	0.019	0.132
N4	0.045	0.023	0.022	0.023	-0.001	-1.796	0.031	-0.131
N3'	0.002	0.001	0.001	0.001	0.000	-0.167	0.010	-0.059
O1'	-0.001	0.000	-0.001	0.000	0.000	-0.392	-0.008	-0.079
F1'	0.000	0.000	0.000	0.000	0.000	-0.025	0.007	-0.031
F2'	0.001	0.000	0.000	0.000	0.000	-0.041	0.007	-0.037
F3'	-0.001	0.000	0.000	0.000	0.000	-0.028	-0.007	-0.033
C1'	0.000	0.000	0.000	0.000	0.000	0.147	0.001	0.057
C2'	0.000	0.000	0.000	0.000	0.000	-0.231	0.001	-0.066
C3'	0.000	0.000	0.000	0.000	0.000	0.066	0.004	0.044
C4'	0.000	0.000	0.000	0.000	0.000	-0.225	0.005	-0.066
C5'	0.000	0.000	0.000	0.000	0.000	0.084	0.004	0.047
C6'	0.000	0.000	0.000	0.000	0.000	-0.077	0.005	-0.046
C7'	0.000	0.000	0.000	0.000	0.000	-0.136	0.004	-0.055
C8'	0.000	0.000	0.000	0.000	0.000	-0.139	0.005	-0.056
C9'	0.000	0.000	0.000	0.000	0.000	-0.210	0.003	-0.064
H1'	0.000	0.000	0.000	0.000	0.000	0.018	0.004	0.028
H2'	0.001	0.000	0.000	0.000	0.000	0.044	0.007	0.038
H3'	-0.001	0.000	0.000	0.000	0.000	0.000	-0.008	-0.004
H4'	0.000	0.000	0.000	0.000	0.000	0.016	0.003	0.027
H5'	0.000	0.000	0.000	0.000	0.000	0.021	0.006	0.030
H6'	0.000	0.000	0.000	0.000	0.000	0.014	0.005	0.026
H7'	0.000	0.000	0.000	0.000	0.000	-0.010	0.002	-0.024
H8'	0.000	0.000	0.000	0.000	0.000	-0.010	0.005	-0.023
H9'	0.000	0.000	0.000	0.000	0.000	-0.002	0.005	-0.014
H10'	0.000	0.000	0.000	0.000	0.000	0.017	0.006	0.028
H11'	0.000	0.000	0.000	0.000	0.000	0.009	-0.006	0.023
H12'	0.000	0.000	0.000	0.000	0.000	0.001	0.006	0.012
H13'	0.000	0.000	0.000	0.000	0.000	0.010	0.005	0.023
H14'	0.000	0.000	0.000	0.000	0.000	-0.004	0.006	-0.018

**Table A2.19:** Contributions at the N5 atomic basin along the N5-N4 bond for the EE molecular system; LS, SF%,  $LS_{\alpha}$ ,  $LS_{\beta}$ ,  $LS_s$ ,  $SF_s\%$  are respectively the Local source, the Source Function atomic percentage for  $\rho(\mathbf{r})$ , the Local source alfa and beta, the Local Source for  $s(\mathbf{r})$  and the Source Function atomic percentage for  $s(\mathbf{r})$ .  $R_{SF}$  ( $R_{FSS}$ ) are evaluated as in tab A2.1

$\Omega$	LS	SF%	$LS_{\alpha}$	$LS_{\beta}$	$LS_s$	$SF_s\%$	$R_{SF}$	$R_{FSS}$
Cu1	0.001	0.305	0.001	0.000	0.002	1145.081	0.044	0.676
N1	-0.001	-0.115	0.000	0.000	0.000	-44.475	-0.031	-0.229
N2	-0.001	-0.307	-0.001	-0.001	0.000	-31.036	-0.044	-0.203
N5'	0.000	-0.065	0.000	-0.001	0.001	606.369	-0.026	0.547
N4'	-0.001	-0.155	-0.001	0.000	-0.001	-527.187	-0.035	-0.522
N3	0.235	51.110	0.118	0.117	0.000	374.562	0.240	0.466

O1	-0.001	-0.290	-0.001	0.000	0.000	-367.983	-0.043	-0.463
F1	0.000	0.011	0.000	0.000	0.000	-15.313	0.014	-0.161
F2	0.001	0.182	0.000	0.000	0.000	-21.551	0.037	-0.180
F3	0.000	0.003	0.000	0.000	0.000	-14.702	0.009	-0.158
C1	0.000	-0.005	0.000	0.000	0.000	79.827	-0.011	0.278
C2	0.001	0.144	0.000	0.000	0.000	-137.233	0.034	-0.333
C3	0.000	0.100	0.000	0.000	0.000	37.772	0.030	0.217
C4	0.000	0.026	0.000	0.000	0.000	46.130	0.019	0.232
C5	0.000	0.085	0.000	0.000	0.000	-129.573	0.028	-0.327
C6	0.000	0.054	0.000	0.000	0.000	-46.032	0.024	-0.232
C7	0.000	0.061	0.000	0.000	0.000	-86.509	0.025	-0.286
C8	0.000	0.046	0.000	0.000	0.000	-114.501	0.023	-0.314
C9	0.000	-0.014	0.000	0.000	0.000	-152.820	-0.016	-0.346
H1	-0.001	-0.190	0.000	0.000	0.000	16.180	-0.037	0.163
H2	0.001	0.248	0.001	0.001	0.000	29.175	0.041	0.199
H3	0.000	0.100	0.000	0.000	0.000	0.912	0.030	0.063
H4	-0.001	-0.138	0.000	0.000	0.000	16.734	-0.033	0.165
H5	0.001	0.195	0.000	0.000	0.000	16.505	0.037	0.165
H6	0.001	0.128	0.000	0.000	0.000	11.405	0.033	0.145
H7	0.000	0.045	0.000	0.000	0.000	-5.367	0.023	-0.113
H8	0.000	0.033	0.000	0.000	0.000	-5.369	0.021	-0.113
H9	0.000	0.060	0.000	0.000	0.000	-1.190	0.025	-0.068
H10	0.001	0.131	0.000	0.000	0.000	9.807	0.033	0.138
H11	0.000	0.054	0.000	0.000	0.000	5.030	0.024	0.111
H12	0.000	0.074	0.000	0.000	0.000	0.942	0.027	0.063
H13	0.001	0.110	0.000	0.000	0.000	5.576	0.031	0.115
H14	0.001	0.119	0.000	0.000	0.000	-2.355	0.032	-0.086
Cu1'	0.000	-0.062	0.000	-0.001	0.001	621.262	-0.026	0.552
N1'	-0.001	-0.135	0.000	0.000	0.000	-17.267	-0.033	-0.167
N2'	-0.001	-0.120	0.000	0.000	0.000	7.296	-0.032	0.125
N5	0.019	4.107	0.010	0.009	0.002	1167.256	0.104	0.681
N4	0.199	43.216	0.098	0.100	-0.002	-1694.383	0.227	-0.771
N3'	0.002	0.359	0.001	0.001	0.000	-92.719	0.046	-0.293
O1'	-0.001	-0.201	-0.001	0.000	0.000	-213.065	-0.038	-0.386
F1'	0.000	0.106	0.000	0.000	0.000	-12.460	0.031	-0.150
F2'	0.001	0.126	0.000	0.000	0.000	-20.496	0.032	-0.177
F3'	-0.001	-0.113	0.000	0.000	0.000	-14.089	-0.031	-0.156
C1'	0.000	-0.002	0.000	0.000	0.000	73.747	-0.008	0.271
C2'	0.000	0.004	0.000	0.000	0.000	-117.966	0.010	-0.317
C3'	0.000	0.034	0.000	0.000	0.000	34.191	0.021	0.210
C4'	0.000	0.020	0.000	0.000	0.000	43.006	0.017	0.226
C5'	0.000	0.041	0.000	0.000	0.000	-116.782	0.022	-0.316
C6'	0.000	0.038	0.000	0.000	0.000	-40.463	0.022	-0.222
C7'	0.000	0.020	0.000	0.000	0.000	-71.486	0.018	-0.268
C8'	0.000	0.042	0.000	0.000	0.000	-72.193	0.023	-0.269
C9'	0.000	0.010	0.000	0.000	0.000	-110.344	0.014	-0.310
H1'	0.000	0.041	0.000	0.000	0.000	9.224	0.022	0.136
H2'	0.001	0.139	0.000	0.000	0.000	22.996	0.034	0.184
H3'	-0.001	-0.194	0.000	0.000	0.000	-0.250	-0.037	-0.041

H4'	0.000	0.016	0.000	0.000	0.000	8.317	0.016	0.131
H5'	0.000	0.073	0.000	0.000	0.000	10.618	0.027	0.142
H6'	0.000	0.052	0.000	0.000	0.000	7.107	0.024	0.124
H7'	0.000	0.005	0.000	0.000	0.000	-5.338	0.011	-0.113
H8'	0.000	0.056	0.000	0.000	0.000	-4.846	0.025	-0.109
H9'	0.000	0.047	0.000	0.000	0.000	-1.136	0.023	-0.067
H10'	0.000	0.107	0.000	0.000	0.000	8.975	0.031	0.134
H11'	0.000	-0.100	0.000	0.000	0.000	4.970	-0.030	0.110
H12'	0.000	0.092	0.000	0.000	0.000	0.747	0.029	0.059
H13'	0.000	0.044	0.000	0.000	0.000	5.277	0.023	0.113
H14'	0.000	0.089	0.000	0.000	0.000	-2.238	0.029	-0.085

**Table A2.20:** Contributions at the bcp along the N5-N4 bond for the EE molecular system; LS, SF%,  $LS_{\alpha}$ ,  $LS_{\beta}$ ,  $LS_s$ ,  $SF_s\%$  are respectively the Local source, the Source Function atomic percentage for  $\rho(\mathbf{r})$ , the Local source alpha and beta, the Local Source for  $s(\mathbf{r})$  and the Source Function atomic percentage for  $s(\mathbf{r})$ .  $R_{SF}$  ( $R_{FS_s}$ ) are evaluated as in tab A2.1

$\Omega$	LS	SF%	$LS_{\alpha}$	$LS_{\beta}$	$LS_s$	$SF_s\%$	$R_{SF}$	$R_{FS_s}$
Cu1	0.000	0.000	0.000	-0.001	0.001	21.001	-0.007	0.297
N1	-0.001	0.000	0.000	0.000	0.000	-0.764	-0.008	-0.098
N2	-0.001	0.000	0.000	0.000	0.000	0.012	-0.008	0.024
N5'	0.052	0.026	0.027	0.025	0.003	56.442	0.032	0.413
N4'	98.337	49.555	99.165	99.172	-0.008	-167.819	0.396	-0.594
N3	0.002	0.001	0.001	0.001	0.000	-3.404	0.010	-0.162
O1	-0.001	-0.001	-0.001	0.000	0.000	-7.430	-0.009	-0.210
F1	0.001	0.000	0.000	0.000	0.000	-0.381	0.007	-0.078
F2	0.001	0.000	0.000	0.000	0.000	-0.629	0.007	-0.092
F3	0.000	0.000	0.000	0.000	0.000	-0.428	-0.006	-0.081
C1	0.000	0.000	0.000	0.000	0.000	2.283	-0.002	0.142
C2	0.000	0.000	0.000	0.000	0.000	-3.738	0.003	-0.167
C3	0.000	0.000	0.000	0.000	0.000	1.102	0.005	0.111
C4	0.000	0.000	0.000	0.000	0.000	-3.817	0.005	-0.168
C5	0.000	0.000	0.000	0.000	0.000	1.385	0.004	0.120
C6	0.000	0.000	0.000	0.000	0.000	-1.348	0.005	-0.119
C7	0.000	0.000	0.000	0.000	0.000	-2.397	0.004	-0.144
C8	0.000	0.000	0.000	0.000	0.000	-2.358	0.005	-0.143
C9	0.000	0.000	0.000	0.000	0.000	-3.672	0.003	-0.166
H1	0.000	0.000	0.000	0.000	0.000	0.302	0.006	0.072
H2	0.001	0.000	0.000	0.000	0.000	0.748	0.008	0.098
H3	-0.001	-0.001	-0.001	-0.001	0.000	-0.019	-0.009	-0.029
H4	0.000	0.000	0.000	0.000	0.000	0.268	0.004	0.069
H5	0.000	0.000	0.000	0.000	0.000	0.341	0.006	0.075
H6	0.000	0.000	0.000	0.000	0.000	0.232	0.006	0.066
H7	0.000	0.000	0.000	0.000	0.000	-0.171	0.003	-0.060
H8	0.000	0.000	0.000	0.000	0.000	-0.155	0.006	-0.058
H9	0.000	0.000	0.000	0.000	0.000	-0.036	0.006	-0.036
H10	0.001	0.000	0.000	0.000	0.000	0.297	0.007	0.072
H11	-0.001	0.000	0.000	0.000	0.000	0.172	-0.007	0.060
H12	0.001	0.000	0.000	0.000	0.000	0.025	0.007	0.031



H13	0.000	0.000	0.000	0.000	0.000	0.174	0.006	0.060
H14	0.000	0.000	0.000	0.000	0.000	-0.071	0.007	-0.045
Cu1'	0.000	0.000	0.001	0.000	0.001	27.133	0.007	0.324
N1'	0.000	0.000	0.000	0.000	0.000	-0.990	-0.007	-0.107
N2'	-0.001	-0.001	-0.001	0.000	0.000	-0.378	-0.009	-0.078
N5	0.000	0.000	0.001	0.000	0.001	17.831	0.006	0.281
N4	-0.001	-0.001	-0.001	0.000	-0.001	-16.057	-0.010	-0.272
N3'	0.046	0.023	0.023	0.023	0.000	7.464	0.031	0.211
O1'	-0.002	-0.001	-0.001	-0.001	0.000	-9.100	-0.010	-0.225
F1'	0.000	0.000	0.000	0.000	0.000	-0.441	0.003	-0.082
F2'	0.001	0.000	0.000	0.000	0.000	-0.620	0.008	-0.092
F3'	0.000	0.000	0.000	0.000	0.000	-0.435	-0.004	-0.082
C1'	0.000	0.000	0.000	0.000	0.000	2.282	-0.002	0.142
C2'	0.001	0.000	0.000	0.000	0.000	-3.853	0.007	-0.169
C3'	0.000	0.000	0.000	0.000	0.000	1.038	0.006	0.109
C4'	0.000	0.000	0.000	0.000	0.000	-3.505	0.006	-0.164
C5'	0.000	0.000	0.000	0.000	0.000	1.262	0.004	0.116
C6'	0.000	0.000	0.000	0.000	0.000	-1.223	0.005	-0.115
C7'	0.000	0.000	0.000	0.000	0.000	-2.271	0.005	-0.142
C8'	0.000	0.000	0.000	0.000	0.000	-2.876	0.005	-0.153
C9'	0.000	0.000	0.000	0.000	0.000	-3.974	-0.004	-0.171
H1'	-0.001	0.000	0.000	0.000	0.000	0.411	-0.008	0.080
H2'	0.001	0.000	0.000	0.000	0.000	0.785	0.008	0.099
H3'	0.000	0.000	0.000	0.000	0.000	0.018	0.005	0.028
H4'	0.000	0.000	0.000	0.000	0.000	0.402	-0.007	0.080
H5'	0.001	0.000	0.000	0.000	0.000	0.423	0.008	0.081
H6'	0.000	0.000	0.000	0.000	0.000	0.285	0.007	0.071
H7'	0.000	0.000	0.000	0.000	0.000	-0.148	0.005	-0.057
H8'	0.000	0.000	0.000	0.000	0.000	-0.147	0.005	-0.057
H9'	0.000	0.000	0.000	0.000	0.000	-0.033	0.005	-0.035
H10'	0.001	0.000	0.000	0.000	0.000	0.263	0.007	0.069
H11'	0.000	0.000	0.000	0.000	0.000	0.136	0.004	0.055
H12'	0.000	0.000	0.000	0.000	0.000	0.024	0.006	0.031
H13'	0.000	0.000	0.000	0.000	0.000	0.150	0.006	0.057
H14'	0.000	0.000	0.000	0.000	0.000	-0.066	0.007	-0.043

**Table A2.21:** Contributions at the N4 atomic basin along the N5-N4 bond for the EE molecular system; LS, SF%,  $LS_{\alpha}$ ,  $LS_{\beta}$ ,  $LS_s$ ,  $SF_s\%$  are respectively the Local source, the Source Function atomic percentage for  $\rho(\mathbf{r})$ , the Local source alpha and beta, the Local Source for  $s(\mathbf{r})$  and the Source Function atomic percentage for  $s(\mathbf{r})$ .  $R_{SF}$  ( $R_{FSS}$ ) are evaluated as in tab A2.1

$\Omega$	LS	SF%	$LS_{\alpha}$	$LS_{\beta}$	$LS_s$	$SF_s\%$	$R_{SF}$	$R_{FSS}$
Cu1	-0.001	-0.125	0.000	-0.001	0.001	241.723	-0.032	0.403
N1	-0.001	-0.224	-0.001	-0.001	0.000	-11.404	-0.039	-0.145
N2	-0.001	-0.214	-0.001	-0.001	0.000	-3.144	-0.039	-0.095
N5'	0.247	49.369	0.126	0.121	0.005	1044.505	0.237	0.656
N4'	0.231	46.077	0.113	0.118	-0.004	-965.036	0.232	-0.639
N3	0.001	0.258	0.001	0.001	0.000	-43.260	0.041	-0.227

O1	-0.001	-0.190	-0.001	0.000	0.000	-88.018	-0.037	-0.288
F1	0.001	0.115	0.000	0.000	0.000	-3.937	0.031	-0.102
F2	0.001	0.132	0.000	0.000	0.000	-6.533	0.033	-0.121
F3	0.000	-0.060	0.000	0.000	0.000	-4.359	-0.025	-0.106
C1	0.000	-0.005	0.000	0.000	0.000	23.886	-0.011	0.186
C2	0.000	0.018	0.000	0.000	0.000	-39.945	0.017	-0.221
C3	0.000	0.042	0.000	0.000	0.000	12.125	0.022	0.148
C4	0.000	0.067	0.000	0.000	0.000	-42.890	0.026	-0.226
C5	0.000	0.028	0.000	0.000	0.000	15.314	0.020	0.161
C6	0.000	0.052	0.000	0.000	0.000	-15.575	0.024	-0.161
C7	0.000	0.016	0.000	0.000	0.000	-27.859	0.016	-0.196
C8	0.000	0.063	0.000	0.000	0.000	-26.436	0.026	-0.193
C9	0.000	0.016	0.000	0.000	0.000	-41.814	0.016	-0.224
H1	0.001	0.110	0.000	0.000	0.000	3.331	0.031	0.097
H2	0.001	0.196	0.001	0.000	0.000	8.276	0.038	0.131
H3	-0.001	-0.247	-0.001	-0.001	0.000	-0.300	-0.041	-0.043
H4	0.000	0.043	0.000	0.000	0.000	2.947	0.023	0.093
H5	0.000	0.099	0.000	0.000	0.000	3.756	0.030	0.100
H6	0.000	0.067	0.000	0.000	0.000	2.597	0.026	0.089
H7	0.000	0.008	0.000	0.000	0.000	-1.876	0.013	-0.080
H8	0.000	0.067	0.000	0.000	0.000	-1.693	0.026	-0.077
H9	0.000	0.068	0.000	0.000	0.000	-0.387	0.026	-0.047
H10	0.001	0.163	0.000	0.000	0.000	3.401	0.035	0.097
H11	-0.001	-0.149	0.000	0.000	0.000	2.096	-0.034	0.083
H12	0.001	0.132	0.000	0.000	0.000	0.286	0.033	0.043
H13	0.000	0.074	0.000	0.000	0.000	1.994	0.027	0.081
H14	0.001	0.118	0.000	0.000	0.000	-0.763	0.032	-0.059
Cu1'	0.000	0.032	0.001	0.000	0.001	226.618	0.021	0.394
N1'	0.000	-0.083	0.000	0.000	0.000	-7.423	-0.028	-0.126
N2'	-0.001	-0.145	0.000	0.000	0.000	-0.506	-0.034	-0.052
N5	0.001	0.216	0.001	0.000	0.001	170.606	0.039	0.358
N4	-0.002	-0.327	-0.001	0.000	-0.001	-158.360	-0.045	-0.350
N3'	0.017	3.471	0.009	0.009	0.000	15.150	0.098	0.160
O1'	-0.002	-0.303	-0.001	-0.001	0.000	-76.249	-0.043	-0.274
F1'	0.000	0.010	0.000	0.000	0.000	-4.270	0.014	-0.105
F2'	0.001	0.157	0.000	0.000	0.000	-6.036	0.035	-0.118
F3'	0.000	-0.053	0.000	0.000	0.000	-4.302	-0.024	-0.105
C1'	0.000	-0.002	0.000	0.000	0.000	22.058	-0.008	0.181
C2'	0.000	0.092	0.000	0.000	0.000	-36.456	0.029	-0.214
C3'	0.000	0.074	0.000	0.000	0.000	9.728	0.027	0.138
C4'	0.000	0.054	0.000	0.000	0.000	-32.533	0.024	-0.206
C5'	0.000	0.018	0.000	0.000	0.000	11.840	0.017	0.147
C6'	0.000	0.038	0.000	0.000	0.000	-11.198	0.022	-0.145
C7'	0.000	0.033	0.000	0.000	0.000	-20.579	0.021	-0.177
C8'	0.000	0.033	0.000	0.000	0.000	-25.360	0.021	-0.190
C9'	0.000	-0.012	0.000	0.000	0.000	-35.484	-0.015	-0.212
H1'	-0.001	-0.134	0.000	0.000	0.000	3.575	-0.033	0.099
H2'	0.001	0.158	0.000	0.000	0.000	7.207	0.035	0.125
H3'	0.000	-0.001	0.000	0.000	0.000	0.143	-0.007	0.034

H4'	0.000	-0.072	0.000	0.000	0.000	3.444	-0.027	0.098
H5'	0.001	0.106	0.000	0.000	0.000	3.785	0.031	0.101
H6'	0.000	0.071	0.000	0.000	0.000	2.514	0.027	0.088
H7'	0.000	0.029	0.000	0.000	0.000	-1.405	0.020	-0.072
H8'	0.000	0.030	0.000	0.000	0.000	-1.377	0.020	-0.072
H9'	0.000	0.040	0.000	0.000	0.000	-0.314	0.022	-0.044
H10'	0.000	0.086	0.000	0.000	0.000	2.430	0.028	0.087
H11'	0.000	0.010	0.000	0.000	0.000	1.245	0.014	0.070
H12'	0.000	0.054	0.000	0.000	0.000	0.221	0.024	0.039
H13'	0.000	0.067	0.000	0.000	0.000	1.397	0.026	0.072
H14'	0.000	0.084	0.000	0.000	0.000	-0.625	0.028	-0.055

**Table A2.22:** Contributions at the bcp along the N4-N3 bond for the EE molecular system; LS, SF%,  $LS_{\alpha}$ ,  $LS_{\beta}$ ,  $LS_s$ ,  $SF_s\%$  are respectively the Local source, the Source Function atomic percentage for  $\rho(\mathbf{r})$ , the Local source alpha and beta, the Local Source for  $s(\mathbf{r})$  and the Source Function atomic percentage for  $s(\mathbf{r})$ .  $R_{SF}$  ( $R_{FSs}$ ) are evaluated as in tab A2.1

$\Omega$	LS	SF%	$LS_{\alpha}$	$LS_{\beta}$	$LS_s$	$SF_s\%$	$R_{SF}$	$R_{FSs}$
Cu1	-0.001	-0.002	0.000	-0.001	0.001	117.395	-0.013	0.527
N1	-0.001	-0.003	-0.001	-0.001	0.000	-6.773	-0.016	-0.204
N2	-0.001	-0.003	-0.001	-0.001	0.000	-3.009	-0.016	-0.156
N5'	45.422	99.828	22.713	22.709	0.004	370.279	0.500	0.774
N4'	0.060	0.131	0.028	0.031	-0.003	-262.580	0.055	-0.690
N3	0.001	0.002	0.000	0.001	0.000	-22.428	0.014	-0.304
O1	-0.001	-0.002	-0.001	0.000	0.000	-43.371	-0.013	-0.378
F1	0.001	0.001	0.000	0.000	0.000	-1.758	0.012	-0.130
F2	0.001	0.001	0.000	0.000	0.000	-2.931	0.012	-0.154
F3	0.000	0.000	0.000	0.000	0.000	-1.919	-0.008	-0.134
C1	0.000	0.000	0.000	0.000	0.000	10.761	-0.004	0.238
C2	0.000	0.000	0.000	0.000	0.000	-18.245	0.007	-0.284
C3	0.000	0.001	0.000	0.000	0.000	5.702	0.009	0.192
C4	0.000	0.001	0.000	0.000	0.000	-20.633	0.011	-0.295
C5	0.000	0.000	0.000	0.000	0.000	7.270	0.008	0.209
C6	0.000	0.001	0.000	0.000	0.000	-7.716	0.009	-0.213
C7	0.000	0.000	0.000	0.000	0.000	-13.858	0.005	-0.259
C8	0.000	0.001	0.000	0.000	0.000	-12.692	0.010	-0.251
C9	0.000	0.000	0.000	0.000	0.000	-20.222	0.006	-0.293
H1	0.001	0.002	0.000	0.000	0.000	1.561	0.013	0.125
H2	0.001	0.002	0.001	0.001	0.000	3.903	0.015	0.170
H3	-0.001	-0.003	-0.001	-0.001	0.000	-0.146	-0.015	-0.057
H4	0.000	0.001	0.000	0.000	0.000	1.388	0.009	0.120
H5	0.001	0.001	0.000	0.000	0.000	1.777	0.012	0.130
H6	0.000	0.001	0.000	0.000	0.000	1.247	0.010	0.116
H7	0.000	0.000	0.000	0.000	0.000	-0.887	0.005	-0.103
H8	0.000	0.001	0.000	0.000	0.000	-0.799	0.010	-0.100
H9	0.000	0.001	0.000	0.000	0.000	-0.180	0.010	-0.061
H10	0.001	0.002	0.001	0.000	0.000	1.669	0.014	0.128
H11	-0.001	-0.002	0.000	0.000	0.000	1.088	-0.014	0.111
H12	0.001	0.002	0.000	0.000	0.000	0.141	0.013	0.056

H13	0.000	0.001	0.000	0.000	0.000	0.978	0.011	0.107
H14	0.001	0.001	0.000	0.000	0.000	-0.353	0.012	-0.076
Cu1'	0.000	0.000	0.000	0.000	0.001	88.766	0.006	0.481
N1'	0.000	-0.001	0.000	0.000	0.000	-2.635	-0.010	-0.149
N2'	-0.001	-0.001	0.000	0.000	0.000	0.458	-0.012	0.083
N5	0.001	0.003	0.001	0.000	0.001	71.225	0.016	0.447
N4	-0.001	-0.003	-0.001	0.000	-0.001	-67.100	-0.016	-0.438
N3'	0.010	0.023	0.005	0.005	0.000	-0.288	0.030	-0.071
O1'	-0.001	-0.003	-0.001	-0.001	0.000	-29.627	-0.016	-0.333
F1'	0.000	0.000	0.000	0.000	0.000	-1.820	0.005	-0.132
F2'	0.001	0.002	0.000	0.000	0.000	-2.589	0.013	-0.148
F3'	0.000	-0.001	0.000	0.000	0.000	-1.856	-0.010	-0.132
C1'	0.000	0.000	0.000	0.000	0.000	9.407	-0.001	0.227
C2'	0.000	0.001	0.000	0.000	0.000	-15.299	0.010	-0.267
C3'	0.000	0.001	0.000	0.000	0.000	4.074	0.010	0.172
C4'	0.000	0.001	0.000	0.000	0.000	-13.567	0.009	-0.257
C5'	0.000	0.000	0.000	0.000	0.000	4.975	0.006	0.184
C6'	0.000	0.000	0.000	0.000	0.000	-4.635	0.008	-0.180
C7'	0.000	0.000	0.000	0.000	0.000	-8.457	0.007	-0.219
C8'	0.000	0.000	0.000	0.000	0.000	-10.271	0.007	-0.234
C9'	0.000	0.000	0.000	0.000	0.000	-14.414	-0.005	-0.262
H1'	-0.001	-0.001	0.000	0.000	0.000	1.425	-0.012	0.121
H2'	0.001	0.002	0.000	0.000	0.000	2.975	0.012	0.155
H3'	0.000	0.000	0.000	0.000	0.000	0.059	-0.006	0.042
H4'	0.000	-0.001	0.000	0.000	0.000	1.372	-0.009	0.120
H5'	0.000	0.001	0.000	0.000	0.000	1.547	0.011	0.125
H6'	0.000	0.001	0.000	0.000	0.000	1.018	0.009	0.108
H7'	0.000	0.000	0.000	0.000	0.000	-0.594	0.007	-0.091
H8'	0.000	0.000	0.000	0.000	0.000	-0.580	0.007	-0.090
H9'	0.000	0.000	0.000	0.000	0.000	-0.133	0.008	-0.055
H10'	0.000	0.001	0.000	0.000	0.000	1.011	0.010	0.108
H11'	0.000	0.000	0.000	0.000	0.000	0.515	0.003	0.086
H12'	0.000	0.001	0.000	0.000	0.000	0.091	0.009	0.048
H13'	0.000	0.001	0.000	0.000	0.000	0.583	0.009	0.090
H14'	0.000	0.001	0.000	0.000	0.000	-0.265	0.010	-0.069

**Table A2.23:** Contributions at the N3 atomic basin along the N4-N3 bond for the EE molecular system; LS, SF%,  $LS_{\alpha}$ ,

$LS_{\beta}$ ,  $LS_s$ ,  $SF_s\%$  are respectively the Local source, the Source Function atomic percentage for  $\rho(\mathbf{r})$ , the Local source alfa and beta, the Local Source for  $s(\mathbf{r})$  and the Source Function atomic percentage for  $s(\mathbf{r})$ .  $R_{SF}$  ( $R_{FSS}$ ) are evaluated as

in tab A2.1

$\Omega$	LS	SF%	$LS_{\alpha}$	$LS_{\beta}$	LSs	SFs%	$R_{SF}$	$R_{FSs}$
Ni1	1.540	96.918	0.766	0.774	-0.009	73.646	0.495	0.452
S2	0.017	1.076	0.008	0.009	-0.001	6.915	0.110	0.205
S3	0.007	0.457	0.003	0.004	-0.001	5.660	0.083	0.192
C4	0.002	0.095	0.001	0.001	0.000	0.054	0.049	0.041
H5	0.002	0.138	0.001	0.001	0.000	0.205	0.056	0.064
C6	0.001	0.059	0.000	0.001	0.000	2.024	0.042	0.136
C7	0.000	-0.007	0.000	0.000	0.000	-0.521	-0.021	-0.087
C8	0.000	0.030	0.000	0.001	-0.001	5.024	0.034	0.184
H9	0.002	0.155	0.001	0.001	0.000	0.733	0.058	0.097
C10	0.000	0.014	0.000	0.000	0.000	-2.840	0.026	-0.153
H11	0.003	0.157	0.001	0.001	0.000	0.905	0.058	0.104
C12	0.001	0.053	0.000	0.001	-0.001	6.268	0.040	0.199
H13	0.002	0.147	0.001	0.001	0.000	0.669	0.057	0.094
C14	0.001	0.080	0.001	0.001	0.000	-0.988	0.046	-0.107
H15	0.002	0.135	0.001	0.001	0.000	0.758	0.055	0.098
C16	0.001	0.076	0.000	0.001	0.000	2.857	0.046	0.153
H17	0.002	0.141	0.001	0.001	0.000	0.745	0.056	0.098
N18	0.002	0.138	0.001	0.001	0.000	0.223	0.056	0.065

**Table A2.24:** Contributions at the CD along the Ni1-S2 bond for the adt CpNi(dithiolene)<sup>•</sup> radical complex molecular system; LS, SF%,  $LS_{\alpha}$ ,  $LS_{\beta}$ , LSs, SFs% are respectively the Local source, the Source Function atomic percentage for  $\rho(\mathbf{r})$ , the Local source alfa and beta, the Local Source for  $s(\mathbf{r})$  and the Source Function atomic percentage for  $s(\mathbf{r})$ .  $R_{SF}$  ( $R_{FSs}$ ) are evaluated as in tab A2.1

$\Omega$	LS	SF%	$LS_{\alpha}$	$LS_{\beta}$	LSs	$SF_S - SF_{S_{mag}} \%$	$R_{SF}$	$R_{SFS - SFS_{mag}}$
Ni1	1.525	95.923	0.750	0.774	-0.024	209.952	0.493	0.640
S2	0.019	1.174	0.010	0.009	0.001	-6.526	0.114	-0.201
S3	0.008	0.529	0.004	0.004	0.000	-4.189	0.087	-0.174
C4	0.002	0.098	0.001	0.001	0.000	-0.376	0.050	-0.078
H5	0.002	0.138	0.001	0.001	0.000	0.187	0.056	0.062
C6	0.001	0.062	0.000	0.001	0.000	1.632	0.043	0.127
C7	0.000	-0.007	0.000	0.000	0.000	-0.547	-0.021	-0.088
C8	0.001	0.063	0.000	0.001	0.000	0.564	0.043	0.089
H9	0.003	0.159	0.001	0.001	0.000	0.183	0.058	0.061
C10	0.001	0.034	0.001	0.000	0.001	-5.589	0.035	-0.191
H11	0.003	0.158	0.001	0.001	0.000	0.822	0.058	0.101
C12	0.001	0.083	0.001	0.001	0.000	2.159	0.047	0.139
H13	0.002	0.151	0.001	0.001	0.000	0.009	0.057	0.022
C14	0.002	0.100	0.001	0.001	0.000	-3.736	0.050	-0.167
H15	0.002	0.136	0.001	0.001	0.000	0.614	0.055	0.092
C16	0.002	0.105	0.001	0.001	0.000	-1.027	0.051	-0.109
H17	0.002	0.144	0.001	0.001	0.000	0.344	0.056	0.076
N18	0.002	0.139	0.001	0.001	0.000	0.220	0.056	0.065

**Table A2.25:** Contributions at the CD along the Ni1-S2 bond for the adt CpNi(dithiolene)<sup>•</sup> radical complex molecular system given by the relaxation MO; LS, SF%,  $LS_{\alpha}$ ,  $LS_{\beta}$ , LSs,  $SF_S - SF_{S_{mag}} \%$  are respectively the Local source, the Source Function atomic percentage for  $\rho(\mathbf{r})$ , the Local source alfa and beta, the Local Source for  $s(\mathbf{r})$  and the Source Function atomic percentage for  $s(\mathbf{r})$  obtained by the relaxation (reaction) orbitals.  $R_{SF}$  ( $R_{SFS - SFS_{mag}}$ ) are the ray of the sphere that are proportional to the atomic contribution to  $\rho(\mathbf{r})$  ( $s(\mathbf{r})$ ) evaluated as

$$R_{SF} = 0.5 * (SF\% / 100)^{1/3}$$

$$R_{SFS - SFS_{mag}} = 0.5 * (SF_S - SF_{S_{mag}}\% / 100)^{1/3}$$

All the reported quantity are reported in a.u.

$\Omega$	LSs	SF <sub>Smag</sub> %
Ni1	0.016	-136.307
S2	-0.002	13.440
S3	-0.001	9.849
C4	0.000	0.430
H5	0.000	0.018
C6	0.000	0.392
C7	0.000	0.025
C8	-0.001	4.460
H9	0.000	0.550
C10	0.000	2.749
H11	0.000	0.083
C12	0.000	4.109
H13	0.000	0.660
C14	0.000	2.749
H15	0.000	0.144
C16	0.000	3.884
H17	0.000	0.400
N18	0.000	0.003

**Table A2.26:** Contributions at the CD along the Ni1-S2 bond for the adt CpNi(dithiolene)<sup>•</sup> radical complex molecular system given by the SOMO; LS<sub>S</sub> and SF<sub>Smag</sub> % are respectively the Local source and the Source Function atomic percentage for s(**r**) R<sub>FSmag</sub> are the ray of the sphere that are proportional to the atomic contribution to s(**r**) evaluated as

$$R_{SFs-SFsmag} = 0.5 * (SF_S - SF_{Smag} \% / 100)^{1/3}$$

All the reported quantity are reported in a.u.

$\Omega$	LS	SF%	$LS_{\alpha}$	$LS_{\beta}$	LSs	SFs%	$R_{SF}$	$R_{FSs}$
Ni1	0,014	8,758	0,009	0,006	0,003	163,547	0,222	0,589
S2	0,125	76,334	0,063	0,062	0,001	36,953	0,457	0,359
S3	0,004	2,535	0,002	0,002	-0,001	-27,874	0,147	-0,327
C4	0,006	3,625	0,003	0,003	0,000	-2,079	0,165	-0,137
H5	0,003	1,968	0,002	0,002	0,000	-1,639	0,135	-0,127
C6	0,001	0,875	0,001	0,001	0,000	-13,711	0,103	-0,258
C7	0,000	-0,050	0,000	0,000	0,000	3,535	-0,040	0,164
C8	0,000	-0,118	0,000	0,000	0,000	-20,031	-0,053	-0,293
H9	0,001	0,819	0,001	0,001	0,000	-4,094	0,101	-0,172
C10	-0,001	-0,623	0,000	-0,001	0,000	15,227	-0,092	0,267
H11	0,001	0,715	0,001	0,001	0,000	-5,450	0,096	-0,190
C12	0,000	0,133	0,000	0,000	0,000	-26,442	0,055	-0,321
H13	0,001	0,833	0,001	0,001	0,000	-3,703	0,101	-0,167
C14	0,001	0,524	0,000	0,000	0,000	5,287	0,087	0,188
H15	0,001	0,779	0,001	0,001	0,000	-3,826	0,099	-0,168
C16	0,001	0,521	0,000	0,001	0,000	-10,535	0,087	-0,236
H17	0,001	0,798	0,001	0,001	0,000	-3,776	0,100	-0,168
N18	0,002	1,488	0,001	0,001	0,000	-1,496	0,123	-0,123

**Table A2.27:** Contributions at the CC along the Ni1-S2 bond for the adt CpNi(dithiolene)<sup>•</sup> radical complex molecular system; LS, SF%,  $LS_{\alpha}$ ,  $LS_{\beta}$ , LSs, SFs% are respectively the Local source, the Source Function atomic percentage for  $\rho(\mathbf{r})$ , the Local source alfa and beta, the Local Source for  $s(\mathbf{r})$  and the Source Function atomic percentage for  $s(\mathbf{r})$ .  $R_{SF}$  ( $R_{FSs}$ ) are evaluated as in tab A2.1



$\Omega$	LS	SF%	$LS_{\alpha}$	$LS_{\beta}$	LSs	$SF_S - SF_{S_{mag}} \%$	$R_{SF}$	$R_{SFS} - SFS_{mag}$
Ni1	0,010	5,975	0,004	0,006	-0,002	-88,888	0,195	-0,481
S2	0,127	77,590	0,065	0,062	0,003	150,799	0,459	0,573
S3	0,005	3,062	0,003	0,002	0,000	19,867	0,156	0,292
C4	0,006	3,669	0,003	0,003	0,000	1,875	0,166	0,133
H5	0,003	1,970	0,002	0,002	0,000	-1,496	0,135	-0,123
C6	0,001	0,902	0,001	0,001	0,000	-11,262	0,104	-0,241
C7	0,000	-0,048	0,000	0,000	0,000	3,708	-0,039	0,167
C8	0,000	0,077	0,000	0,000	0,000	-2,414	0,046	-0,144
H9	0,001	0,854	0,001	0,001	0,000	-1,007	0,102	-0,108
C10	-0,001	-0,480	0,000	-0,001	0,001	28,154	-0,084	0,328
H11	0,001	0,721	0,001	0,001	0,000	-4,938	0,097	-0,183
C12	0,001	0,312	0,000	0,000	0,000	-10,164	0,073	-0,233
H13	0,001	0,874	0,001	0,001	0,000	-0,040	0,103	-0,037
C14	0,001	0,653	0,001	0,000	0,000	17,005	0,093	0,277
H15	0,001	0,787	0,001	0,001	0,000	-3,093	0,099	-0,157
C16	0,001	0,690	0,001	0,001	0,000	4,782	0,095	0,181
H17	0,001	0,821	0,001	0,001	0,000	-1,738	0,101	-0,130
N18	0,002	1,488	0,001	0,001	0,000	-1,479	0,123	-0,123

**Table A2.28:** Contributions at the CC along the Ni1-S2 bond for the adt CpNi(dithiolene)<sup>\*</sup> radical complex molecular system given by the relaxation MO; LS, SF%,  $LS_{\alpha}$ ,  $LS_{\beta}$ , LSs,  $SF_S - SF_{S_{mag}} \%$  are respectively the Local source, the Source Function atomic percentage for  $\rho(\mathbf{r})$ , the Local source alfa and beta, the Local Source for  $s(\mathbf{r})$  and the Source Function atomic percentage for  $s(\mathbf{r})$  obtained by the relaxation (reaction) orbitals.  $R_{SF}$  ( $R_{SFS} - SFS_{mag}$ ) are the ray of the sphere that are proportional to the atomic contribution to  $\rho(\mathbf{r})$  ( $s(\mathbf{r})$ ) evaluated as in Tab A2.25.

$\Omega$	Ls	SF <sub>S<sub>mag</sub></sub> %
Ni1	0,005	252,435
S2	-0,002	-113,847
S3	-0,001	-47,741
C4	0,000	-3,954
H5	0,000	-0,143
C6	0,000	-2,449
C7	0,000	-0,174
C8	0,000	-17,617
H9	0,000	-3,087
C10	0,000	-12,927
H11	0,000	-0,512
C12	0,000	-16,278
H13	0,000	-3,663
C14	0,000	-11,718
H15	0,000	-0,733
C16	0,000	-15,317
H17	0,000	-2,038
N18	0,000	-0,017

**Table A2.29:** Contributions at the CC along the Ni1-S2 bond for the adt CpNi(dithiolene)<sup>•</sup> radical complex molecular system given by the SOMO; LS<sub>S</sub> and SF<sub>S<sub>mag</sub></sub> % are respectively the Local source and the Source Function atomic percentage for s(**r**) R<sub>F<sub>S<sub>mag</sub></sub></sub> are the ray of the sphere that are proportional to the atomic contribution to s(**r**) evaluated as in Tab. A2.26

